

The evolution of the Patagonian Ice Sheet from 35 ka to the present day (PATICE)

Bethan J. Davies, Christopher M. Darvill, Harold Lovell, Jacob M. Bendle, Julian A. Dowdeswell, Derek Fabel, Juan-Luis García, Alessa Geiger, Neil F. Glasser, Delia M. Gheorghiu, Stephan Harrison, Andrew S. Hein, Michael R. Kaplan, Julian R.V. Martin, Monika Mendelova, Adrian Palmer, Mauri Pelto, Ángel Rodés, Esteban A. Sagredo, Rachel Smedley, John L. Smellie, Varyl R. Thorndycraft



PII: S0012-8252(19)30623-3

DOI: <https://doi.org/10.1016/j.earscirev.2020.103152>

Reference: EARTH 103152

To appear in: *Earth-Science Reviews*

Please cite this article as: B.J. Davies, C.M. Darvill, H. Lovell, et al., The evolution of the Patagonian Ice Sheet from 35 ka to the present day (PATICE), *Earth-Science Reviews* (2020), <https://doi.org/10.1016/j.earscirev.2020.103152>

This is a PDF file of an article that has undergone enhancements after acceptance, such as the addition of a cover page and metadata, and formatting for readability, but it is not yet the definitive version of record. This version will undergo additional copyediting, typesetting and review before it is published in its final form, but we are providing this version to give early visibility of the article. Please note that, during the production process, errors may be discovered which could affect the content, and all legal disclaimers that apply to the journal pertain.

# The evolution of the Patagonian Ice Sheet from 35 ka to the Present Day (PATICE)

Bethan J. Davies<sup>1\*</sup>, Christopher M. Darvill<sup>2</sup>, Harold Lovell<sup>3</sup>, Jacob M. Bendle<sup>1</sup>, Julian A. Dowdeswell<sup>4</sup>, Derek Fabel<sup>5</sup>, Juan-Luis García<sup>6</sup>, Alessa Geiger<sup>6</sup>, Neil F. Glasser<sup>7</sup>, Delia M. Gheorghiu<sup>5</sup>, Stephan Harrison<sup>8</sup>, Andrew S. Hein<sup>9</sup>, Michael R. Kaplan<sup>10</sup>, Julian R.V. Martin<sup>1</sup>, Monika Mendelova<sup>9</sup>, Adrian Palmer<sup>1</sup>, Mauri Peltó<sup>11</sup>, Ángel Rodés<sup>5</sup>, Esteban A. Sagredo<sup>6,12,13,14</sup>, Rachel Smedley<sup>15</sup>, John L. Smellie<sup>16</sup>, Varyl R. Thorndycraft<sup>1</sup>.

\*Corresponding author: Bethan.davies@rhul.ac.uk

<sup>1</sup>Centre for Quaternary Research, Department of Geography, Royal Holloway University of London, Egham Hill, Egham, Surrey, TW20 0EX, UK

<sup>2</sup>Department of Geography, The University of Manchester, Oxford Road, Manchester M13 9PL, UK

<sup>3</sup>School of the Environment, Geography and Geosciences, University of Portsmouth, Buckingham Building, Lion Terrace, Portsmouth PO1 3HE, UK

<sup>4</sup>Scott Polar Research Institute, University of Cambridge, Cambridge CB2 1ER, UK

<sup>5</sup>Scottish Universities Environmental Research Centre (SUERC), Rankine Avenue, East Kilbride G75 0QF, UK

<sup>6</sup>Instituto de Geografía, Facultad de Historia, Geografía y Ciencia Política, Pontificia Universidad Católica de Chile, Avenida Vicuña Mackenna 4860, Macul, Santiago 782-0436, Chile

<sup>7</sup>Faculty of Earth and Life Sciences, Prifysgol Aberystwyth University, Campws Penglais / Penglais Campus, Aberystwyth, Ceredigion, SY23 3DB, UK

<sup>8</sup>College of Life and Environmental Sciences, University of Exeter, Cornwall Campus, Penryn, TR10 9EZ, UK

<sup>9</sup>School of GeoSciences, University of Edinburgh, Drummond Street, Edinburgh EH8 9XP, UK

<sup>10</sup>Lamont-Doherty Earth Observatory of Columbia University, Palisades, NY, 10964, USA

<sup>11</sup>Nichols College, 121 Centre Road, PO Box 5000, Dudley MA 01571, USA

<sup>12</sup>Millenium Nuclei Palaeoclimate, ANID Millennium Science Initiative. Santiago, Chile

<sup>13</sup>Estación Patagonia de Investigaciones Interdisciplinarias UC. Pontificia Universidad Católica de Chile.

<sup>14</sup>OHM-I, LabEx DRIIHM. Programme "investissements d'avenir": ANR-11-LABX-0010), INEE-CNRS, Paris, France



<sup>15</sup>School of Geography and Planning, University of Liverpool, Liverpool L69 7ZT, UK

<sup>16</sup>School of Geography, Geology and the Environment, University of Leicester, University Road, Leicester LE1 7RH, UK

## Key words:

Patagonia, ice sheet, geochronology, Quaternary, glaciation, geomorphology

## Abbreviations

- GIS Geographical Information System
- LGM Last Glacial Maximum
- LLGM Local Last Glacial Maximum
- PIS Patagonian Ice Sheet
- ACR Antarctic Cold Reversal
- Lago GCBA Lago General Carrera/Buenos Aires
- Lago CP Lago Cochrane/Pueyrredón
- UE/BV Última Esperanza/Bella Vista - Río Gallegos Lobe
- SWW Southern Westerly Winds
- m asl metres above sea level
- ka thousands of years ago
- cal. ka BP calibrated thousand years ago
- Gt Gigatonnes
- DEM Digital Elevation Model
- MIS Marine Isotope Stage
- SLE Sea Level Equivalent
- ACC Antarctic Circumpolar Current
- SAM Southern Annular Mode
- MSL Monte San Lorenzo
- OSL Optically stimulated luminescence
- SD Standard deviation
- $\mu$  Mean

## Abstract

We present PATICE, a GIS database of Patagonian glacial geomorphology and recalibrated chronological data. PATICE includes 58,823 landforms and 1,669 geochronological ages, and extends from 38°S to 55°S in southern South America. We use these data to generate new empirical reconstructions of the Patagonian Ice Sheet (PIS) and subsequent ice masses and ice-dammed palaeolakes at 35 ka, 30 ka, 25 ka, 20 ka, 15 ka, 13 ka (synchronous with the Antarctic Cold Reversal), 10 ka, 5 ka, 0.2 ka and 2011 AD. At 35 ka, the PIS covered of  $492.6 \times 10^3 \text{ km}^2$ , had a sea level equivalent of  $\sim 1,496 \text{ mm}$ , was 350 km wide and 2090 km long, and was grounded on the Pacific continental shelf edge. Outlet glacier lobes remained topographically confined and the largest generated the suites of subglacial streamlined bedforms characteristic of ice streams. The PIS reached its maximum extent by 33 – 28 ka from 38°S to 48°S, and earlier, around 47 ka from 48°S southwards. Net retreat from maximum positions began by 25 ka, with ice marginal stabilisation then at 21 – 18 ka, which was then followed by rapid irreversible deglaciation. By 15 ka, the PIS had separated into disparate ice masses, draining into large ice-dammed lakes along the eastern margin, which strongly influenced rates of recession. Glacial readvances or stabilisations occurred at least at 14 – 13 ka, 11 ka, 6 – 5 ka, 2 – 1 ka, and 0.5 – 0.2 ka. We suggest that 20<sup>th</sup> century glacial recession ( $\% \text{ a}^{-1}$ ) is occurring faster than at any time documented during the Holocene.

## 1 Introduction

Glacier recession is accelerating in Patagonia (Aniya, 1999; Davies and Glasser, 2012; Meier et al., 2018; Braun et al., 2019), causing sea level rise (Gardner et al., 2013; Malz et al., 2018), enlarging glacial lakes and increasing flood risk (Loriaux and Cassassa, 2013; Wilson et al., 2018), and affecting water availability and hydropower opportunities (Huss and Hock, 2018; Milner et al., 2017). The Southern Andes region had a mass loss of 1,208 Gt from 1961 to 2016, and is the largest contributor to global sea level rise outside of Greenland and Alaska (Zemp et al., 2019). This mass loss from global glaciers provides a global contribution of  $0.92 \pm 0.39 \text{ mm a}^{-1}$  to global sea-level rise (totalling  $27 \pm 22 \text{ mm}$  from 1961 – 2016), accounting for 25 – 30% of total observed sea level rise; this is equivalent to mass loss from the Greenland Ice Sheet and exceeds loss from Antarctica (Zemp et al., 2019). In order to understand how future climate change will influence the world's glaciers, and how this will affect societies, it is imperative to model future climate, glacier response and hydrology. Detailed analyses of past glacier-climate interactions can be used to constrain and test numerical models and to untangle externally driven changes versus internally forced changes (e.g. climate compared with calving, ice divide change and topography).

During past glacial periods, the Patagonian Ice Sheet (PIS) was centred on the central chain of the Andes, stretched from  $\sim 38^\circ\text{S}$  to  $55^\circ\text{S}$ , consisted of terrestrial lobes that retreated into large palaeolakes on the east,

and is inferred to have reached the continental shelf on the west coast. The past behaviour of the PIS during different climate states and during rapid climatic transitions could shed insights into the ways in which the region is sensitive to changes and could respond to future climate change. Reconstruction of the evolution of the former PIS provides a unique insight into past terrestrial cryospheric and climatic change in the southern mid-latitudes, a particularly data-sparse area of the globe, and forms an important proxy for changes in circum-hemispheric atmospheric and oceanic systems during global deglaciation (Harrison and Glasser, 2011; Kilian and Lamy, 2012). Improved understanding of the ice-ocean-atmosphere dynamics across the large latitudinal expanse of Patagonia also has the potential to yield insights into the past north/south contraction and expansion of the Southern Westerly Winds (SWW) during key palaeoclimatic transitions (Kohfeld et al., 2013; Sime et al., 2013). The SWW are one of the most important climatic controls of the Patagonian Andes and are responsible for driving major changes in ocean currents, resulting in cryospheric change in West Antarctica (Rignot et al., 2019). However, large uncertainties in the long-term dynamics of the SWW make it challenging to contextualise recent change in this atmospheric circulation system.

Data-calibrated numerical models provide insights into ice sheet and glacier response to periods of rapid climate change (e.g. Briggs et al., 2014; Ely et al., 2019; Golledge et al., 2014; Patton et al., 2017; Stokes et al., 2015; Tarasov et al., 2012). Well-constrained numerical models are used to test hypotheses regarding ice-sheet behaviour under different climatic regimes (e.g. Golledge et al., 2012, 2014; Hulton et al., 2002; Patton et al., 2016, 2017; Stokes and Tarasov, 2010), allowing insights into likely future glacier behaviour. They also yield insights into the mechanisms and climatic controls forcing palaeo ice sheets (e.g. Hubbard et al., 2005), and assist in assessments of the vulnerability of ice masses to future climatic change. Data-calibrated numerical model simulations are reliant on high quality empirical data of glacier fluctuations with well-understood and quantified uncertainties. Improved, open source, ice sheet models such as PISM (Winkelmann et al., 2011), BISICLES (Martin et al., 2013) and GLIMMER (Rutt et al., 2009) now make it possible to simulate PIS evolution from the Last Glacial Maximum (LGM) to present. However, such models clearly require a robust geological framework (including accurate inferences of the direction of ice flow, timing of ice-free conditions, ice-marginal locations, extent and thickness, with an evaluation of uncertainty, at different times), against which they can be calibrated (cf. Ely et al., 2019; Hughes et al., 2016).

There is a large volume of ages and geomorphology constraining past ice sheet extent and dynamics across Patagonia. The first quantified reconstructions of the evolution of the PIS with chronological constraints relied on radiocarbon dating (Mercer, 1968; Mercer, 1970; Porter, 1981). Chronologies of pre-LGM ice extent used  $^{40}\text{Ar}/^{39}\text{Ar}$  (and K-Ar) dating of interbedded moraines and volcanic sequences (e.g. Singer et al., 2004a, b; Clague et al. 2020). Glacier recession over the last few centuries has been mapped using lichenometry (Winchester and Harrison, 2000; Garibotti and Villalba, 2017), dendrochronology (e.g.

Winchester et al., 2014), and historical documents dating from the exploration era (e.g. Casassa et al., 1997). Note that since there is debate about whether the “Little Ice Age” is a global event, in this article we use the term “Late Holocene” for the most recent glacier expansion, dating from 0.5 – 0.2 ka BP. More recently, the application of innovative forms of cosmogenic nuclide exposure-age dating (Ackert et al., 2008; Douglass et al., 2006; García et al., 2012; Hein et al., 2011; Kaplan et al., 2005, 2011; Cogeze et al., 2018), cosmogenic nuclide depth profiles (Darvill et al., 2015b; Hein et al., 2009), optically stimulated luminescence dating (Blomdin et al., 2012; Smedley et al., 2016; Garcia et al., 2019), tephrochronology (Kilian et al., 2003; Stern, 2008; Stern et al., 2016; Weller et al., 2015) and varve-age dating (Bendle et al., 2017a, 2019) has resulted in new insights into the timing and dynamics of both ice-sheet behaviour and palaeolake development.

However, age calculation techniques differ between studies, at times using different erosion corrections (often untested), outlier-removal strategies, marine reservoir effects for radiocarbon dating, and different calibration curves. Further, the calibration of radiocarbon dating (Hogg et al., 2013; Ortlieb et al., 2011; Stuiver et al., 2009) and cosmogenic nuclide dating (Borchers et al., 2016; Kaplan et al., 2011; Lal, 1991; Stone, 2000) has improved over time, making inter-study comparisons difficult given the varying times at which data were gathered and published. Moreover, research has long highlighted the importance of ice-dammed proglacial palaeolake development in eastern Patagonia during deglaciation (e.g., Bell, 2009; Bendle et al., 2017b; Caldenius, 1932; García et al., 2014; Thorndycraft et al., 2019a; Turner et al., 2005), but these have not been included in previous ice sheet reconstructions.

While geomorphological data has been compiled previously (Glasser et al., 2008), a geomorphological and chronological database of palaeolake development throughout southern South America has not been attempted. To date, no attempt has been made to gather these numerous geochronological ages and geomorphological data from across Patagonia into a single database, recalibrate ages using the latest protocols, and assess their reliability. Although LGM ice extent has previously been reconstructed (e.g. Caldenius, 1932; Coronato and Labassa, 2011), no attempt has been made to calculate ice volume from empirical data, assess confidence in ice-marginal positions, or reconstruct the entire ice sheet and its changing palaeolakes through time. This is required as a first step to improving data-calibrated numerical modelling of the PIS.

Here, we present an original, pan-ice sheet, empirical reconstruction (PATICE) of the PIS (38°S to 56°S) from 35 ka to 2011 AD (0 ka) in 5000 year increments, with additional reconstructions at periods of significant ice-margin stabilisation (13 ka, coeval with the ACR, and during the Late Holocene, 0.2 ka). We do not include pre-35 ka glacial fluctuations of the PIS due to a lack of data across the study area, but note that there is evidence of extensive ice prior to 35 ka in southern Patagonia (cf. Garcia et al., 2018; Darvill et al., 2015). We use volume-area scaling to provide a new estimate of ice volume for each time slice. Our reconstruction

compiles existing geomorphological and chronological data, which have been robustly standardised, together with an assessment of the reliability of each age. Our new PATICE database includes 58,823 landforms, 1,669 geochronological ages that constrain ice-free conditions (all recalibrated according to the latest protocols), and spans the breadth of the published literature from 38°S to 56°S centred around the Andes in southernmost South America. It is the first large-scale synthesis to integrate both the terrestrial and offshore geomorphology and chronology. We generate an assessment of confidence (low, medium and high) for each reconstructed ice margin, based on multiple lines of geomorphological and chronological evidence. We interrogate and reveal spatial and temporal variability in ice-mass change over the last 35,000 years, made manifest in terrain and landform evolution. In doing so, we present a novel reconstruction from maximum glaciation, to the present small glaciers, ice caps and ice fields incorporating palaeolake evolution and drainage. In our synthesis (Section 6), we compare our new empirical LGM and post-LGM reconstructions directly with published empirical reconstructions (Caiuleni, 1932; Clapperton 1993; Coronato and Rabassa, 2011) and modelled reconstructions (e.g. Hubbard et al., 2005; Hulton et al., 2002). Our reconstruction yields important insights into rates of change for the PIS during deglaciation, emphasises where ice margins are well constrained or poorly constrained and highlights priorities for future work, and presents a framework that can be used to tune and test future ice-sheet models.

In this paper, Section 2 outlines and describes the study area (geology, topography, present-day climate and proxy records of palaeoclimate). Section 3 summarises the geomorphological and chronological methods used, with more information provided in the Supplementary Methods. Section 4 presents a new analysis of the four key glacial land systems in Patagonia: upland land-terminating glacier, lowland land-terminating glacier, glaciolacustrine and glaciomarine. Section 5 presents the new PATICE reconstruction for the six sectors of the study area: the Chilean Lake District (38°S – 42°S), Isla de Chiloe and Archipiélago de los Chonos and the adjacent mainland (42°S – 46°S), the Northern Patagonian Icefield (46°S to 48°S), the Southern Patagonian Icefield (48°S – 52°S), Gran Campo Nevado (52°S – 53°S), and Cordillera Darwin (53°S – 56°S). Section 6 synthesises these data, examines the timing and characteristics of the key advances, and highlights latitudinal variations in glaciation. We compare our empirical reconstruction to published numerically modelled reconstructions. We also highlight rates of ice and palaeolake area and volume change, and identify key research questions and gaps in knowledge.

## 2 Study area

### 2.1 Geological setting

Topography and geology are key influencers of Quaternary and recent glaciation. Patagonia is located at the junction of four key continental plates; the Nazca, Antarctic, South American and Scotia plates (Figure 1). North of the Chile Triple Junction, the Nazca Plate is subducting beneath the South American plate in a north-easterly direction at 66 mm/yr (Rosenau et al., 2006). South of the Triple Junction, the Antarctic Plate has been subducted at a rate of about 20 mm/yr. Patagonia is bounded to the north by the Gastre Fault System, a major dextral shear zone and geological boundary with perhaps 500 km of lateral displacement. The Gastre Fault System is a fundamental crustal structure, regarded as an intraplate boundary that divides thick cratonic crust to the north from thinner continental crust beneath southern Patagonia, and it marks the northern limit of the Mesozoic-Cenozoic Patagonian Batholith, an important part of one of the largest Cordilleran batholiths on Earth (Rapela and Pankhurst, 1992).

The western edge of Patagonia contains outcrops of low-grade metasedimentary rocks and glaucophane-bearing metabasites (Figure 1). Together, they form a metamorphic complex interpreted as a Late Palaeozoic accretionary prism that was subsequently intruded by the Patagonian batholith (Hervé et al., 2003). The batholith forms a prominent north—south-trending zone about 100 km wide that is dominated by evolved I-type granitoids (mainly tonalities, granodiorites and granites) and associated widespread coeval volcanism, with an age range of Jurassic to Neogene (c. 120 – 15 Ma; Hervé et al., 2007; Rapela et al., 2005). Pliocene and younger products of the magmatic arc are represented by calc-alkaline volcanism that occupies a linear zone on the same axis as the batholith. About 60 volcanic centres are recognised, including 40 of Holocene age. In southern Chile and Tierra del Fuego, back-arc basin strata called the Rocas Verdes were created during Late Jurassic extension (Dainiel et al., 1974; Fildani and Hessler, 2005), together with voluminous bimodal, mainly felsic volcanism that forms a large igneous province (Chon Aike Province). In the north of the study region, these volcanoes provide a local nucleus for glacierisation (Braun et al., 2019; Reindthaler et al., 2019).

Finally, extensive outcrops of Eocene and Plio-Pleistocene alkaline back-arc flood basalts are also present in the east and have been related to the passage of windows in the oceanic slab subducted under the Andean arc (Forsyth and Prior, 1992). This past volcanism has aided the dating of Cenozoic glaciation (Singer et al., 2004a).

*Figure 1. Geology of the study region, after Schenk et al. (1997). Plate boundaries from Bird (2003). Gastre Fault and Cenozoic fold-and-thrust belt from Rosenau et al. (2006). Inset shows wider arrangement of plate boundaries.*

## 2.2 Topography

The Andes stretch for 7,000 km along the west coast of South America, and form a major barrier to the prevailing Southern Westerly Winds (Ackert et al., 2008). Patagonia incorporates part of this mountain range and extends from about 38°S to the southern tip of the continent at 56°S. Mountain summits reach 4,000 m high, decreasing to 1,500 – 2,000 m in the south of the study region (Figure 2).

East of the Andes, Argentine Patagonia and Tierra del Fuego feature low lying (100–200 m asl) steppe-like plains extending for hundreds of kilometres to the Atlantic Ocean (Gareau et al., 2013). The wide continental shelf mostly less than 150 m deep on the eastern Atlantic margin extends hundreds of kilometres offshore (Ponce et al., 2011) (Figure 2, Figure 3). Iceberg ploughmarks are present on the sea floor as far north as 45°S, but these are mainly derived from the full-glacial Antarctic Ice Sheet (López-Martínez et al., 2011). Over-deepened basins east of the Andes are occupied by large proglacial lakes.

The continental shelf on the western, Pacific, margin of Patagonia is located close (tens of kilometres) to the present-day coast. The western Patagonian coastline comprises many channels, islands and fjords, carved out by repeated Cenozoic glaciations. The western coastline receives freshwater from direct precipitation, surface runoff, groundwater and major rivers draining the Patagonian icefields, such as the Baker, Pascua and Bravo rivers. The fjords typically have an estuarine circulation, with rivers discharging at their upstream end to build sedimentary deltas. These fjords have irregular and sometimes over-deepened seafloor topography and sills relating to their excavation by glaciers during full-glacial periods (Syvitski et al., 1987). They are infilled by tens of metres of Holocene fine-grained, laminated sediments (DaSilva et al., 1997; Dowdeswell et al., 2016b, 2016c; Bertrand et al., 2017).

## 2.3 Glaciers and Icefields

Today, the Patagonian Andes support four main icefields: the Northern Patagonian Icefield at 46.4°S to 47.5°S, the Southern Patagonian Icefield at 48.3°S to 52°S, the Gran Campo Nevado at 52.8°S, and the Cordillera Darwin icefield at 54.5°S. The region also hosts numerous small icefields and mountain glaciers, often centred on volcanoes, and the lowest Southern Hemisphere latitude at which glaciers reach the sea today are found in the Chilean fjords at 47°S in the Northern Patagonian Icefield (Dowdeswell and Vásquez, 2013).

In total, present-day icefields and glaciers comprise around 617 glaciers amounting to a total area of 22,718 km<sup>2</sup> in 2011 (Davies and Glasser, 2012) (Figure 2). This equates to a total volume of  $5,955 \pm 1,191$  km<sup>3</sup> ( $5,458 \pm 1,092$  Gt) of ice or  $15.1 \pm 3.0$  mm of sea level equivalent (Carrivick et al., 2016). The region has a specific annual mass change of  $-1.18 \pm 0.38$  m w.e. a<sup>-1</sup>, or  $-34 \pm 11$  Gt a<sup>-1</sup> (2006 to 2016) (Zemp et al., 2019).

During glacial maxima, the icefields coalesced to form a single large ice mass extending westwards to the continental shelf edge and eastwards into steppe-like plains (Caldenius, 1932; Clapperton and Clapperton, 1993; Coronato and Rabassa, 2011; Glasser and Jansson, 2008; Glasser et al., 2011b; Glasser et al., 2008; Hein et al., 2010; McCulloch et al., 2000; Mercer, 1968, 1976). During ice recession, a series of large proglacial lakes formed along the eastern ice margin, dammed between the ice sheet and higher ground or moraines (Bourgois et al., 2016; Caldenius, 1932; Glasser et al., 2016b; García et al., 2014; Lovell et al., 2012; Martinod et al., 2016; McCulloch and Bentley, 1998; Sagredo et al., 2011; Thorndycraft et al., 2019a; Turner et al., 2005). On the eastern side of the Andes, terminal moraines from these maxima often form the present-day continental watershed divide, following lake drainage events causing Atlantic to Pacific drainage reversals and underfit valleys in the sectors 42 – 49°S and 51 – 53°S (Thorndycraft et al., 2019a). Some of these palaeolakes, such as Pico (Caldenius, 1932) and Cienas (García et al., 2019) drained completely, while others dropped to their current level, dammed by sills at their outflows.

*Figure 2. Study area, the Patagonian Icefields and key placenames mentioned in text. Mapped glaciers are shown (from Davies and Glasser, 2012, part of the Randolph Glacier Inventory) overlain on a GEBCO GDEM. Bathymetry shows location of the continental shelf. Inset shows location of Patagonia within South America. Location of marine cores mentioned in the text are shown. The Chilean Lake District, Isla de Chiloé, Archipiélago de los Chonos, Northern Patagonian Icefield, Southern Patagonian Icefield, Gran Campo Nevado and Cordillera Darwin are highlighted*

## 2.4 Present-day climate and oceanography

The modern climate of southern South America has been thoroughly reviewed by Aravena and Luckman (2009) and Garreaud et al. (2013, 2009). South of 40°S, the climate regime is temperate owing to its location between the Sub-Tropical and Sub-Antarctic Fronts (Kohfeld et al., 2013) and the strong influence of the circumpolar Southern Westerly Winds (SWW) (Figure 3). The SWW bring precipitation to Patagonia from the Pacific Ocean. Western Patagonia has annual mean precipitation in the region of 5,000 to 10,000 mm per year (Garreaud et al., 2013; Lenaerts et al., 2014) (Figure 3B). Rainfall decreases rapidly eastwards, resulting in a significant rain shadow east of the Andes (Aravena and Luckman, 2009). Eastern Patagonia tends to have a continental climate dominated by the SWW, with highly evaporative conditions at the surface (Garreaud et al., 2013). Increases in the strength of the SWW will result in a decreased amplitude of the local temperature



annual cycle (Garreaud et al., 2013). These climatic gradients lead to strong westwards and southwards variations in the vegetation communities in Patagonia (Montade et al., 2019), and have likely played a role in controlling past glaciation.

In the southernmost parts of Patagonia this precipitation is evenly distributed throughout the year, but to the north, around Puerto Montt (Figure 2), it falls mostly during the austral winter (Aravena and Luckman, 2009; Rodbell et al., 2009). West of the Andes, seasons with stronger SWW augment precipitation, but east of the Andes, increases in the SWW decrease local precipitation. Thus, SWW strength and precipitation are generally anti-correlated between the west and east sides of the Andes. This includes a possible weakening of the orographic effect; studies have also recently highlighted that for southern Patagonia, when the SWW are relatively weak, easterly-derived moisture can be important on the Atlantic side of the continent (e.g., Mayr et al., 2007; Quade and Kaplan, 2017). For example, high lake levels east of the Andes (e.g. at around 10 ka at Lago Cardiel), may be associated with reduced glacier extent. Such periods, with increased easterly moisture delivery, may include the warmer periods of the Holocene, perhaps due to intensity or displacement of the westerlies far to the south.

Over decadal timescales, large-scale climate cycles such as the El Niño Southern Oscillation (ENSO) influence Patagonian climate variability, largely through atmospheric teleconnections that modulate westerly airflow and thus regional heat and moisture distribution (Aravena and Luckman, 2009; Garreaud et al., 2009). Between 45°S and 55°S, strongly positive El Niño years result in approximately 15% less precipitation as a result of a decreased strength in the SWW (Schneider and Gies, 2004).

Other large-scale climatic oscillations include the Southern Annular Mode (SAM; also known as the Antarctic Oscillation). During SAM positive phases, there is a poleward expansion of the band of stronger westerlies, affecting the Antarctic periphery, while the winds weaken between ~40 – 50°S (Moreno et al., 2018). In Patagonia, cold and wet conditions are associated with negative SAM modes; conversely, warm and dry conditions are associated with positive SAM modes (Quade and Kaplan, 2017; Moreno et al., 2018). Quade and Kaplan (2017) suggested that dominantly positive or negative SAM-like conditions can persist for centuries, influencing ecologic and glacier systems. The most recent cold/wet negative SAM interval was contemporaneous with the European “Little Ice Age” (Moreno et al., 2018), which suggests that interhemispheric correlation of centennial-scale events over the last millennium was apparently mediated through changes in the position and intensity of the SWW (*ibid.*).

Wind stress from the SWW (Figure 3D) drives the Antarctic Circumpolar Current (ACC) through the deep-water Drake Passage, the channel between Patagonia and Antarctica, exerting control on physical, chemical, and biological exchanges between the Pacific and Atlantic Oceans (Toggweiler, 2009) (Figure 2), and

dominating ocean surface circulation around Patagonia. The ACC brings cold, Subantarctic water to the Pacific coast (Kaiser et al., 2007). Around 43°S, this splits into the southward-flowing Cape Horn Current and the equator-ward flowing Peru-Chile Current (Figure 2). Low-salinity Chilean Fjord water, fed by freshwater input from glaciers, flows northward within 150 – 200 km of the coast (Kaiser et al., 2007). Sea surface temperatures at 47°S are 10°C, decreasing to 7°C at 55°S (*ibid.*), meaning that the fjords of Patagonia are a relatively mild environment with abundant freshwater delivered by glaciers and icefields (Dowdeswell et al., 2016a).

*Figure 3. A. Mean annual air temperature (°C) (1970 – 2000) at 30 Arc Seconds resolution, from the WorldClim2 dataset (Fick and Hijmans, 2017). B. Mean annual precipitation (mm) (1970 – 2000) at 30 Arc Seconds resolution, from the WorldClim2 dataset. C. Mean annual air wind speed ( $\text{m s}^{-1}$ ) (1970 – 2000) at 30 Arc Seconds resolution, from the WorldClim2 dataset. Location of the northerly limit of the mean present-day SWW and Subtropical Front after Kohlfeld et al. (2013). D. Approximate distribution of the SWW and oceanic polar fronts that control Patagonia's climate. The westerlies bring rain and snowfall to the west coast of Patagonia. The Subtropical Front (STF) sits at the northern limit of the westerly wind belt.*

## 2.5 Proxy records of Patagonian palaeoclimate

### 2.5.1 The Last Glacial Maximum

Variations in the position and strength of the SWW were a key control on palaeoclimate in Patagonia through glacial-interglacial cycles. During glacial cycles, a reduction in the strength of the ACC through the Drake Passage (Figure 3D) has been linked to a northward shift in the SWW (Lamy et al., 2015). This was associated with a decrease in strength of the SWW over their present core zone in the northern Drake Passage during colder intervals (Lamy et al., 2010, 2015). At the same time, stronger SWW extended northwards, bringing enhanced precipitation to the PIS. While the relationship between wind strength, precipitation and temperature is well understood, the relative importance of this for glacier mass balance is poorly constrained empirically.

Continuous palaeoclimate records reaching back to the full glacial period are not common in Patagonia. Kilian and Lamy (2012) provide a review of the existing records, which are summarised briefly here to contextualise the glacial fluctuations analysed in this study. In the northerly parts of the study area, Heusser et al. (1999) record progressive cooling during Marine Isotope Stage (MIS) 3 from 47  $^{14}\text{C}$  ka BP on Isla Grande de Chiloé, where Subantarctic Evergreen Forest was replaced with parkland. In the lowlands of the Chilean Lake District (41°S), palynological records suggest colder conditions between 24.0 and 23.4 cal. ka BP, with a slight warming from 23.4 to 22.6 cal. ka BP (Moreno et al., 2015). Cooler conditions and a depression in the regional treeline returned from 22.6 to 21.8 cal. ka BP. Warming conditions then occurred until 19.3 cal. ka

BP, resulting in a rising treeline and an increase in arboreal abundance (Moreno et al., 2015). Abrupt cooling with hyperhumid conditions occurred from 19.3 to 17.8 cal. ka BP, with a decrease in arboreal pollen.

Moreno et al. (2015) interpret this to reflect a stronger influence of the SWW at this time, with extreme glacial conditions. The last glacial termination in the Chilean Lake District began at ~17.7 cal. ka BP, with a relatively rapid warming pulse and establishment of *Northofagus*, with drier and warmer conditions.

Further south, palynological records from marine core MD07-3088 at 46°S (Figure 2) indicate lower precipitation than the present-day prior to 18 cal. ka BP (Montade et al., 2019), and cooler mean winter temperatures (*ca* 3°C). However, low pollen counts due to reduced vegetation during the glacial period mean that these interpretations must be treated cautiously.

Marine sediment core MD07-3128 (53°S, off the Pacific entrance of the Strait of Magellan; Figure 2) dates back to 60 ka (Caniupán et al., 2011). The core indicates that sea surface temperatures were ~8°C lower during full glacial periods, with millennial-scale fluctuations (Kilian and Lamy, 2012). This strong cooling suggests a substantial northward expansion of polar water masses and the Southern Ocean fronts, with the Sub-Antarctic front likely close to this site. The coldest sea surface temperatures were recorded at ~19 ka, which has been related to an increase in cold melt water from the PIS. This core also shows pronounced pulses of iceberg-rafted debris between 30 and 13 ka BP, associated with fluctuations of the nearby ice sheet.

Laguna Potrok Aike in the Province of Santa Cruz, Southern Patagonia (51° 57' 47"S, 70° 22' 46"W; Figure 2), provides a unique continuous palaeoclimate record through the last glacial cycle (Recasens et al., 2012). Palynological records from this maar lake suggest cooler and drier conditions during glacial periods. The Lateglacial and Holocene record is characterised by warming and wetter conditions, with increased primary production.

### 2.5.2 The Late Glacial period

The late glacial palaeoclimate of Patagonia (*ca* 15 to 11.5 ka) has been reconstructed using numerous proxy records, mostly located east of the ice fields (Kilian and Lamy, 2012). Several studies have compiled such records to infer broad changes in atmospheric circulation (Björck et al., 2012; Fletcher and Moreno, 2012; Iglesias et al., 2016; Kilian and Lamy, 2012; Lamy et al., 2010; Mancini et al., 2005; Montade et al., 2019; Moreno et al., 2015). In general, deglaciation began after 18 ka (Bendle et al., 2017a, 2019), during a period of warmer conditions (Kilian and Lamy, 2012).

In the northern part of the study area, the Chilean Lake District (41°S; Figure 2), pollen records reflect long term cool and wet conditions between 16 and 11 cal. ka BP, with enhanced variability in the late glacial

(Moreno, 2004; Moreno and Videla, 2016). Particular cold periods have been identified during the Antarctic Cold Reversal (ACR), Younger Dryas, and Huelmo–Mascardi Cold Reversal (a cool episode between 11,400 and 10,200  $^{14}\text{C}$  yr BP, or 13.2 to 11.8 cal. ka BP) (Hajdas et al., 2003; Massafiero et al., 2014; Moreno and Videla, 2016). A marine core (MD07-3088; Figure 2) taken off the Taitao Peninsula at 46°S records the development of North Patagonian Rainforest following the last deglaciation, with expansion of Magellanic Moorland, associated with cooler temperatures and increased precipitation, during the ACR (Montade et al., 2013, 2019). This agrees with proxy oceanic data, which record cooling in the South Atlantic and all regions south of 40°S (Pedro et al., 2016). Increases in the strength of the SWW are suggested by elevated dust deposition in Tierra del Fuego during the ACR (Vanneste et al., 2015), associated with a glacial readvance.

South of the Chilean Lake District at 44°S, the isotopic and pollen records from Lago Nos Niños and Laguna La Pava indicate low but variable moisture levels over the same time (Iglesias et al., 2016), suggesting a cold climate characterised by increased precipitation with major wet periods between 13.4 and 11.8 cal. ka BP (Villa-Martínez et al., 2012). South of the Southern Patagonian Ice field from Laguna Potrol Aike (51°S; Figure 2), palynological records and transfer functions are interpreted to indicate a relatively dry late glacial period (Schäbitz et al., 2013), with precipitation increasing into the Holocene (Tonello et al., 2009). Weaker westerlies in the early Holocene may have allowed increased precipitation east of the Andes, with increased easterly derived moisture. Late-Glacial temperatures were broadly warm, but with a colder period coeval with the ACR in Fuego-Patagonia (53°S) (Mansilla et al., 2016), as at sites to the north. In Torres del Paine (50°S), glacial readvance occurred during a cold episode from 14.8 to 12.6 ka (Moreno et al., 2009, García et al. 2012), with warming occurring after 11.5 ka.

Due to a strong relationship between westerly airflow and precipitation in southern South America (Garreaud, 2007), precipitation proxies have been used to infer the timing and nature of past latitudinal shifts and expansion and contraction of the SWW belt. As with temperature and precipitation reconstructions, there are discrepancies between studies (see e.g. Kilian and Lamy, 2012), but some broad patterns emerge between proxies and sites. During the late glacial, SWW strength was generally low, but increased during the ACR and Younger Dryas, perhaps as the core of the SWW also migrated northwards (Fletcher and Moreno, 2012; Mayr et al., 2013; Montade et al., 2019; Moreno and Videla, 2016; Oehlerich et al., 2015; Vanneste et al., 2015). A lake sediment record from Lago Pichilaguna (51°S) in the Chilean Lake District indicates strong westerlies during the ACR, favourable for glacier growth, followed by anomalously low intensity during the Early Holocene (Moreno et al., 2018).

### 2.5.3 *The Holocene*

Multiple proxy records from the Chilean Lake District (41°S) to southern Patagonia (52°S) indicate that the Holocene began with an extended warm and dry period (Caniupán et al., 2011; Iglesias et al., 2016; Mansilla et al., 2016; Moreno et al., 2018; Moreno and Videla, 2016; Siani et al., 2010; Villa-Martínez et al., 2012). Although, as mentioned above, the east side of the continent may have experienced slightly higher precipitation during this time due to weakening of the westerlies (e.g., Quade and Kaplan, 2017). The mid-Holocene was characterised on both sides of the Andes at several sites from 41°S to 47°S by cooler and wetter periods with reduced fire activity (Iglesias et al., 2016; Moreno, 2004; Moreno and Videla, 2016; Villa-Martínez et al., 2012). In contrast to farther north, southern Patagonian (52°S) pollen, charcoal and lake level records provide evidence for a dry period at some point in the mid-Holocene (Kilian and Lamy, 2012; Schäbitz et al., 2013; Mansilla et al., 2016), although this is not replicated everywhere (Tonello et al., 2009). The late Holocene was generally characterised by centennial switches between cold-wet and warm-dry conditions from 41°S to 52°S (Álvarez et al., 2015; Elbert et al., 2013; Haberzettl et al., 2009; Moreno and Videla, 2016; Schäbitz et al., 2013; Tonello et al., 2009; Moreno et al., 2018).

The strength of the SWW generally decreased into the early Holocene before increasing during the middle Holocene, coinciding with the onset of Holocene neoglaciations (Porter, 2000; Moreno et al., 2018). An increase in wind strength in central Patagonia (45°S) supports the hypothesis that the wind belt broadened during the early and mid-Holocene (Van Daele et al., 2016). In the late Holocene, wind intensity reduced towards conditions similar to present (Lamy et al., 2010; Oehlerich et al., 2015). Sites to the west of the Andes suggest an anti-phasing between the winds' core and northern margin during the Holocene, with a stronger core and weaker northern margin during the early Holocene and the opposite occurring in the late-Holocene (Lamy et al., 2010). During the Holocene, nine positive SAM events occurred at a centennial scale since 5.8 ka, that alternate with cold and wet intervals, favourable for glacier growth (Moreno et al., 2018).

## 3 Methods: PATICE database and ice-sheet reconstruction

### 3.1 *Geomorphological mapping*

Our overall methodology is shown in Figure 4. The geomorphological data in this reconstruction provide detailed information on former ice sheet margins, ice-dammed palaeolake evolution, and ice-flow direction. Mapping of moraines underpins the empirical reconstruction, providing information on the shape and position of the ice margin, and the pattern of retreat (cf. Ely et al., 2019). In Patagonia, the pioneering work of Caldenius (1932), Mercer (1965, 1968, 1970, 1976), Denton et al. (1999), Andersen et al. (1999), McCulloch and Bentley (1998) and McCulloch et al. (2005b) laid the foundations for subsequent compilation and mapping of glacial geomorphology by Glasser and Jansson (2008). Our compilation builds on the Glasser

and Jansson (2008) “Glacial Map of South America” with updates from around the former PIS (e.g., Ackert et al., 2008; Bendle et al., 2017b; Coronato et al., 2009; Darvill et al., 2014, 2015a; De Muro et al., 2018; García 2012, García et al., 2014; Izagirre et al., 2018; Lovell et al., 2011, 2012; Waldmann et al., 2010, Davies et al., 2018; Thorndycraft et al., 2019b) and original mapping by the authors of this study of key landforms in data-sparse regions.

At the scale of the PIS, glacial landforms were mapped from remotely sensed images, particularly satellite imagery (for details on overall methods, see: Boulton and Clark, 1990; Chandler et al., 2018; Clark, 1997; Clark et al., 2012, 2018; Glasser and Jansson, 2008; Jansson and Glasser, 2005). The most commonly used sensors in previous mapping efforts in Patagonia are Landsat 8 OLI and Landsat 7 ETM+ scenes (30 m resolution, 15 m when pan-sharpened), and ASTER (15 m spatial resolution) satellite images, as well as the higher resolution Digital Globe images now widely available in Google Earth Pro and ESRI ArcGIS. Satellite images are commonly overlaid on a Digital Elevation Model (DEM) to provide topographic context, the most commonly used elevation models being the Shuttle Radar Topography Mission (SRTM) DEM, ASTER GDEM (30 m spatial resolution), and the GEBCO 2019 DEM for bathymetric data (The General Bathymetric Chart of the Oceans; GEBCO Compilation Group, 2019). Aerial photographs, where available, have also proven to be useful for more detailed mapping of smaller areas of complex terrain (García et al., 2014; Darvill et al., 2014, 2017).

Our compiled geomorphological record includes moraines, trimlines, glacial lineations (bedrock and sedimentary), meltwater palaeochannels, outwash plains, shorelines, deltas, and cirques. Our compiled maps also display related landforms and topographic features such as rivers, lakes and volcanoes. The detailed criteria used to identify these different landforms on the basis of their morphology, colour, structure and texture are listed by Glasser and Jansson (2008; their Table 1), Martin et al. (2019; their Table 1) and Bendle et al. (2017b; their Table 2).

Compared to the terrestrial record, relatively little has been published on the glacier-influenced marine geomorphology in the fjords around the Patagonian icefields (Araya-Vergara, 2008; Boyd et al., 2008; Dowdeswell et al., 2016c; Dowdeswell and Vásquez, 2013; Fernández et al., 2017; Lastras and Dowdeswell, 2016). In addition to the multibeam echo-sounder data on seafloor morphology described and interpreted in these papers (horizontal resolution usually a few tens of metres), we used the GEBCO 2019 15 Second Arc Grid (GEBCO Compilation Group, 2019) to investigate the geomorphology of the continental shelf edge around Patagonia. The resolution of the GEBCO 2019 DEM is too coarse to map many types of submarine glacial landforms, but allows mapping of major glacial troughs and the possible suggestion of some moraines. Published bathymetric mapping is included in our compilation (Dowdeswell et al., 2016a, b, c).

Our PATICE compilation also includes an updated version of the 2011 AD inventory of 617 glaciers mapped by Davies and Glasser (2012). The inventory now includes a further 393 small mountain glaciers on plateaux and mesetas around the modern icefields, mapped using satellite imagery from 2011 AD. Shapefiles of present-day glacier extent and mapped glacial landforms are provided in the Supplementary Information to facilitate further research.

### 3.2 Chronology

#### 3.2.1 Compilation of ages

Fluctuations of Patagonian outlet glaciers have been dated using multiple techniques, listed in Tables 1 and 2. Each of the techniques is applied within a specific set of circumstances that directly challenge comparison, even when corrected to calendar years. For instance, radiocarbon methods can date the onset of ice-free conditions, but represent minimum deglacial ages for the associated ice limits. In contrast, cosmogenic nuclide exposure dating of boulders on a moraine crest provides a more direct age for landform deposition (and onset of glacial retreat), but invariably may still represent a minimum age given post-depositional processes can then act to reduce the cosmogenic nuclide concentrations. OSL dating of outwash plains has been used to constrain when the ice limit was positioned on the moraine (Smedley et al., 2016). Each of the methods used, and the corrections and calibrations we apply, is discussed in detail in the Supplementary Methods.

Compiling published ages from the literature (census date August 2019) gives us greater confidence in reconstructing glacial chronology than considering different studies in isolation. Here, we use a compilation of ages that provides insights into the lateral and vertical extents of the PIS and the later ice fields the PIS disintegrates into (Tables 1 and 2). Our compilation builds on earlier efforts to produce databases of ages (Coronato and Rabassa, 2011; Hare et al., 2017; Martínez et al., 2011; Mendelova et al., 2017; Rabassa et al., 2011). These databases were cross-checked, and additional published literature was scoured for data pertaining to the geographical position of ages, which were further cross-checked in ArcGIS using the maps and datasets provided. In some instances, errors were found in original papers and where possible these were rectified via communication with the original authors. In a few rare cases, errors in ages or geographical location meant that published ages were excluded from the dataset. Compiled ages are recalibrated according to the methodology set out in the Supplementary Methods, and use the Kaplan et al. (2011) production rate. Throughout this study, ages are given as before 1950 AD, except for lichenometry and dendrochronology ages, which are given in calendar years AD. Ages are presented with the age formats shown in Table 1.



All final ages were mapped in ArcGIS as ESRI point shapefiles (\*.shp), projected to UTM Zone 18S (datum: WGS 84). Each individual age contains attribute information including the publication reference, location (latitude, longitude, description), altitude (masl), site name, dating method, comments regarding sample characteristics, material dated, stratigraphic context, our own assessment of age reliability and any other applicable information (see Supplementary Methods and Figure 4). Each age in our compilation has a unique ID (Table 1) that can be cross-referenced between the Supplementary Information (Excel datasets and GIS shapefiles). This PATICE database uses datasets from 148 peer-reviewed publications spanning some 50 years (Table 1; Table 2). See 'Data Availability' for more information.

*Table 1. Unique IDs for the different categories of ages within the PATICE database; see Table 2 for more information and Supplementary Information for the full database.*

Type of age and format used in text and on figures	Age format	Unique ID in database	Number of ages	Number of publications
Ar/Ar	ka	>1	16	3
Cosmogenic nuclide exposure age ( $^{10}\text{Be}$ , $^{26}\text{Al}$ )	ka	>101	581	36
Calibrated Radiocarbon	cal. ka BP	>1000	903	77
Uncalibrated Radiocarbon	$^{14}\text{C}$ ka BP			
Cosmogenic depth profiles	ka	>2000	2	1
Tephrochronology	ka	>3000	31	10
Dendrochronology	years AD	>4000	21	5
Lichenometry	years AD	>4500	29	2
Historical sources	years AD	>5000	9	4
Varve age	ka	>6000	3	1
Cosmogenic nuclide exposure age ( $^3\text{He}$ )	ka	>7001	13	1
Cosmogenic nuclide exposure age ( $^{36}\text{Cl}$ )	ka	>8001	11	2
Optically stimulated luminescence (OSL)	ka	>9001	50	6
<i>Total</i>			<i>1,669</i>	<i>148</i>

*Table 2. Publications included in the PATICE compilation, with number and type of ages produced. See Supplementary Information for the full database. Some ages appear in more than one publication. Ages are listed only once, with the reference being the original publication where they were first published. Only ages relevant to reconstructing the glacial history of Patagonia are included.*

Publication	Number of Ages	Publication	Number of Ages
<b>Ar/K</b>		<b>Radiocarbon</b>	
Singer et al. (2004a)	6	Ashworth et al. (1991)	1
Singer et al. (2004b)	1	Bennett et al. (2000)	4
Wenzens (2006)	9	Bentley (1997)	14
		Boyd et al. (2008)	4



<b><sup>10</sup>Be exposure ages</b>		Breuer et al. (2013)	1
Ackert et al. (2008)	9	Clapperton et al. (1995)	26
Boex et al. (2013)	18	Coronato et al. (2009)	5
Bourgois et al. (2016)	20	Denton et al. (1999)	278
Davies et al. (2018)	8	de Porras et al. (2012)	1
Douglass et al. (2005)	19	de Porras et al. (2014)	1
Douglass et al. (2006)	40	Fernandez et al. (2012)	1
Evenson et al. (2009)	4	García (2012)	2
Fogwill and Kubik (2005)	4	García et al. (2019)	6
García et al. (2012)	27	Gordillo et al. (1992)	1
García et al. (2018)	64	Glasser et al. (2002)	10
García et al. (2019)	4	Haberle and Bennett (2004)	2
Glasser et al. (2006a)	3	Hall et al. (2013)	13
Glasser et al. (2011b)	10	Hall et al. (2019)	83
Glasser et al. (2012)	15	Henriquez et al. (2017)	2
Harrison et al. (2008)	3	Heusser (1989)	2
Hein et al. (2009)	23	Heusser (1998)	7
Hein et al. (2010)	13	Heusser (1999)	1
Hein et al. (2011)	13	Heusser (2003)	1
Hein et al. (2017)	25	Heusser et al. (1989)	1
Kaplan et al. (2004)	12	Heusser et al. (1995)	2
Kaplan et al. (2005)	18	Denton et al. (1999); Heusser et al. (1999)	174
Kaplan et al. (2007)	23	Horta et al. (2019)	4
Kaplan et al. (2008)	14	Iglesias et al. (2011)	1
Kaplan et al. (2016)	69	Kaplan et al. (2004)	3
McCulloch et al. (2005b)	10	Kilian et al. (2003)	3
Menounos et al. (2013)	9	Kilian et al. (2007a)	2
Moreno et al. (2009)	15	Kilian et al. (2007b)	4
Nimick et al. (2016)	11	Kilian et al. (2013b)	1
Reynhout et al. (2019)	30	Kröner, Martini et al. (1996)	6
Sagredo et al. (2018)	24	Lowen et al. (1995)	1
Sagredo et al. (2011)	4	Lumley and Switsur (1993)	1
Sagredo et al. (2016)	3	Marden and Clapperton (1995)	6
Strelin et al. (2014)	15	McCulloch and Bentley (1998)	3
Thorndycraft et al. (2019a)	6	McCulloch and Davies (2001)	1
Turner et al. (2005)	2	McCulloch et al. (2005a; 2005b)	24
		Mercer (1965)	3
<b><sup>36</sup>Cl exposure ages</b>		Mercer (1968)	1
Ackert et al. (2008)	1	Mercer (1976)	8
Douglass et al. (2005)	2	Mercer and Ager (1983)	2
		Montade et al. (2013)	1
<b><sup>3</sup>He exposure ages</b>		Moreno (1998) and Denton et al. (1999)	2
Kaplan et al. (2004)	13	Moreno et al. (1999)	9
		Moreno et al. (2009)	12
<b>Cosmogenic depth profile</b>		Moreno et al. (2015)	28
Darvill et al. (2015b)	2	Nimick et al. (2016)	1
		Porter (1981)	5
<b>Optically stimulated luminescence</b>		Porter (1990)	4
García et al. (2019)	8	Porter et al. (1984)	1
Glasser et al. (2016b)	17	Porter et al. (1992)	3
Harrison et al. (2008)	3	Rabassa and Clapperton (1990)	1
Harrison et al. (2012)	6	Rabassa et al. (1998)	1
Nimick et al. (2016)	3	Rabassa et al. (2000)	3
Smedley et al. (2016)	13	Roig et al. (1996)	3
		Sagredo et al. (2011)	13

		Stern (1990), in Marden and Clapperton (1995)	1
<b>Tephrochronology</b>		Stern (1992)	4
Biester et al. (2003)	1	Strelin et al. (2011)	6
Breuer et al. (2013)	2	Strelin et al. (2014)	42
Kilian et al. (2013b)	2	Turner et al. (2005)	14
Kilian et al. (2003)	3	Uribe (1982), in Clapperton (1995) and McCulloch et al. (2005a; 2005b)	2
McCulloch et al. (2005a)	1	Van Daele et al. (2016)	1
Stern (1992)	3	Villa-Martínez et al. (2012)	2
Stern et al. (2016)	10	Villagran (1988)	2
Stern et al. (2015)	2	Waldmann et al. (2010)	2
Van Daele et al. (2016)	1	Weller et al. (2015)	4
Weller et al. (2015)	4	Weller et al. (2017)	1
		Wenzens (1999)	12
		Wenzens (2005)	15
<b>Dendrochronology</b>			
Koch and Kilian (2005)	3		
Masiokas et al. (2009b)	10		
Winchester et al. (2014)	5	<b>Historical documents</b>	
Winchester et al. (2001)	1	Casassa et al. (1997)	3
Winchester and Harrison (2000)	2	Rivera et al. (2012b)	2
		Araneda et al. (2007)	3
<b>Lichenometry</b>		Garibotti and Villalba (2017)	1
Garibotti and Villalba (2009)	11		
Garibotti and Villalba (2017)	18	<b>Varve years</b>	
		Bendle et al. (2007a)	3

### 3.2.2 Consistency and quality control of published ages

We assign all ages in the PATICE database a quality control rating to aid interpretation over the scale of an entire ice sheet and to enable the identification of poorly resolved ages (Figure 4). This approach is pragmatic given the resolution of isochrones produced (5 kyr), the size of the area analysed, and the scale and quantity of ages compiled. This rating scheme should not be taken to indicate that the ages or associated studies are perceived to be of low, medium or high quality themselves, and we strongly urge readers to consult original studies when using our compilation to investigate a particular area or higher-resolution time-step. Principally, the quality index reflects the availability of data needed to recalculate ages from the original publication, whether samples are outliers or are part of a group that replicates the same age, and whether they are *in situ* with well constrained geomorphic or stratigraphic context.

Following the approach used by recent studies that encourage model-data comparisons (e.g. Hughes et al., 2016; Small et al., 2017; Ely et al., 2019), ages are assigned a quality index rating of 1, 2 or 3, based on the criteria in Table 3. Decisions are made by the lead and co-authors at the time of writing. These ages are symbolised with green, amber or red circles respectively in the figures in this article.

1. All criteria are met and the age is considered reliable (green);
2. Most of the criteria are met and the age is probably reliable (amber);

3. No criteria met or the age is an outlier; the age is considered unreliable (red).

Key criteria for assessing reliability of all samples include a clearly defined geomorphic context and recording of the geographical and geological context, as well as the degree to which standard protocols are followed for given dating methods (Table 3). The “All samples” criteria are considered first, and then dating method-specific criteria are applied. The number of ages in each category is shown in Table 4.

The evolution and development of dating protocols over time means that ages published a longer time ago may now be deemed less reliable. Some older radiocarbon ages are rated as (2) because  $\delta^{13}\text{C}$  was not measured or provided, for example. Where ages are rated as (3), there is an explanation in the attribute table of the ESRI Shapefile.

For our reconstruction, the ratings of cosmogenic nuclide ages are most critical as only highly (1) rated  $^{10}\text{Be}$  ages are used to generate mean landform ages. Of particular importance, we emphasize that our goal is to define ice margin positions; hence, our quality control ratings should consider our rationalization for rating. As an example, a single  $^{14}\text{C}$  age may provide precise and unparalleled information on the timing of an event, but within the stratigraphy it may tell little about where the ice margin was at that moment; in comparison, cosmogenic date directly ice margin positions, which is our main desired output. Where  $^{14}\text{C}$  studies are arguably most abundant, such as in the Chilean Lake District, the change to our main reconstructions and findings are insignificant with different ratings on individual ages, e.g., a 1 or 2. While some may decide that individual datasets warrant higher ratings, such decisions would not affect the overall 5kyr reconstructions that we present to the community, and so would not affect our conclusions.

Table 3. Criteria for assessing the reliability of published ages once compiled in the PATICE database.

Dating technique	Indicators of reliability
All samples	Sample appears <i>in situ</i> ; Age uncertainty specified; Geomorphic context defined; Geographical and geological context provided; sample can be accurately located; Considered reliable by original authors. Outliers identified by original authors score 3.
Cosmogenic nuclide dating ( $^{10}\text{Be}$ , $^{26}\text{Al}$ , $^3\text{He}$ , $^{36}\text{Cl}$ ): surface exposure age dating	Multiple ( $\geq$ ideally 3) samples from the same landform or site. Ages are internally consistent; spread in ages similar to measurement uncertainty. Uncertainties overlapping with others from same landform/site. Data provided to recalibrate ages using latest published calibration models (cf. Lowe and Walker, 2015).
Cosmogenic nuclide dating: depth profiles	Ideally, modelled profile age compared to separate surface cobble ages. Several samples in profile ( $\geq$ ideally 5), including at least one sample $>1.5$ m deep. Profile ages internally consistent and clustered. Geomorphological situation is accounted for: (1) terraces stabilised shortly after moraine deposition;

	<p>(2) nuclide inheritance is low;</p> <p>(3) post-depositional shielding is minimal;</p> <p>(4) terrace sediment not mixed post-depositionally</p>
Radiocarbon dating ( $^{14}\text{C}$ )	<p>Known and uncontaminated sample material. Material dated is clear.</p> <p>Organic content &gt;5% LOI.</p> <p>Bulk samples (including gyttja, organic silt, carbonate clasts etc.) considered lower quality than samples from individual plants and macrofossils.</p> <p>Uncalibrated age provided with full errors to enable recalibration with modern calibration curves.</p> <p>Multiple or stratigraphically consistent ages if in a core.</p> <p>Appropriate <math>\delta^{13}\text{C}</math> values: -25‰ to -32‰ for terrestrial plants; -15‰ for marine plants; -0‰ for marine carbonates (Lowe and Walker, 2015).</p> <p>Within calibration range of SHCal 13 / Marine13 dataset (Hogg et al., 2013; Reimer et al., 2013).</p> <p>For marine radiocarbon ages, <math>\Delta R</math> is well understood</p> <p>Not from aquatic taxa (freshwater plants), since algae and aquatic mosses build carbon from dissolved inorganic carbon, and reflect the <math>^{14}\text{C}</math>:<math>^{12}\text{C}</math> ratios of the water from which they grew. These aquatic taxa are vulnerable to the hard water effect, dissolved carbonate from surrounding rocks, the residence time of the bog or lake, and other factors. As a result, the <math>^{14}\text{C}</math> activity of the dissolved inorganic carbon is <math>^{14}\text{C}</math> depleted, resulting in artificial ageing with wide variation (Hatté and Jull, 2013).</p>
Optically stimulated luminescence (OSL)	<p>Any potential for partial bleaching has been addressed using small aliquot/single grain measurements.</p> <p>The proglacial outwash sample can be directly linked with the corresponding moraine</p> <p>Multiple or stratigraphically consistent ages.</p> <p>Dose rate information and equivalent described in source.</p> <p>Ages determined for K-feldspar address the potential impacts of anomalous fading.</p> <p>Age is not determined using an experimental analysis protocol.</p>
Tephrochronology	<p>Tephra age is consistent and in stratigraphic order with other tephra layers and independent <math>^{14}\text{C}</math> dating within the core.</p> <p>Tephra is geochemically analysed and compared with other tephras.</p> <p>Tephra layer is independently dated.</p>
Dendrochronology	<p>Eccentricity is calculated and provided</p> <p>Growth rate is calculated and provided</p> <p>Sample context is clear</p> <p>Age of tree is calculated clearly.</p>
Historical documents	<p>Textural source is identified and errors and uncertainties are discussed.</p> <p>Ice margin is clearly located in textural /historical source.</p>
Varve records	<p>Process model of varve formation is provided.</p> <p>Multiple varve counts are carried out by independent analysts.</p> <p>Varve count uncertainty is expressed.</p> <p>The 'floating' varve chronology is anchored in absolute time (e.g. using tephrochronology or radiocarbon dating).</p>

Table 4. Number of ages assigned to each category in the PATICE database. Ages marked “unassigned” either predate 35 ka but are included because older ages help to constrain the LGM ice limit, or could not be recalibrated.

Dating Method	Green (1)	Amber (2)	Red (3)	Unassigned	Total Ages
<sup>10</sup> Be exposure age	446	94	28	13	582
<sup>36</sup> Cl exposure age			11		11
<sup>3</sup> He exposure age	6	1	5	1	13
Tephra	28	3			31
Ar/Ar				16	16
OSL	37	3	10		50
Radiocarbon	312	461	129	1	903
Depth profile	2				2
Dendrochronology	15	6			21
Lichenometry	29				29
Historical documents	9				9
Varve age	3				3
<b>Total Number</b>	<b>887</b>	<b>568</b>	<b>183</b>	<b>31</b>	<b>1,669</b>

### 3.2.3 Calculation of landform mean ages

Where multiple <sup>10</sup>Be cosmogenic nuclide exposure ages ( $\geq 2$ ) exist for a particular moraine or landform, we have generated mean ( $\mu$ ) ages, which we present with one standard deviation (SD), based on high quality (green) ages only (see section 3.2.2), and using external uncertainties. The presentation of mean ages with standard deviations follows guidelines from Lambrook (2008) and Curran-Everett and Benos (2004) for presentation of statistical data. They argue that the standard deviation is a single value that quantifies scatter, and should not follow a plus and minus symbol. Therefore, in this paper, mean ages of landforms are presented as, for example, 5.2 ka (SD 0.5). This makes them clearly distinguishable from individual ages with a measured uncertainty, which are shown as, for example,  $5.2 \pm 0.5$  ka.

Outliers without overlapping uncertainties at 2 sigma are excluded from this calculation. This approach reduces and simplifies the data, and facilitates inter-regional comparison and identification of key ice margins in different parts of Patagonia. It also allows an evaluation of the spread of the ages on each landform, without being biased by measurement uncertainty. This is because the laboratory measured uncertainty in <sup>10</sup>Be ages may not be representative of the uncertainty in the age, which can be greatly influenced by geological factors. Presenting the spread of <sup>10</sup>Be ages on a particular landform instead provides a more robust estimate of the uncertainty in the age of a landform. Landform mean <sup>10</sup>Be ages ( $\mu$ ) with standard deviations (SD) are represented with pink crosses on figures in this study.

Varve years provide a direct age for a moraine with a measured uncertainty (shown as  $\pm$ ). Bracketing tephra, radiocarbon or OSL ages inside and outside the ice margin are used as a check for the mean moraine age but

are not included in the landform mean age calculation. If the bracketing ages were to suggest that the mean landform age was incorrect, this would be highlighted, but we have not found this to be the case. For more information, see Supplementary Methods.

*Figure 4. Workflow model, showing the different stages in the methodology for our new empirical reconstruction. See also Figure 5.*

### 3.3 Palaeo-glaciological reconstruction

#### 3.3.1 Ice extent in isochrones

Following the methodology used in several recent reviews of Antarctic Laurentide and pan-European glaciation (Bentley et al., 2014; Hillenbrand et al., 2014; Hodgson et al., 2014; Hughes et al., 2016; Larter et al., 2014; Ó Cofaigh et al., 2014; Margold et al., 2018), at well dated ice-marginal positions we generated short, isolated isochrones of ice-sheet extent at 5 kyr intervals from analysis of published ages and geomorphology. These isochrones are therefore drawn along well-dated moraine positions. Reconstructions at a resolution finer than 5 kyr time-slices were not possible due to the scarcity of dating in many regions of Patagonia. The density of published ages varies spatially and temporally, and multiple techniques have been applied in different settings. Published ages tend to occur in clusters around the more accessible parts of the palaeo ice-margin. In addition, some data reduction is necessary to make the most useful palaeo ice-sheet reconstructions. However, in some places (e.g. eastern Northern Patagonian Icefield, Torres del Paine), there is enough dating resolution to separate out time-slices at 15, 13 and 10 ka, which allows us to generate a specific ice advance coeval with the ACR. Another additional time-slice through the Late Holocene uses published data (Davies and Glasser, 2012; Glasser et al., 2011a; Meier et al., 2018) and new geomorphic mapping to constrain ice extent at 0.5 – 0.2 ka.

In drawing the isochrones, context was used to assess whether ages related directly to an ice margin (e.g.,  $^{10}\text{Be}$  ages on a moraine), or whether they denoted a minimum age for ice-free conditions (e.g.,  $^{14}\text{C}$  ages from a peat bog inside a moraine), or maximum ages for ice advance. Tephrae are taken to denote ice-free conditions and provide a chronological tie point across multiple sites. They are particularly important for dating palaeolake evolution (e.g., Bendle et al., 2017a; McCulloch et al., 2005a; Thorndycraft et al., 2019a). All of these data (ages, isochrones, moraines) are available in the Supplementary Information as ESRI Shapefiles.

### 3.3.2 *Interpolation of isochrones*

New and published glacial geomorphological mapping were used to reconstruct ice-sheet limits (Figure 4, Figure 5). We interpolated between isochrones using these geomorphological and topographical data to produce the maps of past ice-sheet extent. Reconstructions of ice limits were conducted ‘blind’: relying on geomorphological, chronological and topographical data, but without comparison to established LGM reconstructions.

We assume that prominent moraines indicate a period when the ice margin stabilised and, therefore, in the absence of dating control, that moraines adjacent to dated ice limits or a similar distance from the ice divide have a similar age. Where no moraines were visible from previously published mapping or from new analysis of satellite imagery, ice limits in immediately adjacent valleys with the same orientation were assumed to have reached a similar position and elevation. Reconstructing former ice limits from the geomorphological record was also complicated by the presence of high ground (flat-topped mesetas) beyond the present ice fields. For example, the pattern of latero-terminal moraines from major outlet lobes of the eastern ice sheet suggests they separated and flowed around mesetas. However, determining where ice lobes became topographically confined between mesetas is hard to assess reliably, as broad, high plateaus could have sustained independent ice fields, contributing to the outlet lobes. In such instances, we relied on landform evidence: some mesetas show little geomorphic evidence of glaciation and are dominated by fluvial geomorphology, with steeply incised valleys. They typically have lateral moraines on their sides, suggesting ice was confined to the valley. These are considered not to have been glaciated at any time in our reconstruction. We do note that areas with cold-based glaciation would have left little geomorphic impact, and could be erroneously excluded from the reconstruction. Mesetas closer to the ice divide possess alpine glacial geomorphology (Araos et al., 2018; Glasser and Jansson, 2008; Glasser et al., 2008). The presence of abandoned cirques, truncated spurs, parabolic valleys and arêtes suggests that even if they are not glacierised today, these areas at least supported valley glaciation during past glacial cycles. In the absence of sufficient geomorphic or chronological data, we assume that if mesetas are glacierised today, they contributed ice to outlet lobes during glaciation. More work is required to ascertain the lateral margins of the major outlet ice lobes at different times during the last glaciation.

An additional challenge is inferring an ice margin’s position in places where there is limited or no published chronological data. For example, where there is no clear LGM limit for a particular ice lobe, we keep the ice in the same position from 35 – 20 ka, or until dating controls are available. For many lobes, the 15 ka and ACR ice extents are indistinguishable, and so are held constant between these two time-slices. For the 5 ka ice extent, where geomorphological or chronological data are unavailable, we hold the ice margin position at the Late Holocene (0.2 ka) ice extent (therefore a minimum estimate). Likewise, the updated 0.2 ka ice

extent is still largely derived from Davies and Glasser (2012), which is also considered a minimum estimate because where no other data (geomorphic or otherwise) are available, the ice margin is mapped using the earliest available satellite imagery (1970s or 1980s). In areas with limited or no dating of mapped ice limits, the ice limits are mapped using geomorphological data and relative chronology (where the outermost landforms are assumed to be oldest).

Our approach contains assumptions in areas where the geomorphology of ice limits is unclear or where there has been limited or no dating of landforms. In these places, we essentially construct a relative chronology, with the caveat that this is an imperfect approach, and has been shown to be problematic in parts of Patagonia (e.g. Darvill et al., 2015b). Nonetheless, we highlight such locations (which have a *low confidence* ice margin; see below) as ideal targets for testing in future dating campaigns.

### 3.3.3 Uncertainty estimate of ice-sheet extent

Empirical ice-sheet reconstructions should have clearly quantified ice-margin uncertainties, indicating where there are data (e.g., mapped moraines) or interpretations (e.g. interpolated ice margin positions where moraines are absent) (Stokes et al., 2015). These data can then be used in data-calibrated model ensembles and provide targets for further work. In our reconstruction, each ice limit is assigned a level of confidence (e.g., see Figure 5):

- *High confidence* ice limits have both well-defined moraines and a well-constrained chronology.
- *Medium confidence* ice limits are defined by geomorphology or topography and lie close to published ages (e.g., Figure 2). For example, if outlet lobes immediately to the north or south have a well-defined chronology, we can make a reasonable estimate of the ice extent if there is well defined glacial geomorphology.
- *Low confidence* limits have no well-defined geomorphology, and no nearby published ages. These ice limits are interpretations, interpolated from mapped moraines where possible. In such areas, we view the reconstructed ice limits as a first tentative hypothesis that requires testing using field surveys or numerical modelling.

Unlike the Hughes et al. (2016) reconstructions of the Eurasian Ice Sheet, we do not provide minimum, maximum and 'best estimate' extents for each time-slice, as our resolution is lower, and the density of dated material is sparser. Our ice-sheet extents at each time interval are simply a best estimate.



*Figure 5. Demonstration of the stages in ice sheet reconstruction around the eastern margin of the Southern Patagonian Icefield (49–51°S) at 35 ka. See also Figure 4 for an overview of the methods. A. Development of isochrones at moraine limits where there are sufficient high quality ages and geomorphology. Current ice catchments are shown in black with white outline. Cosmogenic and Ar/Ar ages older than MIS 3 are not shown. B. The ice margin location is calculated by interpolating between isochrones. Note the high confidence in ice extent areas with both ages and geomorphology relevant to the time slice, medium confidence where there is clear geomorphology but a lack of ages (but there may be published ages nearby); and low confidence where there is an absence of ages or geomorphology. Interlobate areas tend to be particularly difficult to constrain, typically resulting in low confidence margins. C. Development of palaeo ice-flow lines and ice divides using mapped geomorphology and topography.*

### 3.3.4 Palaeo ice-flow and ice divides

We use the orientation of streamlined glacial lineations (including *ocine moutonnées*, whalebacks, drumlins and flutes), topography, bathymetric troughs, fjords and moraines (lateral and terminal) to determine palaeo ice-flow direction (Clark, 1993; Figure 5C). However, in comparison to the much larger Laurentide and Eurasian ice sheets during the last glacial cycle, glacial lineations in Patagonia are largely focused in topographically constrained outlet glacier corridors and demonstrate a consistent ice-flow direction with little evidence of significant changes in drainage patterns. We did not identify the complex cross-cutting flow-sets that are indicative of changes in palaeo ice-flow patterns (cf. Stokes et al., 2015). This suggests that the main corridors for ice flow remained relatively unchanged, and topographically constrained, through time. Palaeo ice-flow is used to identify the location of the ice divides. Interpreted ice divides are provided for indicative use only and have low confidence in the absence of ice-sheet elevation data. We suggest that the ice divides are located along the Andes, orthogonal to ice flow.

### 3.3.5 Glacier area and volume calculations

The total area of each reconstructed time-slice was calculated in ArcGIS 10.3. To give a first-order estimate of total ice-sheet volume, the areas of each individual closed GIS polygon at each time-slice was converted to volume using the relationship in equation (1):

(1)

$$\log V = 1.23(\log A - 1)$$

where  $V$  = volume in  $\text{km}^3$ , and  $A$  = area in  $\text{km}^2$ , following Hughes et al. (2016). This relationship between ice-sheet area and volume is derived from a logarithmic relationship of the area and volume of the world's largest present-ice sheets and ice caps (e.g. Bahr et al., 2014b; Paterson, 1994). This relationship is based on

observations of present-day ice masses and so may underestimate ice volume during colder periods of time, when ice masses likely had steeper surface gradients due to the greater stiffness of colder ice, although this is likely to present less of an issue in temperate regions like Patagonia. Alternatively, where ice sheets rest on soft beds and are thinning and retreating with many fast-flowing outlet ice streams, this equation may tend to over-estimate volume (Hughes et al., 2016). The estimate of ice volume therefore likely becomes increasingly erroneous as deglaciation progressed, and the ice sheet thinned. We use this equation on the PIS from 30 to 20 ka.

We use different volume-area scaling relationships as the PIS breaks down into smaller ice masses (ice fields, ice caps and glaciers) from 15 ka onwards. Throughout our reconstruction, each ice mass (an enclosed GIS polygon) is given an attribute of ice sheet, ice field, mountain ice cap or glacier following standard protocols (Rau et al., 2005; Raup and Khalsa, 2010; Raup et al., 2007). Appropriate volume-area scaling laws were then applied (Bahr, 2014; Bahr et al., 2014a, b). For glaciers and dome-shaped mountain ice caps, ice volume ( $\text{km}^3$ ) is therefore calculated using equation (2):

(2)

$$V = kA^\gamma$$

where  $k$  and  $\gamma$  are constants:  $k = 0.033 \text{ km}^{\gamma-2\gamma}$ ;  $\gamma = 1.36$  for glaciers and icefields, and 1.22 for dome-shaped mountain ice caps. For the present-day ice volume, we use an already published calculation that uses a more sophisticated method (Carrivick et al., 2016).

For ice sheets, ice fields, glaciers and mountain ice caps, conversion of ice volume in  $\text{km}^3$  to gigatonnes (Gt) assumes an ice density of ice of  $0.9167 \text{ Gt/km}^3$ . To convert ice volume to sea level equivalent, we use a global surface ocean area of  $361.8 \text{ Mkm}^2$  and a sea water density of  $1028 \text{ kg m}^3$ . This gives an ice:water density ratio of 0.892 and assumes that sea water replaces ice grounded below sea level (cf. Hughes et al., 2016). However, in our reconstruction we note that ice grounded below sea level is fairly minimal due to the shallow Pacific continental shelf and the extensive sea level lowering at the LGM (Guilderson et al., 2000). Therefore, our calculated sea level equivalent is likely over-estimated where ice is grounded below sea level. Regrettably, in the absence of a three-dimensional ice surface and well-reconstructed relative sea levels across the study area, this uncertainty is challenging to quantify without a numerical model that can account for isostatic adjustment.

### 3.3.6 *Palaeolakes*

We map the extent of ice-dammed palaeolakes at each timeslice. The extent of the palaeolakes is constrained by published geomorphology and chronology (Bell, 2009; Bendle et al., 2017b; Caldenius, 1932; García et al., 2014; García et al., 2019; Glasser et al., 2016b; Hein et al., 2010; Horta et al., 2019; Martin et al., 2019; Martinod et al., 2016; Thorndycraft et al., 2019a; Turner et al., 2005). The ASTER GDEM dataset was used to interpolate lake levels between mapped shorelines or other datapoints. Differential isostasy is not taken into account in these reconstructions, apart from around the Northern Patagonian Icefield (Thorndycraft et al., 2019a). In other cases, glacial lakes are reconstructed following analysis of the DEM where our reconstruction indicates that current drainage routes are blocked. For each lake, we identify a drainage col spillway and drainage pathway. In this way, we are able to reconstruct drainage pathway reversals for the Patagonian palaeolakes. For comparison purposes, we also provide the areas of those palaeolakes that remain today as proglacial lakes following recession of the glaciers. Palaeolake area is calculated in Esri ArcGIS. In the absence of detailed palaeolake bathymetry, it is difficult to robustly calculate glacial lake volume where current lakes remain in the over-deepening, and so we present only the change in glacial lake area.

### 3.4 *Relative sea level record*

We use the relative sea level datapoints in Table 5 throughout our reconstruction figures, where we alter the GEBCO (GEBCO Compilation Group, 2019; [www.gebco.net/](http://www.gebco.net/)) marine bathymetry dataset to reflect relative sea level (Table 5). We use published data from the Argentinian Atlantic coast (Guilderson et al., 2000; Peltier and Drummond, 2002; Schellmann and Radtke, 2010; Isla, 2013). There is a dearth of data for the Pacific margin during the LGM, late glacial and Holocene, and sea level change in the northern part of the study area may be overestimated in our reconstruction. Sediments on the Argentine continental shelf in southern Patagonia suggest a local relative sea level lowering of 150 m at the LGM (Guilderson et al., 2000) (Figure 6). During glacial maxima, the fall in eustatic sea level and increased isostatic depression in western South America relative to the broad Argentinian shelf in the east (Peltier and Drummond, 2002) would have contributed to the formation of ice-dammed lakes east of the PIS.

Following the global LGM, the Argentinian record from shells on the continental shelf indicates that there was a rapid increase in relative sea level between 20 and 15 ka (-150 to -120 m), with further rises in relative sea level following the ACR (Guilderson et al., 2000) (Figure 6). By 10 ka, geological data indicate that local relative sea level here was -45 m. Globally, three periods of rapid sea level rise are recognised; from 19.5 – 18.8 ka (10 m rise), one commonly termed Melt Water Pulse 1A (14.8 to 13.0 ka; 20 m rise) and one termed

Meltwater Pulse 1B (11.5 to 11.1 ka; 16 m rise) (Harrison et al., 2019). These data imply rising regional sea levels throughout the Late Glacial and early Holocene.

The mid-Holocene sea level high-stand in southern Patagonia was reached at  $\sim 7.4$  cal. ka BP (Schellmann and Radtke, 2010; Porter et al., 1984), with sea levels reaching +2 to +3 m above modern sea level. There were also significant falls of 1 and 1-2 m at  $\sim 6.6$  cal. ka BP and  $\sim 2.3$  cal. ka BP respectively. The general trend in relative sea level fall since the mid-Holocene transgression was predominantly driven by glacio-isostasy (Schellmann and Radtke, 2010).

Further north, at San Matías Gulf (41°S, 62°W; Argentinian continental shelf), *in situ* pieces of wood from 70 m below sea level yielded radiocarbon ages of  $11.3 \pm 0.15$  cal. ka BP (Isla, 2013). The mid-Holocene highstand of +6 m was reached at 6 ka BP. Sea level fell to near present by 2.6 cal. ka BP.

Table 5. Regional relative sea levels used in the PATICE reconstruction.

Time-slice	Regional relative sea level	Reference
35 ka	-150 m asl	Guilderson et al., 2000
30 ka	-150 m asl	Guilderson et al., 2000
25 ka	-150 m asl	Guilderson et al., 2000
20 ka	-150 m asl	Guilderson et al., 2000
15 ka	-120 m asl	Guilderson et al., 2000
13 ka	-120 m asl	Guilderson et al., 2000
10 ka	-45 m asl	Guilderson et al., 2000
5 ka	+1 m	Schellmann and Radtke, 2010
0.2 ka	0 m asl	
0 ka	0 m asl	

Figure 6. Relative sea level curve for the Argentine Shelf from the ICE-4G viscoelastic model and geological data (Guilderson et al., 2000). Grey bars highlight timing of meltwater pulses 1A and 1B.

#### 4 Glacial landsystems of Patagonia

Today, Patagonia contains outlet glaciers terminating in the full range of environments possible for temperate glaciation (land-terminating, lake-terminating and tidewater-terminating; Glasser et al., 2009). This was also the case during the Pleistocene (Coronato and Rabassa, 2011; Glasser et al., 2005; Martínez et al., 2011; Rabassa, 2008; Rabassa et al., 2011), and glacial landforms included in PATICE are listed in Table 6.

Table 6. Summary of landforms mapped in this study

Landform	Number
Shorelines	2,507
River terraces	8
Perched deltas	269
Alluvial fan and contemporary deltas	61
Lineations (lines)	3,926
Lineations (polygons)	1,390
Bedrock lineations	9,603
Moraines	25,009
Sandur	594
Empty cirques	4,309
Rivers	1,225
Lakes	3,359
Glaciers	1,010
Volcanoes	31
Peaks over 3000 m	7
Bathymetric trough edge	40
Palaeochannels	4,536
Trimlines	939
Total	58,323

In general, there are four distinct temperate glacial sediment-landform assemblages across the Patagonian Andes:

- i. An upland glacier landsystem, with an assemblage of cirques, lateral and terminal moraines, some mountain glaciers and snow patches, flutes, and lakes within the overdeepened basins (Aroas et al., 2018; Martin et al. 2019);
- ii. In the lowlands, a land-terminating glacial landsystem, with an assemblage of nested lateral-frontal moraine arcs, outwash plains, meltwater channels, sedimentary glacial lineations (including drumlins) and inset hummocky terrain (e.g. Bendle et al., 2017b; Coronato et al., 2009; Darvill et al., 2014; Ercolano et al., 2004; Lovell et al., 2012; Martin et al., 2019; Ponce et al., 2013);
- iii. A lowlands glaciolacustrine landsystem, with landforms such as deltas and shorelines, and localised ice-contact glaciofluvial features (e.g. Bell, 2008; Bell, 2009; Bendle et al., 2017b; Davies et al., 2018; García et al., 2014; Thorndycraft et al., 2019a; Turner et al., 2005);
- iv. An offshore glaciomarine landsystem with fjords, offshore moraine ridges, streamlined sedimentary lineations, turbidity-current channels, raised fluvial deltas and slope failures (Dowdeswell and Vásquez, 2013; Dowdeswell et al., 2016c).

#### 4.1 Upland glacier landsystem

The upland mountains of Patagonia beyond the present-day icefields bear evidence of an upland, Alpine-style of glaciation. This landsystem comprises amphitheatre-shaped cirques, some still occupied by glaciers (Glasser et al., 2008; García, 2012; Araos et al., 2018; Martin et al., 2019). Some cirques host remnant moraine-dammed lakes, eroded lateral moraines, closely-spaced frontal moraines and lineations interpreted as flutes (*ibid.*). The fresh lateral and terminal moraines associated with these cirques have allowed the reconstruction of mountain glaciers during the most recent advance at 0.5 - 0.2 ka (Glasser et al., 2011; Davies and Glasser, 2012; Meier et al., 2018).

In the Chilean Lake District, Alpine-style glaciation occurred, with discrete piedmont glaciers constrained by mountains and deep lake basins (García, 2012). The landform assemblage here includes cirques, well-developed lateral and end-moraine sets, ice-contact kame terraces, moraine-dammed lakes, meltwater channels and spillways, and outwash plains. These landforms were associated with an active, temperate glacial regime, with erosive, wet-based ice (García, 2012).

#### 4.2 Lowland land-terminating glacial landsystem

The broad valleys distributed along the eastern margin of North and Southern Patagonian Icefields, and east and west of the Andes in the Chilean Lake District, comprise over-deepened glacial troughs, often occupied by lakes, indicating the action of effluent ice sheet outlet lobes and smaller glaciers flowing away from the Andean divide (Araos et al., 2018). This large-scale sediment-landform assemblage typically comprises multiple moraine sets, for example those in the areas formerly occupied by the large eastern outlet glaciers (Glasser and Jansson, 2005). The terminal moraines are generally complex features with multiple ridges and crests (Figure 7). Throughout Patagonia there are also many smaller moraines close to the contemporary ice margins, which represent mid and late Holocene and Twentieth Century glacier recession (Glasser et al., 2005). Late Holocene erosional trimlines are vegetation free, are typically developed close to the snouts of many contemporary glaciers, and can merge down-glacier with lateral and terminal moraines. They mark a recent time in the last two centuries when ice was thicker, followed by glacier recession (Glasser et al., 2011a; Davies and Glasser, 2012; Meier et al., 2018). Large tracts of ice-scoured and sometimes streamlined bedrock are present along major ice discharge routes to the east of the contemporary icefields, as well as in and around the fjord areas of Patagonia (Glasser and Ghiglione, 2009; Glasser and Harrison, 2005; Glasser et al., 2009).

Glacial outwash plains (sandur) and meltwater channels are widespread in Patagonia, especially east of the Andes where they are associated with the large terminal moraine complexes (Cogez et al., 2018; Bendle et al., 2017b; Hein et al., 2009, 2011; Smedley et al., 2016) (Figure 7). Sub-parallel lateral and marginal meltwater channels are also common features along the lateral margins of former outlet glaciers (Benn and Clapperton, 2000; Lovell et al., 2012).

Glacial lineations have previously been interpreted as being associated with large, fast-flowing outlet glaciers are present throughout Patagonia (Bendle et al., 2017b; Glasser and Jansson, 2005). Lineations are predominantly found at lower elevations (e.g., Clapperton, 1989; Ponce et al., 2013, 2018) and in discrete topographically controlled corridors (Bendle et al., 2017b; Glasser and Jansson, 2005). They range from streamlined bedrock to elongate sedimentary drumlins in the lowlands (Clapperton, 1989; Ponce et al., 2013, 2018). They are larger in scale than the smaller flutes restricted to upland cirques (cf. Martin et al., 2019).

*Figure 7. Key landforms associated with the lowland land-terminating glacial landsystem. A: Latero-frontal moraines at the eastern margin of Lago GCBA. B: outwash fan. Centre: Geomorphological map showing key land-terminating landforms, such as outwash plains, moraines and meltwater channels. C: Detail of meltwater channels. D: Detail of moraines and meltwater channels. Location of photographs is shown on the central map.*

### 4.3 Glaciolacustrine landsystem

This sediment-landform assemblage is dominated by large flat-topped sediment bodies, interpreted as deltas, or perhaps subaqueous fans modified by subsequent falling lake levels (Figure 8), all deposited into former ice-dammed lakes. These were common along the shores of the lakes located east of the contemporary icefields (Bell, 2008, 2009; Bendle et al., 2017b; Davies et al., 2018; De Muro et al., 2018; Glasser et al., 2016b; Hein et al., 2010; Thorndycraft et al., 2019a; Turner et al., 2005). Marine terraces, documenting former sea level high stands following the LGM, have also been mapped in southern Patagonia especially (e.g. Bentley and McCulloch, 2005; De Muro et al., 2017, 2018; Feruglio, 1933; Porter et al., 1984).

At Lago GCBA and Lago CP, the glaciolacustrine delta fans have a classic Gilbert form with a braided delta top and a steeply inclined delta front. Adjacent to the fans are concave beach embayments that formed parallel with the deltas as they prograded into the lake. The delta sediments consist predominantly of matrix- and clast-supported gravels (Bell, 2009; Figure 8B). Underflows forming turbidity currents are also likely to be relatively common, given the lack of a density difference between river and lake water, as compared with meltwater entering the marine system and rising to form buoyant plumes of suspended sediment (Syvitski, 1989). The palaeolake assemblage also includes subaqueous morainal banks (Figure 8C, D; Bendle et al.,

2017b; Davies et al., 2018; García et al., 2014, 2015; Hein et al., 2010) and palaeo shorelines etched into the hillsides (typically cut into glacial sediments; Figure 8E, F). Shorelines typically have a sloping beachward face and can be tens to hundreds of metres wide. In Torres del Paine, García et al. (2014) and Solari et al. (2012) described substantial glaciolacustrine terraces that flank the valley sides, with consistent elevations over several kilometres. These terraces occur as both continuous and discontinuous fragments that are cut into bedrock and lake sediments. Over 10s of kilometres shorelines are warped upwards towards the Andean Cordillera reflecting glacioisostasy (Thorndycraft et al, 2019a; Turner et al., 2005).

Associated with these glaciolacustrine geomorphological features are extensive deposits of glaciolacustrine rhythmically (and sometimes annually) bedded silts and clays (Caldenius, 1932; Bendle et al., 2017a). These sequences are associated in places with bedded gravel deposits (García et al., 2014, 2015). Tephra horizons may be interbedded within annually-laminated (varved) glaciolacustrine units, and provide the potential for time-anchored, high resolution chronologies for ice-margin recession and palaeolake evolution (Bendle et al., 2017a; Thorndycraft et al, 2019a).

*Figure 8. Glaciolacustrine landsystem around Lago Cochrane and Lago Esmeralda, east of the Northern Patagonian Icefield. A: Raised glaciofluvial delta terraces above Lago Cochrane. B: Perched delta and modern delta, Lago General Carrera. C: Morainal bank, Esmeralda Moraines (see Davies et al. 2018). D: Photograph illustrating the Esmeralda morainal bank. E, F: Palaeolake shorelines around Lago Juncal. G: Geomorphological map highlighting glaciolacustrine landforms around Lago Cochrane. For more information see Davies et al. 2018; Thorndycraft et al, 2019a; Martin et al. 2019. See also Figure 21.*

#### 4.4 Glaciomarine landsystem

The 15 arc-second GEBCO dataset (GEBCO, 2019) permits a relatively low-resolution visualisation of the wider Patagonian continental shelf. The western, Pacific continental shelf is characterised by 12 relatively deep cross-shelf troughs up to 200 km long between 42° and 55°S (Figure 9A). Troughs are not apparent on the corresponding Atlantic continental shelf, which is typically <100 m deep, gradually deepening to 200 m on the outer shelf before the sharp break in slope at the continental shelf edge. The Pacific coast troughs emanate from the narrow, deep, inter-island fjords that characterise the western Patagonian coastline (Figure 9A). The inner fjords between the islands reach depths of more than 1000 m below sea level and are 3 to 10 km wide. Beyond the coastline, on the continental shelf, the troughs shallow and broaden, reaching depths of ~200 m below sea level and widths of 11 to 38 km). The fjords and troughs often follow a dendritic pattern, with several fjords converging in a single trough on the middle and outer continental shelf edge. Although mapping at a regional scale is sparse, the 27,000 km<sup>2</sup> of fjord floors for which relatively high-resolution multibeam echo-sounder data are available contain a landsystem assemblage that has been interpreted to represent a climatically mild, meltwater-dominated fjord setting (Dowdeswell and Vásquez,



2013). Such meltwater-dominated systems are characterised by relatively rapid delivery of fine-grained sorted sediments from meltwater plumes emanating from tidewater-glacier termini and glaciofluvial systems where ice does not reach the sea (Dowdeswell and Vasquez, 2013).

Where fjord floors have been mapped in detail using multibeam echo-sounders, transverse moraine ridges, glaciofluvial and fluvial deltas and turbidity-current channels have commonly been identified (Dowdeswell and Vasquez, 2013) (Figure 9B-D). The moraine ridges are relatively large and are interpreted to represent still-stands of tidewater glaciers during deglacial retreat through the fjord systems of western Patagonia (e.g. Dowdeswell and Vasquez, 2013; Lastras and Dowdeswell, 2016); the broad ridges often protrude through and are draped by Holocene basin-fill (e.g. DaSilva et al., 1997; Boyd et al., 2008). Several moraine ridges are located at the mouths of fjords, which represent likely pinning-points where water deepens by tens to hundreds of metres immediately beyond the ridges (Dowdeswell et al., 2016c). Streamlined subglacial landforms are rarely observed, probably because relatively high rates of Holocene sedimentation after regional deglaciation have buried any subglacially produced landforms under several tens of metres of fine-grained sediment derived from fluvial and glaciofluvial rivers that reach the sea and built prominent deltas (Boyd et al., 2008; DaSilva et al., 1997; Dowdeswell and Vasquez, 2013; Fernández et al., 2012).

Well-developed turbidity-current channels have been mapped in several fjords, appearing to emanate from relatively steep delta fronts (Dowdeswell and Vasquez, 2013). Turbidity-current activity probably continues today, an inference supported by the observation that such channels remain unburied by Holocene sedimentation. The irregular seafloor depressions produced by the ploughing action of iceberg keels, so typical of most glacier-influenced continental shelves (e.g. Lopez-Martinez et al., 2011), are almost absent from the floors of Patagonian fjords despite the presence of calving tidewater-glacier termini. This is probably because heavily crevassed tidewater glaciers, such as Jorge Montt, Tempango and Pio XI (Warren and Aniya, 1999), produce only small icebergs of irregular shape and with shallow keels, similar to many Northern Hemisphere tidewater glacier settings (e.g. Dowdeswell and Forsberg, 1992). These small icebergs rarely ground in the deep fjords of Patagonia and are therefore unable to plough the seafloor.

The fjordlands of Chilean Patagonia represent the mildest climatic and oceanographic end-member of a continuum of glacier-influenced marine settings where ice reaches the sea today (Dowdeswell and Vasquez, 2013); an environment somewhat similar to south-east Alaska in the Northern Hemisphere where glaciers accumulate in mountain ranges and typically have a large altitudinal range and high mass throughput (Cai et al., 1997; Powell and Molnia, 1989). Fjords and associated trough systems similar to these have been observed on the continental shelf around South Georgia (Graham et al., 2008), the Antarctic Peninsula continental shelf (Ó Cofaigh et al., 2014), and in West Antarctica (Ó Cofaigh et al., 2005). They are interpreted to have been formed by palaeo-ice streams during periods of Quaternary glacial maxima. The

cross-shelf troughs on the Patagonian continental shelf appear to show over-deepening by glacial erosion in the inner shelf, with depths decreasing seaward, in a similar way to those observed on other continental shelves (Batchelor and Dowdeswell, 2014). On the basis of their morphology, cross-shelf alignment, connection to present-day fjords and characteristically deep fjord bathymetry, we interpret the probable origin of these troughs as a product of enhanced glacial erosion during periods of past glacial maxima. Cross-shelf trough systems in other locations have been associated with trough-mouth fans (Ó Cofaigh et al., 2003), but the resolution of the GEBCO 2019 dataset does not allow the identification or otherwise of fans on the western Chilean outer-shelf and upper-slope of what is a very active continental margin where rapid sediment transfer down-slope by mass-wasting may in any case limit fan growth.

*Figure 9. Examples of marine glacial geomorphology around Patagonia. A: Cross-shelf troughs on the Patagonian continental shelf. Yellow stars indicate location of panels B-D. B: Terminal moraine ridge, transverse ridges and streamlined lineations associated with Tempango Glacier, Southern Patagonian Icefield. C: Swath bathymetry of the 100 m high recessional moraine in Europa Fjord. D: Glaciofluvial delta in Bernardo Fjord, with a braided river. Bernardo Glacier is just to the southeast of the image. Adapted from Dowdeswell et al. (2016c).*

## 5 PATICE Reconstruction (35 – 0 ka)

This section provides brief summaries of the geomorphological and chronological data that underpin our ice sheet reconstruction, followed by the results of our 5 ka reconstructions from 35 ka to present. For simplicity, we have sub-divided the former PIS into six key sectors spanning the full latitudinal range of the study area from 38°S to 56°S (Figure 10). From north to south, we refer to these as: Chilean Lake District (38° – 42°S), Isla de Chiloé and Archipiélago de los Chonos and the adjacent mainland (42° – 46°S), Northern Patagonian Icefield sector (46° – 48°S), Southern Patagonian Icefield sector (48° – 52°S), Gran Campo Nevado sector (52° – 53°S) and Cordillera Darwin sector (53° – 56°S).

*Figure 10. Location of six key sectors of the former Patagonian Ice Sheet and distribution of selected landforms and all published ages used in this study.*

### 5.1 The Chilean Lake District (38 – 42°S)

#### 5.1.1 Present-day characteristics

The Chilean Lake District owes its name to numerous glacially derived lakes in the “Valle Central”, located between Cordillera de la Costa to the west and the Andes to the east (Moreno et al., 1999) (Figure 11). The

region has a highly maritime climate, with a pronounced west-east precipitation gradient. Precipitation reaches  $3 \text{ m a}^{-1}$  near the coast (Aravena and Luckman, 2009), but data are limited at higher altitudes (Paul and Mölg, 2014). Seno Reloncaví, a seaway, forms the southernmost boundary of the Chilean Lake District (Figure 2; Figure 11). Mountains and volcanoes reach 1,800 - 2,500 m asl (lower than the peaks in the Patagonian icefields), except for the more substantial extinct stratovolcano Mount Tronador (3,500 m asl), and isolated peaks are capped by small snowfields (Figure 11). Glaciers on these mountains are topographically controlled, with steep slopes allowing only limited accumulation and small glaciers (Paul and Mölg, 2014). Where plateaux allow greater accumulation, icefields are able to form; e.g. in Mount Tronador.

The great majority of these mountain glaciers are presently shrinking (Bown and Rivera, 2007; Braun et al., 2019; Davies and Glasser, 2012; Rivera et al., 2005), driven by decreasing precipitation and upper atmosphere warming. The active volcanic centres frequently cover the glaciers with ash layers, which may insulate the glaciers and reduce ablation (Adhikary et al., 2002; Rivera et al., 2005), although geothermal heating may also enhance basal melt (Rivera et al., 2006). These northerly glaciers tend to be higher, steeper and smaller than the more southerly glaciers and icefields, and may therefore have relatively rapid response times and steep mass balance gradients (Davies and Glasser, 2012).

*Figure 11. Location of glaciers and published geomorphology and chronological data (MIS 3 to present) constraining ice mass extent in the Chilean Lake District (38°S – 42°S) (data from Andersen et al., 1999; Bentley, 1997; Davies and Glasser, 2012; Denton et al., 1999; Glasser and Jansson, 2008; Heusser et al., 1999; Mercer, 1976; Moreno et al., 1999; Porter, 1981). Isochrones are labelled with blue numbers.*

#### 5.1.2 Evidence for glaciation

Deposits of the last glaciation (the “Llanquihue Glaciation” of Heusser, 1974) have allowed reconstruction of numerous smaller and four larger piedmont lobes in the western Chilean Lake District (Denton et al., 1999; Lowell et al., 1995; Mercer, 1972; Moreno et al., 2015; Porter, 1981), which excavated deep depressions that are today infilled with lakes (Figure 11). These lakes are surrounded by extensive inset moraines (Bentley, 1996). At their maximum extents, the icefields were confined to the valleys, and expanded laterally onto the plain. The moraine belts feature ridges (10–20 m relief), hummocky terrain, outwash plains outside the moraine limits and prominent kame terraces inside the moraines alongside Lago Llanquihue and northern Seno Reloncaví (Andersen et al., 1999; Denton et al., 1999; Moreno et al., 2015). Other landforms include ice-contact slopes (30-80 m high), and ice-marginal meltwater channels with spillways at the head of the ice-contact slopes. Geomorphological mapping of moraines north of Lago Puyehue indicates that the glaciers in

the northern Lake District also formed smaller piedmont lobes on the plain west of the Andes at the LGM (Andersen et al., 1999; Denton et al., 1999; Glasser and Jansson, 2008; Glasser et al., 2008).

Moraines around Lago Llanquihue and Seno de Reloncaví are largely composed of stratified glaciofluvial deposits, over-thrusted on their proximal flanks by clay-rich diamictos (Bentley, 1996). Water-saturated, fine, impermeable sediments in the lake basins may have facilitated glacier advance even with negligible ice-surface slope by encouraging sedimentary deformation at the ice-bed interface (Bentley, 1996, 1997; Heirman et al., 2011).

Seismic stratigraphy obtained from Lago Puyehue has revealed a complex sedimentary infill, comprising morainic, ice-contact or outwash deposits, glaciolacustrine sediments, with sediments deposited by underflows from sediment-laden meltwater streams, reflecting the deglacial evolution of the lake basin (Charlet et al., 2008; Heirman et al., 2011).

Morphostratigraphic analysis suggests that there are three age groups of moraines relating to these piedmont ice lobes. The youngest two groups have well-preserved morphology, separated by morphologic breaks and weathering differences. The outermost moraines are more weathered and have subdued expression, and are presumed to be older (Andersen et al., 1999; Denton et al., 1999). These moraines are thoroughly dated with radiocarbon, and we include 452 of these ages in our database (Andersen et al., 1999; Denton et al., 1999; Moreno et al., 2015). Other ages are excluded as they are not as relevant to our reconstruction. Many of these radiocarbon ages are given a reliability rating (see Section 3.3) of 2 rather than 3 as they date bulk material, have  $\delta^{13}C$  values outside of the ideal range, or have an unclear stratigraphic or geomorphic context.

As the chronology here is based on stratigraphy, dating of organics interbedded with till deposits and outwash, it is challenging in places to relate this directly to specific ice margins or moraine sets. The stratigraphy here indicates that the Andean piedmont glaciers achieved glacial maxima numerous times during MIS 4, 3 and 2 (Moreno et al., 2015). This stratigraphic framework is reviewed thoroughly by Moreno et al. (2015) and readers are referred to that publication for more details. The key evidence for the timing of glaciation at Lago Llanquihue is now summarised below.

At “Site 3” (Puerto Octay) (Figure 12), at the top of an ice-contact slope that rises above Bahía Octay of the lake, an outwash slope rests on organic-rich pyroclastic deposits. The outwash slope would have been formed by a glacier positioned at the upper crest of the ice-contact slope (Denton et al., 1999). Radiocarbon dating of organic samples from underneath these outwash sediments yielded a mean age of  $33.6 \pm 0.2$  cal. ka BP (Moreno et al., 2015; Denton et al., 1999).

At “Site 4” (Bahía Frutillar Bajo; Figure 12), flow till rests on a land-surface developed on a pyroclastic flow, near the top of an ice-contact slope (Denton et al., 1999; Moreno et al., 2015). Radiocarbon ages on wood and organics below the flow till yield a mean age of  $30.8 \pm 1.0$  cal. ka BP, indicating that the glacial advance that deposited the flow till post-dated this time (*ibid.*).

The Llanquihue moraine belt around Lago Llanquihue is further dated by maximum-limiting radiocarbon ages from organic clasts reworked into outwash that grades from the moraine ridges (Sites 8, 9, 10, 11; Figure 12). These organic clasts yielded mean ages of ranging from 26.2 to 29.3 cal. ka BP (Denton et al., 1999; Moreno et al., 2015). Minimum-limiting ages are derived from lakeside ice-contact slopes, with organic-rich fills at Canal de la Puntilla (Site 1) and Canal de Chanchán (Site 12) dating from 24.2 to 24.8 cal. ka BP. Site 13 provides another minimum-limiting age of  $23.79 \pm 0.31$  cal. ka BP.

The youngest advance of the Llanquihue ice lobe into its lake reached the innermost ice-contact slope of the Llanquihue moraine belt, where it deposited a large kame terrace, which rests conformably on organic deposits. At Site 18, these uppermost organics samples yielded a mean age of  $18.03 \pm 0.81$  cal. ka BP (Moreno et al., 2015). At Puerto Varas (Sites 19, 20, 16, 17), intact peat is overlain by kame terrace sediments, and yields mean radiocarbon ages of 17.70 to 18.10 cal. ka BP (Denton et al., 1999; Moreno et al., 2015).

Further south, the Seno de Reloncaví lobe is dated at “Site 5”, where wood and fibrous peat from the upper surface of an organic bed is overlain by outwash that is, in turn, overlain by the Llanquihue moraines. The meltwater that deposited this outwash emanated from an ice lobe that reached an ice-contact slope above Seno Reloncaví (Moreno et al., 2015), and which then advanced over the outwash. The organic material underneath the outwash yielded mean radiocarbon ages of  $26.89 \pm 0.17$  cal. ka BP (Denton et al., 1999).

At “Site 7” (Puerto Montt, Seno Reloncaví; Figure 12), a road-cutting section in the Llanquihue Drift shows glacial sediments resting on pyroclastic flow deposits. Organic material on the pyroclastic flow land-surface is preserved underneath the glacial diamicton (Moreno et al., 2015). The stratified, gravelly diamicton is interpreted as gravel-rich sediment-flow deposits from a nearby ice margin, and it is capped by a layer of lodgement till (Denton et al., 1999). Radiocarbon ages from wood from the preserved organic material provide a mean age of  $26.0 \pm 0.7$  cal. ka BP, indicating that ice advance predated this time.

*Figure 12. Map showing numbered key palynological and stratigraphic sites (large filled yellow circles) named in the text in the Chilean Lake District. After Moreno et al., 2015.*

Glacier recession early in the Last Glacial-Interglacial Transition is documented further north, where Volcán Villarrica has generated several large explosive eruptions (Moreno et al., 2015). One eruption early in the

Late Glacial led to the emplacement of the Cucido pyroclastic flow and resulting Licán ignimbrite, with the latter being found up to 40 km away from the volcano, covering an area more than 1000 km<sup>2</sup> in size. The Villarrica and Calafquén outlet lobes (Figure 11) here form well-defined arcuate moraine systems and extensive outwash plains west of their lake basins (*ibid*). The Licán ignimbrite mantles these LGM moraines and also extends as tongues into the Andean valleys. The distribution of the Licán ignimbrite shows that the Villarrica and Calafquén outlet lobes had receded deep into the Andes by the time of the eruption, which has a mean age of  $16.8 \pm 0.1$  cal. ka BP (Moreno et al., 2015; Figure 11). This indicates extensive deglaciation of the northern Chilean Lake District prior to  $16.8 \pm 0.1$  cal. ka BP.

East of the Andes, moraines indicated a more restricted ice extent (Glosser and Jansson, 2008; Tatur et al., 2002). Three morainic arcs with ridge crests up to 100 m high enclose the eastern end of Lago Nahuel Huapi, with the inner moraines purportedly marking the end of the Last Glaciation (Tatur et al., 2002). An ice-dammed lake (Palaeolake Elpalafquén and later Palaeolake Nahuel Huapi; del Valle et al., 2000) in this valley is evidenced by post-glacial lacustrine beaches that eroded the inner slopes of the terminal moraines, with strandlines and fluvio-glacial plains located up to 100 m above present lake level.

### 5.1.3 Ice-sheet reconstruction

Most chronological constraints are focused on radiocarbon dating of the moraines around Lago Puyehue, Lago Llanquihue and Seno de Reloncaví (Figure 11) (Andersen et al., 1999; Bentley, 1997; Denton et al., 1999; Heusser et al., 1999; Lowell et al., 1995; Moreno et al., 1999). In the northern Lake District, a lack of dating control makes determining ice extent problematic; ice extents at 35, 30, 25 and 20 ka are therefore assumed to be coeval (Figure 13). Denton et al. (1999) and Moreno et al. (2015) argued that radiocarbon ages from the piedmont lobes of the southern Lake District show recurrent expansions of the glaciers to the piedmont lobe moraines at 33.5, 30.8, 26.9, and 26.0 cal. ka BP (Figure 11). They provide a clear stratigraphic record for ice expansion; however, as the chronology is related to stratigraphy rather than directly dating the moraines, the different ice extents at each time are difficult to map. The Seno de Reloncaví outlet lobe is well constrained at the LLGM, with maximal extent at the outer moraines at 35 – 30 ka (Denton et al., 1999), and recession to the current shoreline of the embayment by 20 ka (Porter, 1981).

The youngest advance into the Llanquihue moraine belt occurred at 17.7 – 18.1 cal. ka BP (Moreno et al., 2015). By 16.8 cal. ka BP, ice had retreated from the over-deepenings to the higher ground (Moreno et al., 2015), forming an icefield over the mountains that today sustains only small glaciers. This reconstruction agrees with Bertrand et al. (2008), based on their extrapolated age model from radiocarbon dates from a core from Lago Puyehue. Bentley (1997) demonstrated that the lake was ice-free by  $14.1 \pm 0.8$  cal. ka BP,

although the lake could have been ice-free before this date. By 10 ka, we assume further recession, with most mountain ice caps disappearing by 5 ka; however, these Holocene reconstructions have a *low confidence*. More data are sorely needed at the highest elevations of the northern Lake District on post-glacial changes.

*Figure 13. Reconstruction of glaciers and outlet lobes of the Chilean Lake District. Relative sea level data from Guilderson et al. (2000), symbolised using GEBCO topographic and bathymetric data. Shading is illustrative only and does not represent ice thickness. Inferred ice-flow lines (yellow) are shown for 35 ka in this and subsequent reconstruction figures.*

Palaeolake Elpalafquen encompassed both Lago Nahuel Huapo and Lago Mascardi (del Valle et al., 2000). As the present-day Lago Nahuel Huapi (altitude 770 m) drains toward the Atlantic, this lake was likely dammed by moraines. Around 13 ka BP, Palaeolake Elpalafquen became several smaller lakes, including Palaeolake Nahuel Huapi. In order to encompass both Lago Nahuel Huapo and Lago Mascardi, we reconstruct Palaeolake Elpalafquen at 15 ka at 850 m asl, covering ~470 km<sup>2</sup>. Drainage from Lago Mascardi to the south and west must remain dammed by ice at this time. At 13 ka we reconstruct a smaller ice mass that allows drainage of Palaeolake Elpalafquen and the formation of Lago Mascardi and Lago Nahuel Huapi at 770 m asl. We give both the 15 ka and 13 ka ice margins here a *low confidence* and highlight this as an area for further work (Figure 13).

## 5.2 Isla de Chiloé and Archipiélago de los Chonos and adjacent mainland (42°S – 46°S)

### 5.2.1 Present day characteristics

The Isla de Chiloé-Archipiélago de los Chonos sector comprises the mainland Chiloé region, and the two large archipelagos to the west of the Andes (Figure 14). The Andes are over 2000 m asl in this sector and host occasional ice caps, e.g. Cerro Barros Arana (43.9°S) and Macizo Nevado (García, 2012). Water maximum depth between Isla de Chiloé and the mainland to the east is greater than 400 m.

Isla de Chiloé is located at the northern margin of the SWW belt and the ACC, with a steep thermal latitudinal gradient between the ACC and the northward Humbolt Current (Lamy et al., 2004). Isla de Chiloé is separated from the mainland by the Golfo de Ancud and Golfo de Corcovado (Figure 14).

*Figure 14. Location of glaciers and lakes, and chronological and geomorphological evidence for glaciation (MIS 3 to present) in Isla de Chiloé and Archipiélago de los Chonos sector (42°S – 46°S) (Andersen et al., 1999; Caldenius, 1932; Davies and Glasser, 2012; Denton et al., 1999; Douglass et al., 2006; Dowdeswell et al.,*



2016c; García et al., 2019; García, 2012; Glasser and Jansson, 2008; Glasser et al., 2016b; Haberle and Bennett, 2004; Heusser et al., 1999; Lastras and Dowdeswell, 2016; Lowell et al., 1995; Stern et al., 2015; Moreno et al., 2015; Van Daele et al., 2016; Weller et al., 2015). See Figure 15 for more detail in the Río Cisnes valley. Pink crosses indicate uncertainty weighted mean ages for boulder exposure ages. Isochrones are labelled in blue writing.

### 5.2.2 Evidence for glaciation

The western coastal margin of Isla de Chiloé is the southernmost terrestrial area of the western side of Patagonia that remained ice free at the LGM. The island is characterised by deep, wide glacial valleys (Glasser et al., 2008). Moraine evidence in this area consists of extensive south – north oriented belts extending for more than 50 km (Figure 14), contrasting in form with the piedmont lobes of the Chilean Lake District to the north (García, 2012). The moraine belts record westward advances of the Golfo de Ancud and the Golfo de Corcovado lobes from the Andes (Denton et al., 1999). The glacial landscape comprises different generations of landforms, such as sharp-crested moraines, hummocky moraines with irregular, low-relief topography, outwash plains, and meltwater channels and spillways (García, 2012; Anderson et al., 1999). In the eastern foothills of Cordillera de La Costa, streamlined bedrock is evident. In the eastern parts of Isla de Chiloé, till flutings trending NWW are apparent. The region is covered with subglacial tills, with clasts of Andean origin. Radiocarbon ages (Denton et al., 1999; García, 2012; Heusser et al., 1999) allow us to place the ice margin on eastern Isla de Chiloé from 35 – 25 ka. It remains unknown when the ice buttressed against Cordillera de la Costa and built the westernmost Llanquihue moraines and associated principal outwash plains (García, 2012). Moreno et al. (2015) and Denton et al. (1999) also show an advance here at 18 ka. South of Dalcahue on Isla de Grande Chiloé (Figure 14), the 17.8 cal. ka BP advance may have been the most extensive.

At “Site 6” (Teguaco; Isla de Chiloé Figure 12), organic material from a gyttja layer is overlain by glaciolacustrine silt and clay (Denton et al., 1999; Moreno et al., 2015). These sediments were deposited in a palaeolake dammed by the Golfo de Corcovado outlet lobe when it advanced onto the eastern flank of Isla Grande de Chiloé (*ibid.*). The organics yield a mean radiocarbon age of  $26.8 \pm 0.2$  cal. ka BP for flooding by the ice-dammed lake (Denton et al., 1999).

On Archipiélago de los Chonos, Bennett et al. (2000) and Haberle and Bennett (2004) obtained bulk basal radiocarbon ages from a series of small lakes across the archipelago (Figure 14). These data suggest that the islands were ice-covered during the LLGM, but that they were ice-free as early as  $19.4 \pm 0.9$  cal. ka BP.

On the eastern side of the Andes, the Epuyen Valley lobe contains some of the earliest records of glaciolacustrine varve analysis (Caldenius, 1932). Here and in the neighbouring Cholila Lobe, a series of flat-topped deltas and rhythmically laminated silts and clays inside terminal moraines evidence a post-LGM



glacial lake. Lago Epuyen drains into Lago Puelo and out to the Pacific Ocean through Río Puelo; during deglaciation, this drainage route was blocked, causing the formation of the ice-dammed lake. Caldenius (1932) suggested that this ice-dammed palaeolake was extant between the terminal moraine crests and the eastern end of the current Lago Epuyen, meaning that this lake occupied the eastern half of Epuyen valley. Currently chronology for this is lacking, but Caldenius (1932) estimated that the lake was extant for about 200 years. The surface elevation of the lake is also uncertain. Caldenius (1932) also described a glaciolacustrine terrace with a width of 200 m, cut to a height of 550 m. Contour analysis suggests that the col for drainage eastwards to the Atlantic lies at 660 m asl, and the palaeochannel for this spillway is clearly visible on satellite imagery. A height of 660 m asl corresponds with deltas mapped in our study from high-resolution satellite imagery. We reconstruct a 660 m asl glacial lake at 20 ka, as the 15 ka ice sheet is presumably too far receded to block the drainage pathway at 15 ka (although this requires further testing).

Caldenius (1932) also reconstructed a palaeolake in the adjacent Corralillo Lobe. Again, this is evidenced by a series of flat-topped terraces within the terminal moraines, and abandoned palaeochannels demarking the outflow from the palaeolake to the current Atlantic drainage. The col through the terminal moraines lies at 700 m asl, which fits with the height of flat-topped deltas mapped by the authors in this valley.

In the Río Pico valley, four sets of moraines were mapped by Beraza and Vilas (1989) and Lapido (2000), all of which have normal polarity magnetisation and are therefore younger than the Brunhes Palaeomagnetic Chron (i.e. younger than 0.78 Ma) (Rabassa et al., 2011). The innermost 'Las Mulas' drift has previously been attributed to the LGM; however, a sediment core from a small intermorainic lake, Laguna La Pava, 12 km to the east of this, within the Trenenhau drift moraines, yielded a basal radiocarbon age of  $15 \pm 0.5$  cal. ka BP (Iglesias et al., 2016) (Figure 14; Figure 15), suggesting that the LGM limit was actually further east. We place the ice limit at 30 ka at the Chergue drift, with low confidence; this is in keeping with the ice extent reached in the valleys south of here with better chronological controls.

Several moraine belts in the Cisnes valley denote ice extent, with the outermost (CIS I and CIS II) denoting full glacial conditions (García et al., 2019; Figure 15). Basal radiocarbon ages from a core from Lake Shaman within the inner CIS II moraine belt suggest the CIS II moraines were free of ice by  $18.9 \pm 0.3$  cal. ka BP (minimum age; Figure 14; Figure 15). Ice-free conditions at this time are also indicated by the presence of the Ho tephra within the core, dated to 17.4 ka (Stern et al., 2015). There are several sets of moraines inset from these (de Porras et al., 2012). Rapid recession following the LGM is suggested by the presence of the Melimoyu tephra (19.7 ka) at Las Barrancas (Stern et al., 2015), 16.5 km southwest of Lake Shaman (Figure 15). The inner CIS III to V moraines represent still stands during ice retreat. Boulders on the CIS IV moraine dated by  $^{10}\text{Be}$  surface exposure dating (mean age 20.1, SD 0.9 ka) indicate that the ice had receded to the

central part of the valley by 20 ka (García et al., 2019) (Figure 15). This suggests a recession of some 35 km in the Río Cisnes valley between the LGM and 20 ka.

The PIS in this region dammed several lakes during deglaciation, when present-day drainage to the Pacific Ocean was obstructed (García et al., 2019). In the Cisnes valley, shorelines and fluvial terraces denote the palaeolake extent. There are two distinct shorelines at 950-920 m, and 860-850 m. The 920 m lake has a distinct col that leads to drainage towards the Atlantic Ocean. The 920 m lake was extant by 20 ka in front of the CIS IV moraine and likely later also, when the ice margin had receded to the central part of the valley (Figure 15) (García et al., 2019).

Further down the valley, a peat core from Mallín El Embudo (Figure 15A), with basal radiocarbon ages of  $12.9 \pm 0.1$  cal. ka BP (de Porras et al., 2014) allows the 15 ka isochrone to be inferred, showing recession of the ice lobe to the west at this time (Figure 15).

Further south, Palaeolake Nirehuao formed in front of the Lago Coyt outlet lobe, with an initial highstand of 740 m, draining towards the Atlantic. The timing of this highstand is unclear, and it could be earlier or later than 20 ka. Following further deglaciation, the Palaeolake Cisnes and Palaeolake Nirehuao united in both the Coyt and Cisnes valleys, likely by 15 ka, to form Palaeolake Cisnes-Nirehuao (Figure 15) at 660 m asl and draining towards the Pacific (García et al., 2019). García et al. (2019) suggested that this united lake could have formed during the ACR, but this awaits confirmation. Radiocarbon ages suggest that this united lake drained below 200 m asl by 12.1 to 12.4 cal. ka BP, and indicates that the ice masses had begun to fragment at this time.

Evidence of a proglacial lake at 20 ka in front of the Coyhaique outlet lobe (Palaeolake Frío) is present in the form of glacier-contact deposits and moraines (Van Daele et al., 2016). This lake outlet flowed to the east, with a likely altitude of 660 m asl and drainage most likely could have flowed south, around the ice margin, and into Palaeolake Balmaceda (Figure 15).

A series of moraines east of Coyhaique, with elevations of up to 867 m asl, mark the easternmost extent of the Coyhaique outlet lobe (Miranda et al., 2013). Bedforms are predominantly ice-scoured bedrock there, overlain by glaciolacustrine sediments from Palaeolake Balmaceda, which produced shorelines of up to 610 m asl in the Río Huemules valley. The col today is located at 585 m asl, indicating that lowering through moraine incision may have occurred (Figure 15). This palaeolake was likely extant at 20 ka, in agreement with radiocarbon ages presented by Miranda et al. (2013) (unfortunately, insufficient data is available to allow inclusion of these ages in our database), and numerous  $^{40}\text{Ar}/^{39}\text{Ar}$  tephra ages (Weller et al., 2015). The lake is likely to have disappeared by 15 ka with the fragmentation of the ice masses and the opening of the drainage route to the Pacific (Figure 15). The spillway that would drain this lake sits at 585 m asl.

In the western mainland, in Aysén Fjord at 45° 22'S, two major submarine ridges have been mapped across the fjord; the Cuervo Ridge and the Colorada Ridge (Lastras and Dowdeswell, 2016). These ridges are located 25 and 54 km beyond the fjord-head delta at Puerto Aysén respectively (Figure 14). These undated ridges constrain the extent of a tidewater glacier in this fjord, likely originating from the mid to late Holocene.

*Figure 15. A: Detail of published ages and geomorphology in Río Cisnes valley (after García et al., 2019). B, C: Reconstructed glacial lakes (orange) of the Isla de Chiloé and Archipiélago de los Chonos sector at 20 ka and 15 ka respectively. Extent of Panel A is shown in Panel B. Shading of the ice sheet is illustrative only and is not related to ice thickness. Col spillways are shown as yellow stars with red labels.*

### 5.2.3 Ice-sheet reconstruction

The central part of Isla de Chiloé preserves the most extensive glacial advance at this latitude, with a double ice-contact slope in Cordillera de la Costa locations (García, 2012). The outermost moraines are more than 100 km from the Andean catchments, with ice infilling and crossing the Golfo de Corcovado basin. The Golfo de Corcovado lobe did not reach the Pacific Ocean, and no cirques or other glacial landforms are observed on Cordillera de La Costa, indicating that the west coast of northern Isla de Chiloé remained ice-free at the LGM (Denton et al., 1999; García, 2012) (Figure 16). Further south, the western margin of the PIS extended offshore, and is poorly constrained.

In the northern part of the sector, the eastern outlet lobes are poorly dated, but their LGM positions are well marked with moraines, leading to *medium confidence* in the LGM ice extent, if not the exact timing (Figure 16). Although ice extent is well constrained in the Cisnes valley, other lobes lack chronological control for post-LGM recession. Separation of the ice masses by 20 ka is indicated by the lower cols becoming occupied by the palaeolakes, and the drainage of palaeolake Balmaceda and Frío. The palaeolakes drained by 10 ka (García et al., 2019), suggesting a smaller ice mass confined to the higher ground, but we have *low confidence* in ice extent at 15, 10 and 5 ka (Figure 16).

Further south and east of the Andes, ice lobes immediately to the north of the Northern Patagonian Icefield, such as the Balmaceda, Paso Coyhaique and Lago Coyt outlet lobes, have mapped moraines (Glasser and Jansson, 2008) but are poorly constrained chronologically (Figure 14). As is the case further south, it is likely that the outermost moraines of these systems represent an earlier Pleistocene maximum, rather than the LLGM. We tentatively assume that the LLGM (no distinction made from 35–20 ka due to limitations in published ages) is located at the eastern-most of the inner moraines. However, in the absence of quantitative data, confidence in the precise location of the ice limits at each time-slice is low. These ice lobes

are therefore identified as a key target for future research. There is very little published data available constraining the Holocene dynamics of these glaciers.

The Paso Coyhaique outlet lobe has no chronological control associated with the outermost moraines, but a series of cores from small lake basins around 20 km east of the town of Coyhaique yielded the Holocene tephras (17.4 ka) and basal radiocarbon ages of  $17.8 \pm 0.5$  to  $17.9 \pm 0.3$  cal. ka BP (Weller et al., 2015) (Figure 14). A sediment core from Lago Castor suggests that the area was ice-free by 28 cal. ka BP, but radiocarbon dating was inconclusive (Van Daele et al., 2016), and the area being ice free this early is unlikely given the extensive ice cover demonstrated in nearby ice lobes.

The fjord between Isla de Chiloé and the mainland is ice free at 20 ka (Figure 16) due to radiocarbon ages from the coast of Isla de Chiloé indicating ice-free conditions at  $16.3 \pm 0.8$  cal. ka BP (Haberle and Bennett, 2004). However, moraines further south on the Taitao Peninsula suggest that ice persisted, perhaps in the central or higher parts of the island, at this time. We suggest that the deep fjord between the island and the mainland precipitated calving and the separation of the ice masses. However, our reconstruction here has low confidence. We suggest that the northern Isla de Chiloé is ice-free by our 15 ka timeslice.

Limited data constraining mid-Holocene ice dynamics is available for this region. The Late Holocene 0.2 ka advance is constrained by lichenometry and historical photographs from Torrecillas Glacier at 42.7°S, which indicate that a series of nested, fresh-looking moraines date from 1735 AD to 1906 AD (Garibotti and Villalba, 2009).

*Figure 16. Ice sheet reconstruction for Isla de Chiloé and Archipiélago de los Chonos, showing palaeolake development (orange) at 20 and 15 ka. Relative Sea Level data from Guilderson et al. (2000), symbolised using GEBCO topographic and bathymetric data. For more detail see Figure 15. Shading is illustrative only and does not represent ice thickness.*

### 5.3 The Northern Patagonian Icefield (46°S – 48°S)

#### 5.3.1 Present-day characteristics

The Northern Patagonian Icefield stretches for 120 km along the spine of the Andes, from 46°30'S to 47°30'S (Figure 17). It is 70 km wide at its widest, has a mean altitude of 1,340 m asl, and covers 3,976 km<sup>2</sup> (Davies and Glasser, 2012). It contains 1,235 km<sup>3</sup> of ice, with a sea level equivalent of 3.1 mm (Carrivick et al., 2016). It is the largest icefield at this temperate latitude in the Southern Hemisphere. The central high plateau, located on the Andes mountain range, is drained by large outlet glaciers mainly orientated west and east. At present, of the 44 outlet glaciers directly draining the Northern Patagonian Icefield, 26 terminate in lakes, 1 terminates in a tidal lagoon (Glaciar San Rafael) and the rest terminate on land (Glasser et al., 2016a)

(Figure 17). Ice thicknesses reach 1 km for Glaciar San Rafael and Colonia (Gourlet et al., 2016); these bedrock troughs drive fast ice flow to the ice margin. Bed elevation for Glaciar San Rafael reaches sea level.

Between 1987 and 2015 the NPI has undergone substantial changes, including area decreased from 4133 km<sup>2</sup> to 3887 km<sup>2</sup>, while debris-covered ice area increased from 246 km<sup>2</sup> to 311 km<sup>2</sup>. The area occupied by proglacial and ice-proximal lakes increased from 112 km<sup>2</sup> to 198 km<sup>2</sup>. Between 1987 and 2015, the terminal environment of many of the outlet glaciers of the NPI changed from land-terminating to lake-calving, enhancing calving and ablation. The increase in debris cover also increases ablation. The ELA has risen 100 m from 1979 to 2003 (Glasser et al 2016a).

*Figure 17. The Northern Patagonian Icefield and the present-day large lakes dammed against high ground in Argentina. Lago GCBA and Lago CP both drain into Río Baker, which flows westwards into the Pacific Ocean. Key moraines and places named in the text are shown.*

Today, the outlet glaciers of the Northern Patagonian Icefield are receding, with the highest rates of recession in small, land-terminating glaciers (Aniya and Enomoto, 1986; Davies and Glasser, 2012; Meier et al., 2018). Overall, annual rates of recession have increased, with the highest rates of annual area loss observed between 2001 and 2011. Northern Patagonian Icefield glaciers are also thinning (Braun et al., 2019; Jaber et al., 2016), with the highest rates observed at Glaciers Steffen and HPN2 between 2000 and 2014 AD. Glaciar San Rafael is a major outlet glacier on the northwestern side of the Northern Patagonian Icefield and currently drains about 20% of the area of the icefield (Rivera et al., 2007). The glacier terminates in the tidal Laguna San Rafael at 46° 40'S, 73° 55'W, and is the only contemporary tidewater outlet glacier of the Northern Patagonian Icefield and the lowest latitude tidewater glacier on Earth (Warren et al., 1995).

Monte San Lorenzo (MSL) (47° 35'S, 72° 18'W) is situated on the eastern flank of the Andean range, located ca 70 km east of the southern point of the Northern Patagonian Icefield, on the border between Chile and Argentina (Figure 17). At 3,706 m asl it is the third highest peak in the Patagonian Andes (Masiokas et al., 2009b). Up to 102 ice bodies have been mapped on MSL, covering an area of 139.34 km<sup>2</sup> (Falaschi et al., 2013). Alongside Sierra de Sangra to the south (see Section 5.4), these represent the most significant ice masses east of the main Patagonian Icefields, and they may have formed independent ice domes that coalesced with ice coming from the main ice sheet during the LGM (Davies et al., 2018).

### 5.3.2 Evidence for glaciation

The eastern Northern Patagonian Icefield sector has been a strong focus for research, with perhaps the best-constrained PIS outlet lobes during the LGM and Holocene. During glaciations, the Northern Patagonian Icefield was drained to the east by two large outlet lobes: the Lago General Carrera/Buenos Aires (Lago GCBA) lobe, and the Lago Cochrane/Pueyrredón (Lago CP) lobe (Figure 17). The outlet glaciers of the Northern Patagonian Icefield overwhelmed topography and extended far into the foothills. The lobes were separated by flat-topped volcanic mesetas that reach elevations of more than 2,000 m (Caldenius, 1932; Wenzens, 2003). As the land rises farther east of the Andean mountain range, the outlet glacier lobes had a reverse-bed gradient near the terminus positions (Kaplan et al., 2009; Thorndycraft et al. 2019b); hence englacial and subglacial flow were effectively uphill (Barr and Lovell, 2017).

The Lago GCBA outlet lobe is separated from the Lago CP outlet lobe at their maximum extents by Meseta del Lago Buenos Aires (Figure 17; Figure 18), which reaches heights of up to 2300 m asl. This meseta, which covers around 6000 km<sup>2</sup>, is one of the largest basaltic plateaus within the Neogene Patagonian plateau lava province (Wolff et al., 2013). This volcanic plateau lacks geomorphic evidence of glaciation and likely remained largely unglaciated during the last glaciation, save for the Meseta Cuadrada Palaeo Ice Cap on the highest ground (Figure 17), which covered 78 km<sup>2</sup> (Wolff et al., 2013). In the Lago CP valley, mid-Pleistocene glaciers imprinted lateral moraines on the sides of Meseta del Lago Buenos Aires (Figure 18). The best evidence for Mid-Pleistocene and pre-LGM glaciation in Lago GCBA is derived from the lateral moraines; terminal moraines here are heavily eroded by outwash and meltwater systems, which were funnelled along the Moreno scarp and down the Desierto River. During the last glacial cycle, the Local LGM ice extent was reached at ca 35 to 30 ka, well inside the Pleistocene maximum extent (Hein et al., 2009, 2010; Coge et al., 2018). The LGM terminal moraines for Lago GCBA lie at 500 to 600 m asl.

Closer to the ice divide, a small mountain range east of the Northern Patagonian Icefield (Reserva Nacional Lago Jeinemeni), with summits up to 2,000 m asl, divided the major Lago GCBA and Lago CP outlet lobes at the LGM, with substantial and well dated ice limits to the north and south of these mountains. These mountains bear small valley glaciers with numerous down-valley moraines today (Glasser and Jansson, 2008) (Figure 17; Figure 18). An ice divide was likely centred across the icefield, with ice flowing north to contribute to Lago GCBA outlet lobe and south to Lago CP outlet lobe during the LGM.

*Figure 18. Published geomorphology and ages (ka) of Northern Patagonian Icefield outlet lobes from 46°-48°S (data from Araneda et al., 2007; Bendle et al., 2017a; Bendle et al., 2017b; Boex et al., 2013; Bourgois et al., 2016; Davies and Glasser, 2012; Davies et al., 2018; Douglass et al., 2005, 2006; Fernandez et al., 2012; Glasser and Jansson, 2008; Glasser et al., 2006a, 2012, 2016b; Harrison et al., 2008, 2012; Hein et al., 2009, 2010, 2011, 2017; Kaplan et al., 2004, 2005; Lumley and Switsur, 1993; Martin et al., 2019; Mercer, 1976;*

*Nimick et al., 2016; Sagredo et al., 2016, 2018; Singer et al., 2004a; Smedley et al., 2016; Stern et al., 2016; Thorndycraft et al., 2019a; Turner et al., 2005; Villa-Martínez et al., 2012; Wenzens, 2005; Winchester et al., 2014). Red inset boxes A, B and C show location of Figure 19, Figure 21 and the central Río Baker valley, and Figure 23 respectively. Altitude and bathymetry as in Figure 17.*

East of the Northern Patagonian Icefield, major outlet glaciers advanced along reverse-bed slopes (Kaplan et al., 2009), resulting in the formation of large ice-contact proglacial lakes during periods of glacier recession (Bell, 2008, 2009; Bendle et al., 2017a; Bourgois et al., 2016; Glasser et al., 2016b; Hein et al., 2010; Heusser, 2003; Martinod et al., 2016; Turner et al., 2005; Tweed, 2011). The geomorphic evidence of these ice-dammed palaeolakes is substantial, comprising shorelines, terraces, raised deltas and glaciolacustrine sediments. The extent, palaeolake surface elevation and depth of ice-dammed palaeolakes was controlled by the location of ice dams relative to drainage cols and moraines, which became degraded and failed over time (Glasser et al., 2016b; Thorndycraft et al., 2019a). The spatial extent, elevation and timing of the palaeolake levels can therefore assist in identifying the location of outlet glacier ice fronts at particular times. A potential complication specific to palaeolake evidence is that, due to the large size of the former lakes, differential isostasy has resulted in gently dipping shorelines (Bourgois et al. 2016; Martinod et al. 2016; Thorndycraft et al. 2019; Turner et al. 2005), which differ from drainage col heights. For the same reasons, deltas of equivalent height at the far eastern and western ends are of different age. However, trends in shoreline uplift are now reasonably well quantified (Bourgois et al. 2016; Martinod et al. 2016; Thorndycraft et al. 2019) and most of the dated deltas cluster in the centre of former lakes (Glasser et al. 2016), where differential isostasy is less likely to cause error in the ages.

There are few geomorphological or chronological data available to the west of the NPI other than at the more accessible San Rafael and San Quintín ice lobes, largely due to the challenges in conducting fieldwork. Dense forest also makes remotely sensed geomorphological mapping challenging.

Below, we present the evidence for glaciation at each time-slice for the Northern Patagonian Icefield region. The evolution of palaeolakes in this region has been thoroughly reviewed by Thorndycraft et al. (2019) and here we follow their lake evolution model. This model argues that following post-LGM recession from the terminal moraines east of Lago GCBA and Lago CP, large ice-dammed lakes developed and drained eastwards towards the Atlantic Ocean. Ice in the Baker Valley and to the north of the Northern Patagonian Icefield initially impeded the westwards drainage of meltwater to the Pacific Ocean; however, pathways opened up through the course of deglaciation in response to outlet glacier recession.



### 5.3.3 Ice sheet reconstruction

#### 5.3.3.1 35 to 25 ka

Of the numerous moraines that fringe the eastern margin of Lago GCBA, the Fenix III to V moraines represent the LGM (Douglass et al., 2006) (Figure 18; Figure 19). Excluding outliers, Fenix V has a mean age of 28.0 (SD 1.8) ka (Kaplan et al., 2004), Fenix IV of 28.8 (SD 2.1) ka, Fenix III of 23.3 (SD 2.1) ka, and Fenix II of 22.9 (SD 1.4) ka (Douglass et al., 2006). Due to the abundance of ages, we can have *high confidence* in the location of the ice margin at 35 to 25 ka.

Lacustrine sediments between the moraines indicate that ice-dammed lakes infilled the gaps between moraines during glacier recession, and OSL ages of these sands support the ice extent reaching the Fenix moraines at ~30 ka (Smedley et al., 2016). Lateral moraines with a single exposure age ( $32.3 \pm 10.2$  ka) west of Chile Chico at 1,116 m asl provide data on ice-thickness at the LGM (Bourgois et al., 2016). Given that Lago GCBA is > 400 m deep (Murdie et al., 1998), this outlet lobe would have been 1500–1700 m thick at the LGM (Bourgois et al., 2016). At the eastern end of Lago GCBA, cosmogenic nuclide ages from Fenix II and III moraines (Douglass et al., 2006; Kaplan et al., 2004) indicate that the ice margin had receded ~4.5 km by 20 ka (Figure 18).

During the LGM, the Jeinemeni icefield contributed ice to the Lago GCBA outlet lobe (Figure 20). A larger valley glacier is also expected to have flowed east from this icefield. However, overall ice contribution to the Lago GCBA along valleys to the east was likely limited, due to the preservation of stratigraphically older latero-terminal moraines in the Lago GCBA valley. The development of these ice masses and their configuration through time is illustrated in Figure 20.

There is a nested series of moraines at the distal end of the Lago CP valley, recording ice extent there (Figure 17). The oldest and outermost moraines (Hatcher Limit and Canadon de Caracoles limit) yield mid-Pleistocene ages (Hein et al., 2009). The innermost moraines of this sequence, the Rio Blanco Moraines, yield progressively younger cosmogenic nuclide exposure ages. The outer Rio Blanco moraines have a mean age of 29.9 ka (SD 3.0). Boulders on the innermost Rio Blanco moraines yield mean ages of 24.7 ka (SD 0.4) to 21.0 ka (SD 1.0), with a youngest age of  $19.3 \pm 1.8$  ka (Hein et al., 2010). This suggests that the outer Rio Blanco moraines represent the local LGM limit, and that ice remained here until deglaciation began after 20 to 19 ka.

*Figure 19. Published ages and geomorphology, and named moraine sequences, for Lago General Carrera - Buenos Aires (Lago GCBA) (Bendle et al., 2017a; Bourgois et al., 2016; Douglass et al., 2006; Glasser et al., 2016b; Hein et al., 2010; Kaplan et al., 2004; Kaplan et al., 2005; Singer et al., 2004a; Smedley et al., 2016). Overlain on Landsat 7 ETM+ image “p231r092\_7f20010320\_z19\_ps742.tif” (acquired 20<sup>th</sup> March 2001).*



Landform evidence in the Chacabuco Valley provides a means to empirically test numerical simulations of ice thickness east of the current Northern Patagonian Icefield (Hubbard et al., 2005; Hulton et al., 1994). Moraines, periglacial/glacial trimlines, and glacially scoured bedrock on the valley flanks can be used to constrain vertical ice limits of the former PIS. Such landforms can also be readily dated using cosmogenic nuclide dating techniques. Boex et al. (2013) represents the only research to date aimed at reconstructing the upper limits of the LGM PIS. This work used valley side evidence related to the Lago CP Lobe to reconstruct changes in ice sheet thickness. The study used a 60 km west–east transect along the Chacabuco Valley, from Cerro Tamango (1,722 m) in the west, through Cerro Oportus (2,076 m) to Sierra Colorado (1,537 m) in the east. The research demonstrated that at the LGM (mean age for the Sierra Colorado lower limit being 12.8 ka, SD 1.9), the PIS in this area reached a maximum elevation of 1,100 m asl at Sierra Colorado, some 120 km from the ice-sheet centre. The summit of Cerro Oportus at over 2,000 m elevation was ice covered at this time, a similar altitude to that reached by the Lago GCBA outlet glacier at this longitude (Boex et al., 2013). The floor of the Lago CP valley here is ~150 m asl, suggesting that the ice mass was ~1,000 m thick at the LGM near Sierra Colorado.

At the LGM, outlet glaciers to the southeast of MSL converged in the Río Belgrano valley, extending *ca* 70 km from the main massif (Figure 17; Figure 20). The hypothesised LGM ice extent in this location is marked by the outermost terminal moraines (cf. Wenzel, 2003, 2005; Caldenius, 1932). However, dating control is poor, and we are unable to distinguish ice marginal fluctuations there between 35 – 20 ka. We therefore consider the LGM ice margin to be uncertain.

*Figure 20. Reconstruction of Northern Patagonian Icefield outlet lobes. Isochrones used in each time-slice reconstruction are shown in red. Development of ice-dammed palaeolakes is illustrated. Yellow stars indicate drainage cols for ice-dammed lakes. Relative sea level data from Guilderson et al. (2000), symbolised using GEBCO topographic and bathymetric data. Shading is illustrative only and does not represent ice thickness.*

#### 5.3.3.2 20 ka

After removing outliers, the mean ages of  $^{10}\text{Be}$  samples from the Fenix I and II moraines in the northernmost, more lateral parts, of the terminal moraine system have a mean age of 18.9 ka (SD 1.8). The nearby Menucos moraines have mean  $^{10}\text{Be}$  ages of 17.6 ka (SD 0.1) and 17.3 ka (SD 1.0) (Figure 19; Douglass et al., 2006). These cosmogenic ages are complemented by a  $994 \pm 36$  yr varve record from the Río Fenix Chico valley in eastern Lago GCBA (46.58°S, 71.07°W), which is anchored to the calendar-year timescale by the H tephra found *in situ* within the lake deposits, and related to the ages of the moraines through morphostratigraphy and Bayesian age modelling (Bendle et al., 2017a). Using a combination of varve

counting, tephrochronology and  $^{10}\text{Be}$  data yields a start age for the Fenix I moraines of  $18.8 \pm 6.2$  cal. ka BP, and an end age of  $18.1 \pm 0.2$  cal. ka BP. We note that the varve ages represent minimum ages due to the likely short delay in the onset of varve accumulation after retreat from moraines; the immediate ice-proximal area is too high-energy for the formation of varves (see Bendle et al., 2017a).

The onset of significant glacial recession in the Lago GCBA ice lobe and the early formation of an ice-dammed lake therefore occurred at  $18.0 \pm 0.1$  cal. ka BP, likely in response to a southward migration of the SWW (Bendle et al., 2019). By  $18.1 \pm 0.2$  ka, a palaeolake had formed between the LGM moraines and the receding ice mass in Lago GCBA (Figure 20) (Bendle et al., 2017a; Thorndycraft et al, 2019a; Turner et al., 2005). Recession accelerated from  $17.8 \pm 0.1$  cal. ka BP due to a lagged response in the Southern Hemisphere to the gradual ocean-atmosphere warming (Bendle et al., 2019). By  $17.4 \pm 0.1$  cal. ka BP, the Lago GCBA lobe had receded into a deepening proglacial palaeolake, encouraging calving losses and more rapid ice recession, evidenced by an increase in ice rafted debris in the varve record (Bendle et al., 2017a). The “Deseado” palaeolake reached a maximum height of 400 m asl and drained to the Atlantic Ocean via Río Deseado (Figure 22; Thorndycraft et al, 2019a). Palaeolake Deseado expanded due to ice-mass retreat for several thousand years, depositing varves in eastern Lago GCBA between  $\sim 18$  and 17 ka (Bendle et al., 2017a). Likewise, an ice-dammed lake (at the “Caracoles Level”) had formed by this time in front of the receding Lago CP ice lobe, which also drained to the Atlantic through the Caracoles Col (500 m asl) (Hein et al., 2010; Thorndycraft et al, 2019a; Turner et al., 2005).

The Menucos moraine to the northeast of Lago GCBA has a slightly younger  $^{10}\text{Be}$  mean age of 17.3 (SD 1.0) ka when outliers are excluded (Figure 12; Figure 19) (Douglass et al., 2006; Kaplan et al., 2004; recalculated in Kaplan et al., 2011 also). Bayesian age modelling of  $^{10}\text{Be}$  and varve ages provides an age for the Menucos moraine of  $17.7 \pm 0.1$  cal. ka BP and a subsequent (and probably short-lived) ice-margin at the Santa Maria fan  $\sim 4$  km further west ( $17.3 \pm 0.1$  cal. ka BP). Combining these ages with distances of glacier retreat indicate that rates of local ice-margin recession began slowly ( $<11 \text{ m a}^{-1}$  from the Fenix I to Menucos moraine), but accelerated ( $>15 \text{ m a}^{-1}$ ) after  $17.32 \pm 0.1$  cal. ka BP. The persistent formation of varves until  $16.9 \pm 0.1$  cal. ka BP suggests that ice remained in eastern Lago GCBA until at least this time (Bendle et al., 2017a).

The stratigraphically youngest Rio Blanco moraines (3<sup>rd</sup> limit) at the distal end of the Lago CP lobe are the innermost moraines of this sequence, and yield a mean age of 21.0 ka (SD 1.0) (Hein et al. 2010). A small Palaeolake CP at this time drained through a 500 m asl col towards the Atlantic (Hein et al., 2010; Thorndycraft et al, 2019a). The Lago CP ice lobe flowed around Sierra Colorado, forming lateral moraines on this upland region at  $\sim 1,000$  m asl (Boex et al. 2013).

Dating evidence presented in Boex et al. (2013) reveals two phases of PIS retreat in the Lago CP valley; an initial rapid ice lobe recession lobe at ~20.0 ka followed by a phase of rapid surface lowering between 16.0 and 14.7 ka. Their evidence indicates that the former PIS remained close to its LGM extent until at least 19.0 ka here. However, rapid ice sheet thinning from 18.1 ka saw ice at or near its present dimension by 15.5 ka (Boex et al., 2013). Radiocarbon and tephra ages from small lakes (Lago Augusta [440 m asl; -47.087°S, -72.402°W] and Lago Edita [570 m asl; -47.12°S, -72.420°W]) on the high ground between the Chacabuco and Cochrane valleys (Cerro Oportus; Figure 21) indicates that this area was ice-free as early as 19.2 cal. ka BP (Villa-Martinez et al. 2012; Henriquez et al., 2017; Stern et al., 2016), suggesting rapid thinning after 20 ka. Further east, mean  $^{10}\text{Be}$  exposure ages of 17.9 ka (SD 0.5) from elevations of 1,895 m asl on Cerro Oportus constrain the thinning of the ice mass during deglaciation and the separation of ice in the Cochrane and Chacabuco valleys. These data indicate that the ice-sheet surface here reached above this elevation at the LGM. With a surface elevation of 1900 m asl and a lake depth of 400 m at this point in Lago CP (Murdie et al., 1998), there was a minimum LGM ice thickness of 2,186 m at that longitude (72°11'W) in Lago CP.

#### 5.3.3.3 15 ka and 13 ka

Ice margins in this sector had retreated substantially up valley by 15 ka, with the terminus of Soler Glacier situated at the col where Lago GCBA drains into Lago Bertrand (see Figure 17) at  $15.6 \pm 1.0$  to  $14.4 \pm 0.6$  ka (Davies et al., 2018). At that point, Palaeolake Desado was still dammed by ice in the Baker Valley at 400 m asl (Thorndycraft et al, 2019a). By 15.3-15.0 ka, according to radiocarbon dating of organic sedimentation at Lago Augusta (Villa-Martínez et al., 2012), the ice-dammed lake in Lago CP had fallen to 420 – 440 m asl (the “Sub-Caracoles level”), potentially due to the opening up of a new drainage pathway towards the Pacific through the Barrancos Valley (Thorndycraft et al, 2019a).

In the Cochrane valley, the ‘Esmeralda Moraines’ and ‘Salto Moraines’ were deposited by glaciers flowing north from Monte San Lorenzo and the Barrancos Valley (Figure 21) (Davies et al., 2018), as indicated by trimlines and inset sequences of moraines in the valleys (e.g., the ‘Moraine Mounds’ of Glasser et al. (2012)). The Esmeralda Moraines yielded cosmogenic nuclide ages of 13.4 ka (SD 0.2) (Figure 21), when the Monte San Lorenzo outlet glaciers calved into the 350 m Palaeolake Chelanko, which was unified in the Lago GCBA and Lago CP Valleys (Davies et al., 2018; Thorndycraft et al, 2019a). A series of moraines in the Tranquilo Valley (Monte San Lorenzo) document a smaller advance of Glaciar Tranquilo during the ACR (Sagredo et al., 2016; 2018). Excluding outliers, the moraines yield mean  $^{10}\text{Be}$  ages of 13.8 ka (SD 0.5) (RT1); 13.3 ka (SD 0.5) (RT2); 13.7 ka (SD 0.3) (RT4); and 12.1 ka (SD 0.5) (RT5) (Figure 21) (Sagredo et al., 2016; 2018). These moraines, which are high above the level of any palaeolake, together with ACR-aged moraines from NPI-outlet glacier, Glaciar Colonia (mean 13.6 ka, SD 0.7; Nimick et al. 2016), suggest glacier stabilisation during

the ACR (Figure 22). Ice receded following the ACR as evidenced by the recession of Glaciar Calluqueo to the “Moraine Mounds” by 12.8 ka (SD 0.4) (Glasser et al., 2012).

The unified Palaeolake Chelenko was extant between ~14.2 and 12.6 ka, with ice still blocking the Baker valley at the Colonia confluence (Thorndycraft et al, 2019a). The lake drained through the Río Bayo col at 350 m asl (Glasser et al., 2016b), north of the Northern Patagonian Icefield towards the Pacific (Figure 22). Glacier recession from the Baker Valley led to drainage of Palaeolake Chelenko between 12.6 to 11.7 ka (ages from Bayesian age modelling) through the lower Baker (Thorndycraft et al, 2019a). The fall in lake level resulted in separate moraine dammed lakes in the Valle Grande, General Carrera and Cochrane basins, as previously submerged moraines became exposed. Boulder bars immediately downstream of the contemporary Lago CP outflow and the Colonia confluence suggest at least two glacial lake outburst floods drained through the lower Baker valley prior to a flood from Lago GCB. This event was caused by drainage of ~100 km<sup>3</sup> of lake water from Lago GCBA (Thorndycraft et al, 2019a), resulting in a catastrophic flood of ~110,000 m<sup>3</sup>s<sup>-1</sup> and creating megaflood-type landforms along the Baker valley (Benito and Thorndycraft, 2020).

Raised deltas in the Tranquilo Valley indicate that a palaeolake was also extant at this time at 520 m asl (“Palaeolake Tranquilo”) to the north of Monte San Lorenzo (Martin et al., 2019). The lake drained over the Brown Moraines and into Lago Brown (Figure 21; Figure 22), until further recession of Calluqueo Glacier allowed a new outflow into the Salto Valley to form. This resulted in the palaeolake level dropping to 425 m asl and a drainage reversal; however, the timing of this currently remains uncertain. Catastrophic drainage is possible, with boulder bars typical of floods mapped further down Río Salto (Martin et al., 2019).

*Figure 21. Central Baker Valley with published ages and geomorphology (Boex et al., 2013; Davies et al., 2018; Glasser et al., 2012; Henríquez et al., 2017; Martin et al., 2019; Sagredo et al., 2016, 2018; Stern et al., 2016; Thorndycraft et al, 2019; Turner et al., 2005).*

*Figure 22. Glacier and palaeolake evolution through the ACR on the eastern Northern Patagonian Icefield. Ice-sheet shading is illustrative only and does not indicate ice thickness. Data from Davies et al. (2018), Thorndycraft et al. (2019a) and Martin et al. (2019).*

#### 5.3.3.4 10 ka

As glaciers continued to recede during the Holocene, the influence of topography became more important as ice masses ‘unzipped’ around higher ground. By 10 ka, the Northern Patagonian Icefield had evolved into

a series of separate icefields (Figure 20; Figure 22). Some of these disappear by either 5 ka or the LIA, while others, such as Monte San Lorenzo, remain as small mountain icecaps and glaciers today. Dating of boulders on a valley-side lateral moraine at around 1,115 m asl showed that Nef Glacier was over 600 m thicker than today at 11.4 ka (Glasser et al., 2012). Similarly, Leones, Soler Glacier and Colonia glaciers were all larger than present at that time, but remained restricted compared with their ACR extents (Glasser et al., 2012; Nimick et al., 2016). Large moraines bounding Lago Plomo and Lago Negro yield mean  $^{10}\text{Be}$  ages of 11.2 ka (SD 0.1) and 11.4 ka (SD 0.5) respectively (Glasser et al., 2012) (Figure 23), suggesting ice-marginal stabilisation at this time, possibly due to palaeolake drainage and changing calving conditions. By 10 ka, all palaeolakes had likely assumed their current extent (Thorndycraft et al, 2019a) (Figure 22).

One substantial moraine limit (Fachinal moraines; Figure 23) to the north of the Reserva Nacional Lago Jeinemeni icefield is dated by  $^{10}\text{Be}$  and  $^{36}\text{Cl}$  cosmogenic nuclide exposure-age dating (Douglass et al., 2005). The two sets of moraines superimposed on a delta surface 100 m above the current lake level yielded recalculated ages ranging from  $20.3 \pm 4.8$  to  $9.4 \pm 2.9$  ka on individual boulders for the Outer Fachinal moraines, with a wide scatter, but perhaps indicating a Late Glacial ice position around 14-13 ka. The Inner Fachinal moraines yield generally younger  $^{10}\text{Be}$  ages of  $7.1 \pm 2.4$  to  $5.8 \pm 1.9$  ka. We do not calculate a mean age for these moraines due to the wide scatter. Possible deltas at ~400 m asl suggest that the Deseado Level ice-dammed lake may have penetrated deeply into the valley, which suggests that the earlier moraines formed before the formation of the lake, indicating a more retreated glacial position further up-valley. However, the geomorphological context and, specifically, the relationship between these moraines and Palaeolake Deseado is unclear, and combined with the wide scatter, we therefore assign them a lower reliability rating.

The Fachinal moraines represent the only dated ice limits for that icefield, but we assume that the large moraines in the lower valleys surrounding the mountain range are all of a contemporary age. These valley glaciers reached a lower elevation limit of 850 m asl in the south, 615 m asl to the west, 850 m asl to the east, and 350 m asl to the north. Douglass et al. (2005) suggest that the Reserva Nacional Lago Jeinemeni icefield that existed at this time had a palaeo-ELA of  $1,120 \pm 65$  m, ~300m lower than the present-day ELA, which may agree with a Late Glacial interpretation of the moraines.

*Figure 23. Geomorphological map showing Jeinemeni Reserve and the Fachinal Moraines, and the moraines around Lago Plomo and Lago Bertrand. Published ages and geomorphology from Glasser et al. (2006, 2008, 2012), Douglass et al. (2005), Bourgois et al. (2016), Davies et al. (2018) and Thorndycraft et al. (2019).*

On the west of the Northern Patagonian Icefield, a major advance of Glacier San Rafael is marked by a large arcuate moraine system, the Tempanos Moraine, which dams Laguna San Rafael (Harrison et al., 2012; Heusser, 2003; Lawrence and Lawrence, 1959). The Tempanos I, II and III moraines (Heusser, 2003) average 20 – 30 m in height, and mark the position of Glaciar San Rafael when it advanced westwards beyond the Andean mountain front to form a large piedmont lobe (Glasser et al., 2006b) (Figure 18). OSL dating of sediments incorporated in the Tempanos moraine system indicate that Glaciar San Rafael experienced multiple advances between 9.3 to 9.7 ka, 7.7 ka, and again at 5.7 ka (Harrison et al., 2012).

Morphostratigraphically comparable moraine suites exist at the mouths of the Gualas and San Quintin valleys to the north and south of the Laguna San Rafael respectively. The Gualas basin has remained ice free for at least the last  $11.3 \pm 3.0$  ka (Fernandez et al., 2012), although this age represents an extrapolation of the sediment accumulation rate to the base of the core and is therefore considered less reliable than other ages in our compilation. However, if correct, this age suggests that the terminal moraines around Golfo Elefantes are older than their counterparts at Laguna San Rafael. The authors argue that the age of these moraines lies somewhere between the beginning of sedimentation in the Gualas Basin and the end of the local LGM after approximately 12.6 ka (Turner et al., 2005). This supports the view put forward by other authors (Harrison et al., 2012; Warren, 1993) that past glacier fluctuations along the western edge of the Northern Patagonian Icefield were likely asynchronous, with glaciers oscillating at different times.

Bertrand et al. (2012) argue that Glaciar Gualas was close to its present-day position between 5.4 and 4.1 cal. ka BP, with a readvance to the shore of Golfo Elefantes between 4.0 and 0.75 cal. ka BP. Comparison with independent proxy records of precipitation and sea surface temperature suggests that Glaciar Gualas responded most strongly to precipitation, rather than temperature, change since the mid-Holocene (Bertrand et al., 2012). However, the asynchrony of past glacier fluctuations suggests that calving likely played an important role in past glacier dynamics, possibly overwhelming the climate signal on occasion.

#### 5.3.3.5 5 ka

Across the region, where limits at 5 ka are unknown, we place them broadly at the outer limits of the morphostratigraphically fresh Late Holocene moraines. The reconstructed 5 ka ice extent (Figure 20) is therefore likely to be a minimum. Mid-Holocene (Neoglacial) advances in this region of Patagonia began after 6.8 cal. ka BP, coincident with a strong cooling episode at this time and a tendency to negative SAM-like conditions (Moreno et al., 2018). Neoglacial glacier advances in the San Rafael, Colonia and Leones valleys first occurred around  $5.7 \pm 0.6$  ka to  $4.7 \pm 0.2$  ka (Harrison et al., 2012; Nimick et al., 2016). Around Lago Colonia, trees dated by dendrochronology and radiocarbon dating indicate recession behind this limit

followed by a smaller Late Holocene readvance. At Leones Glacier, the 135 m high terminal moraine damming Lago Leones was dated using a combination of OSL on sands deposited within the moraine and  $^{10}\text{Be}$  surface exposure ages on large boulder on its distal side. These data showed that the glacier receded from the eastern edge of the lake by about 2.5 ka BP (Harrison et al., 2008).

The glaciers of Monte San Lorenzo are surrounded by mid-Holocene moraines (Sagredo et al., 2018) (Figure 21). The mid-Holocene (radiocarbon dated to  $5.2 \pm 0.7$  cal. ka BP) limit of Río Lacteo glacier lies *ca* 5 km down valley of the current calving front (Mercer, 1968; Garibotti and Villalba, 2017). To the north of MSL in the Río Tranquilo valley,  $^{10}\text{Be}$  cosmogenic nuclide dating gives latero-terminal moraines a mean  $^{10}\text{Be}$  age of 5.7 ka (SD 0.1) (Sagredo et al., 2016; 2018). Radiocarbon ages from organic sediments within a moraine complex west of Sierra de Sangra (east of the main Andes) yield a basal age of  $4.9 \pm 0.8$  cal. ka BP (Mercer, 1968; Wenzens, 2005) (Figure 21).

Smaller moraines inset up-valley from the larger moraines on the delta north of the Jeinemeni Icefield (Figure 23) are assumed to be 5 ka in age, although it is possible they relate to the LIA. Further dating control is required here. These moraines suggest that by 5 ka, the Jeinemeni Icefield had fragmented into numerous small valley glaciers. Limits on available chronologies and limited detailed mapping means that we have low confidence in the Reserva Nacional Lago Jeinemeni icefield reconstruction and this is highlighted as a key region for future research, especially distinguishing between the 5 ka and 0.2 ka ice limits.

A thrust moraine near the snout of Soler Glacier preserves woody fragments and *in situ* tree remains with radiocarbon ages of 0.5 to 3.1 cal. ka BP (Glasser et al., 2002). This advance precedes the most recent Late Holocene advance (0.2 ka) by several hundred years, and suggests that prior to this time, Soler Glacier was less extensive than present.

#### 5.3.3.6 Late Holocene (0.5–0.2 ka)

In many places, the most recent Late Holocene moraines, typically large and well-defined moraines surrounding ice-scoured bedrock around the edges of the valley glaciers (Davies and Glasser, 2012; Glasser and Jansson, 2008; Glasser et al., 2008, 2011a), reach similar extents to the ice limit at 5 ka (Sagredo et al., 2016; 2018). These moraines are constrained to the last 500 to 200 years by dendrochronology and historical documents on the fresh-looking moraines surrounding these glaciers (Harrison et al., 2007; Nimick et al., 2016; Winchester and Harrison, 2000; Winchester et al., 2001, 2014). Late Holocene moraines of Monte San Lorenzo are additionally constrained by lichenometry (Garibotti and Villalba, 2017). Morphological similarities between these moraines allows extrapolation of the 0.2 ka ice margin across the Northern Patagonian Icefield (Davies and Glasser, 2012; Glasser et al., 2011a). This period of time was associated with



a persistent cold/wet negative SAM interval, which produced conditions favourable for glacier growth (Moreno et al., 2018).

## 5.4 The Southern Patagonian Icefield (48° – 52°S)

### 5.4.1 Present-day characteristics

The Southern Patagonian Icefield (Figure 24) is the largest of the present-day Patagonian ice masses at 13,219 km<sup>2</sup> (as of 2011) and reaches elevations of up to 3,400 m (Davies and Glasser, 2012). Ice thicknesses reach 1.5 km for Glaciar San Occidental, and bed elevation is below sea level for 15 – 20 km inland of the ice margin for Jorge Montt and O'Higgins (Gourlet et al., 2016).

The outlet glaciers of the Southern Patagonian Icefield are temperate and are among the fastest-flowing glaciers in the world, reaching velocities of up to 10.3 km/yr (Mouginot and Rignot, 2015). This fast ice flow is caused by the high mass balance gradient (with high accumulation and high ablation; Schaefer et al., 2015) and high basal sliding associated with the temperate climate and high precipitation of the Andes (cf. Aravena and Luckman, 2009; Garreaud et al., 2009). Seasonal velocity variations are also observed in a number of these glaciers (Mouginot and Rignot, 2015). These can be attributed to seasonal ocean thermal forcing modulating ice melt at the calving margin, combined with seasonal variations in subglacial meltwater discharge (Mouginot and Rignot, 2015).

Most of the Southern Patagonian Icefield outlet glaciers are receding (Davies and Glasser, 2012), with some notable exceptions. For example, Glaciar Perito Moreno, which drains eastwards into Lago Argentino (Figure 24), is in steady-state equilibrium with climate, and experiences periodic fluctuations due to its unique geometry (Stuefer et al., 2007; Davies and Glasser, 2012). In contrast, HPS-12 has receded 13 km from 1985 to 2017. Overall, between 2000 and 2016, the Southern Patagonian Icefield had a mass loss rate of  $-11.84 \pm 3.3 \text{ Gt a}^{-1}$  (Malz et al., 2018). This equates to a specific glacier mass balance of  $-0.941 \pm 0.19 \text{ m w.e. a}^{-1}$  for the whole icefield.

*Figure 24. A. Glaciers, lakes and rivers of the Southern Patagonian Icefield (48°–52°S), and published chronology (ka) and geomorphology (Ackert et al., 2008; Ashworth et al., 1991; Casassa et al., 1997; Davies and Glasser, 2012; Dowdeswell et al., 2016a; Fogwill and Kubik, 2005; García et al., 2012, 2018; Glasser and Jansson, 2008; Glasser et al., 2011b; Horta et al., 2019; Kaplan et al., 2016; Lastras and Dowdeswell, 2016; Marden and Clapperton, 1995; Masiokas et al., 2008; Mercer, 1965, 1968, 1976; Moreno et al., 2009; Sagredo et al., 2011; Strelin et al., 2014; Wenzens, 1999, 2005, 2006). Mean <sup>10</sup>Be ages of moraines are shown in pink crosses. See also Figure 5. B. Scale Map. Red boxes C and D show location of Figure 26. Box E shows location of Figure 28. Isochrones are shown in blue lines with blue labels.*



#### 5.4.2 Evidence for glaciation

Similar to the Northern Patagonian Icefield, geomorphological and geochronological evidence for past glaciation for the Southern Patagonian Icefield is concentrated east of the icefield. There are few data points constraining ice extent and patterns of recession for the western margin of the ice sheet in this region, except for limited radiocarbon ages from the isolated Puerto Eden (Ashworth et al., 1991). We assume that, at glacier maxima, the ice extended westwards to the continental shelf edge. This is a situation similar to most northern hemisphere marine-terminating Quaternary ice sheets (e.g. Hughes et al., 2016) and is linked to the rapid increase in iceberg calving as water-depth increases beyond the continental shelf edge, which prohibits further growth. The eastern margin of the Southern Patagonian Icefield consisted of four main ice lobes, which are constrained chrono-stratigraphically by radiocarbon and cosmogenic ages. From north to south these are the O'Higgins/San Martín lobe (Glasser et al., 2011b; Wenzens, 2005), Lago Viedma and Lago Argentino lobes (Ackert et al., 2008; Kaplan et al., 2016; Strelin et al., 2011, 2014; Wenzens, 1999), and, south of Cordon de los Baguales, the Torres del Paine/Río Coyle and del Toro lobes (García et al., 2012, 2018; Moreno et al., 2009) (Figure 24). The Bella Vista/Última Esperanza lobe is discussed in the Gran Campo Nevado section. During ice sheet recession, ice-dammed lakes formed in the over-deepenings currently occupied by the present-day lakes (García et al., 2014; Glasser et al., 2011b; Horta et al., 2019; Ponce et al., 2018; Sagredo et al., 2011; Strelin et al., 2011) (Figure 24).

The O'Higgins/San Martín Lobe has five major moraine systems (Glasser et al., 2011b). The LGM position of the O'Higgins/San Martín Lobe is placed at  $M_1$  at 34.9 ka (SD 3.1) (Glasser et al., 2011b). The outer  $M_4$  moraine contains scattered ages, making this ice limit difficult to date, with ages ranging from 28.0 to 59.3 ka. However, the recent publication of older MIS 3 and early MIS 4  $^{10}\text{Be}$  ages from the Torres del Paine area (García et al., 2018) suggests that this oldest age may be realistic for the  $M_4$  moraine. Further work is required to clarify LGM ice extent for this lobe. To the south, the Viedma Lobe contains a complex landsystem of glaciotectonic moraines, glacial lineations and crevasse-squeeze ridges located between the glacier maximum moraines and the present-day lake shoreline; Ponce et al. (2018) suggested that such features reflect palaeosurge activity within the lobe at, or following, the LGM.

The Lago Argentino Lobe is clearly delimited by a number of moraine sequences. Little published work is available for the terminal moraines beyond the eastern margin of the lake. However, extensive work on the Puerto Bandera moraines constrains Late Glacial recession from these outer moraines (Ackert et al., 2008; Strelin and Malagnino, 2000; Strelin et al., 2011). Holocene ice dynamics of the Lago Argentino lobe are well dated on the Herminita Peninsula, around Lago Pearson and around Lago Frías (Kaplan et al., 2016; Strelin et al., 2014).

The Torres del Paine/Río Coyle Lobe is denoted by a series of moraines: the outermost RV 1 moraines, which wrap around Sierra Contreras as a series of lateral moraines, the RV II moraines inside of these, and finally the TDP I to IV moraines around Laguna Azul, Lago Sarmiento de Gamboa and Lago del Toro. The RV Moraines (Caldenius, 1932; García et al., 2014, 2018) include multiple concentric moraine ridges deposited over some 15 km, and continue around into the del Toro outlet lobe.

Just north of Lago Argentino, Holocene glacier dynamics resulted in a sequence of progressively less-extensive advances of Glaciar Torre (49.3°S) since the LGM (Reynhout et al., 2019). Glaciar Torre is a smaller, alpine-style glacier, which may be expected to respond sensitively to climatic changes. These moraines have mean  $^{10}\text{Be}$  exposure ages of 16.7 ka (SD 0.6), 13.3 ka (SD 0.3), 9.7 ka (SD 0.3), 6.9 ka (SD 0.1), 6.2 ka (SD 0.2), and 530 years (SD 40). The ages suggest a readvance during the ACR, Mid-Holocene and Late Holocene, with the 0.2 ka advance being only slightly smaller than the Mid-Holocene advance. These Late Holocene moraines were previously dated with dendrochronology to the most recent Late Holocene advance, yielding ages of 1640 AD to 1829 AD (Masiokas et al., 2009a). The  $^{10}\text{Be}$  chronology proposed by Reynhout et al. (2019) revises the ages of these moraines from last 200 years to mid-Holocene and suggest that previous studies have under-estimated the age of moraines in this area.

In the west, tidewater glacier extent during the Late Holocene is constrained by moraines mapped in Iceberg Fjord (48° 43.5'S) around 3 km from the current terminus of Tempango Glacier (Dowdeswell et al., 2016c; Lastras and Dowdeswell, 2016). Associated with these moraines is also a series of sub-parallel ridges orientated in the direction of past ice-flow, together with areas of smoother sea floor. The outermost ridge is *ca* 100 m high and is asymmetrical, with a steeper ice-distal face. The largest moraine is interpreted as dating from the Late Holocene (last two centuries) (Dowdeswell et al., 2016c) (Figure 24). Cross-fjord moraines are also noted about 40 km from the terminus of Europa Glacier, where the fjord joins the deeper Wide Fjord, probably representing a still-stand at a pinning point during regional deglaciation after the LGM (Figure 9). Three other sedimentary ridges are spaced out in the inner fjord between 15 and 25 km from the modern ice front, but remain undated.

#### 5.4.3 Ice sheet reconstruction

Figure 25 shows our ice sheet reconstruction for the Southern Patagonian Icefield section. García et al. (2018) record a series of progressively less extensive glacier positions pre-dating the global LGM in Torres del Paine in the southern parts of the study region, with a LLGM of 47.0 ka recorded at the central part (Río de las Vizcachas) of the Torres del Paine/Río Coyle Lobe. The RV II Lateral moraine, in the north of the study region (Figure 28), has a mean  $^{10}\text{Be}$  age of 35.1 ka (SD 1.2). We assign the ice margin at 35 ka here with *high*

*confidence*. Although we recognise maximum extents earlier than 35 ka, the evidence suggests significant recession (~12 km) by 35 to 30 ka.

At 35 and 30 ka the margin also extended to the moraines at the eastern extents of the glacial over-deepenings currently occupied by Lago Viedma and Lago Argentino to the north. Glasser et al. (2011b) argued that the M3 moraine (dated to  $34.9 \pm 3.1$  ka) in the O'Higgins/San Martín valley is most likely to represent the local LGM (Figure 26A). Palaeolake Tar likely formed by this time (Horta et al., 2019). However, prior to 35 ka, the ice extent in this valley may have been greater, though the timing is difficult to ascertain. We use this to guide the *medium confidence* LLGM positions of the Viedma and Argentino Lobes, which have less chronological control but are delineated by (in some places detailed) geomorphological mapping (Wenzens, 1999; Strelin et al., 2011; Ponce et al., 2013, 2018; García et al., 2014). We assume that ice extended westwards to the continental shelf edge at these time-slices.

*Figure 25. Reconstruction of the Southern Patagonian Icefield at 5 ka time-slices. Ice dammed lakes are highlighted in orange. Relative sea level data from Gulderson et al. (2000), symbolised using GEBCO topographic and bathymetric data. Shading is illustrative only and does not represent ice thickness.*

By 25 ka, the O'Higgins/San Martín Lobe had receded 6 km to the M2 moraine (Figure 26A), and begun to flow around, rather than over, the 1,400 m high landmass at the eastern end of Lago O'Higgins/San Martín. During deglaciation, we assume that the high orographic precipitation would sustain larger glaciers to the west than those ice lobes extending east of the ice divide, but the reconstruction of the western margin should be considered highly speculative. We reconstruct a small Palaeolake Tehuelche at 250 m asl here (cf. Solari et al. 2012), although the col location is uncertain. Palaeolake Tar has formed in front of the O'Higgins/San Martín Lobe (Horta et al., 2019). At 20 ka, the extent of many outlet lobes is uncertain. The Torres del Paine/Río Coyle Lobe is well dated at the TDP I moraines around Lago del Toro to 21.3 ka (SD 1.7) (García et al., 2018). This indicates that in general, the ice lobes had pulled back from the LLGM moraines east of the Southern Patagonian Icefield but continued to occupy their over-deepenings. Palaeolake Tehuelche remains at 250 m asl and occupies a larger extent (cf. Solari et al. 2012). We speculatively place the western ice margin along the present-day coastline of Chile at this time.

*Figure 26. Detailed maps of: (A) the Lago O'Higgins/Lago San Martín/Lago Tar region. Data from Cassassa et al., 1997; Masiokas et al., 2009; Reynhout et al., 2019; Glasser et al., 2011, Wenzens 2005; 2006; Horta et al., 2019. (B) Herminita Peninsula. Numerous sources for published ages and geomorphology (Glasser and Jansson, 2008; Kaplan et al., 2016; Mercer, 1965; Strelin et al., 2014). Pink crosses are mean exposure ages for the landforms. Altitude and symbology as in Figure 24. Lakes are shown in blue.*

At 15 ka, substantial recession has occurred east of the Southern Patagonian Icefield, damming lakes within the over-deepenings. We place the O'Higgins/San Martín Lobe margin at the M1 moraines (mean  $^{10}\text{Be}$  age 14.7 ka, SD 0.5; cf. Glasser et al., 2011b), a recession of some 23 km from the M2 moraines (Figure 26A). In Lago Argentino, the 13 ka ice extent is well defined by the Puerto Bandera moraines (Figure 5; Figure 27) (Strelin et al., 2011). These moraines have been comprehensively dated by cosmogenic nuclide ( $^{10}\text{Be}$  and  $^{36}\text{Cl}$ ) and radiocarbon dating (Ackert et al., 2008; Kaplan et al., 2011), indicating a readvance and ice-marginal stabilisation during the ACR. Minimum-limiting  $^{14}\text{C}$  ages on bogs between the Puerto Bandera moraine crests yield ages older than 12.5 cal. ka BP (Strelin et al., 2011). Given the  $^{14}\text{C}$  chronology, this site was used as the basis for the production rate calibration used in this study (Kaplan et al., 2011). The Puerto Bandera moraines indicate an ice extent mid-way up Lago Argentino (Figure 27), damming a proglacial lake of a similar size to the present-day Lago Argentino at this time. Shorelines at elevations of 200 m asl (Glasser and Jansson, 2008) suggest the lake was slightly higher than today (165 m asl), and likely continued to drain eastwards to the Atlantic.

*Figure 27. Detail of ages and chronology for the Puerto Bandera Moraines, Lago Argentino, Southern Patagonian Icefield. Data from Mercer (1965), Wenzens (1999), Ackert et al. (2008), Glasser et al. (2008), Strelin et al. (2014), Kaplan et al. (2016). Pink crosses are mean exposure ages for the landforms. Altitude and symbology as in Figure 24. Lakes are shown in blue.*

In the Torres del Paine region (Río Coyle / Torres del Paine Lobe; Figure 28A), the mean  $^{10}\text{Be}$  age of the TDP II-IV moraines around Lago Azul and Lago Sarmiento de Gamboa indicate ice-margin stabilisation at 14.4 ka (SD 0.7), with extensive moraines extending southwards bearing similar stratigraphic positions again suggesting ice margin stabilisation during the ACR (García et al., 2012). This is supported by lateral moraines north of Lago Nordenskjöld with mean ages of 14.9 ka (SD 1.1) and 15.0 ka (SD 1.1) (Fogwill and Kubik, 2005; Moreno et al., 2009) (Figure 28). An extensive Palaeolake Tehuelche (Solari et al., 2012) had formed by 15 ka with lake levels at 125–155 m asl, draining southwards towards the Río Gallegos valley (Figure 28C), and

then eastwards towards the Atlantic through Río Gallegos (Sagredo et al., 2011; García et al., 2014, 2015). This extended ice-dammed palaeolake was confluent with Palaeolake Puerto Consuelo to the south (García et al., 2014; Solari et al., 2012) and thus we hereafter refer to the combined Palaeolake Tehuelche-Puerto Consuelo at the 15 ka time-slice. Our reconstruction differs slightly to the reconstruction by Sagredo et al. (2011) and García et al. (2014), in that we maintain the larger conjoined proglacial lake draining eastwards at 15 ka (Figure 28C), due to other constraints on the ice margin, without compromising the basal radiocarbon ages, which are above the 125 m lake level.

*Figure 28. A. Geological data pertaining to glaciation of the Torres del Paine region (Ackert et al., 2008; Fogwill and Kubik, 2005; García et al., 2014; García et al., 2012; Glasser and Jansson, 2008; Kaplan et al., 2016; Kaplan et al., 2007; Moreno et al., 2009; Sagredo et al., 2011; Strelin et al., 2014). B. Palaeolake Tehuelche (250 m altitude; cf. Solari et al., 2012) and Paleolake Puerto Consuelo at 20 ka. C. Palaeolake Tehuelche-Puerto Consuelo is formed by 15 ka, here at 125 m elevation (traced by contour analysis). This reconstructed lake represents the combined extent of both Palaeolake Tehuelche in the Torres del Paine area and Palaeolake Puerto Consuelo in the Río Prat area. D. Palaeolake Tehuelche-Puerto Consuelo and ice-sheet extent at 13 ka (during the ACR). Symbolology, bathymetry and altitude as in Figure 24. Ice-sheet shading is illustrative only and does not represent ice thickness. E. Map extent*

To the west of the Southern Patagonian Icefield, we hypothesise that an independent ice cap may have been supported on Isla Wellington at this time, with moraines dated by radiocarbon dating to  $13.4 \pm 0.4$  cal. ka BP at Puerto Eden suggesting glaciers flowing east from Isla Wellington towards the Southern Patagonian Icefield (Ashworth et al., 1991).

By 10 ka, the ice sheet was near to its present-day configuration in most areas. We assign a *low confidence* to ice-margin uncertainty due to the lack of published ages. One location where there are dates at this time is at the Lago Argentino lobe, where there are several radiocarbon ages at Lago Pearson, on the Herminita Peninsula (Figure 5; Figure 26B) and at the head of Lago Frias. These  $^{14}\text{C}$  ages indicate that recession took place between 13 and 10 ka, after the ACR, and significantly reduced ice extent through the earliest Holocene; ice extent at 10 ka was likely limited to the upper valleys (Kaplan et al., 2016; Strelin et al., 2011, 2014; Wenzens, 1999). Elsewhere, a lack of clear moraines at this time means we have *medium confidence* in this ice margin. It is likely that enlarged ice-dammed lakes persisted at the O'Higgins/San Martín Lobe and Viedma Lobe at this time-slice, but palaeolakes Argentino and Teheulche-Puerto Consuelo had drained (García et al., 2014). We suggest a separation of the Southern Patagonian Icefield from the Northern Patagonian Icefield had occurred between 12.6 and 11.7 ka (Thorndycraft et al, 2019a), based on the lake drainage through Río Baker south of the Northern Patagonian Icefield by this time (see Northern Patagonian

Icefield section), but note that there are few data constraining glacier recession in this region and especially on the timing of this separation.

There are no data available to constrain Southern Patagonian Icefield extent to the west of the Andes at 10 ka. We assume glacier advances in the fjords given that lobes to the east continue to extend at least partway into their over-deepenings.

Our ice sheet reconstruction is relatively unchanged from 5 ka to the LIA, with little evidence of ice extent beyond the 0.5 - 0.2 ka limits. Where there is evidence, such as at the head of Lago Argentino, it suggests that the 5 ka margin was slightly larger than the ice extent during the 0.2 ka maximum (Kaplan et al., 2016; Strelin et al., 2014) (Figure 5).

The series of inset moraines around Laguna Torres record a mid-Holocene stabilisation of Glacier Torres (mean  $^{10}\text{Be}$  ages of 6.9 ka (SD 0.1), 6.2 ka (SD 0.2), and 4.5 ka (SD 0.1)) (Reynhout et al., 2019) (Figure 26A). These moraines (M4 and M4b) are close to the younger Late Holocene moraines, dated to 0.53 ka (SD 0.04) by  $^{10}\text{Be}$  exposure ages.

Around the head of Lago Argentino, mid Holocene and Late Holocene moraines are well dated by  $^{10}\text{Be}$  exposure and  $^{14}\text{C}$  ages on ice-marginal landforms, mainly in three valleys (Strelin et al. 2014; Kaplan et al., 2016) (Figure 26B); these moraines suggest an ice margin stabilised here repeatedly during the interval from ~6 to 1 and 0.6 to 0.3 ka (Kaplan et al., 2016; Strelin et al., 2014). The  $^{10}\text{Be}$  and  $^{14}\text{C}$  chronologies in at least three different sectors of the Lago Argentino (Figure 26B) basin show mid-Holocene limits were more extensive than the limits of the most recent Holocene advance at ~0.6 to 0.2 ka. As the ages here are mainly derived from  $^{10}\text{Be}$  dating on a number of different moraines, as well as supporting  $^{14}\text{C}$  data, we do not calculate mean moraine ages here. In the absence of other data, we use these inferences from this site to predict ice-sheet extent at 5 ka at moraines down-valley of the most recent Late Holocene limits in adjacent valleys (and therefore assign a *medium confidence* classification).

The Late Holocene extent of Glaciar O'Higgins is well constrained with maps based on aerial photographs dating from 1896 AD (Casassa et al., 1997). The extent of Lago Viedma over the last 200 years is well-constrained by dendrochronological dating of moraines (Masiokas et al., 2009b). At the northern section of the Southern Patagonian Icefield, historical photographs date extent and subsequent recession of Glaciar Jorge Montt over the last few hundred years (Rivera et al., 2012a; 2012b).

## 5.5 *Gran Campo Nevado (52° – 53°S)*

### 5.5.1 *Present day characteristics*

Gran Campo Nevado is an ice cap covering 237 km<sup>2</sup> on the Península Muñoz Gamero, 200 km south of the Southern Patagonian Icefield (Davies and Glasser, 2012) (Figure 29A). It has steep outlet glaciers that are currently receding quickly (Schneider et al., 2007), and due to the ice cap's small size and fast response time the glaciers are possibly responding faster to climate change than those of the Southern Patagonian Icefield or Northern Patagonian Icefield (Möller et al., 2007). The mountain range here reaches only 1,000 – 1,700 m high, with the glaciers being sustained by the high volumes of precipitation and cooler mean annual air temperatures (Möller and Schneider, 2008). The glaciers terminate in tidal fjords or in proglacial lakes, with a few land-terminating glaciers.

### 5.5.2 *Evidence for glaciation*

The glacial geomorphology suggests that, at maxima, Gran Campo Nevado ice coalesced with the Southern Patagonian and Cordillera Darwin Icefields to form the southern extent of the PIS (Clapperton, 1993). Multiple ice lobes extended eastwards, including the Última Esperanza/Bella Vista—Río Gallegos Lobe (henceforth UE/BV Lobe), Skyring and Otway lobes (Figure 29). The Magellan and Bahía Inútil lobes are covered in the Cordillera Darwin section.

A series of moraines in the region east of the UE/BV Lobe document extensive Early and Middle Pleistocene glaciations, with interacting glacial, fluvial, volcanic and aeolian systems (Ercolano et al., 2016). The most recent glacial maximum east of the Andes resulted in the formation of a landsystem comprising sedimentary drumlins, moraines and marginal melt water channels (Benn and Clapperton, 2000; Clapperton et al., 1995; Darvill et al., 2017; Ercolano et al., 2016; Ercolano et al., 2004; Glasser and Jansson, 2008; Lovell et al., 2011; Meglioli, 1992; Sagredo et al., 2011) (Figure 29). Ice-dammed lakes formed in glacial over-deepenings to the east of the ice sheet during recession, as drainage to the Pacific was blocked by the remaining ice mass (Kilian et al., 2007b, 2013a; Lovell et al., 2012; Sagredo et al., 2011; Stern, 2011). Glaciolacustrine terraces at 25 – 30 m around the eastern shores of Seno Otway are well constrained to around 14 cal. ka BP (Kilian et al., 2013b).

Retreat is constrained by minimum radiocarbon ages from marine and terrestrial sediment cores east of the ice sheet, mostly from the modern Seno Skyring (Breuer et al., 2013; Kilian et al., 2003, 2007a, 2013b, 2013c). Some of these sediment cores also contain well-dated tephra horizons from the Burney (MB1 and MB2) and Reclus (R1) eruptions (Breuer et al., 2013; Kilian et al., 2003, 2013b). In addition, sediment cores to the west of Gran Campo Nevado at Bahía Beaufort constrain recession through the western fjords (Kilian et



al., 2007a). Ice is assumed to have reached the continental margin in the west at the LGM, but the timing remains ambiguous.

*Figure 29. Map showing published ages and geomorphology associated with Gran Campo Nevado (52° - 53°S) (data from Breuer et al., 2013; Clapperton et al., 1995; Darvill et al., 2015b; Darvill et al., 2017; Evenson et al., 2009; Fernandez et al., 2017; Kaplan et al., 2007; Kaplan et al., 2008; Kilian et al., 2003, 2007a, 2013b, 2013c; Koch and Kilian, 2005; McCulloch et al., 2005a; McCulloch et al., 2005b; Porter et al., 1992; Stern, 1992) and location of glaciers and lakes of Gran Campo Nevado.*

### 5.5.3 Ice sheet reconstruction

Our reconstruction for the Gran Campo Nevado area is shown in Figure 29. At 35 and 30 ka, we place the ice margin towards the outer limits of the glacial over-deepenings. We are confident with the glacial geomorphology based on in-depth published mapping (Darvill et al., 2014; Lovell et al., 2011). The outermost limit of the UE/BV Lobe is well dated by  $^{10}\text{Be}$  exposure ages on the Rio Turbio RT latero-terminal moraines (García et al., 2018), with a mean age of 47.1 ka (SD 1.8). Inboard of this, the Aracuco AR Moraine has a mean  $^{10}\text{Be}$  age of 32.4 ka (SD 1.2). In Sierra Dorotea to the north, the Aracuco AR Moraine has a mean  $^{10}\text{Be}$  age of 33.0 ka (SD 2.8). We therefore place the 35 and 30 ka ice limits with *high confidence* at these moraines.

We give the margins of the Skyring and Otway lobes *Medium confidence* at 35 ka, as the well-constrained Magellan and UE/BV lobes determine the ice lobe configuration here (Darvill et al., 2017; Kaplan et al., 2007, 2008; McCulloch et al., 2005b), but there are few independent limiting ages for these outlets.

By 25 ka, ice receded into the over-deepenings. Palaeolake Blanca, defined by raised shorelines around the present-day Laguna Blanca, was dammed in front of Skyring Lobe, initially draining northwards through a col at 190 m (Darvill et al., 2017; Lovell et al., 2012). Subsequently the lake drained through a col 188 m asl as the Skyring and Otway lobes receded, resulting in a drainage switch to the east and into the Strait of Magellan (Figure 30). However, the timing of lake level fall is poorly constrained, as is the location of the ice margin; it is likely that the ice margin retreated back beyond the lower 188 m asl col by 20 ka, given that outwash sediments show drainage passed in front of the well-constrained Magellan lobe (Darvill et al., 2017; Kaplan et al., 2007; Kaplan et al., 2008; Lovell et al., 2012; McCulloch et al., 2005b).

By 20 ka, the UE/BV Lobe had receded to prominent moraines and located east of Lago Balmaceda (Figure 29), constrained by a small number of minimum radiocarbon ages (Sagredo et al., 2011). Palaeolake Puerto Consuelo started to form in front of this ice margin, draining east through a col at 155 m (Sagredo et al., 2011). Palaeolake Blanca likely drained through the 188 m asl col by 20 ka, and may even have drained



completely (Lovell et al., 2012). There are also minimum tephra and radiocarbon ages in Seno Skyring and Seno Otway, indicating that ice filled these basins at this time (Kilian et al., 2007b). However, it is unclear at what point the Skyring and Otway lobes retreated and began forming their respective palaeolakes.

Palaeolake Puerto Consuelo in front of the UE/BV lobe merged with Palaeolake Tehuelche to the north to form Palaeolake Tehuelche-Puerto Consuelo by 15 ka. The combined palaeolake initially drained east through a col at 155 m asl (Sagredo et al. 2011) (Figure 28), but later drained completely, either southward into Palaeolake Skyring and/or westward into the Pacific between the shrinking independent ice masses. Eventually, Palaeolake Puerto Consuelo became the modern marine fjord, but it is unclear whether the lake level had dropped to sea level by 15 ka (Sagredo et al. 2011). The Skyring and Otway lobes had retreated from the Seno Skyring and Seno Otway over-deepenings (Figure 29; Figure 30), forming new palaeolakes (Palaeolake Skyring and Palaeolake Otway), constrained by shorelines at 15 m asl and the positions of the respective ice margins (Clapperton et al., 1995; Kilian et al., 2013b; Lovell et al., 2011, 2012).

The development and growth of these palaeolakes suggests that substantial retreat of ice had occurred, supported by ages from glacial landforms around the UE/BV lobe and minimum radiocarbon ages and tephra horizons in sediment cores from the modern Seno Skyring and Seno Otway (Breuer et al., 2013; Kilian et al., 2003, 2007b, 2013b, 2013c; Sagredo et al., 2011). However, differing reconstructions for this time lead us to assign low confidence ice margins, particularly as the precise extent of ice is unclear. It is likely that the Gran Campo Nevado, Cordillera Darwin and Southern Patagonian Icefield ice masses had begun to separate around 15 ka, leaving an independent ice cap over Gran Campo Nevado. However, ice must have been much larger than at present to dam the Strait of Magellan and create the palaeolakes. The glaciolacustrine shorelines indicate that the lakes were extensive.

There are few geomorphological or chronological constraints for the Gran Campo Nevado ice mass at 10 ka or 5 ka, with a few scattered ages suggesting rapid recession but yielding inconclusive results. Palaeolake Tehuelche-Puerto Consuelo had likely drained by 10.3 ka (Sagredo et al. 2011; Stern, 2011). We ascribe stepwise retreat of ice between 15 ka and present day in a pattern based on limits further north, and which agrees with similar reconstructions, but give these limits low confidence. The 0.2 ka maximum limit is dated using dendrochronology on some moraines, and relatively clear geomorphology (moraines, trimlines) assumed to be related to the Late Holocene advance has been mapped around the present icefield (Davies and Glasser, 2012; Koch and Kilian, 2005). It is not possible to determine whether ice at 10 ka or 5 ka was more or less extensive than at 0.2 ka or present day.

*Figure 30. Palaeo ice sheet reconstruction for the Gran Campo Nevado region. Yellow stars show location of col spillways for ice-dammed lakes (shown in pink). Relative sea level data from Guilderson et al. (2000),*

symbolised using GEBCO topographic and bathymetric data. Ice-sheet shading is illustrative only and does not represent ice thickness.

## 5.6 Cordillera Darwin (53° – 56°S)

### 5.6.1 Present day characteristics

The 2,300 km<sup>2</sup> Cordillera Darwin Icefield, at the southern tip of the Andean Mountain range, is the third largest ice mass in present-day South America (Bown et al., 2014) (Figure 31). The icefield receives relatively uniform precipitation throughout the year (up to 5,000 mm a<sup>-1</sup>) due to its position in the core of the modern SWW system (Garreaud et al., 2013). Mountain peaks in Cordillera Darwin exceed 2,000 m asl, and the icefield is drained by a mixture of tidewater glaciers calving into fjords and land-terminating glaciers, some of which are now retreating with expanding proglacial lakes (Holmlund and Fuenzalida, 1995) (Izagirre et al., 2018). Meier et al. (2018) identified area change of Patagonia glaciers from 1870 – 2016 with a ~16% area loss of Cordillera Darwin Icefield, with more than half of the loss occurring since 1985. They also noted that Cordillera Darwin Icefield glaciers were retreating fastest between 1986 and 2005; afterwards the rate of retreat has decreased. The retreat has been largest on tidewater glaciers such as Marinelli Glacier and Ventisquero Grande Glacier.

*Figure 31. Location of published ages, geomorphology, glaciers and lakes in Cordillera Darwin, southernmost Patagonia (53° - 56°S) (Boyd et al., 2008; Breuer et al., 2013; Clapperton et al., 1995; Coronato et al., 2009; Darvill et al., 2015b; Darvill et al., 2017; Davies and Glasser, 2012; Evenson et al., 2009; Glasser and Jansson, 2008; Gordillo et al., 1992; Hall et al., 2013, 2019; Heusser, 1989, 1998; Izagirre et al., 2018; Kaplan et al., 2007; Kaplan et al., 2008; Kilian et al., 2013b; Kilian et al., 2007a; Kilian et al., 2003; Kuylensstierna et al., 1996; McCulloch and Bentley, 1998; McCulloch et al., 2005a; McCulloch et al., 2005b; Menounos et al., 2013; Porter, 1990; Porter et al., 1997; Rabassa et al., 2000; Roig et al., 1996; Stern, 1992).*

### 5.6.2 Evidence for glaciation

Here, we focus on the Magellan, Bahía Inutíl–San Sebastián, Fagnano and Beagle Channel lobes, sourced from the Cordillera Darwin area. During the most recent glacial maximum, an enlarged icefield coalesced with the Gran Campo Nevado Icefield ice to the north, forming the southernmost extent of the PIS (Clapperton, 1993). Multiple ice lobes extended from the former ice sheet across Isla Grande de Tierra del Fuego, leaving well-preserved glacial geomorphology (Bentley et al., 2005; Bujalesky et al., 2001; Clapperton et al., 1995; Coronato et al., 2009; Darvill et al., 2014; Fernández et al., 2017; Glasser and Jansson, 2008; Izagirre et al., 2018; Kuylensstierna et al., 1996; Lozano et al., 2018; Strelin et al., 2008) that has been

investigated in numerous studies (e.g. Coronato et al., 2004; McCulloch et al., 2005a, 2005b; Meglioli, 1992; Rabassa, 2008; Rabassa et al., 2000).

The prominent Magellan and Bahía Inútil–San Sebastián ice lobes advanced north and then eastward along the present-day Strait of Magellan, dissected by Isla Dawson. In the southern Central Strait of Magellan and in Bahía Inútil (Figure 31), multibeam data show glacial lineations, and iceberg ploughmarks in the channel floor (Fernández et al., 2017). Seismic facies show high angle or sinuous reflectors, interpreted as ice proximal or subglacial sediments, and parallel reflectors with no internal complex geometries, interpreted as pelagic or distal glaciomarine sediments (*ibid.*). These data indicate that grounded ice occupied Seno Almirantazgo, Whiteside Channel and Bahía Inútil during the last glacial cycle. Evidence for a glacial readvance during the ACR is equivocal here.

The Fagnano and Beagle Channel lobes also extended to the east and southeast, and ice is assumed to have reached the continental margin to the south and west, although the extent and timing remain ambiguous. During retreat, residual ice masses in the Cordillera Darwin range blocked drainage into the Pacific, creating large proglacial lakes that occupied the present-day Strait of Magellan and Bahía Inútil (McCulloch et al., 2005a; Porter et al., 1992). Lower relative sea levels at the same time expanded the Argentinian continental shelf, damming the lakes to the east (Peltier and Drinnon, 2002). The timing of Quaternary ice activity in the region has been described using a range of dating techniques (for recent summaries, see Darvill et al., 2017; Hall et al., 2017).

Evidence for former palaeolake high-stands includes a widespread terrace (18 – 25 m asl) on the Atlantic sector of the Straits of Magellan (De Muro et al., 2017, 2018). This terrace documents a transition from glacio-fluvial-lacustrine conditions to littoral-marine environments. Three lower terraces (at 6 – 11 m asl, 3 – 5 m asl, and 1 – 2 m asl respectively) consist of sedimentary sequences of coastal marine origin, documenting sea level fall during the Holocene (De Muro et al., 2018).

Extensive radiocarbon ages from Fiordo Marinelli and Fiordo Brooks (Figure 32) provide evidence for ice dynamics following the onset of deglaciation (Hall et al., 2013, 2019). These ages show that after the LLGM, ice remained extensive near LGM positions until after 18.4 cal. ka BP (Kaplan et al., 2011; Darvill et al., 2017). Glacier ice then rapidly receded to Bahía Ainsworth and the mouth of Fiordo Brooks by 17.1 cal. ka BP (Hall et al., 2019). This indicates substantial deglaciation from 18.4 – 17.1 cal. ka BP during Heinrich Stadial 1 (Hall et al., 2013, 2019). By 15.8 cal. ka BP, the terminus of the glacier in Fiordo Marinelli was 3 km beyond Narrows Moraine (Figure 32). Holocene glacier dynamics are then well constrained here with a series of radiocarbon ages from the valley sides (Hall et al., 2019; Figure 32).

*Figure 32. Detail of radiocarbon ages and geomorphology from Fiordo Marinelli and Fiordo Brookes, northern Cordillera Darwin Icefield. Data from Boyd et al. (2008), Hall et al. (2013, 2019), Izagirre et al. (2018). Symbology as in Figure 31. Background image is ESRI Basemap World Imagery.*

### 5.6.3 Ice sheet reconstruction

Our reconstruction for the Cordillera Darwin area is shown in Figure 33. We are confident in the lateral margins of the Bahía Inútil–San Sebastián Lobe at 35 to 30 ka given clearly-defined moraine limits (Darvill et al., 2014) and recent cosmogenic dating of outwash gravels on the northern margin (Darvill et al., 2015b), but the full extent of ice off-present-shore remains unclear (Coronato et al., 2004; Rabassa, 2008). We are also relatively confident that, stratigraphically, the Magellan Lobe extended beyond Peninsula Juan Mazía (based on previous dating and reconstructions; see Darvill et al., 2017). However, we note that these recent studies are at significant odds with previous work suggesting that outer glacial limits were deposited prior to the last glacial cycle (Bujalesky et al., 2001; Coronato et al., 2004; Evenson et al., 2009; Kaplan et al., 2007; Rabassa, 2008). Cosmogenic  $^{10}\text{Be}$ ,  $^{26}\text{Al}$  and  $^{36}\text{Cl}$  nuclide exposure dating of erratic boulders from pre-LGM moraines of the Magellan and Bahía Inútil–San Sebastián lobes has yielded ages substantially younger than expected (Evenson et al., 2009; Kaplan et al., 2007). The effect is most apparent for drifts on the southern margin of the Bahía Inútil–San Sebastián lobe, where the broad range in ages (although most <50 ka) has been attributed to post-depositional exhumation and intense erosion of the boulders (Darvill et al., 2015a; Evenson et al., 2009; García et al., 2018; Kaplan et al., 2007).  $^{26}\text{Al}/^{10}\text{Be}$  depth profiles through outwash sediments linked to the northern margin of the Bahía Inútil–San Sebastián lobe show that this ice lobe was extensive at ~30.1 ka and possibly also earlier, at ~45.6 ka (Darvill et al., 2015b).

For the Magellan Lobe,  $^{10}\text{Be}$  and  $^{26}\text{Al}$  exposure ages from erratic boulders at Primera Angostura show that ice was also still extensive at around this time (27.7 ka (SD 1.0) and 25.1 ka (SD 0.9); Kaplan et al., 2008), consistent with more recent exposure dating showing ice was extensive as early as ~60–70 ka (Peltier et al., 2016) (Figure 29). Given the emerging pattern of expansive pre-MIS 2 ice from here and further north in Patagonia (as well as elsewhere in the southern mid-latitudes; Darvill et al., 2016), we opt for extensive limits at 35 ka and 30 ka in this study. The extent and timing of the Fagnano and Beagle lobes, as well as the southern and western ice sheet margins bordering the Pacific coast remain uncertain for 35–10 ka.

At 25 ka, we place limits between those at 30 ka and 20 ka.  $^{10}\text{Be}$  exposure ages on the outer lateral moraines show that the Magellan Lobe was likely back at Península Juan Mazía by ~27.4–29.9 ka, suggesting significant retreat occurred shortly after 30 ka (Kaplan et al., 2008; McCulloch et al., 2005b). Exposure ages with a mean age of 25.1 ka (SD 0.9) from the recessional moraines of the Magellan Lobe constrain ice extent at 25 ka (Kaplan et al., 2007). However, we also note that there is geomorphological evidence of readvance at this time and cannot be sure that the 25 ka limits were not less extensive than we portray here.

The extent of the Fagnano and Beagle lobes at 25 ka is unclear but we assume they remained relatively extensive, in a similar manner to the larger ice lobes to the north (Bujalesky et al., 1997; Coronato et al., 2009). Seismic and sedimentary data from the Fagnano basin suggest post-LGM retreat of ice was punctuated by numerous still-stands or re-advances into a lake level higher than the present Lago Fagnano (Waldmann et al., 2010). Final retreat of the Fagnano Lobe into the Cordillera Darwin range allowed drainage into the Almirantazgo Fjord and Strait of Magellan and lowering of the lake level to present (Waldmann et al., 2010). It is assumed that a palaeolake must have formed in front of the retreating Magellan Lobe, blocked by the Primera Angostura moraine limit (Clapperton et al., 1995; McCulloch et al., 2005b), although the time at which it formed, and its extent are uncertain. Similar palaeo-lakes may not yet have formed in front of the other ice lobes given that drainage was still possible towards the Atlantic and the Bahía Inútil–San Sebastián Lobe had not yet retreated into its over-deepening (Porter et al., 1992).

Ice extent is relatively well-constrained at 20 ka. The major ice lobes skirted their respective over-deepened basins (Darvill et al., 2017) and geomorphological evidence suggests that the Magellan and Bahía Inútil–San Sebastián ice lobes might have re-advanced to these positions (Benn and Clapperton, 2000; Bentley et al., 2005; Clapperton et al., 1995; Darvill et al., 2017; McCulloch et al., 2005b). These lobes may have displayed surge-like behaviour, with an assemblage of thrust moraines and highly elongate streamlined glacial lineations suggesting rapid ice flow, combined with an asymmetry in lobate marginal positions (Darvill et al., 2017; Lovell et al., 2012).  $^{10}\text{Be}$  exposure ages demonstrate that the Magellan Lobe reached this limit by  $\sim 18.3 - 23.2$  ka (Kaplan et al., 2008; McCulloch et al., 2005b) and cosmogenic exposure ages from prominent trains of erratic boulders on the southern side of the Bahía Inútil–San Sebastián lobe generally cluster around  $17.6 - 24.9$  ka (Darvill et al., 2015a, 2015b; Evenson et al., 2009; Kaplan et al., 2007, 2008; McCulloch et al., 2005b). The extent of the Magellan Lobe at 20 ka is thus constrained by  $^{10}\text{Be}$  exposure ages on moraines near the margin of the current fjord on Peninsula Juan Mazía, with mean moraine ages of 19.6 ka (SD 0.1) and 19.9 ka (SD 1.9) (Kaplan et al., 2008). As in the north, an ice margin stabilisation at  $\sim 19$  ka is apparent, followed by rapid deglaciation after that time. We reconstruct a small Palaeolake Magellan in front of the Magellan Lobe at 20 ka, with a drainage col at 10 m above present-day sea level.

Several lines of evidence now suggest rapid retreat of ice occurred well before 15 ka around Cordillera Darwin (Hall et al., 2017, 2019). In early studies, numerous minimum radiocarbon ages suggest that ice retreat had begun by at least 14–15 ka, if not well before (Anderson and Archer, 1999; Clapperton et al., 1995; McCulloch and Bentley, 1998; McCulloch et al., 2005b; Porter et al., 1992). Radiocarbon ages as old as 16.8 ka from peat bogs close to the centre of Cordillera Darwin imply large-scale, rapid retreat of the Magellan and Bahía Inútil–San Sebastián lobes from LGM positions, perhaps to within a few kilometres of present ice extent (Hall et al., 2013). These ages are supported by minimum radiocarbon ages of up to  $\sim 15.7$

cal. ka BP in marine sediment cores from Fiordo Almirantazgo, offshore of Bahía Ainsworth (Bertrand et al., 2017; Boyd et al., 2008), as well as marine geological evidence (Fernandez et al., 2017). Such rapid recession may have been driven or exacerbated by broad, decoupled terminic calving into a large combined Palaeolake Magellan–Bahía Inútil (Boyd et al., 2008; Darvill et al., 2017; Porter et al., 1992). The lake could have existed for hundreds or even thousands of years between 20 ka and 15 ka, and the presence of the well-dated Reclús tephra within lake sediments on the northern shore of Bahía Inútil implies that drainage may not have been before ~14.3 ka (McCulloch et al., 2005b). However, this would have required key drainage routes within Cordillera Darwin to have remained blocked despite extensive deglaciation (Hall et al., 2013, 2017; Mansilla et al., 2016), and is at odds with marine conditions in Seno Almirantazgo, radiocarbon dated to ~15.5 cal. ka BP (Boyd et al., 2008; Fernández et al., 2017). The precise timing and extent of the deglacial Palaeolake Magellan–Bahía Inútil requires further examination and we do not include the lake in our 20 ka or 15 ka time-slices. However, a large glacial lake existed at some point between 20 and 15 ka, and we indicate this on our reconstruction (Figure 33). Lastly, further south, along the eastern Beagle Channel,  $^{10}\text{Be}$  exposure ages with a mean of 13.5 ka (SD 1.3) and 14.3 ka (SD 0.2) indicate cirque glaciation during the ACR interval (Menounos et al., 2013).

Radiocarbon ages from Fiordo Marinelli indicate that ice from the Cordillera Darwin Icefield was 3 km outboard of Narrows Moraine (Figure 32) at 15.7 cal. ka BP (Hall et al. 2019). There is no evidence of a strong advance during the ACR at this location; ice here terminated inside of this site at 13 ka, most likely at Narrows Moraine. Ice extent during the Early Holocene was similar to, or smaller than present.

*Figure 33. Reconstruction of ice in Cordillera Darwin. Ice-dammed palaeolakes are shown in pink. Relative sea level data from Guilderson et al. (2000), symbolised using GEBCO topographic and bathymetric data. Shading is illustrative only and does not represent ice thickness.*

The precise extent of Cordillera Darwin ice at 10 ka and 5 ka is well constrained in Fiordo Marinelli, which suggests that ice was near to the present-day configuration (Bertrand et al., 2017; Fernandez et al., 2011; Hall et al. 2013, 2019). Basal peat from Isla Dawson suggests that Palaeolake Magellan–Bahía Inútil had drained west into the Pacific by ~11.8 cal. ka BP (McCulloch et al., 2005b), as ice dams breached during retreat. Sea-level rise during this time would also have formed an island and fjord system similar to present. Many outlet glaciers of the Cordillera Darwin Icefield would have calved and retreated into fjords. Minimum radiocarbon ages from Bahía Ainsworth show that Ensenada Pigafetta was likely ice-free by ~8.0 cal. ka BP (Boyd et al., 2008), demonstrating the reduced nature of the icefield. Marine sediments also suggest a possible readvance of outlet glaciers at 7.3 – 5.7 cal. ka BP, but not to extents greater than at 10 ka (Boyd et

al., 2008). Hence we can be confident that glaciers were restricted, and not dissimilar to most recent Late Holocene (0.5 – 0.2 ka) positions just beyond present day extents.

New data from Fiordo Marinelli indicates that during the Holocene there were several periods when ice extent was less than that of 1984 AD. A readvance into the fjord was dated to 6.5 – 5.6 cal. ka BP, with ice reaching nearly to Narrows Moraine. Ice extent from 5.4 – 4.7 cal. ka BP was similar to present, or smaller. There was a late Holocene expansion at 3.8 cal. ka BP (Hall et al., 2019). Another glacier expansion is dated to 2.4 – 1.7 cal. ka BP.

We are relatively confident about ice extent during the Late Holocene given clear geomorphology related to this time period (Davies and Glasser, 2012). Prominent moraines, some of which were captured in historical records (e.g. de Agostini, 1956; de Gasperi, 1922; Izagirre et al., 2018), demonstrate that glaciers were more extensive than present in the last two centuries (Fernández et al., 2011; Izagirre et al., 2018). Dendrochronology suggests Glaciario Marinelli, a large outlet to the north of the Cordillera Darwin range, advanced to leave a prominent moraine during the last two millennia (Hall et al., 2019) and 0.5 – 0.2 ka (Porter and Santana, 2003), supported by data from marine cores (Boyd et al., 2008). Other geomorphologically and stratigraphically similar moraines around the present icefield are assumed to be correlatives, and formed during the last millennium.

## 6 Synthesis

### 6.1 Patagonian Ice Sheet reconstruction at the LGM (PATICE)

Our new PATICE reconstruction demonstrates, for the first time, Patagonian Ice Sheet changes from 35 ka to the present day (Figure 34). The original empirical reconstruction is provided with a level of confidence for each time slice (*high, medium, and low confidence*) and we include the extent and height of ice-dammed lakes. Our reconstruction of maximum ice extent provides a systematic revision of LGM ice sheet extent that—like previously published reconstructions—still has similarities with the work of early researchers (e.g. Caldenius, 1932; Mercer, 1968, 1976; Coronato and Rabassa, 2011; Harrison and Glasser, 2011) (Figure 35). Changes are particularly prominent for several of the eastern outlet lobes, following recent chronostratigraphic work in these areas. Detailed geomorphological data, and the topographic control of glacier ice-flow patterns, allow us to reconstruct icefield separation and the dynamics of ice through time. Our compilation highlights areas where further work is needed and allows a detailed assessment of regional trends in ice-sheet response to climatic forcing and the role of palaeolakes in recession dynamics.



*Figure 34. Patagonian Ice Sheet reconstruction at 5 ka time-slices from 35 ka to present day, with additional time-slices through periods of ice advance during the ACR (13 ka) and Late Holocene (0.2 ka). Ice-dammed lakes are highlighted in orange. Yellow stars indicate location of drainage cols. Sea level reconstruction is from geological data in Guilderson et al. (2000), symbolised using the GEBCO marine bathymetry dataset. Ice-sheet shading is illustrative only and does not represent ice thickness.*

The Patagonian Ice Sheet covered  $492.6 \times 10^3 \text{ km}^2$  at 35 ka. We derive an estimate of ice volume of  $548.1 \times 10^3 \text{ Gt}$  ( $597.5 \times 10^3 \text{ km}^3$ ) at 30 ka, which equates to a sea level equivalent of  $\sim 1.5 \text{ m}$ . The ice sheet was 350 km wide and 2090 km long and was most probably grounded on the Pacific continental shelf edge. Our new 35 ka reconstruction indicates an ice sheet that is larger than previous reconstructions. Coronato and Rabassa (2011) estimated an ice-covered area of  $431.0 \times 10^3 \text{ km}^2$  in our study region. Excluding outlying ice masses, our 35 ka reconstruction covers  $491.9 \times 10^3 \text{ km}^2$ , indicating that the new reconstruction is 60,960  $\text{km}^2$ , or 12%, larger than previous attempts. The differences are greatest in southern Patagonia, where recent research indicates more extensive ice lobes than were previously documented.

Early reconstructions using numerical ice-sheet modelling produced a slightly smaller reconstruction. Hulton et al. (2002) applied a numerical model to South America for the LGM period. In their modelled reconstruction, disparate ice masses along the Andes joined up to form a continuous mass of ice from  $38^\circ\text{S}$  to the southern tip of South America. Fast-flowing ice zones were constrained at their margins by active calving. The modelled change in ice volume from the LGM to present-day was  $\sim 500 \times 10^3 \text{ km}^3$  of ice, equivalent to a sea-level change of  $\sim 1.2 \text{ m}$  (Hulton et al., 2002). Hubbard et al. (2005) used a time-dependent model to investigate the PIS between  $45^\circ$  and  $48^\circ\text{S}$  during the LGM. These modelling experiments suggested that to reach the LGM moraines bounding Lago GLBA, a lowering of the ELA by  $\sim 900 \text{ m}$  is required. These modelled experiments suggested that the PIS was highly dynamic, with mean ice thicknesses of 1130 m drained by large ice streams to the western margin and fast-flowing outlet lobes to the east. This model, forced with the Antarctic ice core record of past climate, also recognised a stabilisation during the Antarctic Cold Reversal and rapid collapse after that time, shrinking to near its present-day margins by 11 ka.

We use our geomorphological database (including bathymetric troughs, over-deepened lakes and basins, glacial lineations in both rock [roche moutonnées, whalebacks] and sediment [large streamlined drumlins, smaller flutes in upland regions], fjords, trimlines, parabolic valleys and orientation), topographic data, and the pattern of recession revealed by moraines to determine palaeo ice-flow lines (Figure 35). The LLGM PIS was drained by fast flowing outlet lobes that flowed orthogonally from a north-south ice divide extending the length of the Patagonian Andean mountain chain (although this has low confidence in the absence of ice thickness data). We assume that the ice divide remained more or less over the highest points of the Andes, given the topographically confined nature of the outlet lobes. Subsidiary ice divides were likely above the

topographic lows between the present-day Northern and Southern Patagonian ice fields. Ice masses centred on mountains located to the east of the main ice divide, such as Monte San Lorenzo and San Sangra, were likely confluent with the main outlet lobes, but retained some radial flow, and likely remained as ice dispersal centres throughout the LLGM. The large fjords and bathymetric troughs located west of the main present-day icefields suggest the presence of large, well-established outlet lobes with a dendritic flow pattern, characteristic of fast-flowing glaciers and ice streams. Outlet lobes to the east remained topographically confined and followed terrestrial valleys and bathymetric troughs on the continental shelf. Growth on the Pacific margin was likely limited by deepening water beyond the continental shelf edge, which increased mass loss through enhanced iceberg calving. Outlet lobes on the western side of the Andes were likely larger than those on the east, as they are today, reflecting an orographic precipitation gradient. This is apparent in our LLGM reconstructions, in which ice extended further to the west than the present-day icefields compared with the east (Figure 35).

In the Chilean Lake District, LLGM outlet lobes were relatively small when measured along the reconstructed flowlines, with maximum lengths (ice divide to terminus) of ca 70 km (Lago Ranco), 92 km (Lago Llanquihue), and 110 km (Seno de Reloncaví) (Figure 35). Ice lobes were larger further south around the present-day Northern Patagonian Icefield, reaching lengths of up to 180 km (Lago GCBA), and 186 km (Lago CP), and with widths of 40 – 50 km. Outlet lobes of the Southern Patagonian Icefield attained lengths of ~130 km (Lago Viedma and Lago Argentino). The most substantial lobes were formed in the far south around Tierra del Fuego, with the Magellan Lobe reaching 230 km, and the Bahía Inútil Lobe reaching 300 km in length (40 km in width) (Figure 35). The topographically influenced, highly convergent flow and attenuated bedforms mapped around some larger outlet lobes in the south (Clapperton, 1989; Darvill et al., 2017; Ercolano et al., 2004; Lovell et al., 2012; Ponce et al., 2013, 2018) satisfy the criteria for being considered ice streams (Stokes and Clark, 1999). Further work is required to investigate the potential for the diagnostic offshore trough-mouth fans along the Pacific margin, in order to establish whether marine-terminating ice streams were present on the eastern side of the PIS, which is likely.

Ice-dammed lakes featured prominently along the eastern ice sheet margin during ice sheet recession (Figure 34), due to higher ground east of the ice sheet and glacial over-deepening, exacerbated by isostatic depression and eustatic sea level fall during glacial maxima (Barr and Lovell, 2014; Kaplan et al., 2009; Thorndycraft et al., 2019b). These large, deep lakes likely strongly influenced calving, outlet glacier mass balance and rates of recession (Porter et al., 1992), and should be included in numerical modelling efforts. Ice-cliff instability would likely have encouraged rapid calving (Pattyn et al., 2017; Pollard et al., 2015), especially as glaciers retreated and thinned in over-deepened lake basins, and as lake levels changed

dynamically as new spillways opened during recession. Incorporating hydrological and glaciological models, which can account for changing lake levels and calving dynamics, remains a research priority.

*Figure 35. A. Comparison of our 35 ka LGM reconstruction with that of Coronato and Rabassa (2011). Sea level reconstruction (-150m at the LGM on the Argentine Shelf) is from geological data in Guilderson et al. (2000), symbolised using the GEBCO marine bathymetry dataset. Outlet, the abbreviations: BV/RG/UE = Bella Vista/Río Gallegos/Ultima Esperanza; Corcovado = Golfo de Corcovado, Ancud = Golfo de Ancud; GCBA = Lago General Carrera/Buenos Aires; CP = Lago Cochrane/Pueyrredón; MS = Monte San Lorenzo. B. Reconstruction of ice flow pathways and ice divide for the 35 ka ice sheet. Flowlines are reconstructed using mapped geomorphology (glacial lineations, moraines, bathymetric troughs, topography, etc) and the pattern of recession. Ice divide has low confidence and is assumed to lie over the Andean mountain chain.*

Our reconstruction lacks detail on the western side of the Patagonian Andes between 46°S and 53°S. While there have been numerous studies on glacier limits to the east of the current North and Southern Patagonian Icefields, very few moraines have been dated on the wetter western flanks of the Icefields (Mercer, 1970). This is partly a function of the relative absence of Late Quaternary moraines as many western outlet glaciers of the current icefields and expanded PIS calved into deep fjords during the Pleistocene and much of the Holocene (Gassler et al., 2008; Harrison et al., 2012). In addition, post-glacial sea level rise has covered much of the geomorphological evidence of past glacier fluctuations. Dating of pre- to near-recent neoglacial moraines and glacier fluctuations to the west of the icefields is also difficult. No cosmogenic dates have thus far been successfully obtained from the wet and heavily vegetated western side, and this restricts analysis of ice sheet and glacier fluctuations to OSL, radiocarbon dating and analysis of offshore sedimentary records. As a result of these issues, few attempts have been made to date Late Quaternary glacier behaviour there, and we suggest that this represents a significant gap in our understanding of the dynamics and evolution of Patagonian ice masses and palaeoclimate forcing (cf. Harrison et al., 2012).

## 6.2 Characteristics of key advances

Analysis of the  $^{10}\text{Be}$  ages of moraines and other published ages across our large latitudinal transect allows some interpretation of the key timings of glacial advances within the time frame of this study. Focusing on

moraine mean ages allows concentration on timings of ice-margin stabilisation; other ages may be distributed between moraines, or not related directly to a period of ice-margin stabilisation. However,  $^{10}\text{Be}$  moraine ages are not evenly distributed; rather, they are clearly focused along particular latitudes, with accessible outlet lobes forming the foci for regional assessment. Analysis of the moraine mean ages across the study region indicates clusters of ages at 40 – 27 ka, a stabilisation with moraine formation at 18 – 19 ka, a clear cluster coincident with the ACR (15 – 13 ka), evidence of a small stabilisation of outlet glaciers at ~11 ka, and clusters of ages coincident with Holocene advances at 5 – 6 ka, 1 – 2 ka and at 0.5 – 0.2 ka (Figure 36A, B, C).

#### 6.2.1 Local Last Glacial Maximum: 40–30 ka

The LLGM in Patagonia is well dated by radiocarbon dating (especially in the Chilean Lake District) and cosmogenic nuclide dating (Figure 36). Nested terminal moraines consistently yield Early and Middle Pleistocene ages for the outermost moraine belts across Patagonia, with inset moraines yielding Late Pleistocene ages ranging from ~47 to 19 ka. The spread of ages across the Late Pleistocene terminal moraines indicates that at least some the outlet lobes achieved their last glacial cycle maximum positions during MIS 3 (60 to 25 ka; Siddall et al., 2008), with minor recession and stabilisation at inset moraines through the global LGM (23 to 19 ka; Hughes et al., 2013), and rapid deglaciation after ~18 to 19 ka (Figure 36B, D).

In the Chilean Lake District (38°S to 42°S), radiocarbon ages show recurrent expansions of the piedmont glaciers to the moraines at 33.6, 30.8, 26.9, and 26.0 cal. ka BP (Moreno et al., 2015). There is little dating control available in the eastern part of the Andes at this latitude. Moving south, the Río Cisnes Lobe (44.6°S) shows substantial recession from the LGM moraines by 20.1 ka (SD 0.9).

At 46°S, the Lago GCBA Lobe has the best-dated limits (Figure 35), where a range of older Middle Pleistocene ages at the outer moraines (Moreno I, II and III moraines) delimit the maximum possible extent (Hein et al., 2017; Kaplan et al., 2005). Here, the Fenix V Moraines yield a mean age of 28.0 ka (SD 1.8) (Douglass et al., 2006). The ice margin remained in this area, forming the nearby Fenix IV moraines at 28.8 ka (SD 2.1), and the Fenix III moraines at 23.3 ka (SD 2.1) (Douglass et al., 2006). The Fenix II and Fenix I moraines yield mean ages of 22.9 ka (SD 1.4) and 20.9 ka (SD 1.5) respectively (Figure 36D).

Further south (47°S), the LGM limit of the Lago CP outlet lobe of the Northern Patagonian Icefield is similarly well dated, again with outer Middle Pleistocene moraines at the Hatcher moraines limiting the maximum possible LGM extent (Hein et al., 2009). The Río Blanco Moraines yielded mean exposure ages of 29.9 ka (SD

3.0) and 27.0 ka (SD 0.5) (Hein et al., 2009, 2010; Smedley et al., 2016). The innermost Río Blanco moraines yield a mean age of 21.0 ka (SD 1.0).

The Southern Patagonian Icefield moraines are dated at the San Martín/O'Higgins Lobe, where again older Middle Pleistocene moraines indicate a relatively restricted LLGM ice extent when compared with older glaciations (Glasser et al., 2011b). Here (49°S), the M4 Moraine yields a mean  $^{10}\text{Be}$  age of 32.9 ka (SD 4.9). The Torres del Paine/Río Coyle Lobe (51°S) is well dated at the Río de las Vizcachas (RV I) terminal moraine (García et al., 2018), with a mean age of 47.0 ka (SD 0.6). The RV I lateral moraine yields a mean age of 39.2 ka (SD 3.3), and the RV II moraine has a mean age of 35.1 ka (SD 1.2). The TDP I moraine has a mean age of 21.3 ka (SD 1.7) (García et al., 2018), synchronous with the global LGM in MIS 2, with recession of circa 50 km between the LLGM at 47.0 ka and 20 ka.

The UE/BV Lobe, at the southern margin of the Southern Patagonian Icefield, is constrained by the Río Turbio Moraine Complex (51.5°S), with mean ages of 47.1 ka (SD 1.8) (García et al., 2018). The Dos Laguna Moraine Complex is dated to 36.3 ka (SD 0.7), and the AR moraine to 33.0 ka (SD 2.8) and 32.4 ka (SD 1.2) (García et al., 2018; Sagredo et al., 2011). Together with the older ages associated with the San Martín and Río Coyle lobes, this could suggest that the Southern Patagonian Icefield reached its maximum earlier than the Chilean Lake District, Isla de Chiloé area and the Northern Patagonian Icefield (cf. Figure 36D).

In Tierra del Fuego (52°S), the Magellan Lobe reached its maximum extent at a minimum age of 25.1 ka (SD 0.9) (Kaplan et al., 2008), although older moraines exist beyond that site, suggesting that the LLGM may have been earlier (Peltier et al., 2016). The Bahía Inútil-San Sebastián Lobe (53°S) has a series of cosmogenic exposure and depth profile ages (Figure 31), which suggest that the LLGM here was at 30 ka or even 45 ka (Darvill et al., 2015b; Kaplan et al., 2008).

Overall, these data indicate that the PIS reached its local maximum extent well before the global LGM of 19–23 ka (Clark et al., 2009; Hughes et al., 2013) and global sea-level lowstand of 29–19 ka (Harrison et al., 2019). This PIS instead reached its maximum extent during the last glacial cycle most likely between 47 and 30 ka across most of Patagonia (Figure 36D). We therefore use our 35 ka time-slice as our local LGM reconstruction. Outlet glaciers may have remained near that extent through the global LGM, although some are known to have receded markedly (Darvill et al., 2015b; García et al., 2018). These data suggest that the PIS reached its local LGM position earlier than the Antarctic Peninsula Ice Sheet, which reached its LLGM at 18 ka BP (Davies et al., 2012). However, further work is needed to constrain LLGM extent and timing beyond the few lobes that have a well-developed chronology. For example, there is limited work constraining the LGM timing in the eastern Chilean Lake District, southern Isla de Chiloé and Archipiélago de los Chonos, the area west of the PIS and for large parts of Cordillera Darwin.

The reason for this early LLGM is poorly understood in Patagonia (Darvill et al. 2015; García et al., 2018). However, it reproduces early local glacial maxima observed across the Pacific in New Zealand at ~44 ka, 41 ka, 35 ka, 27 ka and 20 ka (Kelly et al., 2014; Doughty et al., 2015; Strand et al. 2019). It is apparent that unlike the Northern Hemisphere ice sheets, that are linked by Milankovitch forcing to summer insolation at 65°N, the behaviour of the southern mid-latitude glaciers was not tied to summer insolation intensity (Doughty et al., 2015). In New Zealand at least, Doughty et al. (2015) inferred that the larger glacier extents between 41.2 ka and 18.29 ka were aligned with Southern Ocean surface temperatures and with low atmospheric carbon dioxide. This hypothesis needs to be evaluated more comprehensively for Patagonia, building on García et al. (2018).

*Figure 36. A. Latitudinal transect of mean  $^{10}\text{Be}$  ages (reliability of 1) and standard deviations (SD) for moraines in Patagonia (using external uncertainties). Grey bars indicate timing of significant advances, during the Local LGM (LLGM), ACR (Pedro et al., 2016), Mid-Holocene and Late Holocene. The global LGM (gLGM) is marked (Hughes et al., 2013). B: Frequency histogram of  $^{10}\text{Be}$  ages for moraines in Patagonia, 40 ka to present day. C. Gaussian probability density function (“camel plot”) of all  $^{10}\text{Be}$  ages with an age reliability of 1 or 2 from moraines in Patagonia. D. Box and whisker plot for  $^{10}\text{Be}$  ages on terminal moraines of outlet lobes across the study site.*

### 6.2.2 Onset of deglaciation: 18–19 ka

In the Chilean Lake District, the youngest advance into the Llanquihue moraine belt occurred at 17.7 – 18.1 cal. ka BP (Moreno et al., 2015). In Lago GCB, the Fenix II (north) and Menucos moraines yield mean ages of 18.9 ka (SD 1.8) and 17.3 ka (SD 1.0) respectively (Douglass et al., 2006). Here, the FCMC17 varve record also constrains the age of the Fenix I moraines, with a Bayesian modelled start age of  $18.8 \pm 0.6$  cal. ka BP, and an end age of  $18.1 \pm 0.2$  cal. ka BP (Pendle et al., 2017a). Bayesian modelled varve ages provide an age for the Menucos moraine of  $17.10 \pm 0.2$  ka BP. Other outlet lobes showing a stabilisation at that time include the Lago CP Lobe (Rio Blanco 3<sup>rd</sup> limit; 21.0 ka (SD 1.0); Hein et al., 2010), the TDP I moraines of the Torres del Paine/Río Coyle Lobe (21.3 ka (SD 1.7); García et al., 2018), Magellan Lobe (19.9 ka (SD 1.9); and 19.6 ka (SD 0.1); Kaplan et al., 2008), and the Bahía Inútil Lobe (19.4 ka (SD 0.9); Kaplan et al., 2008). In Cordillera Darwin, extensive ice recession and deglaciation had occurred by 17.2 cal. ka BP. In all these cases, rapid regional deglaciation appeared to begin after 18 – 19 ka, perhaps initiating earlier further north and with ice persisting later further south.

### 6.2.3 Antarctic Cold Reversal (ACR): 14.6 to 12.8 ka

The ACR (14.6–12.8 ka; Blunier et al., 1997; Cuffey et al., 2016; Pedro et al., 2016, 2018; Steig et al., 1998) is captured in our 13 ka time-slice (Figure 34). There is widespread evidence in Patagonia south of ~46°S that

glaciers advanced and stabilised at that time, forming prominent moraines inset from the LGM moraines (Figure 36A, B). In general, where outlet glaciers advanced during the late glacial period, it seems to have been during the ACR rather than during the Northern Hemisphere Younger Dryas (12.9–11.7 ka; Pedro et al., 2016). In several studies that date moraines to both intervals, the ACR limits are more extensive, and lateral moraines are distinctly higher, than limits during the Younger Dryas chronozone (Strelin et al., 2011, 2014; Kaplan et al., 2011; Sagredo et al., 2018; Davies et al., 2018). While glaciers had receded substantially since the LGM, ice remained sufficiently expansive to continue blocking palaeolake drainage to the Pacific Ocean, resulting in the formation of some of the largest ice-dammed lakes at this time (Figure 36).

In the Chilean Lake District, ice was well within the Andean mountains by the ACR (Moreno et al. 2015). Palaeoenvironmental evidence, such as pollen, indicates a cooling period that began during the ACR and ended during the Younger Dryas chronozone here (Hajdas et al., 2003; Marsaferro et al., 2009; Moreno et al., 2001), including to the east of the Andes (Ariztegui et al., 1997). There is no evidence of an ACR advance on Isla de Chiloé or Archipiélago de los Chonos. These sites need further investigation to test the case for an ACR advance here, especially as an advance of tropical glaciers in Peru has been observed at that time (Jomelli et al., 2014), and because oceanic cooling reachings as far north as 40°S (Pedro et al., 2016).

Outlet glaciers extending from the northern part of the Northern Patagonian Icefield underwent asynchronous advances (or relative magnitude of events) during the ACR, with calving dynamics modulating outlet glacier mass balance for those terminating in water (Davies et al., 2018). The Lago GCBA and CP lobes had disintegrated as lobes by the time of the ACR (Boex et al., 2013; Thorndycraft et al., 2019a), but moraines indicating Northern Patagonian Icefield outlet glacier stabilisation during the ACR are common in this region (Davies et al., 2018; Nimick et al., 2016; Thorndycraft et al., 2019a). Just to the east of the Northern Patagonian Icefield, in the San Lorenzo massif, Sagredo et al. (2018) observed ACR moraines from ~13.8 to 13.3 ka. To the west of the Northern Patagonian Icefield, a cold event identified in offshore cores corresponds to the ACR (Montade et al., 2019; Siani et al., 2010).

The Lago Argentino Lobe and outlet glaciers in the Torres Del Paine region advanced from the Southern Patagonian Icefield during the ACR (Fogwill and Kubik, 2005; García et al., 2012; Kaplan et al., 2011; Moreno et al., 2009; Strelin et al., 2011). Dating of the Puerto Bandera moraines at the edge of Lago Argentino provided a maximum limiting age of  $13.0 \pm 0.1$  cal. ka BP, indicating a readvance of 25 km during the ACR (Strelin et al., 2011). This was followed by rapid recession by ~12.5 cal. ka BP to near present-day positions, save for the stabilisation of Glaciar Upsala, around 12.2 ka, at the Herminita moraines (Strelin et al., 2011).

In the Torres Del Paine area of the southern Southern Patagonian Icefield, the Torres del Paine/Rio Coyle outlet glaciers advanced during the ACR at *ca* 14.9 ka (SD 1.1) to 13.7 ka (SD 0.1) (Fogwill and Kubik, 2005;



García et al., 2012; Moreno et al., 2009). The maximum extent was reached at  $\sim 14.4$  ka, forming the TDP II-IV moraines over 45 km from the present-day icefield and within close proximity of the MIS 2 TDP I limits (García et al., 2012). Following the ACR, there was major glacier recession (García et al., 2012), with some reports of subsequent advances of early Holocene age (Marden and Clapperton, 1995; McCulloch et al., 2000) but with limited age precision. A similar pattern is indicated by analysis of  $^{14}\text{C}$  ages from peat and sediment cores from the fjord channel system located to the NE of the present-day Grand Campo Nevado ice cap suggests that the deglaciating Skyring Lobe retreated slowly, and possibly stabilised during the ACR (Kilian et al., 2007a).

The extent of ACR glacier re-advances in the Cordillera Darwin region has been the subject of some debate. McCulloch et al. (2005b) and Sugden et al. (2005) proposed an ACR re-advance from Cordillera Darwin that extended northwards into the Strait of Magellan, reaching Isla Dawson and damming a large proglacial lake. However, Hall et al. (2013) recorded deglaciation ages of  $\sim 16.8$  ka at a location over 100 km to the south of the previously proposed ACR limits, suggesting there is no evidence for an extensive ACR advance in the Cordillera Darwin. Recently, Hall et al. (2019) argued that Cordillera Darwin glaciers were restricted in ice extent during the ACR. Moraines dating clearly to an ACR advance are also lacking in the Strait of Magellan (Fernández et al., 2017). ACR glacier advances in the Cordillera Darwin region were also identified by Menounos et al. (2013), who dated advances ( $\sim 1$  km from the backwall) of alpine glaciers in relatively small cirques surrounding Ushuaia to 13.5 ka (SD 1.3) and 14.3 ka (SD 0.2) (mean ages).

#### 6.2.4 Late Pleistocene/Early Holocene transition: 12 – 10 ka

In some valleys, there are minimum-limiting  $^{14}\text{C}$  ages that morphostratigraphically relate to the moraines, and lie in the Northern Hemisphere Younger Dryas chronozone (e.g., Marden and Clapperton, 1995; Mercer, 1968, 1976; Strelin and Malagino, 2000; Wenzens, 1999). At Lago Argentino, the Herminita moraine system is dated to 12.2 cal. ka BP (Strelin et al., 2011). There are often not enough dates or  $^{14}\text{C}$  data are minimum-limiting, or it is in general not clear how such stillstands or advances relate specifically to the Younger Dryas events in the Northern Hemisphere. Furthermore, in valleys mapped with sufficient resolution, numerous cross-valley moraines, post-dating maximum ACR ice position, are identified (e.g. Martin et al., 2019). This is indicative of active recession, with glaciers frequently stabilising and forming moraines. The post-ACR moraines dated to 10 – 11 ka around the Northern Patagonian Icefield and the Nef valley (Glasser et al., 2012) could be part of this active recession, or a dynamic response to palaeolake drainage as ice dams receded past key cols and spillways during a period of rapid regional warming. The early to mid-Holocene Tempanos Moraine from Laguna San Rafael also indicate a period of ice-margin stabilisation and moraine formation post-dating the ACR in the Early Holocene (Harrison et al., 2012).

Paleoclimate data from onshore and immediately offshore along the Taitao Peninsula suggest that the Younger Dryas chronozone was an event characterised by cooler and drier conditions (Massaferro and Brooks, 2002; Siani et al., 2010), but, according to pollen records, did not represent a significant climate reversal as reported further north in the Chilean Lake District. In southern Patagonia, Moreno et al. (2009) inferred that after the ACR, conditions were slightly warmer but still cold and variable until the start of the Holocene early thermal maximum.

The alpine glaciers in cirques surrounding Ushuaia also contain the only record of glacier activity of Younger Dryas age in that part of southernmost Patagonia, represented by a single recessional moraine dated to 12.38 - 12.01 ka (Menounos et al., 2013). Palaeoenvironmental evidence for Younger Dryas cooling in the Strait of Magellan has been the subject of great debate, with a particular focus on whether cooling was climate-driven or by other factors (Heusser and Rabassa, 1987; Heusser et al., 2000; Markgraf, 1993; McCulloch and Davies, 2001). Evidence from Fiordo Marinelli in Cordillera Darwin supports highly restricted ice extent from 8 cal. ka BP, during the Early Holocene (Hall et al., 2019).

#### 6.2.5 Mid-Holocene: 6 – 4 ka

Figure 36A, B and C reveals a consistent set of moraine ages indicating a mid-Holocene neoglaciation, and the first major glacier stabilisation since the end of the ACR. They include mean  $^{10}\text{Be}$  ages of 5.4 ka (SD 0.2) in front of Lago Colonia (47.3°S) (Nimick et al., 2015). The first deglaciation of the Glaciar Gualas lagoon occurred by  $5.3 \pm 0.2$  cal. ka BP, indicating ice extent near this point until the mid-Holocene (Fernandez et al., 2012). For MSL, a mean age of 5.7 ka (SD 0.1) was obtained on the RT6 moraines of Tranquilo Glacier (47.5°S) (Sagredo et al., 2016). An overgrown tree within moraines surrounding an eastward-flowing outlet glacier of MSL provide a maximum age for glacial advance of  $5.3 \pm 0.7$  cal. ka BP (Mercer, 1976). Lichenometric data further supports a period of glacier stabilisation and moraine formation for Glacier San Lorenzo and Glaciar Rio Lacteo at 5.8 to 4.5 ka (Garibotti and Villalba, 2017).

Around the Southern Patagonian Icefield, moraines have  $^{10}\text{Be}$  exposure ages ranging from  $5.2 \pm 0.4$  to  $4.6 \pm 0.4$  ka on the outer Pearson moraines near Lago Argentino (49.9°S), and ranging from  $5.7 \pm 0.5$  to  $4.5 \pm 0.4$  ka on the Herminita Peninsula at 50.0°S (Kaplan et al., 2016; Strelin et al., 2014). In the most south-westerly part of the Lago Argentino basin, Holocene moraines date to around 6.1 to 5.7 ka around Lago Frias (50.6°S) (Kaplan et al., 2016; Strelin et al., 2014). Just to the north of Lago Viedma, Glacier Torres has a sequence of progressively inset moraines with mean  $^{10}\text{Be}$  ages of 6.9 ka (SD 0.1), 6.2 ka (SD 0.2) and 4.5 ka (SD 0.1) (Reynhout et al., 2019). These  $^{10}\text{Be}$  ages agree with the more widespread limiting  $^{14}\text{C}$  ages that indicate ice margins close to the most recent 0.5 – 0.2 ka maximum extent before or by 5 ka. For example, radiocarbon

ages of  $3.6 \pm 0.2$  and  $4.8 \pm 0.5$  cal. ka BP inside moraines from Río Condor and Río Guanaco, respectively, constrain a mid-Holocene ice advance east of the Southern Patagonian Icefield (Wenzens, 1999). For Cordillera Darwin, there is strong evidence of glacier advances at  $6.7 - 5.4$  cal. ka BP, synchronous with ice advances reported in the Southern Patagonian Icefield (Hall et al., 2019).

In all these cases, these mid-Holocene moraines are close to, but just larger than, moraines with ages of  $1 - 2$  ka or  $0.2 - 0.5$  ka. Recent findings, especially in Lago Argentino and at San Lorenzo, support earlier work by Mercer (1968) or inferred larger middle than Late-Holocene limits. The exception are the Leones Moraine, west of the NPI, which does show significant differences between the  $0.5 - 0.2$  ka and early to mid-Holocene advances (Harrison et al., 2008). It is highly likely that moraines of mid-Holocene age are more widespread in Patagonia, but limited work dating these advances has been carried out and many of these moraines may have been re-occupied by glaciers during the last few centuries. However, unlike glaciers in the Northern Hemisphere, which reached their maximum extent during the “Little Ice Age” (cf. Ivy-Ochs et al., 2009; Solomina et al., 2015), this mid (or early)-Holocene advance is likely to be the greatest since the end of the ACR, with relatively more subdued ice advances during the last millennium. Similar Neoglacial mid-Holocene advances have been observed at this time in the sub-Arctic islands (Hall, 2009) and in New Zealand (Bravo et al., 2015; Schaefer et al., 2009).

Kaplan et al. (2016) suggested that the  $6 - 4$  ka mid-Holocene advance is due to a northward expansion of the SWW at this time, bringing colder polar/subpolar air. Moreno et al. (2018) showed that the Mid-Holocene was a time of pervasive or persistent negative SAM-like conditions of cold and wet climate, which forced glacier growth. Using PMIP2 climate model simulations, Bravo et al. (2015) suggest that during the mid-Holocene (6 ka), there were cooler conditions during the austral summer ( $-0.2^{\circ}\text{C}$ ), autumn ( $-0.5^{\circ}\text{C}$ ) and winter ( $-0.4^{\circ}\text{C}$ ), with slightly warmer conditions during the spring ( $+0.2^{\circ}\text{C}$ ). This was accompanied by a seasonal shift in precipitation, with increased precipitation from October to April. This resulted in an ELA that was  $15 - 33$  m lower during the mid-Holocene than at 1750 AD, resulting in slightly larger glacier extents at this time (Bravo et al., 2015). These Neoglacial glacier expansions were followed by warming and glacier recession that drove glacier recession and ice limits similar to present (Moreno et al., 2018).

#### 6.2.6 Last two millennia: $1 - 2$ ka

Figure 36 shows consistent evidence of a Neoglacial readvance at  $1 - 2$  ka, when colder conditions are recorded in Antarctic ice cores (Cuffey et al., 2016). Some of these late Holocene advances are also constrained by OSL or radiocarbon dating. These include moraines dated to  $1.1 \pm 0.2$  ka by OSL and  $^{10}\text{Be}$  at Glacier Leon, an outlet glacier of the Northern Patagonian Icefield (Harrison et al., 2008) ( $46.7^{\circ}\text{S}$ ); the Lago

Onelli moraine at the head of Lago Argentino ( $1.4 \pm 0.1$  ka), moraines on the Herminita Peninsula at  $50^\circ\text{S}$  ( $^{10}\text{Be}$  ages are  $1.2 \pm 0.1$  ka;  $2.1 \pm 0.2$  ka;  $1.4 \pm 0.1$  ka), and moraines from nearby Lago Pearson dating from  $1.6 \pm 0.1$  and  $1.3 \pm 0.1$  ka (Kaplan et al., 2016; Strelin et al., 2014). A series of radiocarbon ages indicate a similar late Holocene readvance in the nearby Agassiz Este Valley (Strelin et al., 2014). Radiocarbon ages indicate a later readvance that predates the 0.5 – 0.2 ka advance at Soler Glacier (Glasser et al., 2002). Finally, radiocarbon ages indicate a late Holocene advance during the last two millennia in Cordillera Darwin, using bracketing inside-outside ages to constrain moraine limits to *ca* 2 ka (Kuylenstierna et al., 1996). Radiocarbon ages from Fiordo Marinelli, Cordillera Darwin, indicate Late Holocene advances at 1.3–1.1 cal. ka BP and 3.8 – 2.4 cal. ka BP (Hall et al., 2019).

Further work is needed to firmly establish glacier limits before a region-wide reconstruction can be attempted for this late Holocene readvance. However, the proximity of dated limits to those dated to 5 ka and the 0.5 – 0.2 ka advance suggest that this ice advance was of a similar magnitude to those occurring in the mid and late Holocene, although this may have varied depending on glacier size or other factors.

#### 6.2.7 Late Holocene: 0.5 – 0.2 ka

A final near-recent Neoglacial readvance is evidenced by historical documents (e.g. Araneda et al., 2007; Casassa et al., 1997; Rivera et al., 2012b), dendrochronology (e.g. Masiokas et al., 2009b; Winchester and Harrison, 2000; Winchester et al., 2001, 2014), lichenometry (Harrison et al., 2007; Garibotti and Villalba, 2009, 2017), and  $^{10}\text{Be}$  dating (Kaplan et al., 2016; Reynhout et al., 2019). The most recent moraines and trimlines, generally assumed to date from the period 0.5 – 0.2 ka, show distinctive differences to older Holocene moraines in terms of vegetation and degradation on satellite imagery (Davies and Glasser, 2012; Glasser et al., 2011a).

In the Isla de Chiloé and Archipiélago de los Chonos sector, lichenometric dating of Glaciar Torrecillas suggests a series of consecutively stratigraphically younger moraines date from 1735 AD to 1934 AD (Garibotti and Villalba, 2009).

At the Northern Patagonian Icefield, chronostratigraphic data record a readvance of Glaciar San Rafael into the lagoon at 1871 AD, followed by recession to present-day limits at 1675 and 1766 AD (Araneda et al., 2007; Winchester and Harrison, 1996). Dendrochronological records indicate advance of Glaciar Benito of the Northern Patagonian Icefield to prominent nearby moraines at 1860 AD (Winchester et al., 2014). On the eastern Northern Patagonian Icefield, Glaciar Nef formed prominent moraines at 1863 AD (Winchester et al., 2001), and moraine crests around Lago Arco date an advance of glacier NPI-24 at 1881 AD (Winchester and Harrison, 2000). In this case, this signifies a significant difference in distance between Mid-Holocene

moraines dated to  $5.4 \pm 0.3$  ka (Nimick et al., 2016) and near-recent moraines for Glaciar Colonia. For Monte San Lorenzo, lichenometric dating indicates ice-margin stabilisation at *ca* 1925 AD (Glaciar Rio Lacteo) and 1795 – 1955 AD (Glaciar San Lorenzo) (Garibotti and Villalba, 2017).

For the Southern Patagonian Icefield, historical documents provide evidence of a substantial advance of Glacier Jorge Montt relative to present at 1898 AD (Rivera et al., 2012a). Glacier O'Higgins likewise advanced into Lago O'Higgins at 1896 AD (Casassa et al., 1997). On the eastern Southern Patagonian Icefield, dendrochronology indicates glacier advance to prominent moraines at 1626 to 1850 AD (Masiokas et al., 2009b). Moraines near Huemul Glaciar are dated from 1481 to 1886 AD by lichenometry (Garibotti and Villalba, 2009).

On the Herminita Peninsula, a number of moraines, just inside the mid-Holocene and last two millennia moraines described above, are dated using  $^{10}\text{Be}$  dating to *ca* 0.2 to 0.6 ka (Kaplan et al., 2016; Strelin et al., 2014). Moraines just inside those of Mid-Holocene age at Glacier Torres have  $^{10}\text{Be}$  exposure ages of 0.5 ka (Reynhout et al., 2019). In the south-western Lago Argentino basin, moraines inside the mid-Holocene limits document an advance of Grande Glacier at 0.2 to 0.5 ka (Kaplan et al., 2016). A Late Holocene advance of the Gran Campo Nevado ice cap is recorded by dendrochronology on glacier moraines dating from AD 1628 to AD 1886 (Koch and Kilian, 2005). An advance of glaciers at Cordillera Darwin is recorded in Fiordo Marinelli, where two advances are dated to  $\sim 480$  and  $\sim 750$  years BP. The most recent of these reached Narrows Moraine (Figure 32), where it remained until historical times (Hall et al., 2019).

Many of the moraines dating from the mid- and late-Holocene are morphologically similar to moraines dated to the last few centuries by dendrochronology, lichenometry, historical documents or geological data. While in some cases a series of inset moraines are present, independently dated to  $\sim 6 - 5$  ka,  $\sim 1 - 2$  ka and  $\sim 0.3$  ka (Kaplan et al., 2016; Strelin et al., 2014), in other places, the same moraines may have been repeatedly occupied. Additionally, some moraines assumed to date from the last two centuries may have initially been formed much earlier. Further work is therefore required to untangle these complex relationships, and we are presently unable to definitively separate out ice extent through these Mid- and Late-Holocene advances at a continental scale.

#### 6.2.8 Latitudinal variations in timings of key advances

The large latitudinal transect covered by the former PIS allows examination of the spatial variation in timings of ice-marginal stabilisation and recession (summarised in Table 7). This in turn can be used to investigate palaeoclimatic controls driving ice sheet dynamics. However, while some of these fluctuations are clearly related to large-scale climatic drivers, it is possible that some ice-marginal fluctuations could have been

driven by glaciodynamic processes, especially changes in glaciomarine or glaciolacustrine calving, as glaciers receded into embayments or created large glacier lakes at their termini (Bendle et al., 2017a; Lovell et al., 2012; Darvill et al., 2017; Davies et al. 2018; Thorndycraft et al., 2019). We also note that thermal regime could evolve or switch as ice volume changed, which could influence glacier response time and lag times between climate and ice extent or dynamics (Glasser and Jansson, 2005). Further work and detailed numerical modelling is required to further investigate the internal versus external drivers of former ice margin variability.

In the Chilean Lake District (38 – 42°S), the piedmont lobe glaciers advanced repeatedly at 33.6, 30.8, 26.9, and 26.0 cal. ka BP (Moreno et al., 2015). On Isla Grande de Chiloé, an ice-dammed lake dated to  $26.8 \pm 0.2$  cal. ka BP indicates that the Golfo de Corcovado outlet lobe was near its maximum extent at that time (Denton et al., 1999). In the central sector of Isla Grande de Chiloé, at Dalcahue, the most extensive advance occurred at 17 – 18 cal. ka BP. The Lago GCBA and Lago CP outlet lobes of the Northern Patagonian Icefield record maximum extents with mean moraine ages of 28.0 ka (SD 1.0) (Douglass et al., 2006) and 29.9 ka (SD 3.0) (Hein et al., 2010) (Table 7). Therefore, the available evidence suggests that from 38°S to 46°S, the LLGM was reached at ca. 33 – 28 ka.

Further south, in the Southern Patagonian Icefield, the LLGM was reached earlier, with the oldest moraines of the Torres del Paine/Río Coyle Lobe pertaining to the last glaciation dated to 47.0 ka (SD 0.6) (Garcia et al., 2018). Associated lateral moraines yielded a mean age of 39.2 ka (SD 3.3) to 35.1 ka (SD 1.2). Similarly, the UE/BV Lobe yielded maximum LLGM ages of 47.1 ka (SD 1.8) (Garcia et al., 2018; Sagredo et al., 2011). Inboard of this, the Aracuco moraines yielded mean ages of 33.0 ka (SD 2.8). Together, these show that the LLGM was reached in the region of 48°S to 52°S during MIS 3, at ca. 47 ka. At 53°S, the Magellan Lobe was extensive at 27.7 ka (SD 1.0) (Kaplan et al., 2008), although the maximum LLGM ice extent may have been reached even earlier, at  $\sim 60 - 70$  ka, during MIS 4 (Peltier et al., 2016). Cosmogenic dating of outwash gravels from the Bahía Inútil-San Sebastián Lobe (53°S) suggests that ice was extensive here at  $\sim 45.6$  ka, and confidently before 30.1 ka (Darvill et al., 2015). We therefore suggest that the currently available evidence also supports an LLGM in this region at 47 ka, or possibly earlier in the last glacial cycle.

The timing of the onset of deglaciation, which we define as when glacier recession accelerated, also varies latitudinally. In the Chilean Lake District, rapid deglaciation was initiated after ca 18 ka, with glaciers retreating into the mountains by 16.8 cal. ka BP. Limited data after that time is available in the sector from 42 – 46°S. In the Northern Patagonian Icefield, the outlet lobes had only minor recession from the LGM until 17 – 18 ka (Lago GCBA) and 21 ka (Lago CP), with deglaciation after this time, similar to the Río Cisnes valley (García et al., 2019). The tephra-constrained FCMC17 varve record at Lago GCBA indicates a phase of ice-lobe recession beginning at  $18.1 \pm 0.2$  cal. ka BP followed by accelerated recession coinciding with calving

dynamics from  $17.3 \pm 0.1$  cal. ka BP (Bendle et al., 2017a; 2019). There is limited data around the Southern Patagonian Icefield, though moraines around the margin of Lago del Toro yield a mean age of 21.3 ka (SD 1.7), suggesting deglaciation after this time. Deglaciation began at ca 19 – 20 ka in the Gran Campo Nevado and Cordillera Darwin regions (52°S – 56°S; Table 7).

Evidence for an ACR glacier stabilisation is absent from 38°S to 46°S, but there is strong evidence of an advance from 14 – 13 ka around the Northern and Southern Patagonian icefields. In that sector (46°S – 52°S), ice remained reasonably extensive until after the ACR, with large ice-dammed lakes forming in front of the icefields. An ACR advance also occurred around Cordillera Darwin. However, glaciation at that time may have been smaller scale, and restricted to upland cirque glacier advance.

Mid-Holocene readvances are well documented around the Northern and Southern Patagonian icefields. A Late-Holocene advance at ~2 ka is also observed between 46°S and 56°S. Further work is required to establish whether the northern parts of Patagonia underwent no glacial advances at this time. Finally, a Late Holocene advance synchronous with the Northern Hemisphere “Little Ice Age” at 0.5 – 0.2 ka is well documented across the latitudinal gradient of Patagonia.

We note that there is a synchronous response to substantial climate changes such as that seen during the period 0.5 – 0.2 ka and at the beginning of the 21<sup>st</sup> century (cf. Meier et al., 2018). This suggests that for larger global climate changes, there is a synchronous response.



Table 7. Summary of evidence of the timing of key advances and during key climatic transitions across the Patagonian latitudinal transect.

Location	Latitude	Local LGM	Global LGM (23 – 19 ka)	Onset of deglaciation	ACR (14.6 – 12.8 ka)	Early Holocene (12 – 10 ka)	Mid-Holocene readvance	Readvances in the last two millennia	Late Holocene advance at 0.5 – 0.2 ka
Chilean Lake District	38°S – 42°S	33.6 – 26.0 ka	Limited data	After 17.7 ka	Strong recession; limited data	Strong recession; limited data	Limited data	Limited data	Advance at 0.5 – 0.2 ka
Isla de Chiloe and Archipiélago de los Chonos	42°S – 46°S	26.8 ka	Limited data	Limited data; recession in Cisnes from 20.1 ka	Limited data, no evidence for advance	No evidence for advance	Limited data	Limited data	Advance at 0.5 – 0.2 ka
Northern Patagonian Icefield	46°S to 48°S	28.0 to 29.9 ka	Moraines near LLGM at 23.3 to 21 ka	After 17.5 ka	13.2 – 13.3 ka	Inset moraines at 11.4 ka. San Rafael moraines 9.3 – 9.7 ka	San Rafael: 7.7, 5.7 ka Gualas: 5.4 – 4.1 ka MSL: 5.7 ka	Leones: 2.5 ka	Advance at 0.5 – 0.2 ka
Southern Patagonian Icefield	48°S – 52°S	O'Higgins: 34.9 ka Rio Coyle: 47 ka UE/BV: 47.1 ka	TDP I moraine 21.2 ka, near LLGM extent	Lago del Toro: after 21 ka	13.3 – 14.1 ka Torres del Paine: 14 ka. Puerto Bandera ~13 ka	Limited data. Glaciar Torre (10 – 9.5 ka)	Glaciar Torre: Multiple small advances 6 – 4 ka. Sierra de Sangra: 4.9 ka	Herminita: 3 – 2 ka; 1.4 – 1.5 ka	Advance at 0.6 – 0.2 ka
Gran Campo Nevado	52°S – 53°S	27.7 ka, though ice may have been more extensive earlier	Limited data	Magellan: after 19.4 ka	Limited data	Limited data	Limited data	Limited data	Advance at 0.5 – 0.2 ka
Cordillera Darwin	53°S – 56°S	45.6 ka	Limited data	After 19.4 – 19.9 ka	Ushuaia: 13.5 – 14.3 ka; small advances. Fiordo Marinelli	Restricted ice extent, similar to present	6.7 – 5.4 cal. Ka BP	3.8 – 2.4 cal. ka BP 1.3 – 1.1 cal. Ka BP	Advance at 0.5 – 0.2 ka

shows restricted  
ice extent.

---

Journal Pre-proof

### 6.3 *Glacier and ice-dammed palaeolake area and volume change*

#### 6.3.1 *Glacier area and volume change*

Our calculated area and volume for the PIS at each time-slice is presented in Table 8 and Figure 37. The reconstructed maximum glacierised area is the best estimate to date of ice-sheet extent through time, although uncertainties remain, particularly at 10 and 5 ka (Figure 34). Ice extent at 0.5 to 0.2 ka and present day (2011 AD) takes into account previous estimates (Davies and Glasser, 2012; Glasser et al., 2011a), but has been updated with our new glaciological mapping. The annualised rate of change between each time slice is an average over the entire time-slice and does not consider periods of time when rates of recession may have been more rapid. It is therefore a useful guide to average rates of change.

Calculated ice volumes (Table 8) are dependent on volume-area scaling using different power laws for ice sheets, ice fields, glaciers and dome-shaped mountain ice caps (see Section 3.3.5). Vertical constraints on ice-sheet thickness are limited (e.g. Boex et al., 2013), meaning that ice volume estimates remain challenging. Though crude, our calculations provide insights into volume change of the PIS and its contribution to sea level change through the late glacial. Present-day ice volume is from Carrivick et al. (2016) using a more sophisticated method, and adjusted for ice volume below sea level. Ice volume at 0.2 ka is likely within errors of the estimate for present-day.

The PIS reached its maximum extent during MII. 3, and was relatively stable from 35 to 30 ka. From a local LGM maximum extent, initial recession and deposition of inboard moraines began by 25 ka (Figure 37), during a period of slight cooling in the Antarctic ice cores (Cuffey et al., 2016; Wais Divide Project Members, 2013) (Figure 37C), and perhaps highlighting the role of atmospheric circulation changes (such as changes in the SWW) in driving ice-sheet dynamics. The maximum extent of the PIS thus preceded the global LGM. To some degree, this may be because the global LGM is defined by  $\delta^{18}\text{O}$ , which is a function of the large ice sheets, which take longer to reach a maximum size, compared with the relatively small and dynamic PIS. An earlier LLGM may also highlight the role of regional atmospheric and oceanic circulation changes in driving ice-sheet dynamics to large extents well before the Laurentide and other ice sheets reached their maxima.

*Table 8. Estimated area and volume of the Patagonian Ice Sheet and associated ice fields, glaciers and mountain ice caps, at each time-slice, and calculated annualised rates of recession. \*Present-day ice volume and SLE was estimated by Carrivick et al. (2016). Volume-area scaling estimates the 2011 extent to be  $2.2 \times 10^3$  Gt. SLE = Sea level equivalent. 0.2 ka ice volume is within errors of present-day ice volume. See also Figure 37.*

Time Slice	Total ice-covered area (km <sup>2</sup> )	Difference (km <sup>2</sup> )	Rate of change (km <sup>2</sup> /yr)	% area change	% area change per annum (% a <sup>-1</sup> )	Volume (Gt)	SLE (mm)
35 ka	$492.6 \times 10^3$		0	0	0	$541.2 \times 10^3$	1496
30 ka	$491.3 \times 10^3$	$1.3 \times 10^3$	0.27	0.3%	0.000%	$539.8 \times 10^3$	1492
25 ka	$465.3 \times 10^3$	$26.0 \times 10^3$	5.20	5.3%	0.001%	$503.5 \times 10^3$	1392
20 ka	$359.6 \times 10^3$	$105.7 \times 10^3$	21.14	22.7%	0.005%	$367.2 \times 10^3$	1015
15 ka	$121.8 \times 10^3$	$237.7 \times 10^3$	47.55	66.1%	0.013 %	$144.8 \times 10^3$	400
13 ka	$116.7 \times 10^3$	$5.1 \times 10^3$	2.57	4.2%	0.002%	$134.2 \times 10^3$	371
10 ka	$63.8 \times 10^3$	$53.1 \times 10^3$	10.61	45.5%	0.009%	$51.0 \times 10^3$	141
5 ka	$31.1 \times 10^3$	$32.5 \times 10^3$	6.50	51.1%	0.010%	$21.7 \times 10^3$	60
0.2 ka	$27.9 \times 10^3$	$3.2 \times 10^3$	0.66	10.4%	0.002%	$5.5 \times 10^3$	$14.7 \pm 2.9$
2011 AD*	$23.3 \times 10^3$	$4.6 \times 10^3$	32.90	16.5%	0.118%	$5.5 \times 10^3$	$14.7 \pm 2.9$

*Figure 37. A. Area of the PIS at each time-slice (see Table 8). Grey line represents glaciated area of the PIS (km<sup>2</sup>). The black line represents the annualised rate of change (km<sup>2</sup>/year) between each time-slice. B. As A, but with percentage area change per annum (% a<sup>-1</sup>). C. Surface air temperatures from West Antarctica (Cuffey et al., 2016). D. Global ice volume sea-level equivalent, with timing of global ice-volume maximum highlighted (from Harrison et al., 2019). Timings of significant Patagonian glacier advances are highlighted in vertical blue bars. Meltwater pulse (MWP) 1A and 1B are highlighted in pink bars.*

Particularly rapid recession and widespread deglaciation occurred after ~18 ka at the end of the late glacial, during a period of rapid Antarctic warming (Cuffey et al., 2016; Wais Divide Project Members, 2013) (Figure 37C), and rapid sea level rise (Figure 6) (Guilderson et al., 2000; Harrison et al., 2019). Rapid retreat in the Lago GCBA Lobe has also been attributed to abrupt southward migration of the SWW, which may have enhanced ablation at the ice sheet surface (Bendle et al., 2019). The PIS potentially contributed ca 615 mm to global eustatic sea level rise between 20 and 15 ka, when we estimate that it shrank from  $359.6$  to  $121.8 \times 10^3$  km<sup>2</sup> (Table 8). Glaciers stabilised or re-advanced during the ACR (Figure 37), although the PIS was by then significantly smaller than during the LLGM at  $116.7 \times 10^3$  km<sup>2</sup>.

Rates of ice recession slowed through the Holocene until after 0.2 ka (with the caveat that some time-slices are highly uncertain). Absolute recession rates ( $\text{km}^2 \text{a}^{-1}$ ) over recent decades rival those seen between 20 and 15 ka for an ice sheet more than two orders of magnitude larger, and relative average rates of recession ( $\% \text{a}^{-1}$ ) are higher between 0.2 ka and 2011 AD than at any time observed in our reconstruction (Table 8). However, more rapid rates of recession are possible during deglaciation, given the 5 kyr resolution of our reconstruction. It is likely that there were periods of time with especially rapid rates of recession during the last glacial-interglacial transition, when many outlet lobes were calving into large, deep, ice-dammed lakes; however, the published chronologies and our compilation are currently not able to capture this.

There are fewer degrees of freedom for ice extent and volume changes during the Holocene than earlier time slices. Ice margins stabilised not far from present-day positions by the early Holocene, and dated moraines suggest that Holocene neoglacial advances were largely similar to advance at 0.2 ka in size. Thus we argue that average rates of ice-marginal recession are currently faster than at any time observed in the Holocene, in line with recent temperature increases observed in Antarctica and Patagonia, following a sustained period of relative stability, and when glacial lake area remains fairly constant (Figure 37C, Table 9; see below). Since observations indicate that rates of recession in Patagonia have accelerated in recent decades, from  $34.3 \text{ km}^2 \text{a}^{-1}$  ( $0.14 \% \text{a}^{-1}$ ) for 1986 – 2001 AD to  $51.2 \text{ km}^2 \text{a}^{-1}$  ( $0.22 \% \text{a}^{-1}$ ) for 2001 – 2011 AD (Davies and Glasser, 2012), this is especially concerning.

### 6.3.2 Ice-dammed palaeolake area change

Table 9 presents calculated ice-dammed lake areas and volumes for 23 palaeolakes for each of the key timeslices. During the LGM, the PIS blocked drainage of palaeolakes to the Pacific, and they drained instead towards the Atlantic Ocean. The ACR was characterised by large ice-dammed palaeolakes filling glacial over-deepening within the LGM terminal moraines, and the start of the fragmentation of the PIS into the modern-day icefields, ice caps and glaciers. During the ACR, glacier recession had allowed some lakes around the Northern Patagonian Icefield to drain towards the Pacific (Thorndycraft et al, 2019a).

Glacial lake area peaked at ~13 ka with an estimated area of  $13,999 \text{ km}^2$  (Table 9), with the enlargement of palaeolakes Chelenko, Tar and Tehuelche-Puerto Consuelo. This is substantially larger than previous estimates of palaeolake area at this time ( $7,400 \text{ km}^2$ ; Glasser et al., 2016; Harrison et al., 2019). These large ice-dammed lakes likely exerted a strong control on glacial recession, as evidenced over the short 17.3 - 17.0 ka period at the end of the FCMC17 varve record (Bendle et al., 2017a), and would have contributed to the rapid absolute rates of recession observed at that time (Figure 37).

Glacial lake area minimum was reached at 10 ka (assuming that all lakes are mapped and known at this time slice; Figure 38). Rapid recession of glaciers from the end of the ACR to *ca* 10 ka led to many of these lakes reaching their current spatial extent and volume. As ice dams receded, this cold, fresh water may have been released suddenly into the Pacific (Thorndycraft et al, 2019a), possibly affecting regional climate (Glasser et al., 2016b). Thorndycraft et al. (2019) noted that opening drainage pathways to the Pacific through separation of ice fields and ice caps in the Northern Patagonian Icefield region led to a  $\sim 1.0 \times 10^5 \text{ km}^2$  increase in watershed drainage area to the Pacific.

Glacial lake area at 5 ka and during the 0.5 to 0.2 ka advance was similar to the present day and is not calculated separately due to the low confidence in most ice margins at 5 ka. In some basins, parts of these palaeolakes remain as the modern proglacial lakes. In addition to these larger glacial lakes, Wilson et al. (2018) mapped 4204 current glacier lakes in our study region, equating to 1,178  $\text{km}^2$  in addition to the glacial lakes noted in Table 9 below.

The remaining lake water today, from lakes that were within the footprint of the palaeolakes, is 6,823.6  $\text{km}^2$ . Overall, between the maximum lake extent at 13 ka and today, there has been a reduction in glacial lake area of 7,175.6  $\text{km}^2$ . It is important to note that although glacial lake area remained relatively constant during the Holocene (Figure 38), rates of glacier recession (percentage change per annum) observed in the 20<sup>th</sup> century are currently far higher than have been observed or reconstructed at any time in the last 10,000 years.

Table 9. Calculated glacier lake area (km<sup>2</sup>). Present-day glacial lake area is also provided for those palaeolakes that still remain today in some form. Palaeolake Magellan-Bahia Inútil likely existed for some time between 20 and 15 ka, but is not included here due to uncertainties in timing.

Sector	Latitude (°S)	Palaeolake Name	Area (km <sup>2</sup> )							Present-day (remaining lake waters)	
			35 ka	30 ka	25 ka	20 ka	15 ka	13 ka	10 ka	Present-day status of glacial lakes	Area (km <sup>2</sup> )
Chilean Lake District	41.0	Nahuel Huapi	-	-	-	-	-	239.8	576	Lago Nahuel Huapi	538.1
	41.1	Elpafquen	-	-	-	-	472.2	-	-	Lago Nahuel Huapi	
Isla de Chiloé-Archipiélago de los Chonos region	42.2	Epuyen	-	-	-	114.9	0	0	0	Drained completely	0
	42.2	Golfo de Ancud	-	-	319.2	366.3	0	0	0	Drained completely	0
	42.5	Cholia	-	-	-	233.35	0	0	0	Drained completely	0
	45.0	Cisnes-Nirehuao	-	-	-	743.1	1126.5	1126.5	0	Drained completely	0
	45.7	Frio	-	-	-	50.4	4.1	4.1	4.1	Small remnant lakes; Lago Frío	4.1
	45.6	Lago Castor	-	-	70.3	Frío, 13.01	13.01	13.01	13.01	Castor and Lago Pollux	13.01
	45.9	Balmaceda	-	-	102.6	345.3	0	0	0	Drained completely	0
Northern Patagonian Icefield	47.3	CP-Chacabuco	120	120.1	153.7	155.23	1965.7	Palaeolake Chelenko	348.8	Lago CP	348.77
	46.5	Deseado	-	-	-	-	3151.5	Palaeolake Chelenko	1803.2	Lago GCBA	1803.15
	46.8	Chelenko	-	-	-	-	-	4740.5	-	Evolved into Lago GCBA/CP	
	47.4	Tranquilo	-	-	-	-	-	20.3	0	Drained completely	0
Southern Patagonian Icefield	49.7	Tar	409.0	409.0	514.5	567.2	797.3	981	711	Lago O'Higgins / San Martin / Tar	1054.2
	51.1	Tehuelche	-	52.2	276.6	829.4	-	-	-	Small remnant lakes; Lago del Toro and Balmaceda	
	51.9	Consuelo	-	-	89.6	217.9	-	-	-		
	51.6	Tehuelche-Puerto Consuelo	-	-	-	-	1369.7	1369.7	269.7		269.7
	49.7	Viedma	-	-	-	-	661.9	662.2	766.2	Lago Viedma	1200.8
	50.2	Argentino	-	-	-	-	124.9	713.2	1083.3	Lago Argentino	1479.5
	50.5	Southern Lago Argentino	-	-	-	-	-	-	248	Joined with Lago Argentino	0
Gran Campo Nevado	52.4	Blanca	-	-	466.9	551.5	112.3	112.3	112.3	Laguna Blanca	112.3
	52.8	Magellan	-	-	1618.7	2162.6	0	0	0	Marine fjord	0
Cordillera	52.6	Skyring	-	-	-	-	1564	1564	0	Marine fjord	0



<b>Darwin</b>	53.1	<b>Otway</b>	-	-	-	-	2452.6	2452.6	0	Marine fjord	0
<b>Total</b>			529.0	581.3	3,612.6	6,350.2	13,815.7	13,999.2	5,935.6		6,823.6

Figure 38. Change in glacier lake area in Patagonia from the LGM to present, visualising data from Table 9.

#### 6.4 Key future research agendas

We suggest the Patagonian research community focus on the following six key priority areas in order to improve future empirical reconstructions of the PIS:

- (1) A major remaining limitation for empirical reconstructions of PIS dynamics is constraints on vertical ice extent, and we call on future studies to target vertical transects constraining the timing of ice-surface elevation lowering (cf. Mackintosh et al., 2007).
- (2) Ice dynamics during the Holocene remain poorly understood, apart from a small number of well constrained outlet lobes. In order to contextualise current change and extend the empirical record of observations of glacier length, further analyses of ice extent in the last few millennia are required.
- (3) The synchronicity of recession from north to south remains challenging to ascertain in the absence of comparable and detailed records detailing the timing of the LLGM, Late Glacial advances and Holocene neoglaciations dynamics. The eastern Chilean Lake District, most outlet lobes in the Isla Grande de Chiloé sector, south-central and western Patagonia through the archipelago and numerous outlet lobes of the Southern Patagonian Ice Field remain poorly dated and poorly understood.
- (4) Detailed studies in different sectors of Patagonia are also required to further untangle the complex interplays between climatic controls on ice dynamics (including the behaviour of the SWW) and local dynamic controls, such as calving and topography. In many places, a strong influence of topography and water depth is expected in influencing ice marginal positions and retreat dynamics, but few studies have attempted to analyse these. Detailed analysis of lacustrine varves offers an opportunity to provide high-resolution studies of outlet lobe recession, building on pioneering early work (Caldenius, 1932). Numerical modelling may also be able to test the links between palaeoclimate and ice-mass behaviour by linking mass-balance sensitivities, topography and ice flow parameters with variations in temperature and precipitation.
- (5) The direction of ice flow and the extent to which flow was topographically controlled is poorly constrained in areas of thickest ice, and the location of the ice divide in these places remains uncertain. The direction of ice flow in extensive areas that are currently not glacierised also remains uncertain.

- (6) Large parts of western Patagonia remain unknown in terms of extent and timing of ice advance and retreat, with limited geomorphological data from the onshore (being well hidden and inaccessible in dense vegetation) or offshore environment. A greater understanding of western-flowing glaciers is a research priority, as these were likely some of the largest and most important outlet lobes of the LGM ice sheet, and formed an important ice-ocean interface.
- (7) We are still largely unable to resolve whether deglacial ice limits result from significant stabilisation or re-advance of glaciers, or a combination of the two over time. Numerical modelling work is needed to establish the likely dynamic behaviour of the ice lobes under complex topographic and climatic conditions.

## 7 Summary and Conclusions

We present the first 2D ice-sheet scale reconstruction of PIS evolution at 5 kyr intervals, from 35 ka to 2011 AD, with additional time-slices at the ACR (13 ka) and late Holocene (0.5- 0.2 ka). The reconstruction is empirically constrained by the PATICE database, a new compilation of published geomorphology (moraines, perched delta terraces, trimlines, bathymetric troughs, palaeochannels, shorelines, glacial lineations, alluvial fans, sandar, cirques) and recalibrated published ages. Our chronological database includes radiocarbon ages, cosmogenic nuclide surface exposure ages ( $^{10}\text{Be}$ ,  $^{26}\text{Al}$ ,  $^{36}\text{Cl}$ ,  $^3\text{He}$ ), cosmogenic depth profiles, OSL, lichenometry, dendrochronology, tephrochronology, varve ages and historical documents. Each age is assigned a reliability rating based on well-defined criteria to aid our pan-ice sheet reconstruction. This new PATICE database thus generates an unprecedented assessment of materials pertinent to southern Patagonia.

At its last maximum, the PIS was 3,100 km wide, 2,091 km long, and covered  $492.6 \times 10^3 \text{ km}^2$ , with a sea-level equivalent of 1,496 mm. Our reconstruction envisages an ice sheet 12% larger than previous reconstructions. It was arranged along the spine of the Andean mountain chain, with prominent outlet lobes flowing orthogonally from the ice divide. The western, Pacific margin of the PIS was likely grounded at the continental shelf edge and outlet lobes here calved into deep water. The emergence of the broad Argentinian continental shelf resulted in an enlarged expanse of land east and towards the Atlantic Ocean. Outlet lobes extended onto this continental plain, following existing topography and often with limited interaction between lobes. Some of the largest outlet lobes satisfy some of the criteria to be considered topographically constrained ice streams.

The timing of the local LGM varied latitudinally, occurring at *ca* 33 to 28 ka in the Chilean Lake District and around the Northern Patagonian Icefield (38°S to 46°S). Further south, the LLGM was reached earlier, at *ca* 47 ka (48°S to 56°S). Maximum ice extent was followed by a period of stabilisation until  $\sim 20$  ka, with a period

of moraine formation and outlet lobe stabilisation at 18 – 19 ka. However, again this varied latitudinally, with ice persisting later in the north and deglaciation beginning earlier, at 20 ka, in the Gran Campo Nevado and Cordillera Darwin sectors.

After 18 ka, rapid recession and thinning occurred during a phase of fast warming observed in Antarctic ice cores. The rapid recession observed in the post-LGM period in the sector south of 46°S was closely associated with palaeolake formation and development, with outlet lobes calving into large, deep lakes. These palaeolakes were likely pivotal in terms of shaping glacial behaviour. Glaciers then stabilised or readvanced during the ACR, before once again receding. Some glaciers may have responded to Younger Dryas cooling, with a minor stabilisation at *ca* 12 – 11 ka. It is also possible that some late glacial moraines formed in response to ice-margin stabilisation due to palaeolake drainage and the cessation of lacustrine calving rather than climatic deterioration. There is currently no evidence for ice readvance during the ACR or Younger Dryas periods in the northernmost Chilean Lake District and Isla Grande de Chiloé sectors of the PIS (38°S to 46°S), or in Cordillera Darwin, south of 54°S, with the exception of a small independent terrestrial glacier in Tierra del Fuego (Menounos et al., 2013). Potentially ice limits could still be offshore in this area during the ACR, or perhaps advances were only small scale here. Further work is needed to investigate this.

A number of well-dated moraines across Patagonia constrain stillstands or readvances at *ca* 5 ka and 2 – 1 ka across our latitudinal transect, usually slightly larger than the 0.5 – 0.2 ka advance. Holocene ice advances were likely more subdued in Cordillera Darwin. This was possibly in response to changes in the core belt of the SWW, as Antarctic ice cores do not record a substantial period of cooling at this time. However, across the study region, glacial chronologies are generally sparse for this time period. Late Holocene glacial limits at 0.5 – 0.2 ka are synchronous with the Northern Hemisphere “Little Ice Age”. However, unlike in the Northern Hemisphere, ice was likely more extensive at *ca* 5 ka than during this period (cf. Mercer, 1968). These data indicate that the PIS generally seems to have responded to climate signals observed in Antarctica, such as the ACR, with some glaciodynamic controls, such as palaeolake drainage. It also highlights the critical role that the SWW, and centennial-scale climatic oscillations, such as the SAM, played in driving glacier advance and recession. Variations in the core belt of the SWW were responsible for the latitudinal gradients observed in the timings and locations of key glacier advances in Patagonia.

Our empirical reconstruction of the PIS and its evolution through time demonstrates that rates of net recession were generally slow through the Holocene, with limited evidence for large-scale advances or extensive glacier recession. However, observations of glacier recession for the last few decades rival rates seen much earlier, for a much larger ice sheet that was calving into large, deep, ice-dammed lakes. This rapid recession is in line with recent temperature increases observed in Patagonia and in Antarctic ice cores, and documents a step-change in rates of recession.

We provide these data (shapefiles and data tables of geomorphology and ice and palaeolake extent; shapefiles and data tables of recalibrated ages, confidence levels in ice margins) as supplementary information in the hope that this will drive forwards data-calibrated numerical modelling of the PIS. Numerical models should be calibrated in locations with *high confidence* in ice-margin position and should integrate calving dynamics in ice-dammed lakes and offshore regions. Our reconstructions highlight regions where ice limits are less well constrained, and these should be used to prioritise future field campaigns.

Our reconstruction highlights key priorities for future research. Data informing the timing of vertical ice sheet thinning as well as improved sea level estimates would better constrain calculations of ice volume, a parameter that remains difficult to assess reliably. We are still largely unable to resolve whether deglacial ice limits result from stabilisation or re-advance of glaciers, or a combination of the two over time. A lack of detailed chronological data across the latitudinal transect makes it challenging to assess variations that may be related to changes in the SWW, and to unpick palaeoclimatic controls on deglaciation. More work is needed to constrain the extent of the Patagonian icefields during the Holocene, including times of reduced ice extent, and to distinguish 0.2 - 0.5 ka and other mid/late Holocene neoglaciations. While there are sufficient data to emphasise confidently ice-sheet stabilisation or glacier advances during the ACR and at 5 ka, 2 – 1 ka and 0.5 – 0.2 ka, there are too few dated moraines at this stage to attempt ice-sheet wide reconstructions for all these time periods in addition to our 5 kyr time-slices.

## Acknowledgements

We thank all other researchers who shared or clarified their data with us. We thank Eñaut Izzagirre for sharing shapefiles of geomorphology around northern Cordillera Darwin. Bethan Davies, Varyl Thorndycraft and Julian Martin acknowledge additional Patagonian fieldwork funding support from the Quaternary Research Association. Bethan Davies and Varyl Thorndycraft also acknowledge support from the Royal Holloway Research Strategy Fund, British Society for Geomorphology and Geologists' Association for this project. Julian Dowdeswell thanks the Servicio Hidrográfico y Oceanográfico de la Armada de Chile (SHOA) for access to their swath-bathymetric data from Chilean fjords. Jacob Bendle acknowledges NERC Doctoral Training Grant NE/L501803/1. Monika Mendelova thanks NERC Doctoral Training Grant NE/L002558/1 and the University of Edinburgh for her PhD studentship. Andy Hein acknowledges NERC CIAF awards 9167/0416, 9036/0407, and the Scottish Alliance for Geoscience, Environment and Society (SAGES). Julian Martin acknowledges NERC Doctoral Training Grant NE/L002485/1. Christopher Darvill acknowledges previous NERC studentship NE/j500215/1 at Durham University, NERC CIAF awards 9127/1012 and 9140/1013, University of Manchester SEED Strategic Research Fund ECR Award, University of Manchester Geography Research Fund, plus fieldwork support from an Explorers Club Exploration Grant, Quaternary Research Association NRW

Award, Santander Mobility Grant, and Durham University. Neil Glasser acknowledges funding from NERC (NER/B/S/2002/00282, NE/G00952X/1, NE/N020693/1) and the Leverhulme Trust, plus NERC CIAF awards 9186-0418, 9166.0416 and 9086.0410. Esteban Sagredo acknowledges the Millennium Science Initiative of the Ministry of Economy, Development and Tourism, grant “Millennium Nuclei Palaeoclimate”, and FONDECYT Grants #1160488 and #1180717. Juan-Luis García acknowledges FONDECYT grant #1161110. Michael Kaplan acknowledges the National Science Foundation specifically NSF BCS 1263474 and NSF EAR-0902363. We thank all Patagonian landowners for allowing access to their property during fieldwork. ASTER GDEM is a product of METI and NASA. We acknowledge GEBCO for the bathymetry data (GEBCO Compilation Group (2019) GEBCO 2019 Grid (doi:10.5285/836f016a-33be-6ddc-e053-6c86abc0788e). We thank Dr Jeremy Ely and two anonymous reviewers whose helpful and constructive comments improved the manuscript. This is LEDO contribution number #XXXX.

## Data availability

The Supplementary Information comprises:

- PATICE logo
- Supplementary Methods
- Animated GIF of glacier extent.

All data used in the PATICE database is available in the Mendeley Data repository, which comprises:

- Full Excel tables of recalibrated published ages (including all data required to rerun the calculations).
- ESRI Shapefiles of each dating technique and compiled geomorphology.
- ESRI Shapefiles of outlines of ice extent and uncertainty in the ice margin.
- ESRI Shapefile of ice flow and ice divide at the LLGM.
- ESRI Shapefile of names of outlet lobes.

## List of Figures

Figure 1. Geology of the study region, after Schenk et al. (1997). Plate boundaries from Bird (2003). Gastre Fault and Cenozoic fold-and-thrust belt from Rosenau et al. (2006). Inset shows wider arrangement of plate boundaries..... 8

Figure 2. Study area, the Patagonian Icefields, and key placenames mentioned in text. Mapped glaciers are shown (from Davies and Glasser, 2012, part of the Randolph Glacier Inventory) overlain on a GEBCO GDEM. Bathymetry shows location of the continental shelf. Inset shows location of Patagonia within South America. Location of marine cores mentioned in the text are shown. The Chilean Lake District, Isla de Chiloé,

Archipiélago de los Chonos, Northern Patagonian Icefield, Southern Patagonian Icefield, Gran Campo Nevado and Cordillera Darwin are highlighted..... 9

Figure 3. A. Mean annual air temperature ( $^{\circ}\text{C}$ ) (1970 – 2000) at 30 Arc Seconds resolution, from the WorldClim2 dataset (Fick and Hijmans, 2017). B. Mean annual precipitation (mm) (1970 – 2000) at 30 Arc Seconds resolution, from the WorldClim2 dataset. C. Mean annual air windspeed ( $\text{m s}^{-1}$ ) (1970 – 2000) at 30 Arc Seconds resolution, from the WorldClim2 dataset. Location of the northerly limit of the mean present-day SWW and Subtropical Front after Kohlfeld et al. (2013). D. Approximate distribution of the SWW and oceanic polar fronts that control Patagonia's climate. The westerlies bring rain and snowfall to the west coast of Patagonia. The Subtropical Front (STF) sits at the northern limit of the westerly wind belt. .... 11

Figure 4. Workflow model, showing the different stages in the methodology for our new empirical reconstruction. See also Figure 5. .... 23

Figure 5. Demonstration of the stages in ice sheet reconstruction around the eastern margin of the Southern Patagonian Icefield ( $49^{\circ}$ – $51^{\circ}\text{S}$ ) at 35 ka. See also Figure 4 for an overview of the methods. A. Development of isochrones at moraine limits where there are sufficient high quality ages and geomorphology. Current ice catchments are shown in black with white outline. Cosmogenic and  $\text{Ar}/\text{Ar}$  ages older than MIS 3 are not shown. B. The ice margin location is calculated by interpolating between isochrones. Note the high confidence in ice extent areas with both ages and geomorphology relevant to the time slice, medium confidence where there is clear geomorphology but a lack of ages (but there may be published ages nearby); and low confidence where there is an absence of ages or geomorphology. Interlobate areas tend to be particularly difficult to constrain, typically resulting in low confidence margins. C. Development of palaeo ice-flow lines and ice divides using mapped geomorphology and topography..... 26

Figure 6. Relative sea level curve for the Argentine Shelf from the ICE-4G viscoelastic model and geological data (Guilderson et al., 2000). Grey bars highlight timing of meltwater pulses 1A and 1B..... 29

Figure 7. Key landforms associated with the lowland land-terminating glacial landsystem. A: Latero-frontal moraines at the eastern margin of Lago GCBA. B: outwash fan. Centre: Geomorphological map showing key land-terminating landforms, such as outwash plains, moraines and meltwater channels. C: Detail of meltwater channels. D: Detail of moraines and meltwater channels. Location of photographs is shown on the central map..... 32

Figure 8. Glaciolacustrine landsystem around Lago Cochrane and Lago Esmeralda, east of the Northern Patagonian Icefield. A: Raised glaciofluvial delta terraces above Lago Cochrane. B: Perched delta and modern delta, Lago General Carrera. C: Morainal bank, Esmeralda Moraines (see Davies et al. 2018). D: Photograph illustrating the Esmeralda morainal bank. E, F: Palaeolake shorelines around Lago Juncal. G: Geomorphological map highlighting glaciolacustrine landforms around Lago Cochrane. For more information see Davies et al. 2018; Thorndycraft et al, 2019a; Martin et al. 2019. See also Figure 21. .... 33

Figure 9. Examples of marine glacial geomorphology around Patagonia. A: Cross-shelf troughs on the Patagonian continental shelf. Yellow stars indicate location of panels B-D. B: Terminal moraine ridge, transverse ridges and streamlined lineations associated with Tempango Glacier, Southern Patagonian Icefield. C: Swath bathymetry of the 100 m high recessional moraine in Europa Fjord. D: Glaciofluvial delta in Bernardo Fjord, with a braided river. Bernardo Glacier is just to the southeast of the image. Adapted from Dowdeswell et al. (2016c). .... 35

Figure 10. Location of six key sectors of the former Patagonian Ice Sheet and distribution of selected landforms and all published ages used in this study. .... 35



- Figure 11. Location of glaciers and published geomorphology and chronological data (MIS 3 to present) constraining ice mass extent in the Chilean Lake District (38°S – 42°S) (data from Andersen et al., 1999; Bentley, 1997; Davies and Glasser, 2012; Denton et al., 1999; Glasser and Jansson, 2008; Heusser et al., 1999; Mercer, 1976; Moreno et al., 1999; Porter, 1981). Isochrones are labelled with blue numbers. .... 36
- Figure 12. Map showing numbered key palynological and stratigraphic sites (large filled yellow circles) named in the text in the Chilean Lake District. After Moreno et al., 2015. .... 38
- Figure 13. Reconstruction of glaciers and outlet lobes of the Chilean Lake District. Relative sea level data from Guilderson et al. (2000), symbolised using GEBCO topographic and bathymetric data. Shading is illustrative only and does not represent ice thickness. Inferred ice-flow lines (yellow) are shown for 35 ka in this and subsequent reconstruction figures. .... 40
- Figure 14. Location of glaciers and lakes, and chronological and geomorphological evidence for glaciation (MIS 3 to present) in Isla de Chiloé and Archipiélago de los Chonos sector (42°S – 46°S) (Andersen et al., 1999; Caldenius, 1932; Davies and Glasser, 2012; Denton et al., 1999; Douglass et al., 2006; Dowdeswell et al., 2016c; García et al., 2019; García, 2012; Glasser and Jansson, 2008; Glasser et al., 2016b; Haberle and Bennett, 2004; Heusser et al., 1999; Lastras and Dowdeswell, 2015; Lowell et al., 1995; Stern et al., 2015; Moreno et al., 2015; Van Daele et al., 2016; Weller et al., 2015). See Figure 15 for more detail in the Río Cisnes valley. Pink crosses indicate uncertainty weighted mean ages for boulder exposure ages. Isochrones are labelled in blue writing. .... 40
- Figure 15. A: Detail of published ages and geomorphology in Río Cisnes valley (after García et al., 2019). B, C: Reconstructed glacial lakes (orange) of the Isla de Chiloé and Archipiélago de los Chonos sector at 20 ka and 15 ka respectively. Extent of Panel A is shown in Panel B. Shading of the ice sheet is illustrative only and is not related to ice thickness. Col spillways are shown as yellow stars with red labels. .... 44
- Figure 16. Ice sheet reconstruction for Isla de Chiloé and Archipiélago de los Chonos, showing palaeolake development (orange) at 20 and 15 ka. Relative Sea Level data from Guilderson et al. (2000), symbolised using GEBCO topographic and bathymetric data. For more detail see Figure 15. Shading is illustrative only and does not represent ice thickness. .... 45
- Figure 17. The Northern Patagonian Icefield and the present-day large lakes dammed against high ground in Argentina. Lago GCBA and Lago CP both drain into Río Baker, which flows westwards into the Pacific Ocean. Key moraines and places named in the text are shown. .... 46
- Figure 18. Published geomorphology and ages (ka) of Northern Patagonian Icefield outlet lobes from 46° – 48°S (data from Araneda et al., 2007; Bendle et al., 2017a; Bendle et al., 2017b; Boex et al., 2013; Bourgois et al., 2016; Davies and Glasser, 2012; Davies et al., 2018; Douglass et al., 2005, 2006; Fernandez et al., 2012; Glasser and Jansson, 2008; Glasser et al., 2006a, 2012, 2016b; Harrison et al., 2008, 2012; Hein et al., 2009, 2010, 2011, 2017; Kaplan et al., 2004, 2005; Lumley and Switsur, 1993; Martin et al., 2019; Mercer, 1976; Nimick et al., 2016; Sagredo et al., 2016, 2018; Singer et al., 2004a; Smedley et al., 2016; Stern et al., 2016; Thorndycraft et al., 2019a; Turner et al., 2005; Villa-Martínez et al., 2012; Wenzens, 2005; Winchester et al., 2014). Red inset boxes A, B and C show location of Figure 19, Figure 21 and the central Río Baker valley, and Figure 23 respectively. Altitude and bathymetry as in Figure 17. .... 47
- Figure 19. Published ages and geomorphology, and named moraine sequences, for Lago General Carrera-Buenos Aires (Lago GCBA) (Bendle et al., 2017a; Bourgois et al., 2016; Douglass et al., 2006; Glasser et al., 2016b; Hein et al., 2010; Kaplan et al., 2004; Kaplan et al., 2005; Singer et al., 2004a; Smedley et al., 2016). Overlain on Landsat 7 ETM+ image “p231r092\_7f20010320\_z19\_ps742.tif” (acquired 20<sup>th</sup> March 2001). .... 49

- Figure 20. Reconstruction of Northern Patagonian Icefield outlet lobes. Isochrones used in each time -slice reconstruction are shown in red. Development of ice -dammed palaeolakes is illustrated. Yellow stars indicate drainage cols for ice -dammed lakes. Relative sea level data from Guilderson et al. (2000), symbolised using GEBCO topographic and bathymetric data. Shading is illustrative only and does not represent ice thickness. .... 50
- Figure 21. Central Baker Valley with published ages and geomorphology (Boex et al., 2013; Davies et al., 2018; Glasser et al., 2012; Henríquez et al., 2017; Martin et al., 2019; Sagredo et al., 2016, 2018; Stern et al., 2016; Thorndycraft et al, 2019a; Turner et al., 2005). .... 53
- Figure 22. Glacier and palaeolake evolution through the ACR on the eastern Northern Patagonian Icefield. Ice-sheet shading is illustrative only and does not indicate ice thickness. Data from Davies et al. (2018), Thorndycraft et al. (2019a) and Martin et al. (2019). .... 53
- Figure 23. Geomorphological map showing Jeinemeni Reserve and the Fagnal Moraines, and the moraines around Lago Plomo and Lago Bertrand. Published ages and geomorphology from Glasser et al. (2006, 2008, 2012), Douglass et al. (2005), Bourgois et al. (2016), Davies et al. (2018), and Thorndycraft et al. (2019). .... 54
- Figure 24. A. Glaciers, lakes and rivers of the Southern Patagonian Icefield (48° -52°S), and published chronology (ka) and geomorphology (Ackert et al., 2008; Ashworth et al., 1991; Casassa et al., 1997; Davies and Glasser, 2012; Dowdeswell et al., 2016a; Fogwill and Kubik, 2005; García et al., 2012, 2018; Glasser and Jansson, 2008; Glasser et al., 2011b; Horta et al., 2019; Kaplan et al., 2016; Lastras and Dowdeswell, 2016; Marden and Clapperton, 1995; Masiokas et al., 2008; Mercer, 1965, 1968, 1976; Moreno et al., 2009; Sagredo et al., 2011; Strelin et al., 2014; Wenzens, 1999, 2005, 2006). Mean  $^{10}\text{Be}$  ages of moraines are shown in pink crosses. See also Figure 5. B. Scale Map. Red boxes C and D show location of Figure 26. Box E shows location of Figure 28. Isochrones are shown in blue lines with blue labels. .... 57
- Figure 25. Reconstruction of the Southern Patagonian Icefield at 5 ka time-slices. Ice dammed lakes are highlighted in orange. Relative sea level data from Guilderson et al. (2000), symbolised using GEBCO topographic and bathymetric data. Shading is illustrative only and does not represent ice thickness. .... 60
- Figure 26. Detailed maps of: (A) the Lago O'Higgins/ Lago San Martin/Lago Tar region. Data from Cassassa et al., 1997; Masiokas et al., 2009; Reynhout et al., 2019; Glasser et al., 2011, Wenzens 2005; 2006; Horta et al., 2019. (B) Herminita Peninsula. Numerous sources for published ages and geomorphology (Glasser and Jansson, 2008; Kaplan et al., 2016, Mercer, 1965; Strelin et al., 2014). Pink crosses are mean exposure ages for the landforms. Altitude and symbology as in Figure 24. Lakes are shown in blue. .... 61
- Figure 27. Detail of ages and chronology for the Puerto Bandera Moraines, Lago Argentino, Southern Patagonian Icefield. Data from Mercer (1965), Wenzens (1999), Ackert et al. (2008), Glasser et al. (2008), Strelin et al. (2014), Kaplan et al. (2016). Pink crosses are mean exposure ages for the landforms. Altitude and symbology as in Figure 24. Lakes are shown in blue. .... 61
- Figure 28. A. Geological data pertaining to glaciation of the Torres del Paine region (Ackert et al., 2008; Fogwill and Kubik, 2005; García et al., 2014; García et al., 2012; Glasser and Jansson, 2008; Kaplan et al., 2016; Kaplan et al., 2007; Moreno et al., 2009; Sagredo et al., 2011; Strelin et al., 2014). B. Palaeolake Tehuelche (250m altitude; cf. Solari et al., 2012) and Paleolake Puerto Consuelo at 20 ka. C. Palaeolake Tehuelche-Puerto Consuelo is formed by 15 ka, here at 125 m elevation (traced by contour analysis). This reconstructed lake represents the combined extent of both Palaeolake Tehuelche in the Torres del Paine area and Palaeolake Puerto Consuelo in the Río Prat area. D. Palaeolake Tehuelche-Puerto Consuelo and ice-

- sheet extent at 13 ka (during the ACR). Symbology, bathymetry and altitude as in Figure 24. Ice-sheet shading is illustrative only and does not represent ice thickness. E. Map extent ..... 62
- Figure 29. Map showing published ages and geomorphology associated with Gran Campo Nevado (52° - 53°S) (data from Breuer et al., 2013; Clapperton et al., 1995; Darvill et al., 2015b; Darvill et al., 2017; Evenson et al., 2009; Fernandez et al., 2017; Kaplan et al., 2007; Kaplan et al., 2008; Kilian et al., 2003, 2007a, 2013b, 2013c; Koch and Kilian, 2005; McCulloch et al., 2005a; McCulloch et al., 2005b; Porter et al., 1992; Stern, 1992) and location of glaciers and lakes of Gran Campo Nevado. .... 65
- Figure 30. Palaeo ice sheet reconstruction for the Gran Campo Nevado region. Yellow stars show location of col spillways for ice-dammed lakes (shown in pink). Relative sea level data from Guilderson et al. (2000), symbolised using GEBCO topographic and bathymetric data. Ice-sheet shading is illustrative only and does not represent ice thickness..... 66
- Figure 31. Location of published ages, geomorphology, glaciers and lakes in Cordillera Darwin, southernmost Patagonia (53° - 56°S) (Boyd et al., 2008; Breuer et al., 2013; Clapperton et al., 1995; Coronato et al., 2009; Darvill et al., 2015b; Darvill et al., 2017; Davies and Glasser, 2012; Evenson et al., 2009; Glasser and Jansson, 2008; Gordillo et al., 1992; Hall et al., 2013, 2019; Heusser, 1989, 1998; Izagirre et al., 2018; Kaplan et al., 2007; Kaplan et al., 2008; Kilian et al., 2013b; Kilian et al., 2007a; Kilian et al., 2003; Kuylenstierna et al., 1996; McCulloch and Bentley, 1998; McCulloch et al., 2005a; McCulloch et al., 2005b; Menounos et al., 2013; Porter, 1990; Porter et al., 1992; Rabassa et al., 2000; Roig et al., 1996; Stern, 1992). .... 67
- Figure 32. Detail of radiocarbon ages and geomorphology from Fiordo Marinelli and Fiordo Brookes, northern Cordillera Darwin Icefield. Data from Boyd et al. (2008), Hall et al. (2013, 2019), Izagirre et al. (2018). Symbology as in Figure 31. Background image is ESRI Basemap World Imagery..... 69
- Figure 33. Reconstruction of ice in Cordillera Darwin. Ice-dammed palaeolakes are shown in pink. Relative sea level data from Guilderson et al. (2000) symbolised using GEBCO topographic and bathymetric data. Shading is illustrative only and does not represent ice thickness..... 71
- Figure 34. Patagonian Ice Sheet reconstruction at 5 ka time-slices from 35 ka to present day, with additional time-slices through periods of ice advance during the ACR (13 ka) and Late Holocene (0.2 ka). Ice-dammed lakes are highlighted in orange. Yellow stars indicate location of drainage cols. Sea level reconstruction is from geological data in Guilderson et al. (2000), symbolised using the GEBCO marine bathymetry dataset. Ice-sheet shading is illustrative only and does not represent ice thickness. .... 73
- Figure 35. A. Comparison of our 35 ka LGM reconstruction with that of Coronato and Rabassa (2011). Sea level reconstruction (-150 m at the LGM on the Argentine Shelf) is from geological data in Guilderson et al. (2000), symbolised using the GEBCO marine bathymetry dataset. Outlet lobe abbreviations: BV/RG/UE = Bella Vista/Río Gallegos/Ultima Esperanza; Corcovado = Golfo de Corcovado; Ancud = Golfo de Ancud; GCBA = Lago General Carrera/Buenos Aires; CP = Lago Cochrane/Pueyrredón; MSL = Monte San Lorenzo. B. Reconstruction of ice flow pathways and ice divide for the 35 ka ice sheet. Flowlines are reconstructed using mapped geomorphology (glacial lineations, moraines, bathymetric troughs, topography, etc) and the pattern of recession. Ice divide has low confidence and is assumed to lie over the Andean mountain chain..... 75
- Figure 36. A. Latitudinal transect of mean  $^{10}\text{Be}$  ages (reliability of 1) and standard deviations (SD) for moraines in Patagonia (using external uncertainties). Grey bars indicate timing of significant advances, during the Local LGM (LLGM), ACR (Pedro et al., 2016), Mid-Holocene and Late Holocene. The global LGM (gLGM) is marked (Hughes et al., 2013). B: Frequency histogram of  $^{10}\text{Be}$  ages for moraines in Patagonia, 40 ka to present day. C. Gaussian probability density function ("camel plot") of all  $^{10}\text{Be}$  ages with an age reliability

of 1 or 2 from moraines in Patagonia. D. Box and whisker plot for  $^{10}\text{Be}$  ages on terminal moraines of outlet lobes across the study site..... 78

Figure 37. A. Area of the PIS at each time-slice (see Table 8). Grey line represents glaciated area of the PIS ( $\text{km}^2$ ). The black line represents the annualised rate of change ( $\text{km}^2/\text{year}$ ) between each time-slice. B. As A, but with percentage area change per annum ( $\% \text{a}^{-1}$ ). C. Surface air temperatures from West Antarctica (Cuffey et al., 2016). D. Global ice volume sea-level equivalent, with timing of global ice-volume maximum highlighted (from Harrison et al., 2019). Timings of significant Patagonian glacier advances are highlighted in vertical blue bars. Meltwater pulses (MWP) 1A and 1B are highlighted in pink bars..... 90

Figure 38. Change in glacier lake area in Patagonia from the LGM to present, visualising data from Table 9. 95

## List of Tables

Table 1. Unique IDs for the different categories of ages within the PATICE database; see Table 2 for more information and Supplementary Information for the full database..... 17

Table 2. Publications included in the PATICE compilation, with number and type of ages produced. See Supplementary Information for the full database. Some ages appear in more than one publication. Ages are listed only once, with the reference being the original publication where they were first published. Only ages relevant to reconstructing the glacial history of Patagonia are included..... 17

Table 3. Criteria for assessing the reliability of published ages once compiled in the PATICE database. .... 20

Table 4. Number of ages assigned to each category in the PATICE database. Ages marked “unassigned” either predate 35 ka but are included because older ages help to constrain the LGM ice limit, or could not be recalibrated..... 22

Table 5. Regional relative sea levels used in the PATICE reconstruction..... 29

Table 6. Summary of landforms mapped in this study ..... 30

Table 7. Summary of evidence of the timing of key advances and during key climatic transitions across the Patagonian latitudinal transect ..... 87

Table 8. Estimated area and volume of the Patagonian Ice Sheet and associated ice fields, glaciers and mountain ice caps, at each time-slice, and calculated annualised rates of recession. \*Present-day ice volume and SLE was estimated by Carrivick et al. (2016). Volume-area scaling estimates the 2011 extent to be  $2.2 \times 10^3$  Gt. SLE = Sea level equivalent. 0.2 ka ice volume is within errors of present-day ice volume. See also Figure 37..... 90

Table 9. Calculated glacier lake area ( $\text{km}^2$ ). Present-day glacial lake area is also provided for those palaeolakes that still remain today in some form. Palaeolake Magellan-Bahia Inútil likely existed for some time between 20 and 15 ka, but is not included here due to uncertainties in timing. .... 93

## References

- Ackert, R.P., Becker, R.A., Singer, B.S., Kurz, M.D., Caffee, M.W., Mickelson, D.M., 2008. Patagonian Glacier Response During the Late Glacial–Holocene Transition. *Science* 321, 392–395.
- Adhikary, S., Yamaguchi, Y., Ogawa, K., 2002. Estimation of snow ablation under a dust layer covering a wide range of albedo. *Hydrological processes* 16, 2853–2865.
- Álvarez, D., Fagel, N., Araneda, A., Jana-Pinninghoff, P., Keppens, E., Urrutia, R., 2015. Late Holocene climate variability on the eastern flank of the Patagonian Andes (Chile): A  $\delta^{18}\text{O}$  record from mollusks in Lago Cisnes (47 S). *The Holocene* 25, 1220–1230.
- Andersen, B., Denton, G.H., Lowell, T.V., 1999. Glacial geomorphologic maps of Llanquihue drift in the area of the southern Lake District, Chile. *Geografiska Annaler: Series A, Physical Geography* 81, 155–166.
- Anderson, D.M., Archer, R.B., 1999. Preliminary evidence of early deglaciation in southern Chile. *Palaeogeography, Palaeoclimatology, Palaeoecology* 146, 295–301.
- Aniya, M., 1999. Recent glacier variations of the Hielos Patagónicos. South America, and their contribution to sea-level change. *Arctic, Antarctic, Alpine Research* 31, 165–173.
- Aniya, M., Enomoto, H., 1986. Glacier variations and their causes in the Northern Patagonia Icefield, Chile, since 1944. *Arctic and Alpine Research* 18, 307–316.
- Araos, J.M., Le Roux, J.P., Kaplan, M.R., Spagnolo, M., 2018. Factors controlling alpine glaciations in the Sierra Baguales Mountain Range of southern Patagonia (50° S), inferred from the morphometric analysis of glacial cirques. *Andean Geology* 45, 357–378.
- Araneda, A., Torrejon, F., Aguayo, M., Torres, L., Cruces, F., Cisternas, M., Urrutia, R., 2007. Historical records of San Rafael glacier advances (North Patagonian Icefield): another clue to 'Little Ice Age' timing in southern Chile? *Holocene* 17, 987–998.
- Aravena, J.C., Luckman, B.H., 2009. Spatio-temporal rainfall patterns in Southern South America. *International Journal of Climatology* 29, 2106–2120.
- Araya-Vergara, J., 2008. 2.2. The submarine geomorphology of the Chilean Patagonian fjords and piedmonts, in: Silva, N., Palma, S. (Eds.), *Progress in the oceanographic knowledge of Chilean interior waters, from Puerto Montt to Cape Horn*. Comité Oceanográfico Nacional - Pontificia Universidad Católica de Valparaíso, Valparaíso, pp. 25–27.
- Ariztegui, D., Bianchi, M.M., Maserferro, J., Lafargue, E., Niessen, F., 1997. Interhemispheric synchrony of Late-glacial climatic instability as recorded in proglacial Lake Mascardi, Argentina. *Journal of Quaternary Science: Published for the Quaternary Research Association* 12, 333–338.
- Ashworth, A.C., Markgraf, V., Villagran, C., 1991. Late Quaternary climatic history of the Chilean Channels based on fossil pollen and beetle analyses, with an analysis of the modern vegetation and pollen rain. *Journal of Quaternary Science* 6, 279–291.
- Bahr, D.B., 2014. Estimation of glacier volume and volume change by scaling methods, *Encyclopedia of Snow, Ice and Glaciers*. Springer, pp. 278–280.
- Bahr, D.B., Pfeffer, W.T., Kaser, G., 2014a. Glacier volume estimation as an ill-posed inversion. *Journal of Glaciology* 60, 922–934.

- Bahr, D.B., Pfeffer, W.T., Kaser, G., 2014b. A Review of Volume-Area Scaling of Glaciers. *Reviews of Geophysics*.
- Barr, I.D., Lovell, H., 2014. A review of topographic controls on moraine distribution. *Geomorphology* 226, 44-64.
- Bassett, S.E., Milne, G.A., Mitrovica, J.X., Clark, P.U., 2005. Ice sheet and solid earth influences on far-field sea-level histories. *Science* 309, 925-928.
- Batchelor, C., Dowdeswell, J., 2014. The physiography of High Arctic cross-shelf troughs. *Quaternary Science Reviews* 92, 68-96.
- Bell, C., 2008. Punctuated drainage of an ice-dammed Quaternary lake in Southern South America. *Geografiska Annaler: Series A, Physical Geography* 90, 1-17.
- Bell, C.M., 2009. Quaternary lacustrine braid deltas on Lake General Carrera in southern Chile. *Andean Geology* 36, 51-65.
- Bendle, J.M., Palmer, A.P., Thorndycraft, V.R., Matthews, I.P., 2017a. High-resolution chronology for deglaciation of the Patagonian Ice Sheet at Lago Buenos Aires (46.5°S) revealed through varve chronology and Bayesian age modelling. *Quaternary Science Reviews* 171, 314-339.
- Bendle, J.M., Palmer, A.P., Thorndycraft, V.R., Matthews, I.P., 2019. Phased Patagonian Ice Sheet response to Southern Hemisphere atmospheric and oceanic warming between 18 and 17 ka. *Scientific Reports* 9, 4133.
- Bendle, J.M., Thorndycraft, V.R., Palmer, A.P., 2017b. The glacial geomorphology of the Lago Buenos Aires and Lago Pueyrredón ice lobes of central Patagonia. *Journal of Maps* 13, 654-673.
- Benito, G. and Thorndycraft, V.R. 2020. Catastrophic glacial lake outburst flooding of the Patagonian Ice Sheet. *Earth-Science Reviews* 200, 102996.
- Benn, D.I., Clapperton, C.M., 2000. Pleistocene glacial tectonic landforms and sediments around central Magellan Strait, southernmost Chile: evidence for fast outlet glaciers with cold-based margins. *Quaternary Science Reviews* 19, 591-612.
- Bennett, K.D., Haberle, S.G., Linsley, S.H., 2000. The last glacial-Holocene transition in southern Chile. *Science* 290, 325-328.
- Bentley, M.J., 1996. The role of lakes in moraine formation, Chilean Lake District. *Earth Surface Processes and Landforms* 21, 493-507.
- Bentley, M.J., 1997. Relative and radiocarbon chronology of two former glaciers in the Chilean Lake District. *Journal of Quaternary Science* 12, 25-33.
- Bentley, M.J., McCulloch, R.D., 2005. Impact of neotectonics on the record of glacier and sea level fluctuations, strait of magellan, southern Chile. *Geografiska Annaler: Series A, Physical Geography* 87, 393-402.
- Bentley, M.J., Ó Cofaigh, C., Anderson, J.B., Conway, H., Davies, B., Graham, A.G.C., Hillenbrand, C.-D., Hodgson, D.A., Jamieson, S.S.R., Larter, R.D., Mackintosh, A., Smith, J.A., Verleyen, E., Ackert, R.P., Bart, P.J., Berg, S., Brunstein, D., Canals, M., Colhoun, E.A., Crosta, X., Dickens, W.A., Domack, E., Dowdeswell, J.A., Dunbar, R., Ehrmann, W., Evans, J., Favier, V., Fink, D., Fogwill, C.J., Glasser, N.F., Gohl, K., Gollidge, N.R., Goodwin, I., Gore, D.B., Greenwood, S.L., Hall, B.L., Hall, K., Hedding, D.W., Hein, A.S., Hocking, E.P.,



- Jakobsson, M., Johnson, J.S., Jomelli, V., Jones, R.S., Klages, J.P., Kristoffersen, Y., Kuhn, G., Leventer, A., Licht, K., Lilly, K., Lindow, J., Livingstone, S.J., Massé, G., McGlone, M.S., McKay, R.M., Melles, M., Miura, H., Mulvaney, R., Nel, W., Nitsche, F.O., O'Brien, P.E., Post, A.L., Roberts, S.J., Saunders, K.M., Selkirk, P.M., Simms, A.R., Spiegel, C., Stollendorf, T.D., Sugden, D.E., van der Putten, N., van Ommen, T., Verfaillie, D., Vyverman, W., Wagner, B., White, D.A., Witus, A.E., Zwart, D., 2014. A community-based geological reconstruction of Antarctic Ice Sheet deglaciation since the Last Glacial Maximum. *Quaternary Science Reviews* 100, 1-9.
- Bentley, M.J., Sugden, D.E., Hulton, N.R.J., McCullough, R.D., 2005. The landforms and pattern of deglaciation in the Strait of Magellan and Bahía Inútil, southernmost South America. *Geografiska Annaler* 87A, 313-333.
- Beraza, L., Vilas, J., 1989. Paleomagnetism and relative age from Pleistocene end moraines at Río Pico valley, Patagonia, Argentina., International geological congress. International Geological Congress, Washington DC, pp. 128-129.
- Bertrand, S., Charlet, F., Charlier, B., Renson, V., Fagel, N., 2008. Climate variability of southern Chile since the Last Glacial Maximum: a continuous sedimentological record from Lago Puyehue (40S). *Journal of Paleolimnology* 39, 179-195.
- Bertrand, S., Huguen, K.A., Lamy, F., Stuut, J.-B., Torrejon, F., Lange, C.B., 2012. Precipitation as the main driver of Neoglacial fluctuations of Gualas glacier, Northern Patagonian Icefield. *Climate of the Past* 8, 519.
- Bertrand, S., Lange, C.B., Pantoja, S., Huguen, K., Van Tol, E., Wellner, J.S., 2017. Postglacial fluctuations of Cordillera Darwin glaciers (southernmost Patagonia) reconstructed from Almirantazgo fjord sediments. *Quaternary Science Reviews* 177, 261-273.
- Biester, H., Martinez-Cortizas, A., Birkenstock, S., Kilian, R., 2003. Effect of peat decomposition and mass loss on historic mercury records in peat bogs from Patagonia. *Environmental science & technology* 37, 32-39.
- Björck, S., Rundgren, M., Ljung, K., Unkel, I., Wallin, Å., 2012. Multi-proxy analyses of a peat bog on Isla de los Estados, easternmost Tierra del Fuego: a unique record of the variable Southern Hemisphere Westerlies since the last deglaciation. *Quaternary Science Reviews* 42, 1-14.
- Blomdin, R., Murray, A., Thomson, K.J., Buylaert, J.-P., Sohbati, R., Jansson, K.N., Alexanderson, H., 2012. Timing of the deglaciation in southern Patagonia: Testing the applicability of K-Feldspar IRSL. *Quaternary Geochronology* 10, 264-272.
- Blunier, T., Schwander, J., Stauffer, B., Stocker, T., Dällenbach, A., Indermühle, A., Tschumi, J., Chappellaz, J., Raynaud, D., Barnola, J.M., 1997. Timing of the Antarctic Cold Reversal and the atmospheric CO<sub>2</sub> increase with respect to the Younger Dryas Event. *Geophysical Research Letters* 24, 2683-2686.
- Boex, J., Fogwill, C., Harrison, S., Glasser, N.F., Hein, A., Schnabel, C., Xu, S., 2013. Rapid thinning of the late Pleistocene Patagonian Ice Sheet followed migration of the Southern Westerlies. *Scientific Reports* 3, 1-6.
- Borchers, B., Marrero, S., Balco, G., Caffee, M., Goehring, B., Lifton, N., Nishiizumi, K., Phillips, F., Schaefer, J., Stone, J., 2016. Geological calibration of spallation production rates in the CRONUS-Earth project. *Quaternary Geochronology* 31, 188-198.
- Boulton, G., Clark, C., 1990. A highly mobile Laurentide ice sheet revealed by satellite images of glacial lineations. *Nature* 346, 813.



- Bourgois, J., Cisternas, M.E., Braucher, R., Bourlès, D., Frutos, J., 2016. Geomorphic Records along the General Carrera (Chile)–Buenos Aires (Argentina) Glacial Lake (46°–48° S), Climate Inferences, and Glacial Rebound for the Past 7–9 ka. *The Journal of Geology* 124, 27–53.
- Bown, F., Rivera, A., 2007. Climate changes and recent glacier behaviour in the Chilean Lake District. *Global and Planetary Change* 59, 79–86.
- Bown, F., Rivera, A., Zenteno, P., Bravo, C., Cawkwell, F., 2014. First Glacier Inventory and Recent Glacier Variation on Isla Grande de Tierra Del Fuego and Adjacent Islands in Southern Chile, in: Kargel, J.S., Leonard, G.J., Bishop, M.P., Kääb, A., Raup, B.H. (Eds.), *Global Land Ice Measurements from Space*. Springer Berlin Heidelberg, pp. 661–674.
- Boyd, B.L., Anderson, J.B., Wellner, J.S., Fernández, R.A., 2008. The sedimentary record of glacial retreat, Marinelli Fjord, Patagonia: Regional correlations and climate ties. *Marine Geology* 255, 165–178.
- Braun, M.H., Malz, P., Sommer, C., Fariás-Barahona, D., Sauter, T., Casassa, G., Soruco, A., Skvarca, P., Seehaus, T.C., 2019. Constraining glacier elevation and mass changes in South America. *Nature Climate Change* 9, 130–136.
- Breuer, S., Kilian, R., Schörner, D., Weinrebe, W., Behrmann, J., Baeza, O., 2013. Glacial and tectonic control on fjord morphology and sediment deposition in the Magellan region (53°S), Chile. *Marine Geology* 346, 31–46.
- Briggs, R.D., Pollard, D., Tarasov, L., 2014. A data-constrained large ensemble analysis of Antarctic evolution since the Eemian. *Quaternary Science Reviews* 103, 91–115.
- Bujalesky, G., Coronato, A., Isla, F., 2001. Ambientes glacifluviales y litorales Cuaternarios de la region del Rio Chico, Tierra del Fuego, Argentina. *Revista de la Asociación Geológica Argentina* 56, 73–90.
- Bujalesky, G.G., Heusser, C.J., Coronato, A.M., Hoig, C.E., Rabassa, J.O., 1997. Pleistocene glaciolacustrine sedimentation at Lago Fagnano, Andes of Tierra del Fuego, Southernmost South America. *Quaternary Science Reviews* 16, 767–778.
- Cai, J., Powell, R.D., Cowan, E.A., Carlson, P.R., 1997. Lithofacies and seismic-reflection interpretation of temperate glaci-marine sedimentation in Tarr Inlet, Glacier Bay, Alaska. *Marine Geology* 143, 5–37.
- Caldenius, C.C., 1932. Las glaciaciones cuaternarias en la Patagonia y Tierra del Fuego. *Geografiska Annaler* 14, 1–164.
- Caniupán, M., Lamy, F., Lange, C.B., Kaiser, J., Arz, H., Kilian, R., Baeza Urrea, O., Aracena, C., Hebbeln, D., Kissel, C., Laj, C., Mollenhauer, G., Tiedemann, R., 2011. Millennial-scale sea surface temperature and Patagonian Ice Sheet changes off southernmost Chile (53°S) over the past ~60 kyr. *Paleoceanography* 26 (3).
- Carrivick, J.L., Davies, B.J., James, W.H.M., Quincey, D.J., Glasser, N.F., 2016. Distributed ice thickness and glacier volume in southern South America. *Global and Planetary Change* 146, 122–132.
- Casassa, G., Brecher, H., Rivera, A., Aniya, M., 1997. A century-long recession record of Glaciar O'Higgins, Chilean Patagonia. *Annals of Glaciology* 24, 106–110.
- Chandler, B.M.P., Lovell, H., Boston, C.M., Lukas, S., Barr, I.D., Benediktsson, Í.Ö., Benn, D.I., Clark, C.D., Darvill, C.M., Evans, D.J.A., Ewertowski, M.W., Loibl, D., Margold, M., Otto, J.-C., Roberts, D.H., Stokes, C.R., Storrar, R.D., Stroeven, A.P., 2018. Glacial geomorphological mapping: A review of approaches and frameworks for best practice. *Earth-Science Reviews* 185, 806–846.

- Charlet, F., De Batist, M., Chapron, E., Bertrand, S., Pino, M., Urrutia, R., 2008. Seismic stratigraphy of Lago Puyehue (Chilean Lake District): new views on its deglacial and Holocene evolution. *Journal of Paleolimnology* 39, 163-177.
- Clague, J.J., Barendregt, R.W., Menounos, B., Roberts, N.J., Rabassa, J., Martinez, O., Ercolano, B., Corbella, H., Hemming, S.R., 2020. Pliocene and Early Pleistocene glaciation and landscape evolution on the Patagonian Steppe, Santa Cruz province, Argentina. *Quaternary Science Reviews* 227, 105992.
- Clapperton, C.M., 1989. Asymmetrical drumlins in Patagonia, Chile. *Sedimentary Geology* 62, 387-398.
- Clapperton, C.M., 1993. Nature of environmental changes in South America at the Last Glacial Maximum. *Palaeogeography, Palaeoclimatology, Palaeoecology* 101, 189-208.
- Clapperton, C.M., 1995. Fluctuations of local glaciers at the termination of the Pleistocene: 18-8 ka BP. *Quaternary International* 28, 41-50.
- Clapperton, C.M., Clapperton, C., 1993. *Quaternary geology and geomorphology of South America*. Elsevier Amsterdam etc.
- Clapperton, C.M., Sugden, D.E., Kaufman, D.S., McCulloch, R.D., 1995. The Last Glaciation in Central Magellan Strait, Southernmost Chile. *Quaternary Research* 44, 135-148.
- Clark, C.D., 1993. Mega-scale Glacial Lineations and Cross-cutting Ice-flow Landforms. *Earth Surface Processes and Landforms* 18, 1-29.
- Clark, C.D., 1997. Reconstructing the evolutionary dynamics of former ice sheets using multi-temporal evidence, remote sensing and GIS. *Quaternary Science Reviews* 16, 1067-1092.
- Clark, C.D., Ely, J.C., Greenwood, S.L., Hughes, A.L.C., Meehan, R., Barr, I.D., Bateman, M.D., Bradwell, T., Doole, J., Evans, D.J.A., Jordan, C.J., Montenegro, X., Pellicer, X.M., Sheehy, M., 2018. BRITICE Glacial Map, version 2: a map and GIS database of glacial landforms of the last British-Irish Ice Sheet. *Boreas* 47, 11-e18.
- Clark, C.D., Hughes, A.L.C., Greenwood, S.L., Jordan, C., Sejrup, H.P., 2012. Pattern and timing of retreat of the last British-Irish Ice Sheet. *Quaternary Science Reviews* 44, 112-146.
- Clark, P.U., Dyke, A.S., Shakun, J.D., Carlson, A.E., Clark, J., Wohlfarth, B., Mitrovica, J.X., Hostetler, S.W., McCabe, A.M., 2009. The Last Glacial Maximum. *Science* 325, 710-714.
- Cogez, A., Herman, F., Pelt, É., Reuschlé, T., Morvan, G., Darvill, C.M., Norton, K.P., Christl, M., Märki, L. and Chabaux, F., 2018. U-Th and <sup>10</sup>Be constraints on sediment recycling in proglacial settings, Lago Buenos Aires, Patagonia. *Earth Surface Dynamics*, 6(1), 121-140.
- Coronato, A., Martínez, O., Rabassa, J., 2004. Glaciations in Argentine Patagonia, southern South America. *Developments in Quaternary Sciences* 2, 49-67.
- Coronato, A., Rabassa, J., 2011. Chapter 51 - Pleistocene Glaciations in Southern Patagonia and Tierra del Fuego, in: Jürgen Ehlers, P.L.G., Philip, D.H. (Eds.), *Developments in Quaternary Sciences*. Elsevier, pp. 715-727.
- Coronato, A., Seppälä, M., Ponce, J., Rabassa, J., 2009. Glacial geomorphology of the Pleistocene lake Fagnano ice lobe, Tierra del Fuego, southern South America. *Geomorphology* 112, 67-81.
- Cronin, T.M., 2012. Rapid sea level rise. *Quaternary Science Reviews* 56, 11-30.

- Cuffey, K.M., Clow, G.D., Steig, E.J., Buizert, C., Fudge, T., Koutnik, M., Waddington, E.D., Alley, R.B., Severinghaus, J.P., 2016. Deglacial temperature history of West Antarctica. *Proceedings of the National Academy of Sciences* 113, 14249-14254.
- Curran-Everett, D., Benos, D.J., 2004. Guidelines for reporting statistics in journals published by the American Physiological Society. *AJP - Gastrointestinal and Liver Physiology* 287(2):G307.
- Darvill, C.M., Bentley, M.J., Stokes, C.R., 2015a. Geomorphology and weathering characteristics of erratic boulder trains on Tierra del Fuego, southernmost South America: Implications for dating of glacial deposits. *Geomorphology* 228, 382-397.
- Darvill, C.M., Bentley, M.J., Stokes, C.R., Hein, A.S., Rodés, Á., 2015b. Extensive MIS 3 glaciation in southernmost Patagonia revealed by cosmogenic nuclide dating of outwash sediments. *Earth and Planetary Science Letters* 429, 157-169.
- Darvill, C.M., Bentley, M.J., Stokes, C.R., Shulmeister, J., 2016. The timing and cause of glacial advances in the southern mid-latitudes during the last glacial cycle based on a synthesis of exposure ages from Patagonia and New Zealand. *Quaternary Science Reviews* 149, 200-214.
- Darvill, C.M., Stokes, C.R., Bentley, M.J., Evans, D.J.A., Lovell, H., 2017. Dynamics of former ice lobes of the southernmost Patagonian Ice Sheet based on a glacial landsystems approach. *Journal of Quaternary Science* 32, 857-876.
- Darvill, C.M., Stokes, C.R., Bentley, M.J., Lovell, H., 2014. A glacial geomorphological map of the southernmost ice lobes of Patagonia: the Bahía Múñiz–San Sebastián, Magellan, Otway, Skyring and Río Gallegos lobes. *Journal of Maps* 10, 500-520.
- DaSilva, J.L., Anderson, J.B., Stravers, J., 1997. Seismic facies changes along a nearly continuous 24° latitudinal transect: the fjords of Chile and the northern Antarctic Peninsula. *Marine Geology* 143, 103-123.
- Davies, B.J., Glasser, N.F., 2012. Accelerating recession in Patagonian glaciers from the "Little Ice Age" (c. AD 1870) to 2011. *Journal of Glaciology* 58, 1063-1084.
- Davies, B.J., Hambrey, M.J., Smellie, J.L., Carrivick, J.L., Glasser, N.F., 2012. Antarctic Peninsula Ice Sheet evolution during the Cenozoic Era. *Quaternary Science Reviews* 31, 30-66.
- Davies, B.J., Thorndycraft, V.R., Fabel, D., Martin, J.R.V., 2018. Asynchronous glacier dynamics during the Antarctic Cold Reversal in central Patagonia. *Quaternary Science Reviews* 200, 287-312.
- Dalziel, I.W., de Wit, M.J., Palmer, K.F., 1974. Fossil marginal basin in the southern Andes. *Nature* 250, 291-294.
- de Agostini, A.M., 1956. Treinta años en Tierra del Fuego. Elefante Blanco, Buenos Aires.
- de Gasperi, G.B., 1922. Scritti vari di geografia e geologia; pubblicazione postuma.
- Del Valle, R.A., Lirio, J.M., Nunez, H.J., Tatur, A., Rinaldi, C.A., 2000. Sedimentary cores from Mascardi Lake, Argentina: a key site to study Elpalafquen paleolake, in: *Southern Hemisphere Paleo-and Neoclimates*. Springer, pp. 275–286.

- De Muro, S., Brambati, A., Tecchiato, S., Porta, M., Ibba, A., 2017. Geomorphology of marine and transitional terraces and raised shorelines between Punta Paulo and Porvenir, Tierra del Fuego, Straits of Magellan – Chile. *Journal of Maps* 13, 311-321.
- De Muro, S., Tecchiato, S., Porta, M., Buosi, C., Ibba, A., 2018. Geomorphology of marine and glacio-lacustrine terraces and raised shorelines in the northern sector of Península Brunswick, Patagonia, Straits of Magellan, Chile AU - De Muro, Sandro. *Journal of Maps* 14, 135-143.
- de Porras, M.E., Maldonado, A., Abarzúa, A.M., Cárdenas, M.L., Francois, J.P., Martel-Cea, A., Stern, C.R., Méndez, C., Reyes, O., 2012. Postglacial vegetation, fire and climate dynamics at Central Chilean Patagonia (Lake Shaman, 44 S). *Quaternary Science Reviews* 50, 71-85.
- de Porras, M.E., Maldonado, A., Quintana, F., Martel Cea, A., Reyes, O., Méndez Melgar, C., 2014. Environmental and climatic changes in Central Chilean Patagonia since the Late Glacial (Mallín El Embudo, 44 S).
- Denton, G.H., Lowell, T.V., Heusser, C.J., Schlüchter, C., Andersen, B.G., Heusser, L.E., Moreno, P.I., Marchant, D.R., 1999. Geomorphology, Stratigraphy, and Radiocarbon Chronology of Llanquihue Drift in the Area of the Southern Lake District, Seno Reloncaví, and Isla Grande de Chiloé, Chile. *Geografiska Annaler: Series A, Physical Geography* 81, 167-229.
- Doughty, A. M., Schaefer, J. M., Putnam, A. E., Denton, G. H., Kaplan, M. R., Barrell, D. J. A., Andersen, B.G., Finkel, R.C., Schwartz, R. 2015. Mismatch of glacier extent and summer insolation in Southern Hemisphere mid-latitudes. *Geology*, 43(5), 407–410.
- Douglass, D., Singer, B., Kaplan, M., Mickelson, D., Caffee, M., 2006. Cosmogenic nuclide surface exposure dating of boulders on last-glacial and late-glacial moraines, Lago Buenos Aires, Argentina: interpretive strategies and paleoclimate implications. *Quaternary Geochronology* 1, 43-58.
- Douglass, D.C., Singer, B.S., Kaplan, M.R., Aclerc, R.P., Mickelson, D.M., Caffee, M.W., 2005. Evidence of early Holocene glacial advances in southern South America from cosmogenic surface -exposure dating. *Geology* 33, 237-240.
- Dowdeswell, J.A., Canals, M., Jakobsson, M., Todd, B.J., Dowdeswell, E.K., Hogan, K.A., 2016a. The variety and distribution of submarine glacial landforms and implications for ice-sheet reconstruction. *Geological Society, London, Memoirs* 46, 519-552.
- Dowdeswell, J.A., Dowdeswell, E.K., Rodrigo, C., 2016b. Pockmarks in the fjords of Chilean Patagonia. *Geological Society, London, Memoirs* 46, 109-110.
- Dowdeswell, J.A., Dowdeswell, E.K., Rodrigo, C., Diaz, J., 2016c. Assemblage of glacial and related landforms in the fjords of southern Chile. *Geological Society, London, Memoirs* 46, 131-134.
- Dowdeswell, J.A., Forsberg, C.F., 1992. The size and frequency of icebergs and bergy bits derived from tidewater glaciers in Kongsfjorden, northwest Spitsbergen. *Polar Research* 11, 81-91.
- Dowdeswell, J.A., Vásquez, M., 2013. Submarine landforms in the fjords of southern Chile: implications for glacial marine processes and sedimentation in a mild glacier-influenced environment. *Quaternary Science Reviews* 64, 1-19.
- Elbert, J., Wartenburger, R., von Gunten, L., Urrutia, R., Fischer, D., Fujak, M., Hamann, Y., Greber, N.D., Grosjean, M., 2013. Late Holocene air temperature variability reconstructed from the sediments of Laguna Escondida, Patagonia, Chile (45° 30' S). *Palaeogeography, Palaeoclimatology, Palaeoecology* 369, 482-492.

- Ely, J. C., Clark, C. D., Hindmarsh, R. C. A., Hughes, A. L. C., Greenwood, S. L., Bradley, S. L., Gasson, E., Gregoire, L., Gandy, N., Stokes, C. R., Small, D. 2019. Recent progress on combining geomorphological and geochronological data with ice sheet modelling, demonstrated using the last British–Irish Ice Sheet. *Journal of Quaternary Science*.
- Ercolano, B., Coronato, A., Tiberi, P., Corbella, H., Marderwald, G., 2016. Glacial geomorphology of the tableland east of the Andes between the Coyle and Gallegos river valleys, Patagonia, Argentina. *Journal of Maps* 12, 304-313.
- Ercolano, B., Mazzoni, E., Vazquez, M., Rabassa, J., 2004. Drumlins and drumlinoid forms of the Lower Pleistocene in southern Patagonia, Province of Santa Cruz. *Rev. Asoc. Geol. Argent* 59, 771-777.
- Evenson, E.B., Burkhart, P.A., Gosse, J.C., Baker, G.S., Jackofsky, D., Meglioli, A., Dalziel, I., Kraus, S., Alley, R.B., Berti, C., 2009. Enigmatic boulder trains, supraglacial rock avalanches, and the origin of “Darwin's boulders,” Tierra del Fuego. *GSA Today* 19, 4-10.
- Falaschi, D., Bravo, C., Masiokas, M., Villalba, R., Rivera, A., 2013. First Glacier Inventory and Recent Changes in Glacier Area in the Monte San Lorenzo Region (47°S), Southern Patagonian Andes, South America. *Arctic, Antarctic, and Alpine Research* 45, 19-28.
- Fernandez, R., Anderson, J., Bertrand, S., Wellner, J., 2012. Galas Glacier sedimentary record of climate and environmental change, Golfo Elefantes, Western Patagonia (46.5° S). *The Holocene* 22, 451-463.
- Fernández, R., Gulick, S., Rodrigo, C., Domack, E., Leventer, A., 2017. Seismic stratigraphy and glacial cycles in the inland passages of the Magallanes región of Chile, southernmost South America. *Marine Geology* 386, 19-31.
- Fernandez, R.A., Anderson, J.B., Wellner, J.S., Hallet, B., 2011. Timescale dependence of glacial erosion rates: a case study of Marinelli Glacier, Cordillera Darwin, southern Patagonia. *Journal of Geophysical Research: Earth Surface* 116.
- Feruglio, E., 1933. I terrazzi marini della Patagonia. Cooperativa Tip. Edit. Paolo Galeati.
- Fick, S.E., Hijmans, R.J., 2017. WorldClim 2: new 1-km spatial resolution climate surfaces for global land areas. *International Journal of Climatology* 37, 4302-4315.
- Fildani, A., Hessler, A.M., 2003. Stratigraphic record across a retroarc basin inversion: Rocas Verdes–Magallanes basin, Patagonian Andes, Chile. *Geological Society of America Bulletin* 117, 1596-1614.
- Fletcher, M.-S., Moreno, P.I., 2012. Have the Southern Westerlies changed in a zonally symmetric manner over the last 14,000 years? A hemisphere-wide take on a controversial problem. *Quaternary International* 253, 32-46.
- Fogwill, C.J., Kubik, P.W., 2005. A Glacial Stage Spanning the Antarctic Cold Reversal in Torres del Paine (51°S), Chile, Based on Preliminary Cosmogenic Exposure Ages. *Geografiska Annaler. Series A, Physical Geography* 87, 403-408.
- Forsyth, R., Prior, D., 1992. Cenozoic continental geology of South America and its relations to the evolution of the Chile triple junction. *Proceedings of the Ocean Drilling Program, Initial Reports* 141, 23-31.
- García, J.-L., Hall, B.L., Kaplan, M.R., Vega, R.M., Strelin, J.A., 2014. Glacial geomorphology of the Torres del Paine region (southern Patagonia): Implications for glaciation, deglaciation and paleolake history. *Geomorphology* 204, 599-616.

- García, J.-L., Hein, A.S., Binnie, S.A., Gómez, G.A., González, M.A., Dunai, T.J., 2018. The MIS 3 maximum of the Torres del Paine and Última Esperanza ice lobes in Patagonia and the pacing of southern mountain glaciation. *Quaternary Science Reviews* 185, 9-26.
- García, J.L., 2012. Late Pleistocene ice fluctuations and glacial geomorphology of the Archipiélago de Chiloé, southern Chile. *Geografiska Annaler: Series A, Physical Geography* 94, 459-479.
- García, J.L., Kaplan, M.R., Hall, B.L., Schaefer, J.M., Vega, R.M., Schwartz, R., Finkel, R., 2012. Glacier expansion in southern Patagonia throughout the Antarctic Cold Reversal. *Geology* 40, 859-862.
- García, J.-L., Maldonado, A., de Porras, M.E., Delaunay, A.N., Reyes, O., Ebensperger, C.A., Binnie, S.A., Lüthgens, C., Méndez, C., 2019. Early deglaciation and paleolake history of Río Cisnes Glacier, Patagonian Ice Sheet (44° S). *Quaternary Research* 91, 194-217.
- García, J.-L., Strelin, J.A., Vega, R.M., Hall, B.L., Stern, C.R., 2015. Deglacial ice-marginal glaciolacustrine environments and structural moraine building in Torres del Paine, Chilean southern Patagonia. *Andean Geology* 42 (2), 190-212.
- Gardner, A.S., Moholdt, G., Cogley, J.G., Wouters, B., Arendt, A.A., Mah, J., Berthier, E., Hock, R., Pfeffer, W.T., Kaser, G., Ligtenberg, S.R.M., Bolch, T., Sharp, M.J., Hagen, J.O., van den Broeke, M.R., Paul, F., 2013. A Reconciled Estimate of Glacier Contributions to Sea Level Rise: 2003 to 2009. *Science* 340, 852-857.
- Garreaud, R., 2007. Precipitation and circulation covariability in the extratropics. *Journal of Climate* 20, 4789-4797.
- Garreaud, R., Lopez, P., Minvielle, M., Rojas, M., 2011. Large-Scale Control on the Patagonian Climate. *Journal of Climate* 26, 215-230.
- Garreaud, R.D., Vuille, M., Compagnucci, R., Marengo, J., 2009. Present-day South American climate. *Palaeogeography Palaeoclimatology Palaeoecology* 281, 180-195.
- Garibotti, I.A., Villalba, R., 2009. Lichenometric dating using *Rhizocarpon* subgenus *Rhizocarpon* in the Patagonian Andes, Argentina. *Quaternary Research* 71, 271-283.
- Garibotti, I.A., Villalba, R., 2017. Colonization of mid- and late-Holocene moraines by lichens and trees in the Magellanic sub-Antarctic province. *Polar Biology* 1-15.
- GEBCO Compilation Group, 2019. GEBCO 2019 Grid (doi:10.5285/836f016a-33be-6ddc-e053-6c86abc0788e) Available at <http://www.gebco.net>.
- Glasser, N., Jansson, K., 2008. The Glacial Map of southern South America. *Journal of Maps* 4, 175-196.
- Glasser, N.F., Ghiglione, M.C., 2009. Structural, tectonic and glaciological controls on the evolution of fjord landscapes. *Geomorphology* 105, 291-302.
- Glasser, N.F., Hambrey, M.J., Aniya, M., 2002. An advance of Soler Glacier, North Patagonian Icefield, at c. AD 1222-1342. *Holocene* 12, 113-120.
- Glasser, N.F., Harrison, S., 2005. Sediment distribution around glacially abraded bedrock landforms (whalebacks) at Lago Tranquilo, Chile. *Geografiska Annaler Series A-Physical Geography* 87A, 421-430.



- Glasser, N.F., Harrison, S., Ivy-Ochs, S., Duller, G.A.T., Kubik, P.W., 2006a. Evidence from the Rio Bayo valley on the extent of the North Patagonian Icefield during the Late Pleistocene - Holocene transition. *Quaternary Research* 65, 70-77.
- Glasser, N.F., Harrison, S., Jansson, K.N., 2009. Topographic controls on glacier sediment-landform associations around the temperate North Patagonian Icefield. *Quaternary Science Reviews* 28, 2817-2832.
- Glasser, N.F., Harrison, S., Jansson, K.N., Anderson, K., Cowley, A., 2011a. Global sea-level contribution from the Patagonian Icefields since the Little Ice Age maximum. *Nature Geoscience* 4, 303-307.
- Glasser, N.F., Harrison, S., Schnabel, C., Fabel, D., Jansson, K.N., 2012. Younger Dryas and early Holocene age glacier advances in Patagonia. *Quaternary Science Reviews* 58, 7-17.
- Glasser, N.F., Holt, T.O., Evans, Z.D., Davies, B.J., Pelto, M., Harrison, S., 2016a. Recent spatial and temporal variations in debris cover on Patagonian glaciers. *Geomorphology* 273, 207-216.
- Glasser, N.F., Jansson, K., Mitchell, W.A., Harrison, S., 2006b. The geomorphology and sedimentology of the 'Tempanos' moraine at Laguna San Rafael, Chile. *Journal of Quaternary Science* 21, 629-643.
- Glasser, N.F., Jansson, K.N., 2005. Fast-flowing outlet glaciers of the Last Glacial Maximum Patagonian Icefield. *Quaternary Research* 63, 206-211.
- Glasser, N.F., Jansson, K.N., Duller, G.A.T., Singarayer, J., Holway, M., Harrison, S., 2016b. Glacial lake drainage in Patagonia (13-8 kyr) and response of the adjacent Pacific Ocean. *Scientific Reports* 6, 21064.
- Glasser, N.F., Jansson, K.N., Goodfellow, B.W., de Argüelles, H., Rodnight, H., Rood, D.H., 2011b. Cosmogenic nuclide exposure ages for moraines in the Lago San Martín Valley, Argentina. *Quaternary Research* 75, 636-646.
- Glasser, N.F., Jansson, K.N., Harrison, S., Klerman, J., 2008. The glacial geomorphology and Pleistocene history of South America between 38°S and 56°S. *Quaternary Science Reviews* 27, 365-390.
- Glasser, N.F., Jansson, K.N., Harrison, S., Rivera, A., 2005. Geomorphological evidence for variations of the North Patagonian Icefield during the Holocene. *Geomorphology* 71, 263-277.
- Golledge, N.R., Mackintosh, A.N., Anderson, B.M., Buckley, K.M., Doughty, A.M., Barrell, D.J.A., Denton, G.H., Vandergoes, M.J., Andersen, R.G., Schaefer, J.M., 2012. Last Glacial Maximum climate in New Zealand inferred from a modelled Southern Alps icefield. *Quaternary Science Reviews* 46, 30-45.
- Golledge, N.R., Menviel, L., Carter, L., Fogwill, C.J., England, M.H., Cortese, G., Levy, R.H., 2014. Antarctic contribution to meltwater pulse 1A from reduced Southern Ocean overturning. *Nature Communications* 5, 5107.
- Gordillo, S., Bujalesky, G.G., Pirazzoli, P.A., Rabassa, J.O., Saliège, J.-F., 1992. Holocene raised beaches along the northern coast of the Beagle Channel, Tierra del Fuego, Argentina. *Palaeogeography, Palaeoclimatology, Palaeoecology* 99, 41-54.
- Gourlet, P., Rignot, E., Rivera, A., Casassa, G., 2016. Ice thickness of the northern half of the Patagonia Icefields of South America from high-resolution airborne gravity surveys. *Geophysical Research Letters* 43, 241-249.



- Graham, A.G.C., Fretwell, P.T., Larter, R.D., Hodgson, D.A., Wilson, C.K., Tate, A.J., Morris, P., 2008. A new bathymetric compilation highlighting extensive paleo-ice sheet drainage on the continental shelf, South Georgia, sub-Antarctica. *Geochemistry, Geophysics, Geosystems* 9, Q07011.
- Guilderson, T., Burckle, L., Hemming, S., Peltier, W., 2000. Late Pleistocene sea level variations derived from the Argentine Shelf. *Geochemistry, Geophysics, Geosystems* 1.
- Haberle, S., Bennett, K., 2004. Postglacial formation and dynamics of North Patagonian Rainforest in the Chonos Archipelago, southern Chile. *Quaternary Science Reviews* 23, 2433-2452.
- Haberzettl, T., Anselmetti, F.S., Bowen, S.W., Fey, M., Mayr, C., Zolitschka, B., Ariztegui, D., Mauz, B., Ohlendorf, C., Kastner, S., 2009. Late Pleistocene dust deposition in the Patagonian steppe-extending and refining the paleoenvironmental and tephrochronological record from Laguna Potrok Aike back to 55 ka. *Quaternary Science Reviews* 28, 2927-2939.
- Hajdas, I., Bonani, G., Moreno, P.I., Ariztegui, D., 2003. Precise radiocarbon dating of Late-Glacial cooling in mid-latitude South America. *Quaternary Research* 59, 70-78.
- Hall, B., Denton, G., Lowell, T., Bromley, G., Putnam, A., 2017. Retreat of the Cordillera Darwin icefield during Termination I. *Cuadernos de Investigación Geográfica* 43, 751-766.
- Hall, B.L., 2009. Holocene glacial history of Antarctica and the sub-Antarctic islands. *Quaternary Science Reviews* 28, 2213-2230.
- Hall, B.L., Porter, C.T., Denton, G.H., Lowell, T.V., Bromley, G.R.M., 2013. Extensive recession of Cordillera Darwin glaciers in southernmost South America during Heinrich Stadial 1. *Quaternary Science Reviews* 62, 49-55.
- Hall, B.L., Lowell, T.V., Bromley, G.R.M., Denton, G.H., Putnam, A.E., 2019. Holocene glacier fluctuations on the northern flank of Cordillera Darwin, southernmost South America. *Quaternary Science Reviews* 222, 105904.
- Harrison, S., Glasser, N.F., 2011. Chapter 54 - The Pleistocene Glaciations of Chile, in: Jürgen Ehlers, P.L.G., Philip, D.H. (Eds.), *Developments in Quaternary Sciences*. Elsevier, pp. 739-756.
- Harrison, S., Glasser, N., Winchester, V., Haresign, E., Warren, C., Duller, G.A.T., Bailey, R., Ivy-Ochs, S., Jansson, K., Kubik, P., 2008. Glacial Leon, Chilean Patagonia: late-Holocene chronology and geomorphology. *Holocene* 18, 643-652.
- Harrison, S., Glasser, N.F., Duller, G.A.T., Jansson, K.N., 2012. Early and mid-Holocene age for the Tempanos moraines, Laguna San Rafael, Patagonian Chile. *Quaternary Science Reviews* 31, 82-92.
- Harrison, S., Smith, D.E., Glasser, N.F., 2019. Late Quaternary meltwater pulses and sea level change. *Journal of Quaternary Science* 34, 1-15.
- Harrison, S., Winchester, V., Glasser, N., 2007. The timing and nature of recession of outlet glaciers of Hielo Patagonico Norte, Chile, from their Neoglacial IV (Little Ice Age) maximum positions. *Global and Planetary Change* 59, 67-78.
- Hatté, C., Jull, A.J.T., 2013. RADIOCARBON DATING |  $^{14}\text{C}$  of Plant Macrofossils, in: Elias, S.A., Mock, C.J.B.T.-E. of Q.S. (Second E. (Eds.), . Elsevier, Amsterdam, pp. 361-367.

- Hein, A.S., Coglez, A., Darvill, C.M., Mendelova, M., Kaplan, M.R., Herman, F., Dunai, T.J., Norton, K., Xu, S., Christl, M., 2017. Regional mid-Pleistocene glaciation in central Patagonia. *Quaternary Science Reviews* 164, 77-94.
- Hein, A.S., Dunai, T.J., Hulton, N.R.J., Xu, S., 2011. Exposure dating outwash gravels to determine the age of the greatest Patagonian glaciations. *Geology* 39, 103-106.
- Hein, A.S., Hulton, N.R., Dunai, T.J., Sugden, D.E., Kaplan, M.R., Xu, S., 2010. The chronology of the Last Glacial Maximum and deglacial events in central Argentine Patagonia. *Quaternary Science Reviews* 29, 1212-1227.
- Hein, A.S., Hulton, N.R.J., Dunai, T.J., Schnabel, C., Kaplan, M.R., Naylor, M., Xu, S., 2009. Middle Pleistocene glaciation in Patagonia dated by cosmogenic-nuclide measurements on outwash gravels. *Earth and Planetary Science Letters* 286, 184-197.
- Heirman, K., De Batist, M., Charlet, F., Moernaut, J., Chapron, E., Brümmer, R., Pino, M., Urrutia, R., 2011. Detailed seismic stratigraphy of Lago Puyehue: implications for the mode and timing of glacier retreat in the Chilean Lake District. *Journal of Quaternary Science* 26, 665-674.
- Henríquez, W.I., Villa-Martínez, R., Vilanova, I., De Pol-Holz, R., Moreno, P.I., 2017. The last glacial termination on the eastern flank of the central Patagonian Andes (47° S). *Climate of the Past* 13, 879-895.
- Hervé, F., Pankhurst, R., Trouw, R., Fanning, C., Dzogolyk, E., Solari, M., Suárez, M., 2003. Geological Observations at the Western Portion of the Scotia–South America plate Boundary: results of the “Penguin” 2003 Cruise, X Congreso Geológico Chileno. CD ROM.
- Hervé, F., Pankhurst, R.J., Fanning, C.M., Calderón, M., Yaxley, G.M., 2007. The South Patagonian batholith: 150 my of granite magmatism on a plate margin. *Lithos* 97, 373-394.
- Heusser, C., 1999. 14 C Age of Glaciation in Estrecho De Magallanes–Bahía Inútil, Chile. *Radiocarbon* 41, 287-293.
- Heusser, C., Heusser, L., Hauser, A., 1979. A 12,000 yr BP tephra layer at Bahia Inutil (Tierra del Fuego, Chile). *Anales del Instituto de la Patagonia* 13, 39-49.
- Heusser, C.J., Heusser, L.E., Lovell, T.V., 1999. Paleoecology of the southern Chilean Lake District-Isla Grande de Chiloé during middle-late Patagonian glaciation and deglaciation. *Geografiska Annaler Series A, Physical Geography* 81, 231-284.
- Heusser, C., Rabassa, J., 1987. Cold climatic episode of Younger Dryas age in Tierra del Fuego. *Nature* 328, 609.
- Heusser, C.J., 1974. Vegetation and climate of the southern Chilean Lake District during and since the last interglaciation. *Quaternary Research* 4, 290-315.
- Heusser, C.J., 1989. Climate and chronology of Antarctica and adjacent South America over the past 30,000 yr. *Palaeogeography, Palaeoclimatology, Palaeoecology* 76, 31-37.
- Heusser, C.J., 1998. Deglacial paleoclimate of the American sector of the Southern Ocean: Late Glacial–Holocene records from the latitude of Canal Beagle (55°S), Argentine Tierra del Fuego. *Palaeogeography, Palaeoclimatology, Palaeoecology* 141, 277-301.
- Heusser, C.J., 2003. *Ice Age Southern Andes*. Elsevier.

- Heusser, C.J., Denton, G.H., Hauser, A., Andersen, B.G., Lowell, T.V., 1995. Quaternary pollen records from the Archipiélago de Chiloé in the context of glaciation and climate. *Andean Geology* 22, 25-46.
- Heusser, C.J., Heusser, L.E., Lowell, T.V., 1999. Paleoecology of the southern Chilean Lake District-Isla Grande de Chiloé during middle-late Llanquihue glaciation and deglaciation. *Geografiska Annaler: Series A, Physical Geography* 81, 231-284.
- Heusser, C.J., Heusser, L.E., Lowell, T.V., 2000. Deglacial palaeoclimate at Puerto del Hambre, subantarctic Patagonia, Chile. *Journal of Quaternary Science* 15, 101-114.
- Hidy, A.J., Gosse, J.C., Pederson, J.L., Mattern, J.P., Finkel, R.C., 2010. A geologically constrained Monte Carlo approach to modeling exposure ages from profiles of cosmogenic nuclides: An example from Lees Ferry, Arizona. *Geochemistry, Geophysics, Geosystems* 11.
- Hillenbrand, C.-D., Bentley, M.J., Stollendorf, T.D., Hein, A.S., Kuhn, G., Graham, A.G.C., Fogwill, C.J., Kristoffersen, Y., Smith, J.A., Anderson, J.B., Larter, R.D., Melles, M., Hodgson, D.A., Mulvaney, R., Sugden, D.E., 2014. Reconstruction of changes in the Weddell Sea sector of the Antarctic Ice Sheet since the Last Glacial Maximum. *Quaternary Science Reviews* 100, 111-136.
- Hodgson, D.A., Graham, A.G.C., Roberts, S.J., Bentley, M.J., Ó Cofaigh, C., Verleyen, E., Vyverman, W., Jomelli, V., Favier, V., Brunstein, D., Verfaillie, D., Colhoun, E.A., Saunders, K.M., Selkirk, P.M., Mackintosh, A., Hedding, D.W., Nel, W., Hall, K., McGlone, M.S., Van der Putten, N., Dickens, W.A., Smith, J.A., 2014. Terrestrial and submarine evidence for the extent and timing of the Last Glacial Maximum and the onset of deglaciation on the maritime-Antarctic and sub-Antarctic islands. *Quaternary Science Reviews* 100, 137-158.
- Hogg, A.G., Hua, Q., Blackwell, P.G., Niu, M., Buck, C.E., Guilderson, T.P., Heaton, T.J., Palmer, J.G., Reimer, P.J., Reimer, R.W., Turney, C.S.M., Zimmerman, S.H., 2013. SHCal13 Southern Hemisphere Calibration, 0–50,000 Years cal BP. *Radiocarbon* 55, 1889-1903.
- Holmlund, P., Fuenzalida, H., 1995. Anomalous glacier responses to 20th century climatic changes in Darwin Cordillera, southern Chile. *Journal of Glaciology* 41, 465-473.
- Horta, L.R., Belardi, J.B., Georgieff, S.M., Carballo Marina, F., 2019. Paleogeographic reconstruction of the Tar – San Martín lacustrine system during late Pleistocene to early Holocene: Landscape availability and hunter-gatherer circulation (Santa Cruz, Argentina). *Quaternary International* 512, 45-51.
- Hubbard, A., Hein, A.S., Kaplan, M.R., Hulton, N.R.J., Glasser, N., 2005. A modelling reconstruction of the Last Glacial Maximum ice sheet and its deglaciation in the vicinity of the Northern Patagonian Icefield, South America. *Geografiska Annaler* 87, 375-391.
- Hughes, A.L., Gyllencreutz, R., Lohne, Ø.S., Mangerud, J., Svendsen, J.I., 2016. The last Eurasian ice sheets—a chronological database and time-slice reconstruction, DATED-1. *Boreas* 45, 1-45.
- Hughes, P.D., Gibbard, P.L., Ehlers, J., 2013. Timing of glaciation during the last glacial cycle: evaluating the concept of a global 'Last Glacial Maximum' (LGM). *Earth-Science Reviews* 125, 171-198.
- Hulton, N.R., Sugden, D.E., Payne, A., Clapperton, C., 1994. Glacier modeling and the climate of Patagonia during the Last Glacial Maximum. *Quaternary Research* 42, 1-19.
- Hulton, N.R.J., Purves, R.S., McCulloch, R.D., Sugden, D.E., Bentley, M.J., 2002. The Last Glacial Maximum and deglaciation in southern South America. *Quaternary Science Reviews* 21, 233-241.

- Huss, M., Hock, R., 2018. Global-scale hydrological response to future glacier mass loss. *Nature Climate Change* 8, 135–140.
- Iglesias, V., Markgraf, V., Whitlock, C., 2016. 17,000 years of vegetation, fire and climate change in the eastern foothills of the Andes (lat. 44° S). *Palaeogeography, Palaeoclimatology, Palaeoecology* 457, 195–208.
- Isla, F.I., 2013. The flooding of the San Matías Gulf: The Northern Patagonia sea-level curve. *Geomorphology* 203, 60–65.
- Ivy-Ochs, S., Kerschner, H., Maisch, M., Christl, M., Kubik, P.W., Schlüchter, C., 2009. Latest Pleistocene and Holocene glacier variations in the European Alps. *Quaternary Science Reviews* 28, 2137–2149.
- Izagirre, E., Darvill, C.M., Rada, C., Aravena, J.C., 2018. Glacial geomorphology of the Marinelli and Pigafetta glaciers, Cordillera Darwin Icefield, southernmost Chile. *Journal of Maps* 14, 269–281.
- Jaber, W.A., Floricioiu, D., Rott, H., 2016. Geodetic mass balance of the Patagonian Icefields derived from SRTM and TanDEM-X data, 2016 IEEE International Geoscience and Remote Sensing Symposium (IGARSS), pp. 342–345.
- Jansson, K.N., Glasser, N.F., 2005. Using Landsat 7 ETM+ imagery and Digital Terrain Models for mapping glacial lineaments on former ice sheet beds. *International Journal of Remote Sensing* 26, 3931–3941.
- Jomelli, V., Favier, V., Vuille, M., Braucher, R., Martin, L., Bourd, P.H., Colose, C., Brunstein, D., He, F., Khodri, M., Bourles, D.L., Leanni, L., Rinterknecht, V., Grancher, T., Francou, B., Ceballos, J.L., Fonseca, H., Liu, Z., Otto-Bliesner, B.L., 2014. A major advance of tropical Andean glaciers during the Antarctic cold reversal. *Nature* 513(7517), 224–228.
- Kaiser, J., Lamy, F., Arz, H.W., Hebbeln, D., 2007. Dynamics of the millennial-scale sea surface temperature and Patagonian Ice Sheet fluctuations in southern Chile during the last 70 kyr (ODP Site 1233). *Quaternary International* 161, 77–89.
- Kaplan, M., Schaefer, J., Strelin, J., Denton, G., Anderson, R., Vandergoes, M., Finkel, R., Schwartz, R., Travis, S., Garcia, J., 2016. Patagonian and southern South Atlantic view of Holocene climate. *Quaternary Science Reviews* 141, 112–125.
- Kaplan, M.R., Ackert, R.P., Singer, B.S., Douglass, D.C., Kurz, M.D., 2004. Cosmogenic nuclide chronology of millennial-scale glacial advances during O-isotope stage 2 in Patagonia. *GSA Bulletin* 116, 308–321.
- Kaplan, M.R., Coronato, A., Hulton, N.R.J., Rabassa, J.O., Kubik, P.W., Freeman, S.P.H.T., 2007. Cosmogenic nuclide measurements in southernmost South America and implications for landscape change. *Geomorphology* 87, 284–301.
- Kaplan, M.R., Douglass, D.C., Singer, B.S., Ackert, R.P., Caffee, M.W., 2005. Cosmogenic nuclide chronology of pre-last glacial maximum moraines at Lago Buenos Aires, 46°S, Argentina. *Quaternary Research* 63, 301–315.
- Kaplan, M.R., Fogwill, C.J., Sugden, D.E., Hulton, N.R.J., Kubik, P.W., Freeman, S.P.H.T., 2008. Southern Patagonian glacial chronology for the Last Glacial period and implications for Southern Ocean climate. *Quaternary Science Reviews* 27, 284–294.
- Kaplan, M.R., Hein, A.S., Hubbard, A., Lax, S.M., 2009. Can glacial erosion limit the extent of glaciation? *Geomorphology* 103, 172–179.

- Kaplan, M.R., Strelin, J.A., Schaefer, J.M., Denton, G.H., Finkel, R.C., Schwartz, R., Putnam, A.E., Vandergoes, M.J., Goehring, B.M., Travis, S.G., 2011. In-situ cosmogenic  $^{10}\text{Be}$  production rate at Lago Argentino, Patagonia: Implications for late-glacial climate chronology. *Earth and Planetary Science Letters* 309, 21-32.
- Kilian, R., Baeza, O., Breuer, S., Ríos, F., Arz, H., Lamy, F., Wirtz, J., Baque, D., Korf, P., Kremer, K., 2013a. Evolución paleogeográfica y paleoecológica del Sistema de fiordos del Seno Skyring y Seno Otway en la región de Magallanes durante el Tardiglacial y Holoceno. *Anales del Instituto de la Patagonia* 41, 5-26.
- Kilian, R., Baeza, O., Breuer, S., Ríos, F., Arz, H., Lamy, F., Wirtz, J., Baque, D., Korf, P., Kremer, K., 2013b. Late Glacial and Holocene palaeogeographical and palaeoecological evolution of the Seno Skyring and Otway fjord systems in the Magellan Region. *Anales del Instituto de la Patagonia* 41, 5-26.
- Kilian, R., Baeza, O., Steinke, T., Arevalo, M., Rios, C., Schneider, C., 2007a. Late Pleistocene to Holocene marine transgression and thermohaline control on sediment transport in the western Magellanes fjord system of Chile (53°S). *Quaternary International* 161, 90-107.
- Kilian, R., Hohner, M., Biester, H., Wallrabe-Adams, H.J., Stern, C.R., 2005. Holocene peat and lake sediment tephra record from the southernmost Chilean Andes (53-55°S). *Revista geologica de Chile* 30, 23-37.
- Kilian, R., Lamy, F., 2012. A review of Glacial and Holocene paleoclimate records from southernmost Patagonia (49–55°S). *Quaternary Science Reviews* 53, 1-23.
- Kilian, R., Lamy, F., Arz, H., 2013c. Late Quaternary variation of the southern westerly wind belt and its influences on aquatic ecosystems and glacier extent within the southernmost Andes [Spätquartäre Variationen der südhemisphärischen Westwindzone und deren Einfluss auf aquatische Ökosysteme sowie Gletscherausdehnung in den südlichen Anden]. *Zeitschrift der Deutschen Gesellschaft für Geowissenschaften* 164, 279-294.
- Kilian, R., Schneider, C., Koch, J., Fesq-Martin, M., Biester, H., Casassa, G., Arévalo, M., Wendt, G., Baeza, O., Behrmann, J., 2007b. Palaeoecological constraints on late Glacial and Holocene ice retreat in the Southern Andes (53°S). *Global and Planetary Change* 59, 49-66.
- Kelley, S. E., Kaplan, M. R., Schaefer, J. M., Andersen, B. G., Barrell, D. J. A., Putnam, A. E., Denton, G.H., Schwartz, R., Finkel, R.C., Doughty, A.M. 2014. High-precision  $^{10}\text{Be}$  chronology of moraines in the Southern Alps indicates synchronous cooling in Antarctica and New Zealand 42,000 years ago. *Earth and Planetary Science Letters*, 405, 194–206.
- Koch, J., Kilian, R., 2005. 'Little Ice Age' glacier fluctuations, Gran Campo Nevado, southernmost Chile. *Holocene* 15, 20-28.
- Kohfeld, K., Graham, R., De Boer, A., Sime, L., Wolff, E., Le Quéré, C., Bopp, L., 2013. Southern Hemisphere westerly wind changes during the Last Glacial Maximum: paleo-data synthesis. *Quaternary Science Reviews* 68, 76-95.
- Kuylensstierna, J.L., Rosqvist, G.C., Holmlund, P., 1996. Late-Holocene glacier variations in the Cordillera Darwin, Tierra del Fuego, Chile. *The Holocene* 6, 353-358.
- Lal, D., 1991. Cosmic ray labeling of erosion surfaces: in situ nuclide production rates and erosion models. *Earth and Planetary Science Letters* 104, 424-439.

- Lamy, F., Kaiser, J., Ninnemann, U., Hebbeln, D., Arz, H.W., Stoner, J., 2004. Antarctic timing of surface water changes off Chile and Patagonian ice sheet response. *Science* 304, 1959-1962.
- Lamy, F., Kilian, R., Arz, H.W., Francois, J.-P., Kaiser, J., Prange, M., Steinke, T., 2010. Holocene changes in the position and intensity of the southern westerly wind belt. *Nature Geoscience* 3, 695-699.
- Lamy, F., Arz, H.W., Kilian, R., Lange, C.B., Lembke-Jene, L., Wengler, M., Kaiser, J., Baeza-Urrea, O., Hall, I.R., Harada, N., Tiedemann, R., 2015. Glacial reduction and millennial-scale variations in Drake Passage throughflow. *Proceedings of the National Academy of Sciences* 112, 13496 LP – 13501.
- Lapido, O., 2000. Carta Geológica de la República Argentina, Escala 1:250.000., Gobernador Costa 4572-II/I. Edición Cartográfica Preliminar. Servicio Geológico Nacional, Buenos Aires.
- Larter, R.D., Anderson, J.B., Graham, A.G.C., Gohl, K., Hillenbrand, C.-D., Jakobsson, M., Johnson, J.S., Kuhn, G., Nitsche, F.O., Smith, J.A., Witus, A.E., Bentley, M.J., Dowdeswell, J.A., Ehrmann, W., Klages, J.P., Lindow, J., Ó Cofaigh, C., Spiegel, C., 2014. Reconstruction of changes in the Amundsen Sea and Bellingshausen Sea sector of the West Antarctic Ice Sheet since the Last Glacial Maximum. *Quaternary Science Reviews* 100, 55-86.
- Lastras, G., Dowdeswell, J., 2016. Terminal and recessional moraines in the fjords of southern Chile. *Geological Society, London, Memoirs* 46, 65-66.
- Lawrence, D.B., Lawrence, E.G., 1959. Recent glacier variations in southern South America. American Geographical Society New York.
- Lenaerts, J.T., Van Den Broeke, M.R., van Wessel, J.M., van de Berg, W.J., van Meijgaard, E., van Uft, L.H., Schaefer, M., 2014. Extreme precipitation and climate gradients in Patagonia revealed by high-resolution regional atmospheric climate modeling. *Journal of climate* 27, 4607-4621.
- López-Martínez, J., Muñoz, A., Dowdeswell, J.A., Linés, C., Acosta, J., 2011. Relict sea-floor ploughmarks record deep-keeled Antarctic icebergs on the Argentine margin. *Marine Geology* 288, 43-48.
- Loriaux, T., Casassa, G., 2013. Evolution of glacial lakes from the Northern Patagonia Icefield and terrestrial water storage in a sea-level rise context. *Global and Planetary Change* 102, 33-40.
- Lovell, H., Stokes, C.R., Bentley, M.J., 2011. A glacial geomorphological map of the Seno Skyring-Seno Otway-Strait of Magellan region, southernmost Patagonia. *Journal of maps* 7, 318-339.
- Lovell, H., Stokes, C.R., Bentley, M.J., Benn, D.I., 2012. Evidence for rapid ice flow and proglacial lake evolution around the central Strait of Magellan region, southernmost Patagonia. *Journal of Quaternary Science* 27, 625-638.
- Lowe, J.J., Walker, M.J.C., 2015. Reconstructing Quaternary Environments. Routledge, Abingdon, Oxon.
- Lowell, T., Heusser, C., Andersen, B., Moreno, P., Hauser, A., Heusser, L., Schlüchter, C., Marchant, D., Denton, G., 1995. Interhemispheric correlation of late Pleistocene glacial events. *Science* 269, 1541-1549.
- Lozano, J.G., Tassone, A., Bran, D.M., Lodolo, E., Menichetti, M., Cerredo, M.E., Esteban, F., Ormazabal, J.P., Ísola, J., Baradello, L., 2018. Glacial-related morphology and sedimentary setting of a high-latitude lacustrine basin: The Lago Chepelmut (Tierra del Fuego, Argentina). *Journal of South American Earth Sciences* 86, 259-270.



- Ludbrook, J., 2008. The presentation of statistics in Clinical and Experimental Pharmacology and Physiology. *Clinical and Experimental Pharmacology and Physiology* 35, 1271–1274.
- Lumley, S.H., Switsur, R., 1993. Late Quaternary chronology of the Taitao Peninsula, southern Chile. *Journal of Quaternary Science* 8, 161–165.
- Mackintosh, A., White, D., Fink, D., Gore, D.B., Pickard, J., Fanning, P.C., 2007. Exposure ages from mountain dipsticks in Mac. Robertson Land, East Antarctica, indicate little change in ice-sheet thickness since the Last Glacial Maximum. *Geology* 35, 551–554.
- Malz, P., Meier, W., Casassa, G., Jaña, R., Skvarca, P., Braun, M., 2018. Elevation and mass changes of the Southern Patagonia Icefield derived from TanDEM-X and SRTM data. *Remote Sensing* 10, 188.
- Mancini, M., Paez, M., Prieto, A., Stutz, S., Tonello, M., Vilanova, I., 2005. Mid-Holocene climatic variability reconstruction from pollen records (32–52 S, Argentina). *Quaternary International* 132, 47–59.
- Mansilla, C.A., McCulloch, R.D., Morello, F., 2016. Palaeoenvironmental change in Southern Patagonia during the Lateglacial and Holocene: Implications for forest refugia and climate reconstructions. *Palaeogeography, Palaeoclimatology, Palaeoecology* 447, 1–11.
- Marden, C.J., Clapperton, C.M., 1995. Fluctuations of the South Patagonian Ice-field during the last glaciation and the Holocene. *Journal of Quaternary Science* 10, 197–206.
- Margold, M., Stokes, C. R., & Clark, C. D. (2018). Recording records of ice streaming and ice margin retreat to produce a palaeogeographic reconstruction of the deglaciation of the Laurentide Ice Sheet. *Quaternary Science Reviews*, 189, 1–30.
- Markgraf, V., 1993. Palaeoenvironments and palaeoclimates in Tierra del Fuego and southernmost Patagonia, South America. *Palaeogeography, Palaeoclimatology, Palaeoecology* 102, 53–68.
- Martin, D., Cornford, S., Peter, S., Le Brech, A., Payne, A., Lipscomb, W., Ng, E., 2013. Resolving Grounding Line Dynamics with the BISICLES Adaptive Mesh, EGU General Assembly Conference Abstracts, p. 12083.
- Martin, J.R.V., Davies, B.J., Thorndyke, V.R., 2019. Glacier dynamics during a phase of Late Quaternary warming in Patagonia reconstructed from sediment-landform associations. *Geomorphology* 337, 111–133.
- Martínez, O., Coronato, A., Rabassa, J., 2011. Chapter 52 - Pleistocene Glaciations in Northern Patagonia, Argentina: An Updated Review, in: Jürgen Ehlers, P.L.G., Philip, D.H. (Eds.), *Developments in Quaternary Sciences*. Elsevier, pp. 729–734.
- Martinod, J., Regard, V., Riquelme, R., Aguilar, G., Guillaume, B., Carretier, S., Cortés-Aranda, J., Leanni, L., Hérail, G., 2016. Pleistocene uplift, climate and morphological segmentation of the Northern Chile coasts (24 S–32 S): Insights from cosmogenic <sup>10</sup>Be dating of paleoshorelines. *Geomorphology* 274, 78–91.
- Masiokas, M., Luckman, B., Villalba, R., Delgado, S., Skvarca, P., Ripalta, A., 2009a. Little Ice Age fluctuations of small glaciers in the Monte Fitz Roy and Lago del Desierto areas, south Patagonian Andes, Argentina. *Palaeogeography, Palaeoclimatology, Palaeoecology* 281, 351–362.
- Masiokas, M.H., Rivera, A., Espizua, L.E., Villalba, R., Delgado, S., Aravena, J.C., 2009b. Glacier fluctuations in extratropical South America during the past 1000 years. *Palaeogeography, Palaeoclimatology, Palaeoecology* 281, 242–268.



- Masiokas, M.H., Villalba, R., Luckman, B.H., Lascano, M.E., Delgado, S., Stepanek, P., 2008. 20th-century glacier recession and regional hydroclimatic changes in northwestern Patagonia. *Global and Planetary Change* 60, 85-100.
- Massaferro, J., Brooks, S.J., 2002. Response of chironomids to Late Quaternary environmental change in the Taitao Peninsula, southern Chile. *Journal of Quaternary Science* 17, 101-111.
- Massaferro, J., Larocque-Tobler, I., Brooks, S.J., Vandergoes, M., Dieffenbacher-Krall, A., Moreno, P., 2014. Quantifying climate change in Huelmo mire (Chile, Northwestern Patagonia) during the Last Glacial Termination using a newly developed chironomid-based temperature model. *Palaeogeography, Palaeoclimatology, Palaeoecology* 399, 214-224.
- Massaferro, J.I., Moreno, P.I., Denton, G.H., Vandergoes, M., Dieffenbacher-Krall, A., 2009. Chironomid and pollen evidence for climate fluctuations during the Last Glacial Termination in NW Patagonia. *Quaternary Science Reviews* 28, 517-525.
- Mayr, C., Wille, M., Haberzettl, T., Fey, M., Janssen, S., Lücke, A., Ohlendörf, C., Oliva, G., Schäbitz, F., Schleser, G.H., Zolitschka, B., 2007. Holocene variability of the Southern Hemisphere westerlies in Argentinean Patagonia (52°S). *Quaternary Science Reviews* 26, 519-529.
- Mayr, C., Lücke, A., Wagner, S., Wissel, H., Ohlendörf, C., Haberzettl, T., Oehlerich, M., Schäbitz, F., Wille, M., Zhu, J., 2013. Intensified Southern Hemisphere Westerlies regulated atmospheric CO<sub>2</sub> during the last deglaciation. *Geology* 41, 831-834.
- McCulloch, R.D., Bentley, M.J., 1998. Late glacial ice advances in the Strait of Magellan, southern Chile. *Quaternary Science Reviews* 17, 775-787.
- McCulloch, R.D., Bentley, M.J., Purves, R.S., Mutton, N.R.J., Sugden, D.E., Clapperton, C.M., 2000. Climatic inferences from glacial and palaeoecological evidence at the last glacial termination, southern South America. *Journal of Quaternary Science* 15, 409-417.
- McCulloch, R.D., Bentley, M.J., Tipping, P.M., Clapperton, C.M., 2005a. Evidence for Late -Glacial ice-dammed lakes in the central Strait of Magellan and Bahía Inútil, southernmost South America. *Geografiska Annaler: Series A, Physical Geography* 87, 335-352.
- McCulloch, R.D., Davies, S.I., 2001. Late-glacial and Holocene palaeoenvironmental change in the central Strait of Magellan, southern Patagonia. *Palaeogeography, Palaeoclimatology, Palaeoecology* 173, 143-173.
- McCulloch, R.D., Fogwill, C.J., Sugden, D.E., Bentley, M.J., Kubik, P.W., 2005b. Chronology of the Last Glaciation in Central Strait of Magellan and Bahía Inútil, Southernmost South America. *Geografiska Annaler. Series A, Physical Geography* 87, 289-312.
- Meglioli, A., 1992. Glacial geology and chronology of southernmost Patagonia and Tierra del Fuego, Argentina and Chile. *Lehigh University, Bethlehem*, p. 298.
- Meier, W.J.-H., Grießinger, J., Hochreuther, P., Braun, M.H., 2018. An updated multi-temporal glacier inventory for the Patagonian Andes with changes between the Little Ice Age and 2016. *Frontiers in Earth Science* 6 (62), 1-21.
- Mendelova, M., Hein, A., McCulloch, R., Davies, B., 2017. The Last Glacial Maximum and deglaciation in central Patagonia, 44° S–49° S. *Cuadernos de Investigación Geográfica*.

- Menounos, B., Clague, J.J., Osborn, G., Davis, P.T., Ponce, F., Goehring, B., Maurer, M., Rabassa, J., Coronato, A., Marr, R., 2013. Latest Pleistocene and Holocene glacier fluctuations in southernmost Tierra del Fuego, Argentina. *Quaternary Science Reviews* 77, 70-79.
- Mercer, J.H., 1965. Glacier Variations in Southern Patagonia. *Geographical Review* 55, 390-413.
- Mercer, J.H., 1968. Variations of some Patagonian glaciers since the Late-Glacial. *American Journal of Science* 266, 91-109.
- Mercer, J.H., 1970. Variations of some Patagonian glaciers since the Late-Glacial; II. *American Journal of Science* 269, 1-25.
- Mercer, J.H., 1972. Chilean glacial chronology 20,000 to 11,000 carbon-14 years ago: some global comparisons. *Science* 176, 1118-1120.
- Mercer, J.H., 1976. Glacial history of southernmost South America. *Quaternary Research* 6, 125-166.
- Mercer, J.H., Ager, T., 1983. Glacial and floral changes in Southern Argentina since 14,000 years ago. *National Geographic Society Research Reports* 15, 457-477.
- Milner, A.M., Khamis, K., Battin, T.J., Brittain, J.E., Barrand, N.E., Freder, L., Cauvy-Fraunié, S., Gíslason, G.M., Jacobsen, D., Hannah, D.M., Hodson, A.J., Hood, E., Lencina, V., Ólafsson, J.S., Robinson, C.T., Tranter, M., Brown, L.E., 2017. Glacier shrinkage driving global changes in downstream systems. *Proceedings of the National Academy of Sciences* 114(37), 9770-9778.
- Miranda, C., Moreno, P., Vilanova, I., Villa-Martínez, R., 2013. Glacial fluctuations in the Coyhaique-Balmaceda sector of central Patagonia (45S-46S) during the last glacial termination. *Bollettino di Geofisica* 54, 268-271.
- Möller, M., Schneider, C., 2008. Climate sensitivity and mass-balance evolution of Gran Campo Nevado ice cap, southwest Patagonia. *Annals of Glaciology* 48, 32-42.
- Möller, M., Schneider, C., Kilian, R., 2007. Glacier change and climate forcing in recent decades at Gran Campo Nevado, southernmost Patagonia. *Annals of Glaciology* 46, 136-144.
- Montade, V., Nebout, N.C., Kissel, C., Haberle, S.G., Siani, G., Michel, E., 2013. Vegetation and climate changes during the last 22,000 yr from a marine core near Taitao Peninsula, southern Chile. *Palaeogeography, Palaeoclimatology, Palaeoecology* 369, 335-348.
- Montade, V., Peyron, O., Favier, C., Francois, J.P., Haberle, S.G., 2019. A pollen-climate calibration from western Patagonia for palaeoclimatic reconstructions. *Journal of Quaternary Science* 34, 76-86.
- Moreno, P.I., 1998. Termination of the last ice age in mid-latitudes of South America. *University of Maine*, p. 187.
- Moreno, P.I., 2004. Millennial-scale climate variability in northwest Patagonia over the last 15 000 yr. *Journal of Quaternary Science* 19, 35-47.
- Moreno, P.I., Denton, G.H., Moreno, H., Lowell, T.V., Putnam, A.E., Kaplan, M.R., 2015. Radiocarbon chronology of the Last Glacial Maximum and its termination in northwestern Patagonia. *Quaternary Science Reviews* 122, 233-249.

- Moreno, P.I., Jacobson Jr, G.L., Lowell, T.V., Denton, G.H., 2001. Interhemispheric climate links revealed by a late-glacial cooling episode in southern Chile. *Nature* 409, 804.
- Moreno, P.I., Kaplan, M.R., François, J.P., Villa-Martínez, R., Moy, C.M., Stern, C.R., Kubik, P.W., 2009. Renewed glacial activity during the Antarctic Cold Reversal and persistence of cold conditions until 11.5 ka in southwestern Patagonia. *Geology* 37, 375-378.
- Moreno, P.I., Lowell, T.V., Jacobson Jr, G.L., Denton, G.H., 1999. Abrupt Vegetation and Climate Changes During the Last Glacial Maximum and Last Termination in The Chilean Lake District: A Case Study from Canal De La Puntilla (41° S). *Geografiska Annaler: Series A, Physical Geography* 81, 285-311.
- Moreno, P.I., Videla, J., Valero-Garcés, B., Alloway, B.V. and Heusser, L.E., 2018. A continuous record of vegetation, fire-regime and climatic changes in northwestern Patagonia spanning the last 25,000 years. *Quaternary Science Reviews* 198, 15-36.
- Moreno, P.I., Videla, J., 2016. Centennial and millennial-scale hydroclimate changes in northwestern Patagonia since 16,000 yr BP. *Quaternary Science Reviews* 149, 326-337.
- Moreno, P.I., Vilanova, I., Villa-Martínez, R., Dunbar, R.B., Mucciaroni, D.A., Kaplan, M.R., Garreaud, R.D., Rojas, M., Moy, C.M., De Pol-Holz, R., 2018. Onset and evolution of southern annular mode-like changes at centennial timescale. *Scientific Reports* 8, 3458.
- Mouginot, J., Rignot, E., 2015. Ice motion of the Patagonian icefields of South America: 1984-2014. *Geophysical Research Letters*, 2014GL062661.
- Murdie, R., Pugh, D., Styles, P., 1998. A lightweight, portable, digital probe for measuring the thermal gradient in shallow water sediments, with examples from Patagonia. *Geo-Marine Letters* 18, 315-320.
- Nimick, D.A., McGrath, D., Mahan, S.A., Friesen, R.A., Leidich, J., 2016. Latest Pleistocene and Holocene glacial events in the Colonia valley, Northern Patagonia Icefield, southern Chile. *Journal of Quaternary Science* 31, 551-564.
- Ó Cofaigh, C., Davies, B.J., Livingstone, S.J., Smith, J.A., Johnson, J.S., Hocking, E.P., Hodgson, D.A., Anderson, J.B., Bentley, M.J., Canals, M., Domack, E., Dowdeswell, J.A., Evans, J., Glasser, N.F., Hillenbrand, C.-D., Larter, R.D., Roberts, S.J., Simms, A.R., 2014. Reconstruction of ice-sheet changes in the Antarctic Peninsula since the Last Glacial Maximum. *Quaternary Science Reviews* 100, 87-110.
- Ó Cofaigh, C., Justin, T., Julian, A. D., Carol, J. P., 2003. Palaeo-ice streams, trough mouth fans and high-latitude continental slope sedimentation. *Boreas* 32, 37-55.
- Ó Cofaigh, C., Larter, R.D., Dowdeswell, J.A., Hillenbrand, C.-D., Pudsey, C.J., Evans, J., Morris, P., 2005. Flow of the West Antarctic Ice Sheet on the continental margin of the Bellingshausen Sea at the Last Glacial Maximum. *Journal of Geophysical Research* 110, B11103.
- Oehlerich, M., Mayr, C., Gussone, N., Hahn, A., Hölzl, S., Lücke, A., Ohlendorf, C., Rummel, S., Teichert, B., Zolitschka, B., 2015. Lateglacial and Holocene climatic changes in south-eastern Patagonia inferred from carbonate isotope records of Laguna Potrok Aike (Argentina). *Quaternary science reviews* 114, 189-202.
- Ortlieb, L., Vargas, G., Saliège, J.-F., 2011. Marine radiocarbon reservoir effect along the northern Chile–southern Peru coast (14–24°S) throughout the Holocene. *Quaternary Research* 75, 91-103.
- Paterson, W., 1994. The physics of glaciers, 480 pp. Pergamon, New York.

- Patton, H., Hubbard, A., Andreassen, K., Auriac, A., Whitehouse, P.L., Stroeve, A.P., Shackleton, C., Winsborrow, M., Heyman, J., Hall, A.M., 2017. Deglaciation of the Eurasian ice sheet complex. *Quaternary Science Reviews* 169, 148-172.
- Patton, H., Hubbard, A., Andreassen, K., Winsborrow, M., Stroeve, A.P., 2016. The build-up, configuration, and dynamical sensitivity of the Eurasian ice-sheet complex to Late Weichselian climatic and oceanic forcing. *Quaternary Science Reviews* 153, 97-121.
- Pattyn, F., Favier, L., Sun, S., Durand, G., 2017. Progress in numerical modeling of Antarctic ice-sheet dynamics. *Current Climate Change Reports* 3, 174–184.
- Paul, F., Mölg, N., 2014. Hasty retreat of glaciers in northern Patagonia from 1985-2011. *Journal of Glaciology* 60, 1033-1043.
- Pedro, J.B., Bostock, H.C., Bitz, C.M., He, F., Vandergoes, M.J., Steig, E.J., Chase, B.M., Krause, C.E., Rasmussen, S.O., Markle, B.R., 2016. The spatial extent and dynamics of the Antarctic Cold Reversal. *Nature Geoscience* 9, 51-55.
- Pedro, J.B., Jochum, M., Buizert, C., He, F., Barker, S., Rasmussen, S.O., 2018. Beyond the bipolar seesaw: Toward a process understanding of interhemispheric coupling. *Quaternary Science Reviews* 192, 27-46.
- Peltier, C., Kaplan, M.R., Schaefer, J.M., Soteres, R., Sagredo, E.A., Aravena, J.C., 2016. A Glacial Chronology of the Strait of Magellan. *AGU Fall Meeting Abstracts*.
- Peltier, W.R., Drummond, R., 2002. A “broad-shelf effect” upon postglacial relative sea level history. *Geophysical Research Letters* 29, 10-11-10-14.
- Pollard, D., DeConto, R.M., Alley, R.B., 2015. Potential Antarctic Ice Sheet retreat driven by hydrofracturing and ice cliff failure. *Earth Planetary Science Letters* 412, 112–121.
- Ponce, J.F., Guillot, M.G., Martinez, O., Palocci, L.D., 2018. Geomorphological evidences of paleosurge activity in Lake Viedma Lobe, Patagonia, Argentina. *Geomorphology* 327, 511-522.
- Ponce, J.F., Rabassa, J., Coronato, A., Borrero, A., 2011. Palaeogeographical evolution of the Atlantic coast of Pampa and Patagonia from the last glacial maximum to the Middle Holocene. *Biological Journal of the Linnean Society* 103, 363-379.
- Ponce, J.F., Rabassa, J., Serrat, E., Martínez, O.A., 2013. El campo de drumlins, flutes y megaflutes de lago Viedma, Pleistoceno Tardío, provincia de Santa Cruz. *Revista de la Asociación Geológica Argentina* 70, 115-127.
- Porter, C., Santana, A., 2003. Rapid 20th century retreat of Ventisquero Marinelli in the Cordillera Darwin icefield. *Anales del Instituto de la Patagonia* 31.
- Porter, S.C., 2000. Onset of Neoglaciation in the Southern Hemisphere. *Journal of Quaternary Science* 15, 395–408.
- Porter, S.C., 1990. Character and ages of Pleistocene drifts in a transect across the Strait of Magellan. *Quaternary of South America and Antarctic Peninsula* 7, 35-50.
- Porter, S.C., Clapperton, C., Sugden, D., 1992. Chronology and dynamics of deglaciation along and near the Strait of Magellan, southernmost South America. *SGU series Ca. Research paper*, 233-239.

- Porter, S.C., 1981. Pleistocene glaciation in the southern Lake District of Chile. *Quaternary Research* 16, 263-292.
- Porter, S.C., Stuiver, M., Heusser, C.J., 1984. Holocene sea-level changes along the Strait of Magellan and Beagle Channel, southernmost South America. *Quaternary Research* 22, 59-67.
- Powell, R.D., Molnia, B.F., 1989. Glacimarine sedimentary processes, facies and morphology of the south-southeast Alaska shelf and fjords. *Marine Geology* 85, 359-390.
- Quade, J., Kaplan, M. R., 2017. Lake-level stratigraphy and geochronology revisited at Lago (Lake) Cardiel, Argentina, and changes in the Southern Hemispheric Westerlies over the last 25 ka. *Quaternary Science Reviews* 177, 173-188.
- Rabassa, J., 2008. Late Cenozoic glaciations in Patagonia and Tierra del Fuego. *Developments in quaternary sciences* 11, 151-204.
- Rabassa, J., Clapperton, C.M., 1990. Quaternary glaciations of the southern Andes. *Quaternary Science Reviews* 9, 153-174.
- Rabassa, J., Coronato, A., Bujalesky, G., Salemme, M., Roig, C., Meglioli, A., Heusser, C., Gordillo, S., Roig, F., Borromei, A., Quattrocchio, M., 2000. Quaternary of Tierra del Fuego, Southernmost South America: an updated review. *Quaternary International* 68-71, 217-240.
- Rabassa, J., Coronato, A., Martinez, O., 2011. Late Cenozoic glaciations in Patagonia and Tierra del Fuego: an updated review. *Biological Journal of the Linnean Society* 103, 316-335.
- Rabassa, J., Heusser, C., Roig, C., Coronato, A., Bujalesky, G., 1998. Palaeoenvironmental conditions during the termination of a glacial stadial in Lago Fagnano, Isla Grande de Tierra del Fuego, Argentina, *Actas VII Congreso Argentino de Paleontología y Biostratigrafía*, p. 132.
- Rapela, C.W., Pankhurst, R.J., 1992. The granites of northern Patagonia and the Gastre Fault System in relation to the break-up of Gondwana. *Geological Society, London, Special Publications* 68, 209-220.
- Rapela, C.W., Pankhurst, R.J., Fanning, C., Herve, F., 2005. Pacific subduction coeval with the Karoo mantle plume: the Early Jurassic Subcordilleran belt of northwestern Patagonia. *Geological Society, London, Special Publications* 246, 217-239.
- Rau, F., Mauz, F., Vogt, S., Khalsa, S.J.S., Raup, B., 2005. Illustrated GLIMS Glacier Classification Manual, Version 1.0. GLIMS (Global Land Ice Measurement from Space), NSIDC, GLIMS Regional Centre, 'Antarctic Peninsula'.
- Raup, B., Khalsa, S.J.S., 2010. GLIMS Analysis Tutorial. GLIMS, Global Land Ice Measurements from Space, NSIDC, [www.GLIMS.org](http://www.GLIMS.org).
- Raup, B., Racoviteanu, A., Khalsa, S.J.S., Helm, C., Armstrong, R., Arnaud, Y., 2007. The GLIMS geospatial glacier database: A new tool for studying glacier change. *Global and Planetary Change* 56, 101-110.
- Recasens, C., Ariztegui, D., Gebhardt, C., Gogorza, C., Haberzettl, T., Hahn, A., Kliem, P., Lisé-Pronovost, A., Lücke, A., Maidana, N., 2012. New insights into paleoenvironmental changes in Laguna Potrok Aike, southern Patagonia, since the Late Pleistocene: the PASADO multiproxy record. *The Holocene* 22, 1323-1335.

- Reimer, P.J., Bard, E., Bayliss, A., Beck, J.W., Blackwell, P.G., Ramsey, C.B., Buck, C.E., Cheng, H., Edwards, R.L., Friedrich, M., 2013. IntCal13 and Marine13 radiocarbon age calibration curves 0–50,000 years cal BP. *Radiocarbon* 55, 1869–1887.
- Reinthal, J., Paul, F., Granados, H. D., Rivera, A., & Huggel, C. 2019. Area changes of glaciers on active volcanoes in Latin America between 1986 and 2015 observed from multi-temporal satellite imagery. *Journal of Glaciology*, 65(252), 542–556.
- Reynhout, S., Sagredo, E.A., Kaplan, M.R., Aravena, J.C., Martini, M.A., Moreno, P.I., Rojas, M., Schwartz, R., Schaefer, J.M., 2019. Holocene glacier fluctuations in Patagonia are modulated by summer insolation intensity and paced by Southern Annular Mode-like variability. *Quaternary Science Reviews* 220, 178–187.
- Rignot, E., Mouginot, J., Scheuchl, B., van den Broeke, M., van Wessem, M. J., & Morlighem, M. (2019). Four decades of Antarctic Ice Sheet mass balance from 1979–2017. *Proceedings of the National Academy of Sciences*, 116(4), 1095–1103. <https://doi.org/10.1073/pnas.1812883116>
- Rivera, A., Benham, T., Casassa, G., Bamber, J., Dowdeswell, J.A., 2007. Ice elevation and areal changes of glaciers from the Northern Patagonia Icefield, Chile. *Global and Planetary Change* 59, 126–137.
- Rivera, A., Bown, F., Casassa, G., Acuña, C., Clavero, J., 2005. Glacier shrinkage and negative mass balance in the Chilean Lake District (40° S)/Rétrécissement glaciaire et bilan massique négatif dans la Région des Lacs du Chili (40° S). *Hydrological Sciences Journal* 50.
- Rivera, A., Bown, F., Mella, R., Wendt, J., Casassa, G., Acuña, C., Rignot, E., Clavero, J., Brock, B., 2006. Ice volumetric changes on active volcanoes in southern Chile. *Annals of Glaciology* 43, 111–122.
- Rivera, A., Corripio, J., Bravo, C., Cisternas, S., 2012a. Glaciar Jorge Montt (Chilean Patagonia) dynamics derived from photos obtained by fixed cameras and satellite image feature tracking. *Annals of Glaciology* 53, 147–155.
- Rivera, A., Koppes, M., Bravo, C., Aravena, J.C., 2012b. Little Ice Age advance and retreat of Glaciar Jorge Montt, Chilean Patagonia. *Climate of the Past* 8, 403–414.
- Rodbell, D.T., Smith, J.A., Mark, B.C., 2009. Glaciation in the Andes during the Lateglacial and Holocene. *Quaternary Science Reviews* 28, 2175–2212.
- Roig, F., Roig, C., Rabassa, J., Boninsegna, J., 1996. Fuegian floating tree-ring chronology from subfossil *Nothofagus* wood. *The Holocene* 6, 469–476.
- Rosenau, M., Melnick, D., Echtler, H., 2006. Kinematic constraints on intra-arc shear and strain partitioning in the southern Andes between 38°S and 42°S latitude. *Tectonics* 25.
- Rutt, I.C., Hagdorn, M., Hulton, N.R.J., Payne, A.J., 2009. The Glimmer community ice sheet model. *Journal of Geophysical Research* 114, F02004.
- Sagredo, E.A., Kaplan, M.R., Araya, P.S., Lowell, T.V., Aravena, J.C., Moreno, P.I., Kelly, M.A., Schaefer, J.M., 2018. Trans-pacific glacial response to the Antarctic Cold Reversal in the southern mid-latitudes. *Quaternary Science Reviews* 188, 160–166.
- Sagredo, E.A., Lowell, T.V., Kelly, M.A., Rupper, S., Aravena, J.C., Ward, D.J., Malone, A.G., 2016. Equilibrium line altitudes along the Andes during the Last millennium: Paleoclimatic implications. *The Holocene* 27, 1019–1033.



- Sagredo, E.A., Moreno, P.I., Villa-Martínez, R., Kaplan, M.R., Kubik, P.W., Stern, C.R., 2011. Fluctuations of the Última Esperanza ice lobe (52°S), Chilean Patagonia, during the last glacial maximum and termination 1. *Geomorphology* 125, 92-108.
- Schäbitz, F., Wille, M., Francois, J.-P., Haberzettl, T., Quintana, F., Mayr, C., Lücke, A., Ohlendorf, C., Mancini, V., Paez, M.M., 2013. Reconstruction of palaeoprecipitation based on pollen transfer functions—the record of the last 16 ka from Laguna Potrok Aike, southern Patagonia. *Quaternary Science Reviews* 71, 175-190.
- Schaefer, J.M., Denton, G.H., Kaplan, M., Putnam, A., Finkel, R.C., Barrell, D.J.A., Andersen, B.G., Schwartz, R., Mackintosh, A., Chinn, T., Schlichter, C., 2009. High-Frequency Holocene Glacier Fluctuations in New Zealand Differ from the Northern Signature. *Science* 324, 622-625.
- Schaefer, M., Machguth, H., Falvey, M., Casassa, G., Rignot, E., 2015. Quantifying mass balance processes on the Southern Patagonia Icefield. *The Cryosphere* 9, 25-35.
- Schellmann, G., Radtke, U., 2010. Timing and magnitude of Holocene sea level changes along the middle and south Patagonian Atlantic coast derived from beach ridge systems, littoral terraces and valley-mouth terraces. *Earth-Science Reviews* 103, 1-30.
- Schenk, C.J., Viger, R.J., Anderson, C.P., 1997. Map showing oil and gas fields and geologic provinces of South America. U.S. Geological Survey, pp. 1-12.
- Schneider, C., Gies, D., 2004. Effects of El Niño–southern oscillation on southernmost South America precipitation at 53 S revealed from NCEP–NCAR reanalyses and weather station data. *International Journal of Climatology* 24, 1057-1076.
- Schneider, C., Schnirch, M., Acuña, C., Casassa, G., Gilian, R., 2007. Glacier inventory of the Gran Campo Nevado Ice Cap in the Southern Andes and glacier changes observed during recent decades. *Global and Planetary Change* 59, 87-100.
- Siani, G., Colin, C., Michel, E., Carel, M., Richter, T., Kissel, C., Dewilde, F., 2010. Late Glacial to Holocene terrigenous sediment record in the Northern Patagonian margin: Paleoclimate implications. *Palaeogeography, Palaeoclimatology, Palaeoecology* 297, 26-36.
- Siddall, M., Rohling, E.J., Thompson, W.G., Waelbroeck, C., 2008. Marine isotope stage 3 sea level fluctuations: Data synthesis and new outlook. *Reviews of Geophysics* 46.
- Sime, L.C., Kohfeld, K.E., Le Qué, C., Wolff, E.W., de Boer, A.M., Graham, R.M. and Bopp, L., 2013. Southern Hemisphere westerly wind changes during the Last Glacial Maximum: model-data comparison. *Quaternary Science Reviews*, 64, 104-120.
- Singer, B.S., Ackert, R.P., Guillou, H., 2004a.  $^{40}\text{Ar}/^{39}\text{Ar}$  and K-Ar chronology of Pleistocene glaciations in Patagonia. *Geological Society of America Bulletin* 116, 434-450.
- Singer, B.S., Brown, L.L., Rabassa, J.O., Guillou, H., 2004b.  $^{40}\text{Ar}/^{39}\text{Ar}$  chronology of late Pliocene and Early Pleistocene geomagnetic and glacial events in southern Argentina. *Timescales of the paleomagnetic field*, 175-190.
- Small, D., Clark, C.D., Chiverrell, R.C., Smedley, R.K., Bateman, M.D., Duller, G.A.T., Ely, J.C., Fabel, D., Medialdea, A., Moreton, S.G., 2017. Devising quality assurance procedures for assessment of legacy geochronological data relating to deglaciation of the last British-Irish Ice Sheet. *Earth-Science Reviews* 164, 232-250.



- Smedley, R., Glasser, N., Duller, G., 2016. Luminescence dating of glacial advances at Lago Buenos Aires ( ~ 46° S), Patagonia. *Quaternary Science Reviews* 134, 59-73.
- Solari, M.A., Le Roux, J.P., Hervé, F., Airo, A., Calderón, M., 2012. Evolution of the Great Tehuelche Paleolake in the Torres del Paine National Park of Chilean Patagonia during the Last Glacial Maximum and Holocene. *Andean Geology* 39, 1-21.
- Solomina, O.N., Bradley, R.S., Hodgson, D.A., Ivy-Ochs, S., Jomelli, V., Mackintosh, A.N., Nesje, A., Owen, L.A., Wanner, H., Wiles, G.C., Young, N.E., 2015. Holocene glacier fluctuations. *Quaternary Science Reviews* 111, 9-34.
- Steig, E., Brook, E., White, J., Sucher, C., Bender, M., Lehman, S., Morse, D., Waddington, E., Clow, G., 1998. Synchronous climate changes in Antarctica and the North Atlantic. *Science* 282, 92-95.
- Stern, C., 1992. Tefrocronología de Magallanes: nuevos datos e implicaciones, *Anales del Instituto de la Patagonia*, pp. 129-141.
- Stern, C., 2011. Evolution of ice-dammed proglacial lakes in Última Esperanza, Chile: implications from the late-glacial R1 eruption of Reclús volcano, Andean Austral Volcanic Zone.
- Stern, C.R., 1990. Tephrochronology of southernmost Patagonia. *National Geographic Society Research* 6, 110-126.
- Stern, C.R., 2008. Holocene tephrochronology record of large explosive eruptions in the southernmost Patagonian Andes. *Bulletin of Volcanology* 70, 435-451.
- Stern, C.R., de Porras, M.E., Maldonado, A., 2015. Tephrochronology of the upper Río Cisnes valley (44 S), southern Chile. *Andean Geology* 42.
- Stern, C.R., Moreno, P.I., Henríquez, W.I., Villalón-Martínez, R., Sagredo, E., Aravena, J.C., de Pol-Holz, R., 2016. Holocene tephrochronology around Cochón ( ~ 47 S), southern Chile. *Andean Geology* 43.
- Stokes, C.R., Clark, C.D., 1999. Geomorphological criteria for identifying Pleistocene ice streams. *Annals of Glaciology* 28, 67-74.
- Stokes, C.R., Tarasov, L., 2010. Ice streaming in the Laurentide Ice Sheet: A first comparison between data-calibrated numerical model output and geological evidence. *Geophysical Research Letters* 37, L01501.
- Stokes, C.R., Tarasov, L., Blomdin, R., Cronin, T.M., Fisher, T.G., Gyllencreutz, R., Hättestrand, C., Heyman, J., Hindmarsh, R.C.A., Hughes, A.L.C., Jakobsson, M., Kirchner, N., Livingstone, S.J., Margold, M., Murton, J.B., Noormets, R., Peltier, W.R., Peteet, D.M., Piper, D.J.W., Preusser, F., Renssen, H., Roberts, D.H., Roche, D.M., Saint-Ange, F., Stroeve, A.P., Teller, J.T., 2015. On the reconstruction of palaeo-ice sheets: Recent advances and future challenges. *Quaternary Science Reviews* 125, 15-49.
- Stone, J.O., 2000. Air pressure and cosmogenic isotope production. *Journal of Geophysical Research* 105, 23753-23759.
- Strand, P. D., Schaefer, J. M., Putnam, A. E., Denton, G. H., Barrell, D. J. A., Koffman, T. N. B., & Schwartz, R. 2019. Millennial-scale pulsebeat of glaciation in the Southern Alps of New Zealand. *Quaternary Science Reviews*, 220, 165-177.

- Strelin, J., Casassa, G., Rosqvist, G., Holmlund, P., 2008. Holocene glaciations in the Elma glacier valley, Monte Sarmiento massif, Tierra del Fuego. *Palaeogeography, Palaeoclimatology, Palaeoecology* 260, 299-314.
- Strelin, J., Denton, G., Vandergoes, M., Ninnemann, U., Putnam, A., 2011. Radiocarbon chronology of the late-glacial Puerto Bandera moraines, southern Patagonian Icefield, Argentina. *Quaternary Science Reviews* 30, 2551-2569.
- Strelin, J.A., Kaplan, M.R., Vandergoes, M.J., Denton, G.H., Schaefer, J.M., 2014. Holocene glacier history of the Lago Argentino basin, southern Patagonian Icefield. *Quaternary Science Reviews* 101, 124-145.
- Strelin, J.A., Malagnino, E.C., 2000. Late-glacial history of Lago Argentino, Argentina, and age of the Puerto Bandera moraines. *Quaternary Research* 54, 339-347.
- Stuefer, M., Rott, H., Skvarca, P., 2007. Glacier Perito Moreno, Patagonia: climate sensitivities and glacier characteristics preceding the 2003/04 and 2005/06 damming events. *Journal of Glaciology* 53, 3-16.
- Stuiver, M., Reimer, P.J., Reimer, R.W., 2009. CALIB 5.0.1. Program and Documentation. <http://www.calib.qub.ac.uk/>.
- Sugden, D.E., Bentley, M.J., Fogwill, C.J., Hulton, N.R.J., McCulloch, R.D., Purves, R.S., 2005. Late-glacial glacier events in southernmost South America: a blend of 'Northern' and 'Southern' hemispheric climate signals? *Geografiska Annaler: Series A, Physical Geography* 87, 273-288.
- Syvitski, J.P.M., 1989. On the deposition of sediment within glacier-influenced fjords: oceanographic controls. *Marine Geology* 85, 301-329.
- Syvitski, J.P.M., Burrell, D.C., Skei, J.M., 1987. *Fjords: processes and products*. Springer Science & Business Media, Berlin.
- Tarasov, L., Dyke, A.S., Neal, R.M., Peltier, W., 2012. A data-calibrated distribution of deglacial chronologies for the North American ice complex from glaciological modeling. *Earth and Planetary Science Letters* 315, 30-40.
- Tatur, A., del Valle, R., Bianchi, M.-M., Outes, V., Villarosa, G., Niegodzisz, J., Debaene, G., 2002. Late Pleistocene palaeolakes in the Andean and Extra-Andean Patagonia at mid-latitudes of South America. *Quaternary International* 89, 135-150.
- Thorndycraft, V.R., Bendle, J.M., Benito, G., Davies, B.J., Sancho, C., Palmer, A.P., Fabel, D., Medialdea, A., Martin, J.R.V., 2019a. Glacial lake evolution and Atlantic-Pacific drainage reversals during deglaciation of the Patagonian Ice Sheet. *Quaternary Science Reviews* 203, 102-127.
- Thorndycraft, V.R., Bendle, J.M., Matthews, I.P., Palmer, A.P., Benito, G., Davies, B.J., Sancho, C., Pike, J.H., Martin, J.R.V., Fabel, D., 2019. Reply to comments by Bourgois et al. (2019) on: "Glacial lake evolution and Atlantic-Pacific drainage reversals during deglaciation of the Patagonia Ice Sheet". *Quaternary Science Reviews* 213, 171-177.
- Toggweiler, J.R., 2009. Shifting Westerlies. *Science* 323, 1434-1435.
- Tonello, M.S., Mancini, M.V., Seppä, H., 2009. Quantitative reconstruction of Holocene precipitation changes in southern Patagonia. *Quaternary Research* 72, 410-420.

- Turner, K., Fogwill, C., McCulloch, R., Sugden, D.E., 2005. Deglaciation of the eastern flank of the North Patagonian Icefield and associated continental-scale lake diversions. *Geografiska Annaler: Series A, Physical Geography* 87, 363-374.
- Tweed, F., 2011. Ice-Dammed Lakes, *Encyclopedia of Snow, Ice and Glaciers*. Springer, pp. 619-621.
- Uribe, P., 1982. Deglaciación en el sector central del Estrecho de Magallanes; consideraciones geomorfológicas y cronológicas, *Anales del Instituto de la Patagonia*. El Instituto, pp. 103-111.
- Van Daele, M., Bertrand, S., Meyer, I., Moernaut, J., Vandoorne, W., Siani, G., Tanghe, N., Ghazoui, Z., Pino, M., Urrutia, R., 2016. Late Quaternary evolution of Lago Castor (Chile, 45.6° S): Timing of the deglaciation in northern Patagonia and evolution of the southern westerlies during the last 17 kyr. *Quaternary Science Reviews* 133, 130-146.
- Vanneste, H., De Vleeschouwer, F., Martínez-Cortizas, A., von Scheffer, C., Piotrowska, N., Coronato, A., Le Roux, G., 2015. Late-glacial elevated dust deposition linked to westerly wind shifts in southern South America. *Scientific Reports* 5.
- Villa-Martínez, R., Moreno, P.I., Valenzuela, M.A., 2012. Deglacial and postglacial vegetation changes on the eastern slopes of the central Patagonian Andes (47°S). *Quaternary Science Reviews* 32, 86-99.
- Villagran, C., 1988. Late quaternary vegetation of southern Isla Grande de Chiloé, Chile. *Quaternary Research* 29, 294-306.
- Wais Divide Project Members, 2013. Onset of deglacial warming in West Antarctica driven by local orbital forcing. *Nature* 500, 440.
- Waldmann, N., Ariztegui, D., Anselmetti, F.S., Coronato, A., Austin Jr, J.A., 2010. Geophysical evidence of multiple glacier advances in Lago Fagnano (51°S), southernmost Patagonia. *Quaternary Science Reviews* 29, 1188-1200.
- Warren, C., Aniya, M., 1999. The calving glaciers of southern South America. *Global and Planetary Change* 22, 59-77.
- Warren, C.R., 1993. Rapid recent fluctuations of the calving San Rafael glacier, Chilean Patagonia: climatic or non-climatic? *Geografiska Annaler. Series A. Physical Geography*, 111-125.
- Warren, C.R., Glasser, N.F., Harrison, S., Winchester, V., Kerr, A.R., Rivera, A., 1995. Characteristics of tide-water calving at Glaciar San Rafael, Chile. *Journal of glaciology* 41, 273-289.
- Weller, D., Miranda, C., Moreno, P., Villa-Martínez, R., Stern, C., 2015. Tephrochronology of the southernmost Andean southern volcanic zone, Chile. *Bulletin of Volcanology* 77, 107.
- Weller, D.J., de Porras, M.E., Maldonado, A., Méndez, C., Stern, C.R., 2017. Holocene tephrochronology of the lower Río Cisnes valley, southern Chile. *Andean Geology* 44, 229-248.
- Wenzens, G., 1999. Fluctuations of outlet and valley glaciers in the Southern Andes (Argentina) during the past 13,000 years. *Quaternary Research* 51, 238-247.
- Wenzens, G., 2003. Comment on: 'The Last Glacial Maximum and deglaciation in southern South America': by NRJ Hulton, RS Purves, RD McCulloch, DE Sugden, MJ Bentley [*Quaternary Science Reviews* 21 (2002) 233–241]. *Quaternary science reviews* 22, 751-754.

- Wenzens, G., 2005. Glacier advances east of the Southern Andes between the Last Glacial Maximum and 5,000 BP compared with lake terraces of the endorheic Lago Cardiel (49°S, Patagonia, Argentina). *Zeitschrift für Geomorphologie*, NF, 433-454.
- Wenzens, G., 2006. Terminal Moraines, Outwash Plains, and Lake Terraces in the Vicinity of Lago Cardiel (49°S; Patagonia, Argentina)—Evidence for Miocene Andean Foreland Glaciations. *Arctic, Antarctic, and Alpine Research* 38, 276-291.
- Wilson, R., Glasser, N.F., Reynolds, J.M., Harrison, S., Anaconda, P.I., Schaefer, M., Shannon, S., 2018. Glacial lakes of the Central and Patagonian Andes. *Global and Planetary Change* 162, 275-291.
- Winchester, V., Harrison, S., 1996. Recent Oscillations of the San Quintin and San Rafael Glaciers, Patagonian Chile. *Geografiska Annaler: Series A, Physical Geography* 78, 35-49.
- Winchester, V., Harrison, S., 2000. Dendrochronology and lichenometry. Colonization, growth rates and dating of geomorphological events on the east side of the North Patagonian Icefield, Chile. *Geomorphology* 34, 181-194.
- Winchester, V., Harrison, S., Warren, C.R., 2001. Recent retreat Glacier Jof, Chilean Patagonia, dated by lichenometry and dendrochronology. *Arctic Antarctic and Alpine Research* 33, 266-273.
- Winchester, V., Sessions, M., Cerda, J.V., Wünderlich, O., Clemmens, S., Glasser, N.F., Nash, M., 2014. Post-1850 changes in Glacier Benito, North Patagonian Icefield, Chile. *Geografiska Annaler: Series A, Physical Geography* 96, 43-59.
- Winkelmann, R., Martin, M.A., Haseloff, M., Albrecht, T., Bueler, E., Khroulev, C., Levermann, A., 2011. The Potsdam Parallel Ice Sheet Model (PISM-PIK)—Part 1: Model description. *The Cryosphere* 5, 715-726.
- Wolff, I.W., Glasser, N.F., Hubbard, A., 2013. The reconstruction and climatic implication of an independent palaeo ice cap within the Andean rain shadow east of the former Patagonian ice sheet, Santa Cruz Province, Argentina. *Geomorphology* 185, 1-15.
- Zemp, M., Huss, M., Thibert, E., Eckert, N., McNabb, R., Huber, J., Barandun, M., Machguth, H., Nussbaumer, S.U., Gärtner-Roer, I., 2019. Global glacier mass changes and their contributions to sea-level rise from 1961 to 2016. *Nature* 568, 382-386.



Royal Holloway  
University of London  
Egham, Surrey  
TW20 0EX

**Dr Bethan Davies**

**BA (Hons) MSc PhD FRGS FHEA**

**Senior Lecturer in Physical  
Geography**

Department of Geography

+44 (0)1784 414 682

Bethan.davies@rhul.ac.uk

[www.royalholloway.ac.uk](http://www.royalholloway.ac.uk)

**Professer Negri**

**Editor, Earth-Science Reviews**

**Thursday, 12 March 2020**

Dear Prof. Negri,

The authors declare no conflicts of interest.

Yours sincerely,

A handwritten signature in cursive script that reads 'Bethan Davies'.

Dr Bethan Davies



Royal Holloway  
University of London  
Egham, Surrey  
TW20 0EX

**Dr Bethan Davies**

**BA (Hons) MSc PhD FRGS FHEA**

**Senior Lecturer in Physical  
Geography**

Department of Geography

+44 (0)1784 414 682

Bethan.davies@rhul.ac.uk

[www.royalholloway.ac.uk](http://www.royalholloway.ac.uk)

**Professor Negri**

**Editor, Earth-Science Reviews**

**Thursday, 12 March 2020**

Dear Prof. Negri,

This author statement file outlines all authors individual contributions.

All authors contributed to writing and reviewing and editing the manuscript.

Bethan Davies: Conceptualisation; Data curation; Formal analysis; Methodology; Roles/Writing – original draft; Writing – review and editing.

Christopher Darvill: Data curation; Formal analysis; Methodology; Roles/Writing – original draft; Writing – review and editing.

Harold Lovell: Data curation; Formal analysis; Methodology; Roles/Writing – original draft; Writing – review and editing.

Jacob Bendle: Data curation; Formal analysis; Methodology; Roles/Writing – original draft; Writing – review and editing.

Julian Dowdeswell: Data curation; Formal analysis; Methodology; Roles/Writing – original draft; Writing – review and editing.

Derek Fabel: Data curation; Formal analysis; Methodology; Roles/Writing – original draft; Writing – review and editing.

Juan-Luis García: Data curation; Formal analysis; Methodology; Roles/Writing – original draft; Writing – review and editing.

Alessa Geiger: Data curation; Formal analysis; Methodology; Roles/Writing – original draft; Writing – review and editing.

Neil Glasser: Data curation; Formal analysis; Methodology; Roles/Writing – original draft; Writing – review and editing.

Delia Gheorghiu: Data curation; Formal analysis; Methodology; Roles/Writing – original draft; Writing – review and editing.

Stephan Harrison: Data curation; Formal analysis; Methodology; Role: /Writing – original draft; Writing – review and editing.

Andrew Hein: Data curation; Formal analysis; Methodology; Role: /Writing – original draft; Writing – review and editing.

Michael Kaplan: Data curation; Formal analysis; Methodology; Roles/Writing – original draft; Writing – review and editing.

Julian Martin: Data curation; Formal analysis; Methodology; Roles/Writing – original draft; Writing – review and editing.

Monika Mendelova: Data curation; Formal analysis; Methodology; Roles/Writing – original draft; Writing – review and editing.

Adrian Palmer: Data curation; Formal analysis; Methodology; Roles/Writing – original draft; Writing – review and editing.

Mauri Pelto: Data curation; Formal analysis; Methodology; Roles/Writing – original draft; Writing – review and editing.

Ángel Rodés: Data curation; Formal analysis; Methodology; Roles/Writing – original draft; Writing – review and editing.

Esteban Sagredo: Data curation; Formal analysis; Methodology; Roles/Writing – original draft; Writing – review and editing.

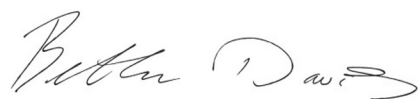
Rachel Smedley: Data curation; Formal analysis; Methodology; Roles/Writing – original draft; Writing – review and editing.

John Smellie: Data curation; Formal analysis; Methodology; Roles/Writing – original draft; Writing – review and editing.

Varyl Thorndycraft: Data curation; Formal analysis; Methodology; Roles/Writing – original draft; Writing – review and editing.



Yours sincerely,

A handwritten signature in black ink, appearing to read 'Bethan Davies'.

Dr Bethan Davies

Journal Pre-proof

## Sedimentary rocks

Quaternary	Q
Tertiary	T
Cretaceous	K
Jurassic-Cretaceous	JK
Jurassic	J
Triassic	Tr
Carboniferous-Permian	CP
Precambrian-Palaeozoic	APZ
Palaeozoic	PZ

## Igneous and Metamorphic rocks

Quaternary volcanics	Qv
Cretaceous-Tertiary volcanics	Cv
Mesozoic volcanics	Mv
Permian volcanics	Pv
Palaeozoic volcanics	PZv
Mesozoic-Cenozoic intrusives	MCI
Palaeozoic-Mesozoic intrusives	PMI
Mesozoic metamorphics	Mv
Palaeozoic metamorphics	PZv
Precambrian undifferentiated	pC

## Other units

Unmapped area	
Volcanoes	▲
Glacier ice	■
Lake	■
River	—
500 m bathymetric contours	—

## Tectonic structures

Plate boundary	—
Subduction plate boundary	—
Plate movement	→

## Faults

Fault	---
Fold	—
Slip	—

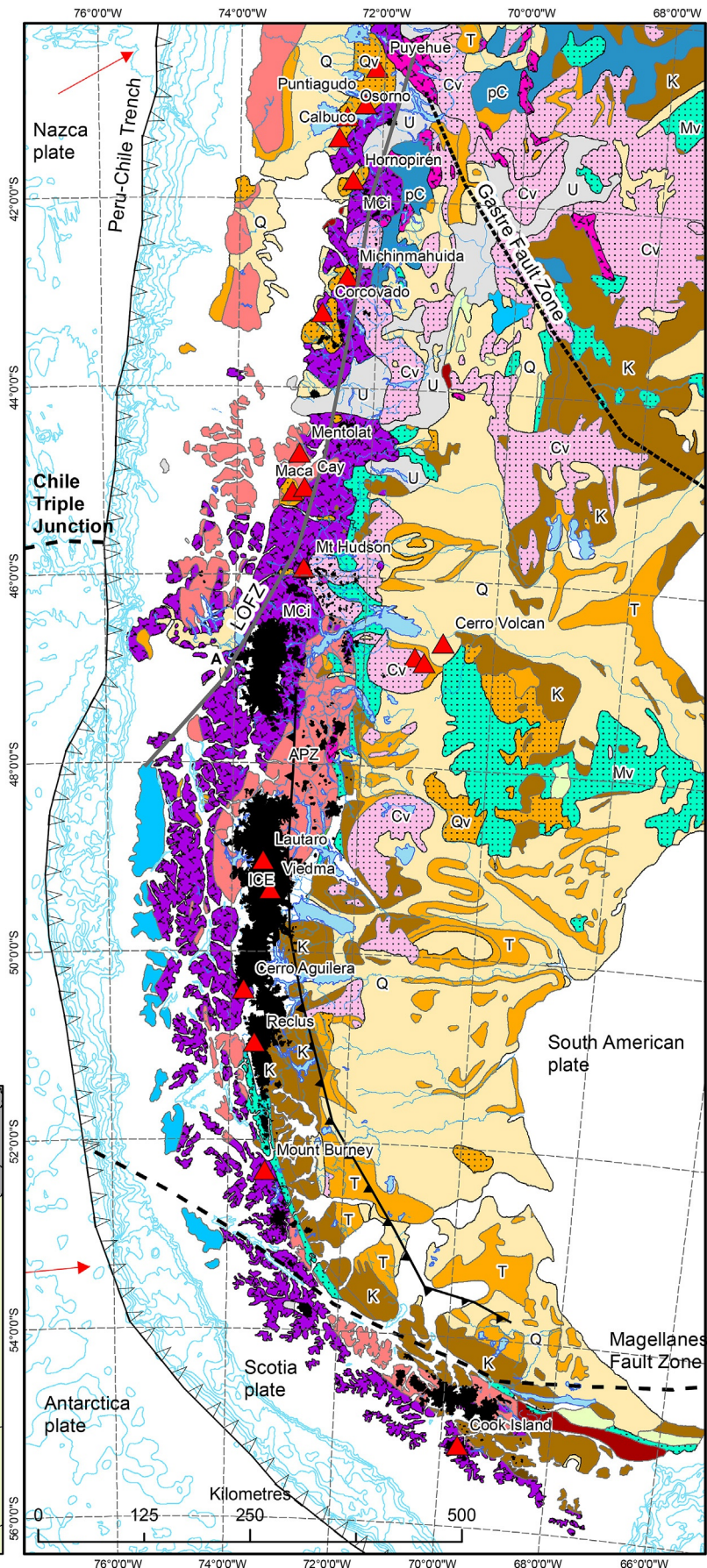


Figure 1



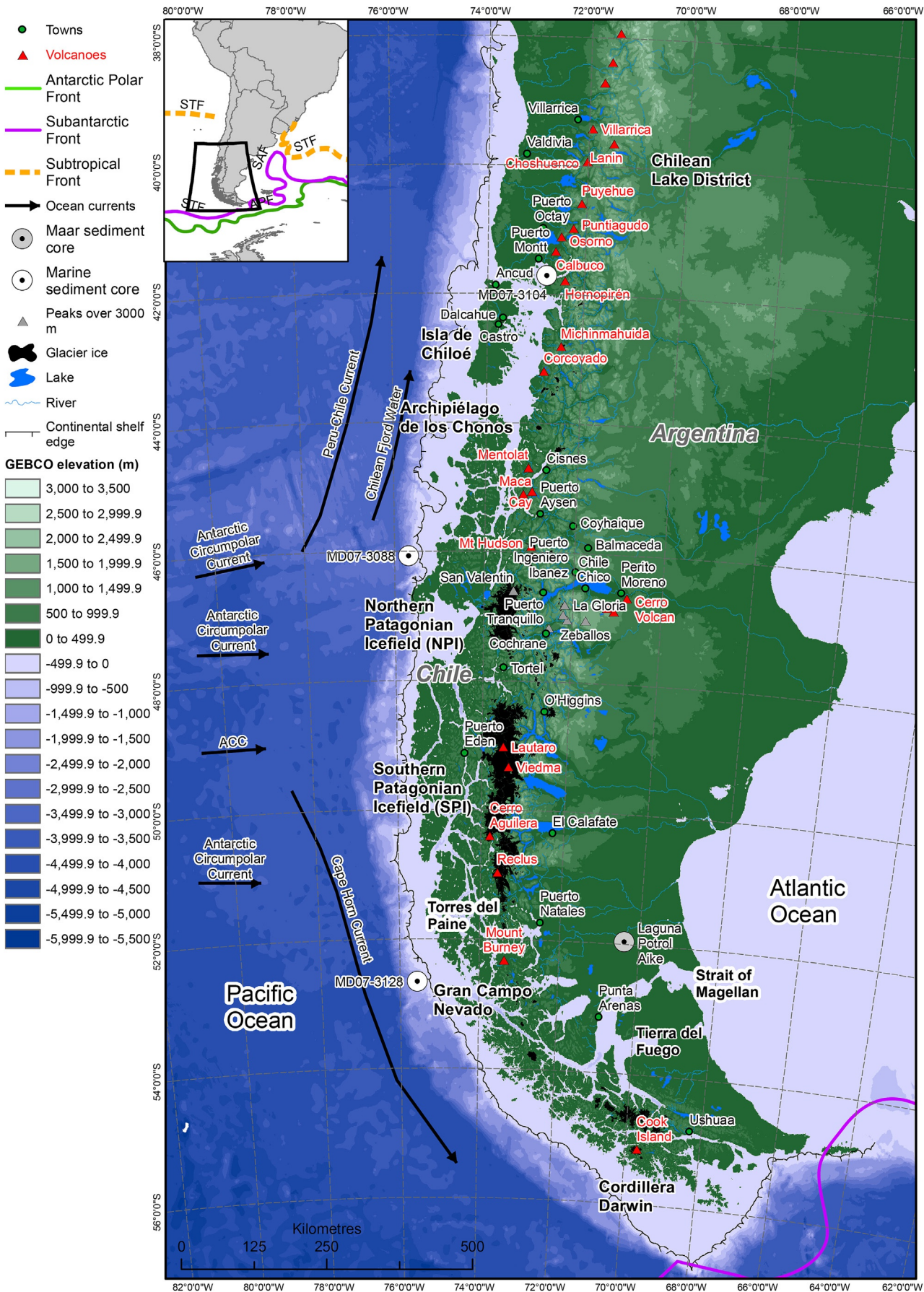


Figure 2



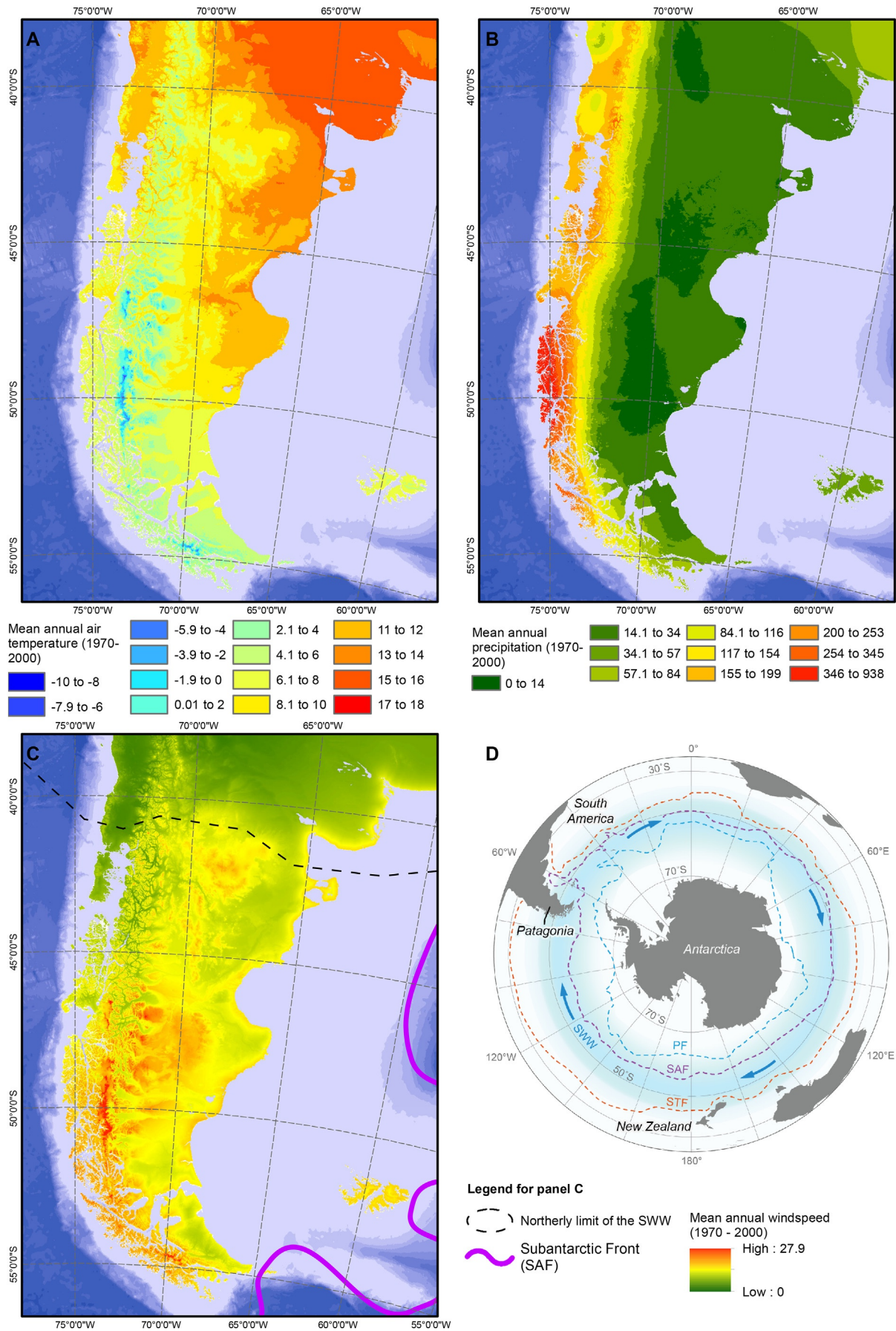


Figure 3

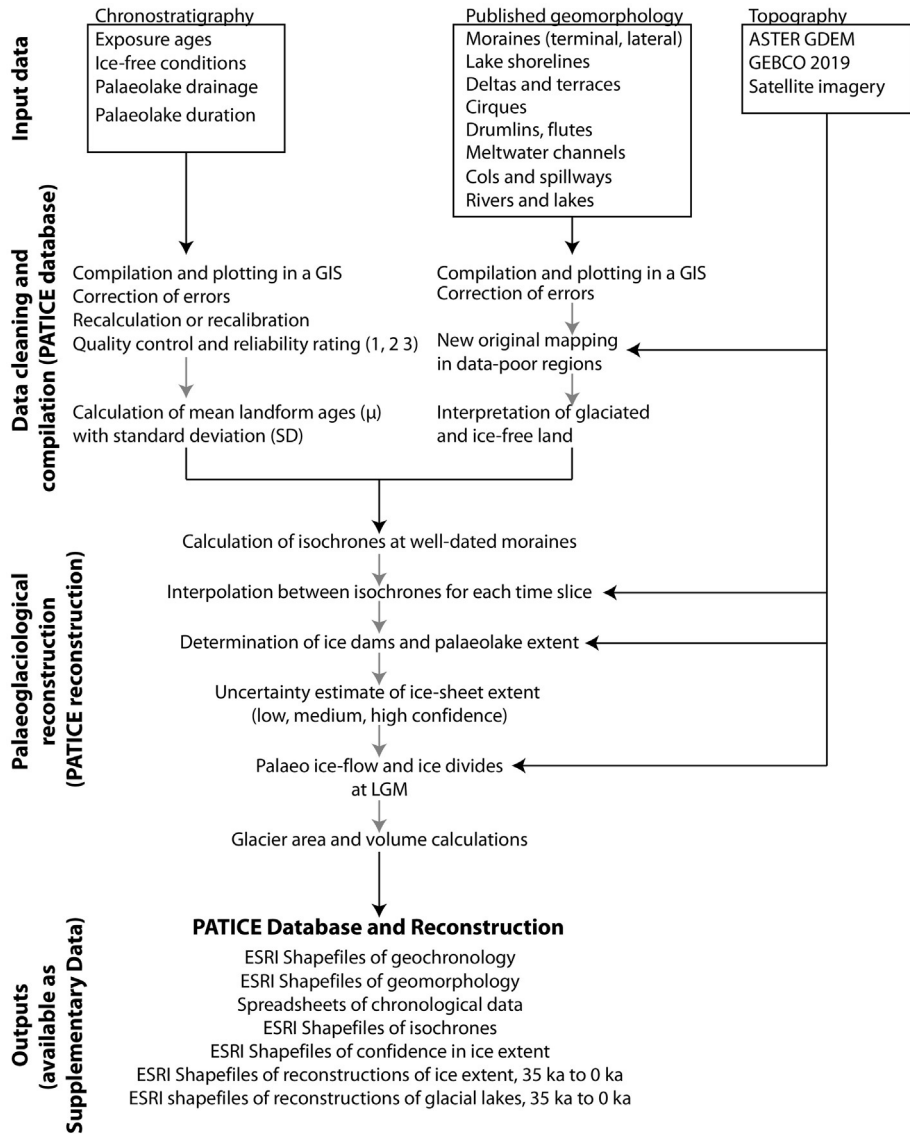


Figure 4



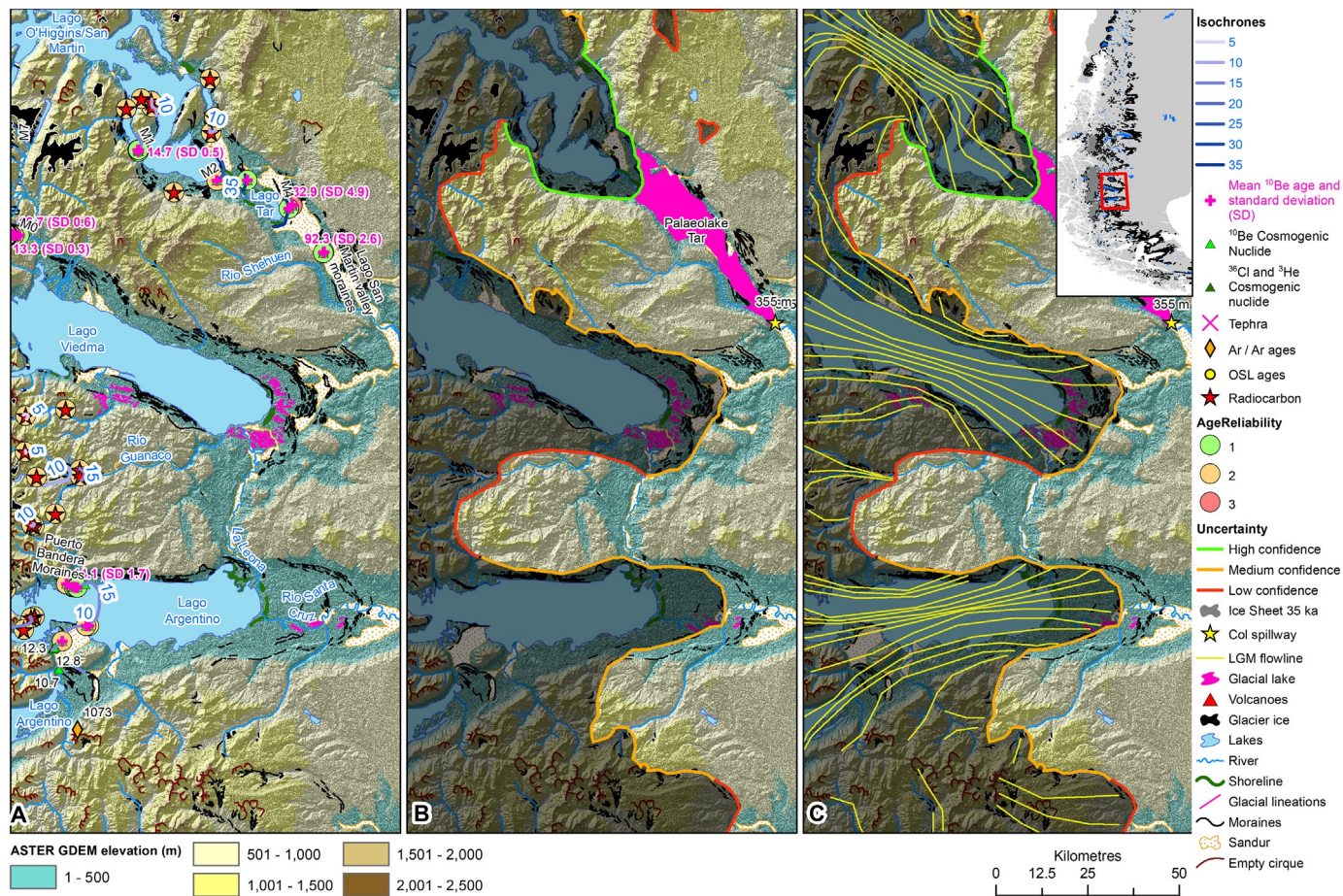


Figure 5

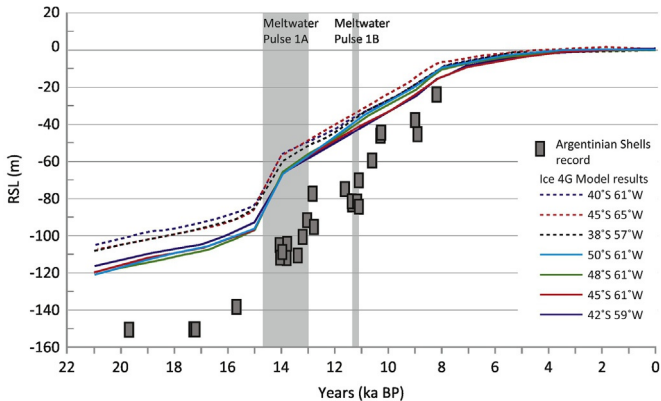


Figure 6



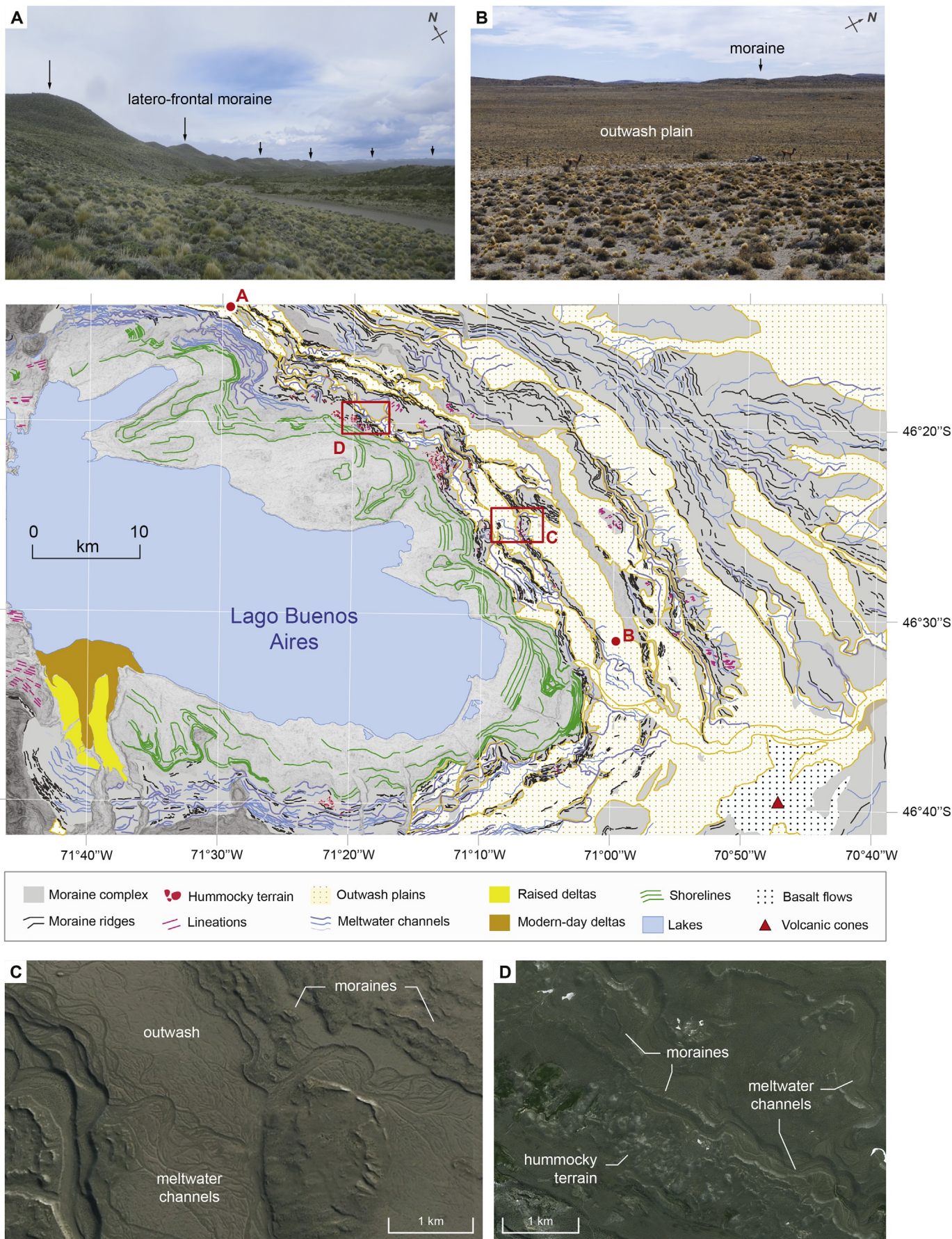


Figure 7



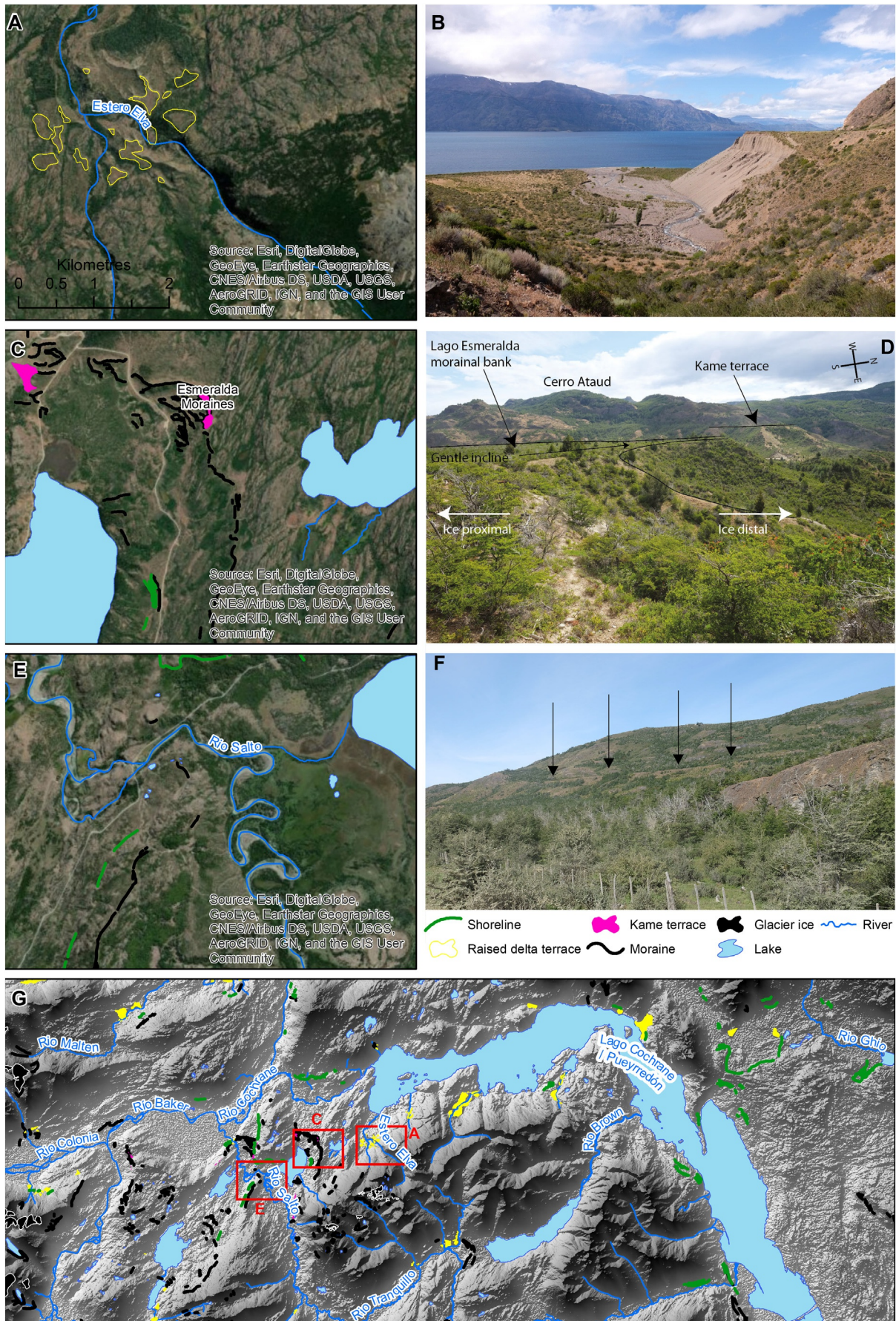
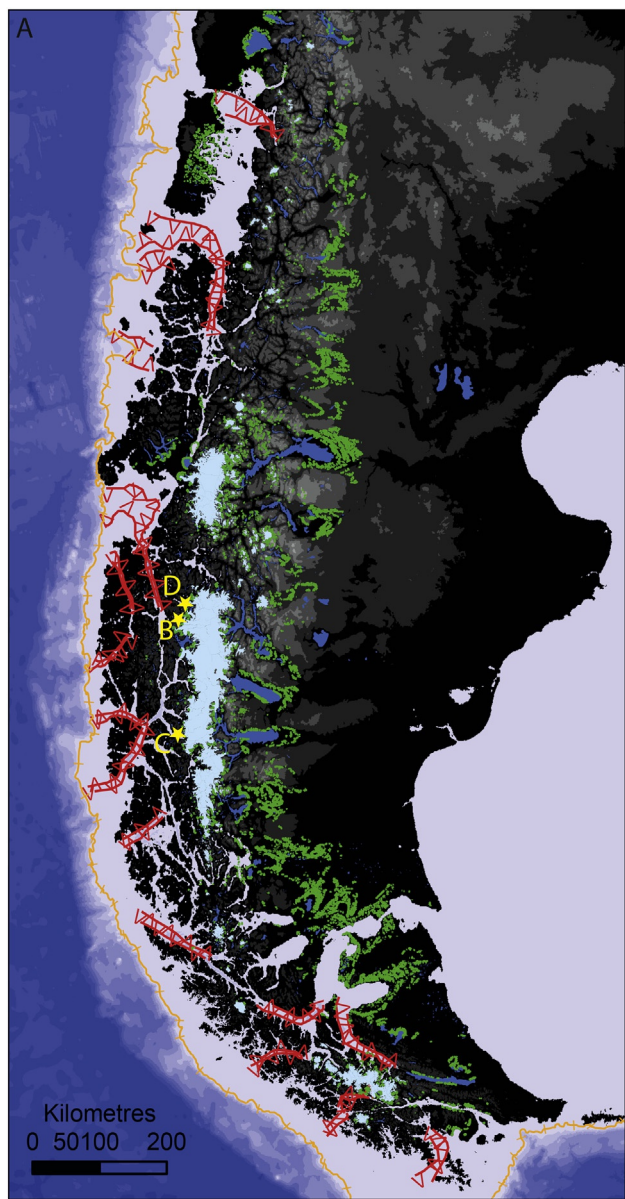


Figure 8





**GEBCO elevation (m)**

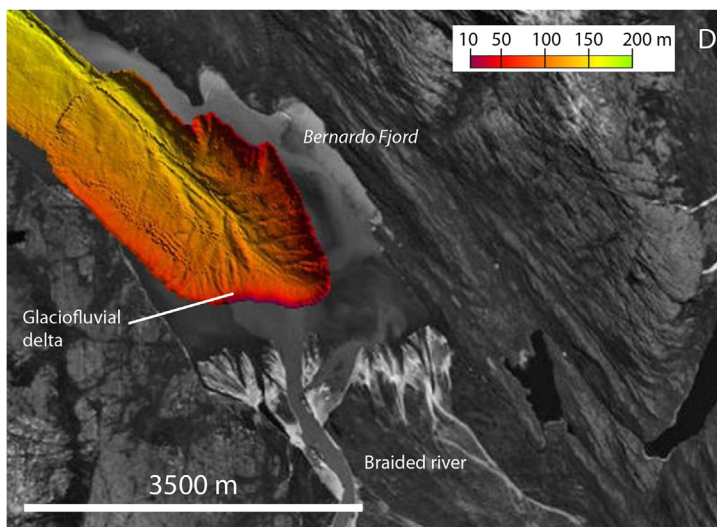
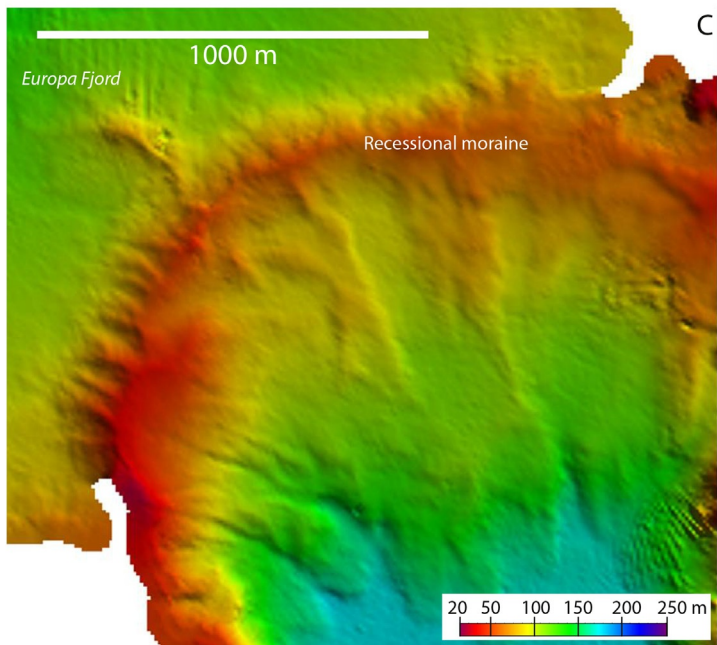
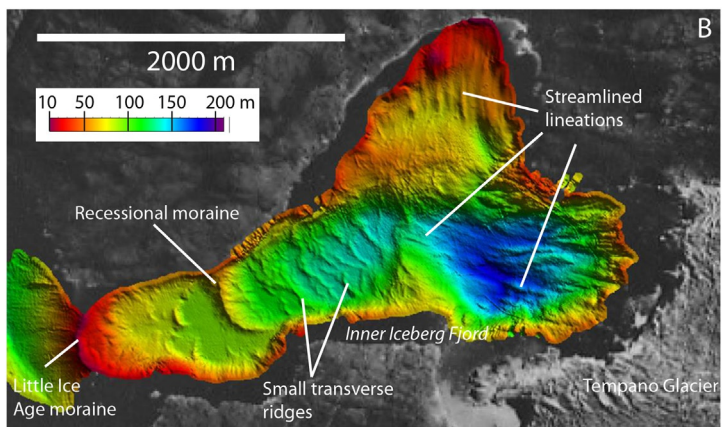
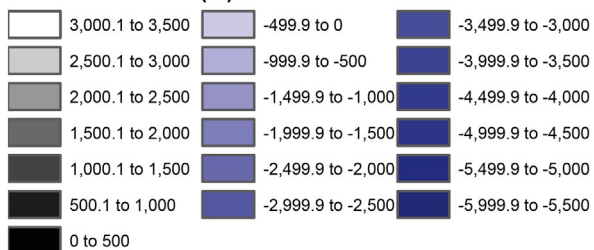


Figure 9



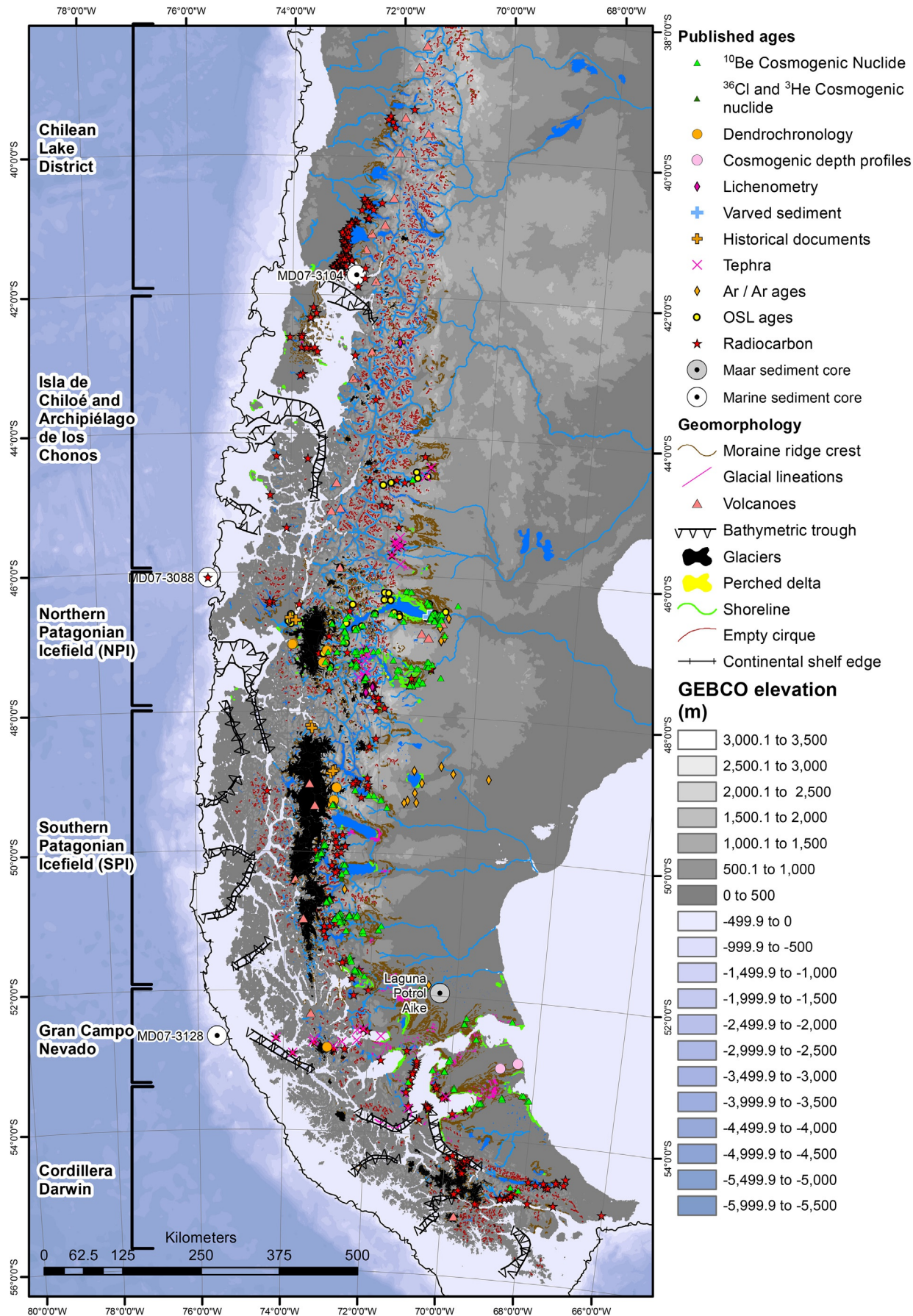


Figure 10



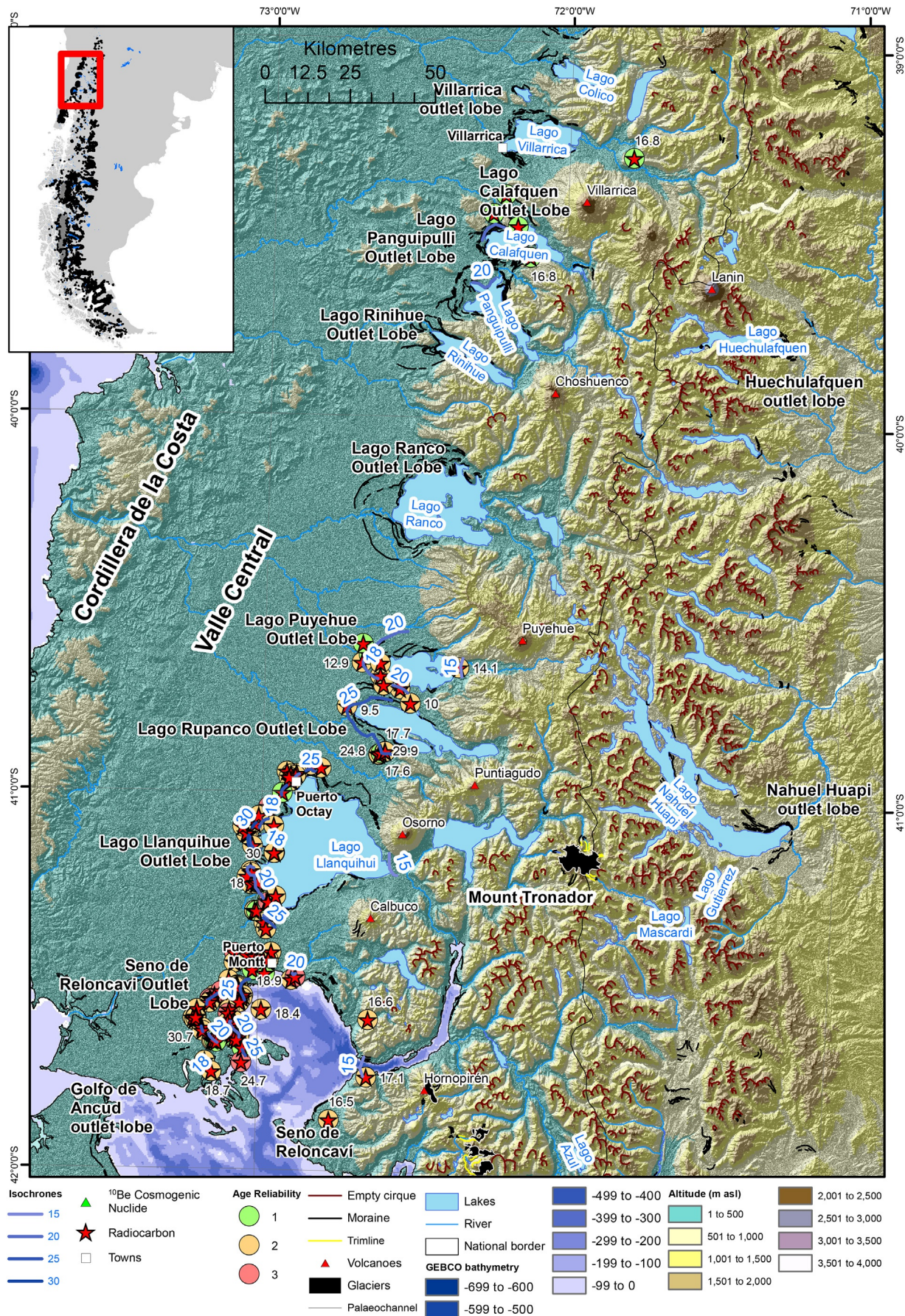
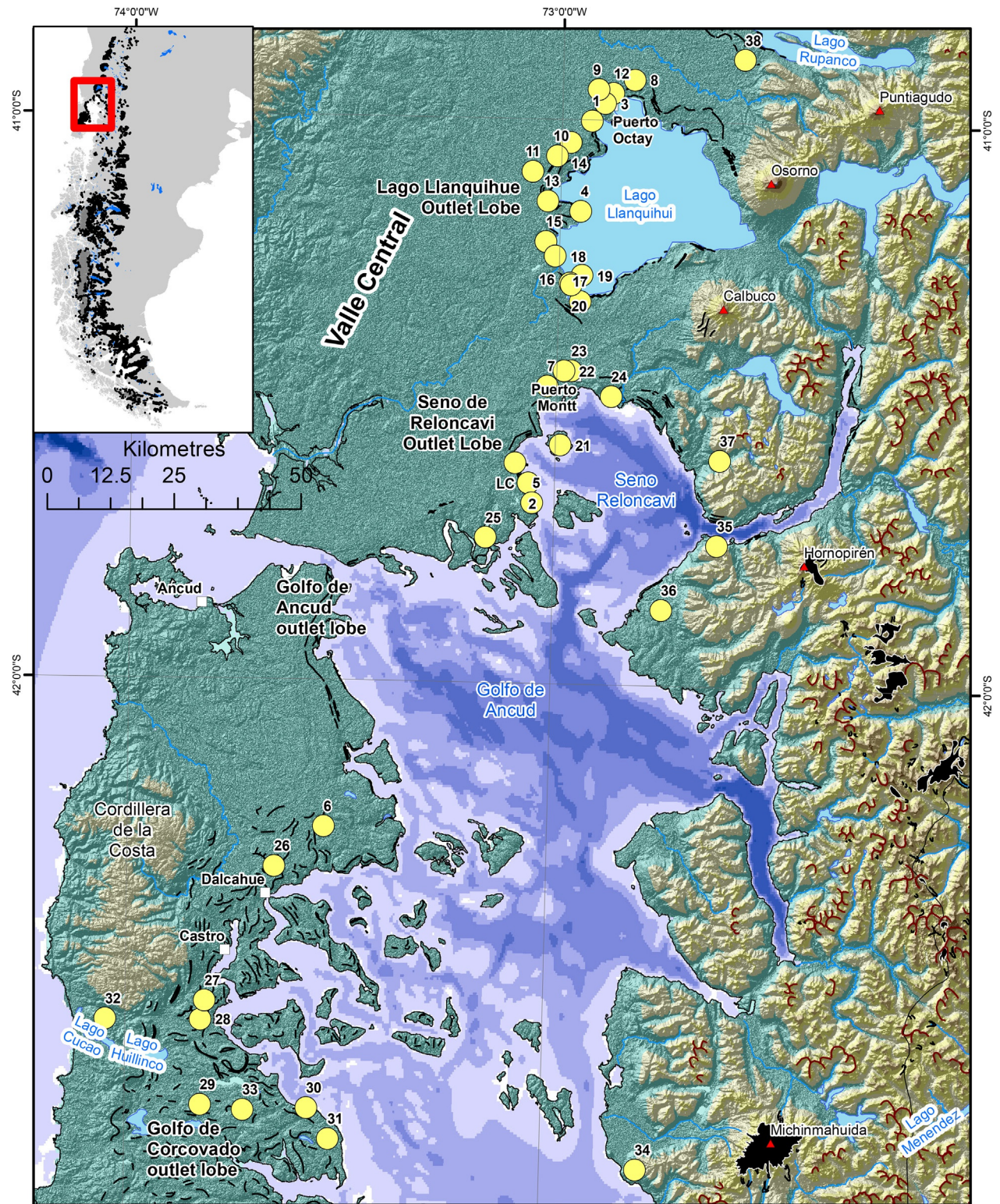


Figure 11





Number	Name	Number	Name	Number	Name	Number	Name
1	Canal de la Puntilla	11	Frutilla Alto	21	Isla Maillen	30	Lago Tahui
2	Huelmo	12	Canal de Chanchan	22	No name	31	Lago Melli
3	Puerto Octay	13	No Name	23	Lago Lepue	32	Lago Taruman
4	Bahia Frutilla Bajo	14	Fundo Linea Pantanosa	24	Punta Penas, upper	33	Lago Lepue
5	Seno Reloncavi, top of organic bed	15	Fundo Llanquihue	25	Near Calbuco, reworked clast in till	34	Chaiten, base of organic bed
6	Teguaco, top of organic bed	16	Puerto Varas Railroad Bridge, lower	26	Dalcahue, top of organic bed	35	Caleta Puelche, base of organic bed
7	Puerto Montt	17	Bella Vista Bluff	27	Mayol	36	Lago Proschle
8	Organic clast reworked into Llanquihue outwash	18	Ulanquihue	28	Esteri Huitanque	37	Lago Reflejos
9	Organic clast reworked into Llanquihue outwash	19	Northwest Bluff	29	Unnamed bog	38	Lago Bonita
10	Organic clast reworked into Llanquihue outwash	20	Calla Santa Rosa, Puerto Varas			LC	Lago Condorito

Figure 12



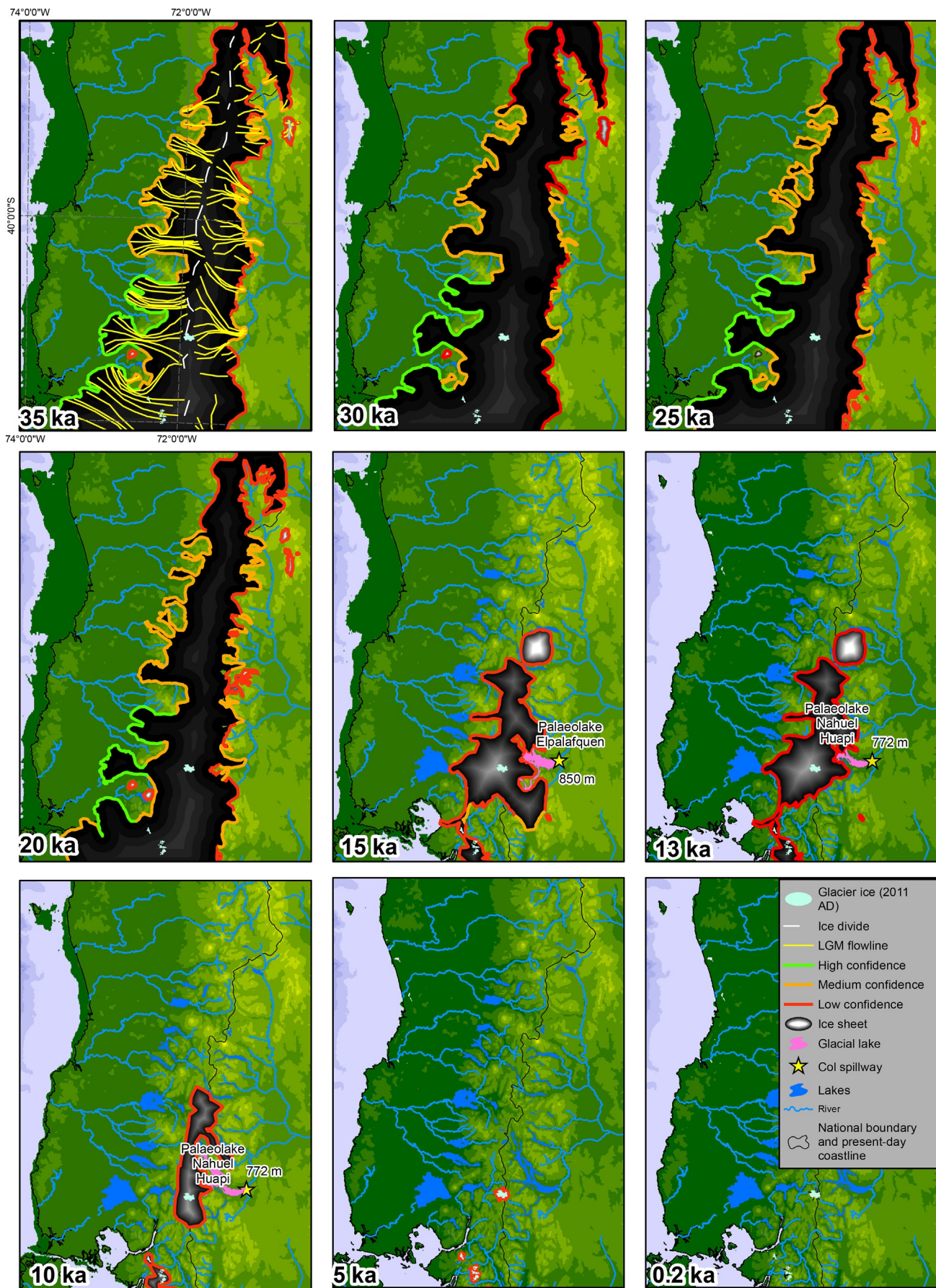


Figure 13



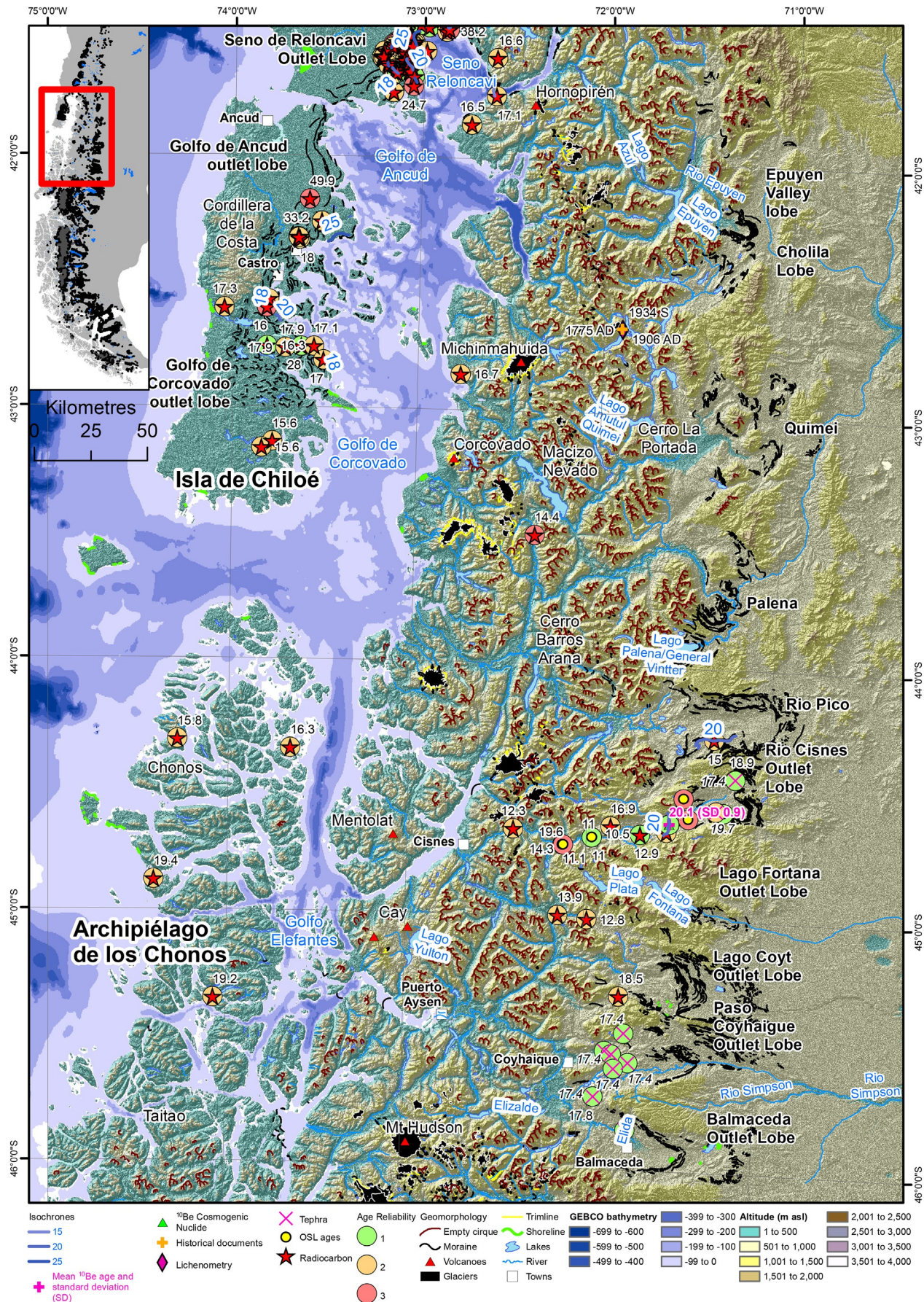


Figure 14



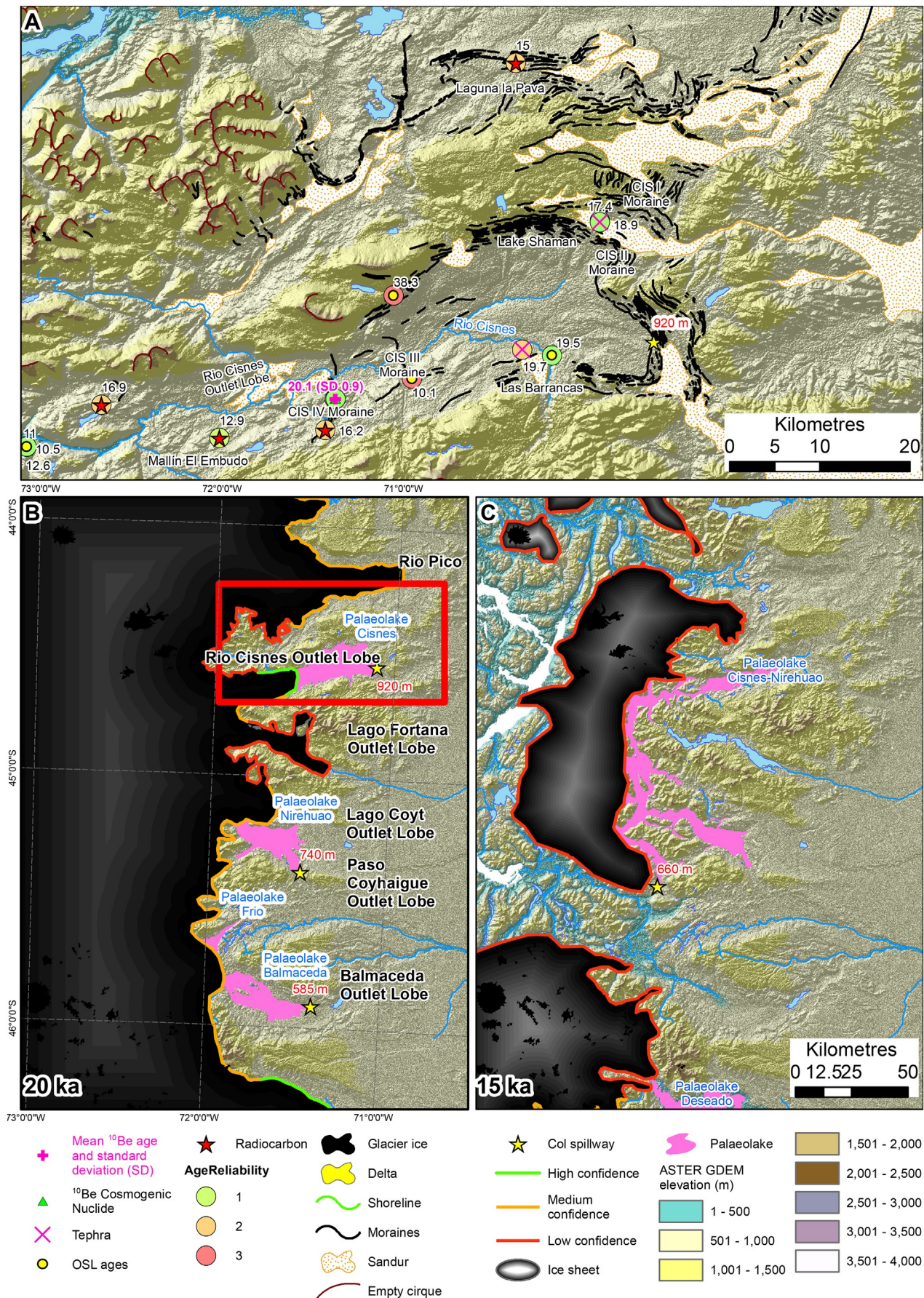


Figure 15



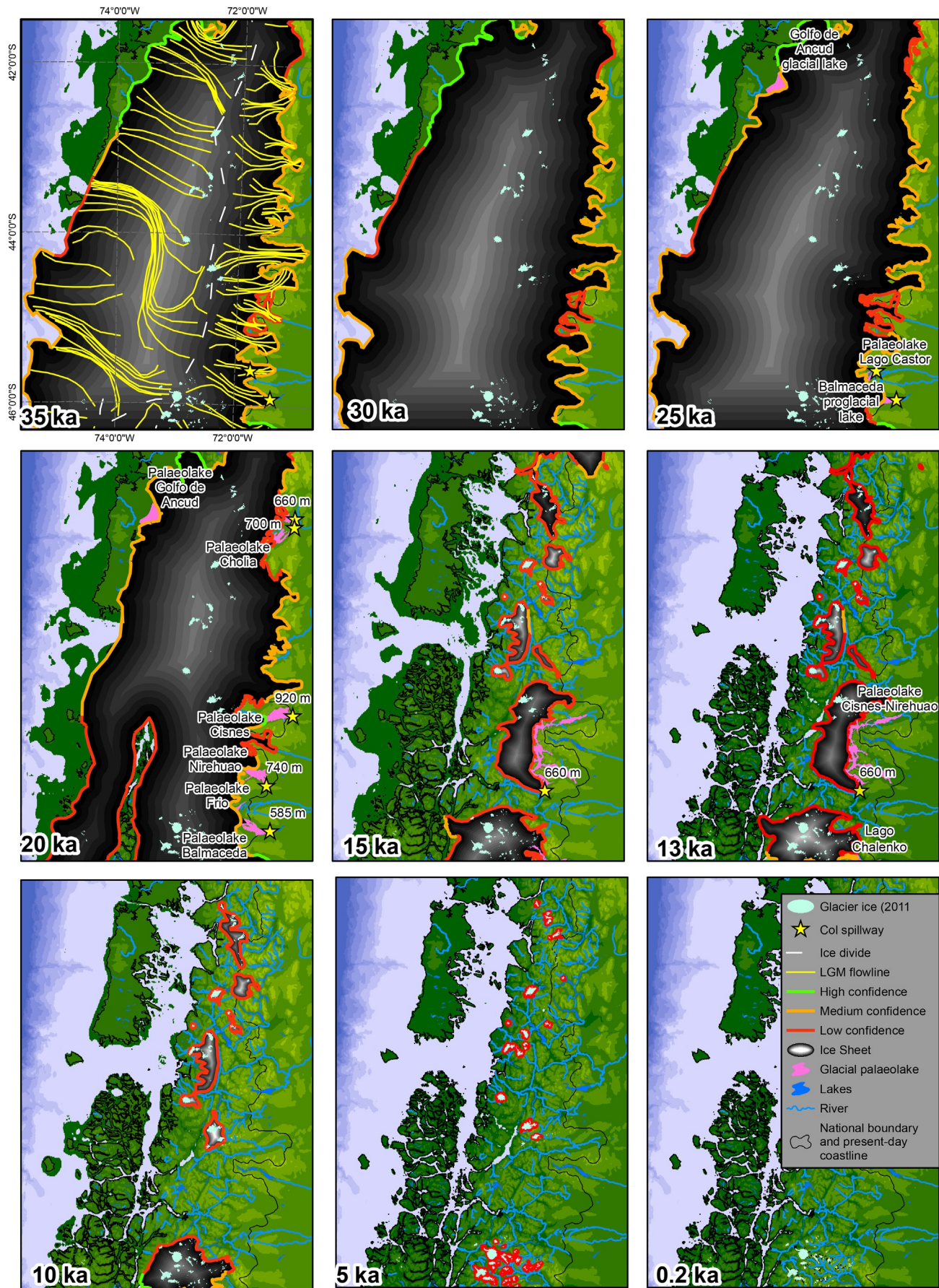


Figure 16



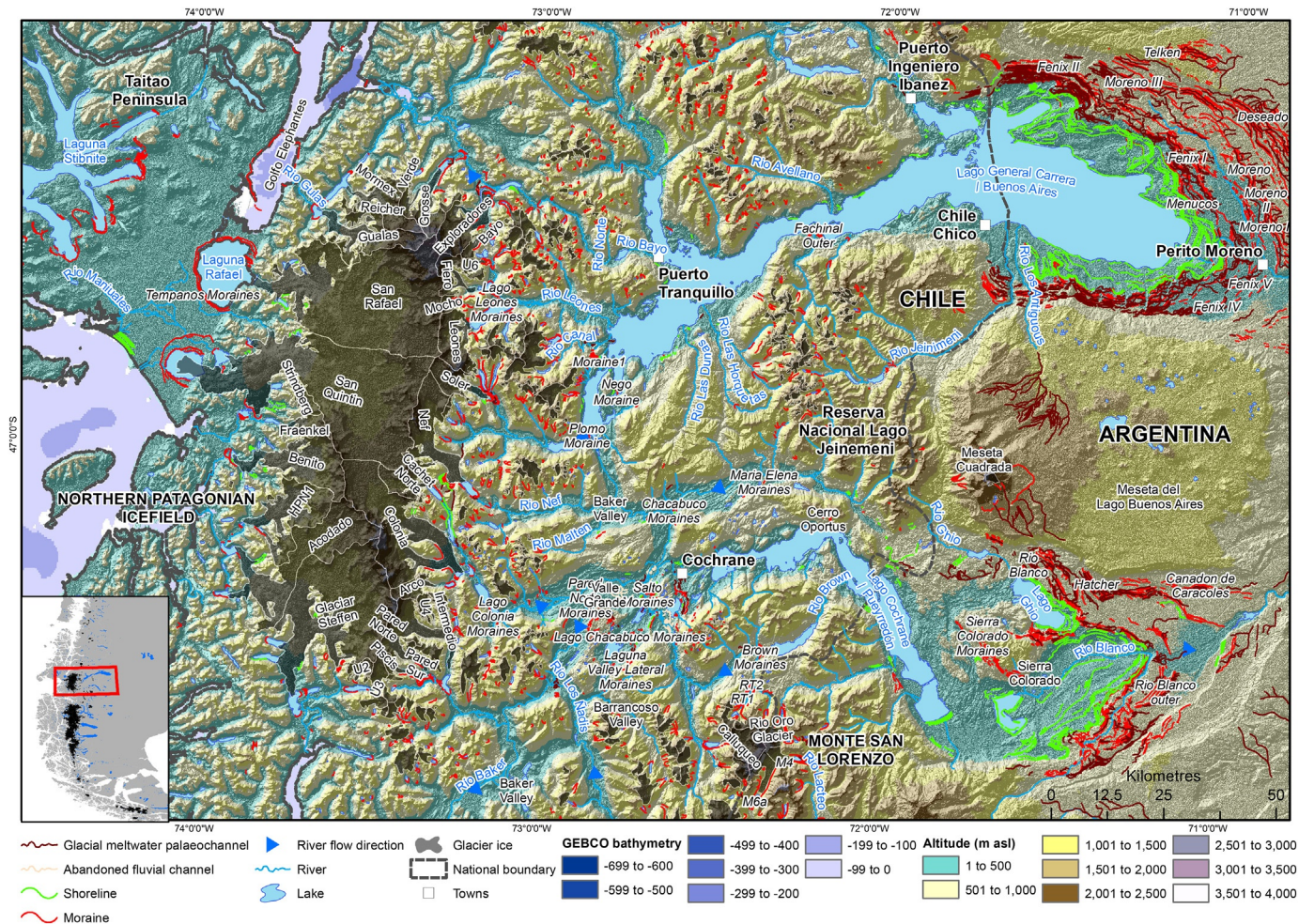


Figure 17



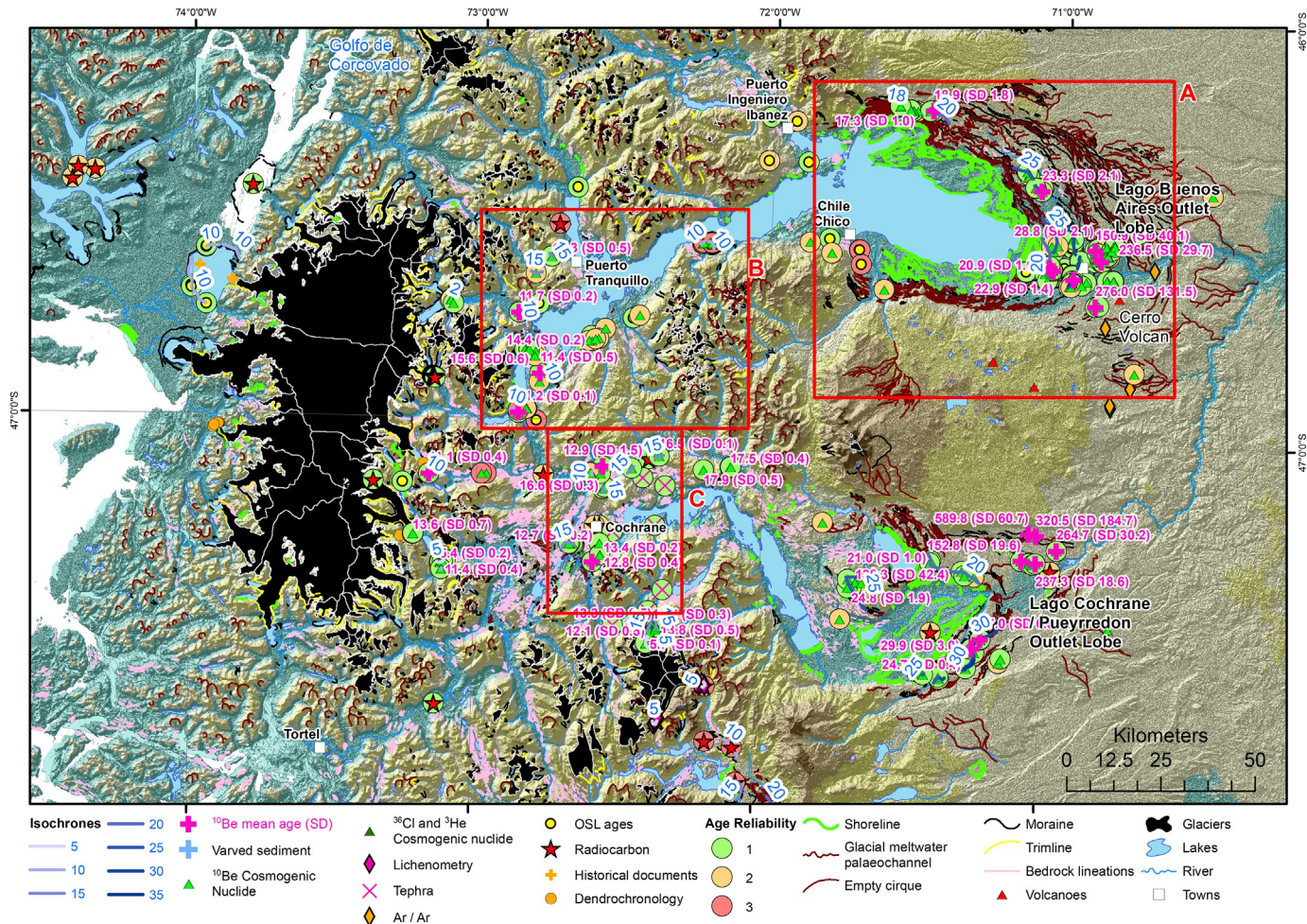


Figure 18



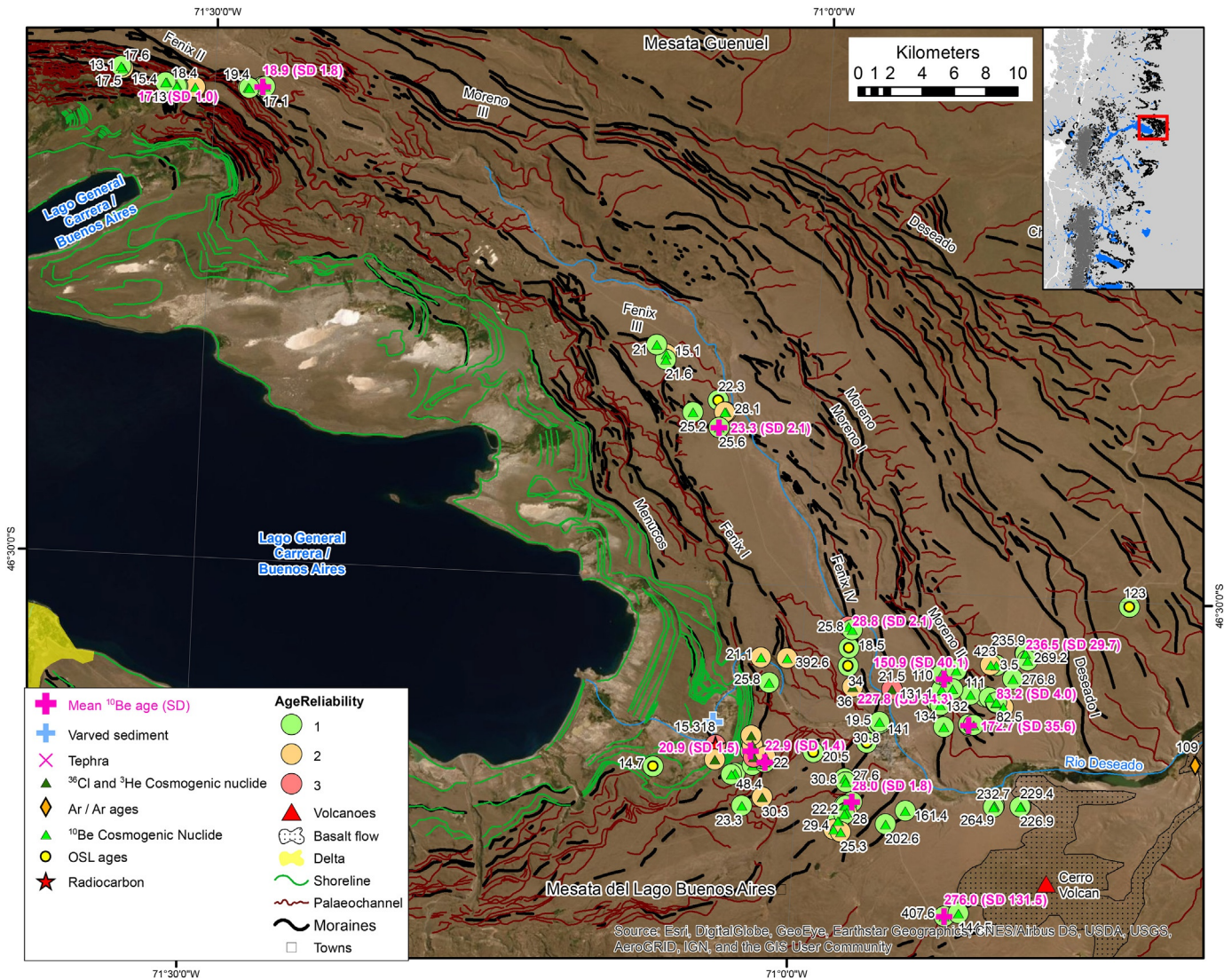


Figure 19



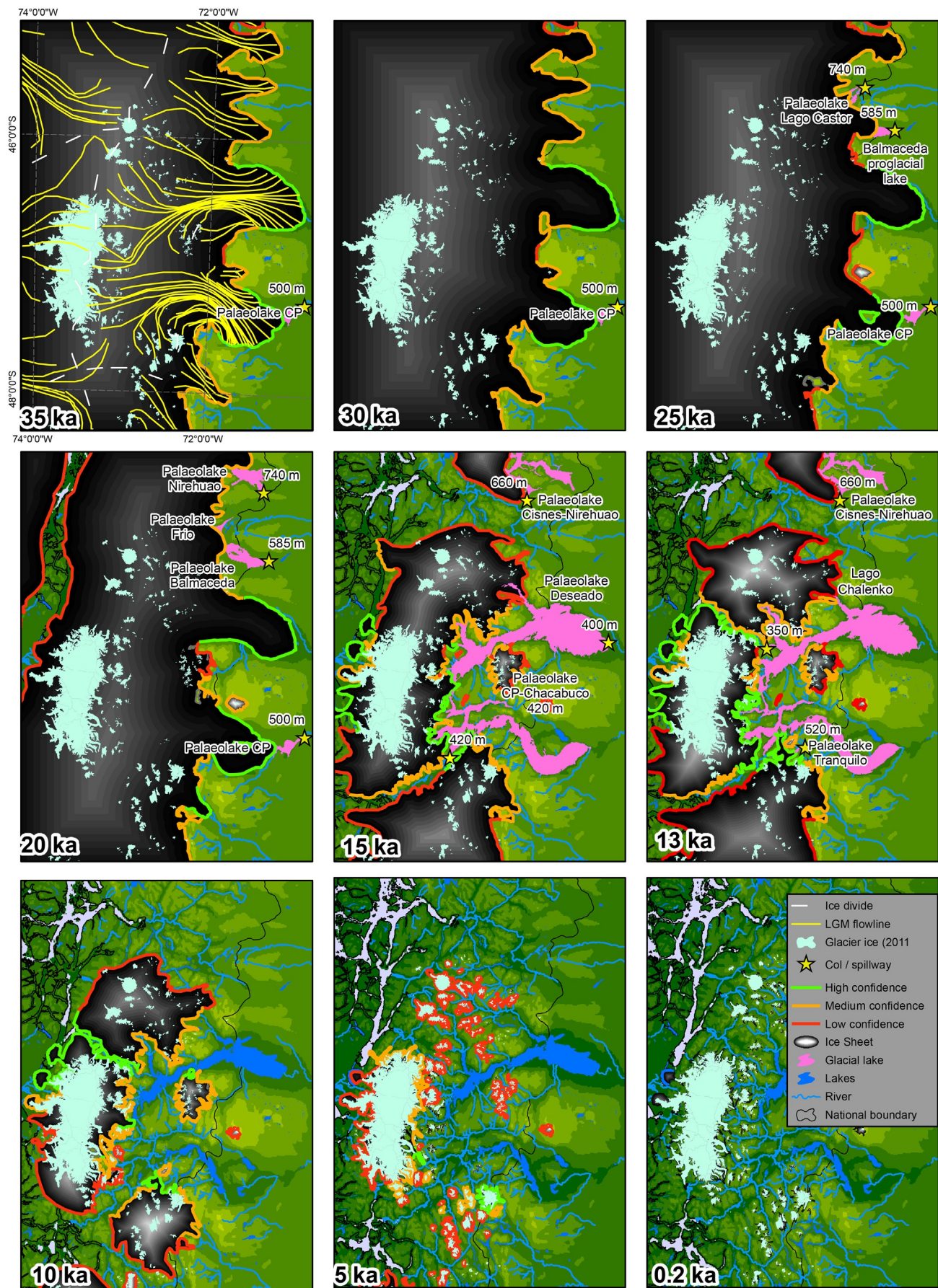


Figure 20







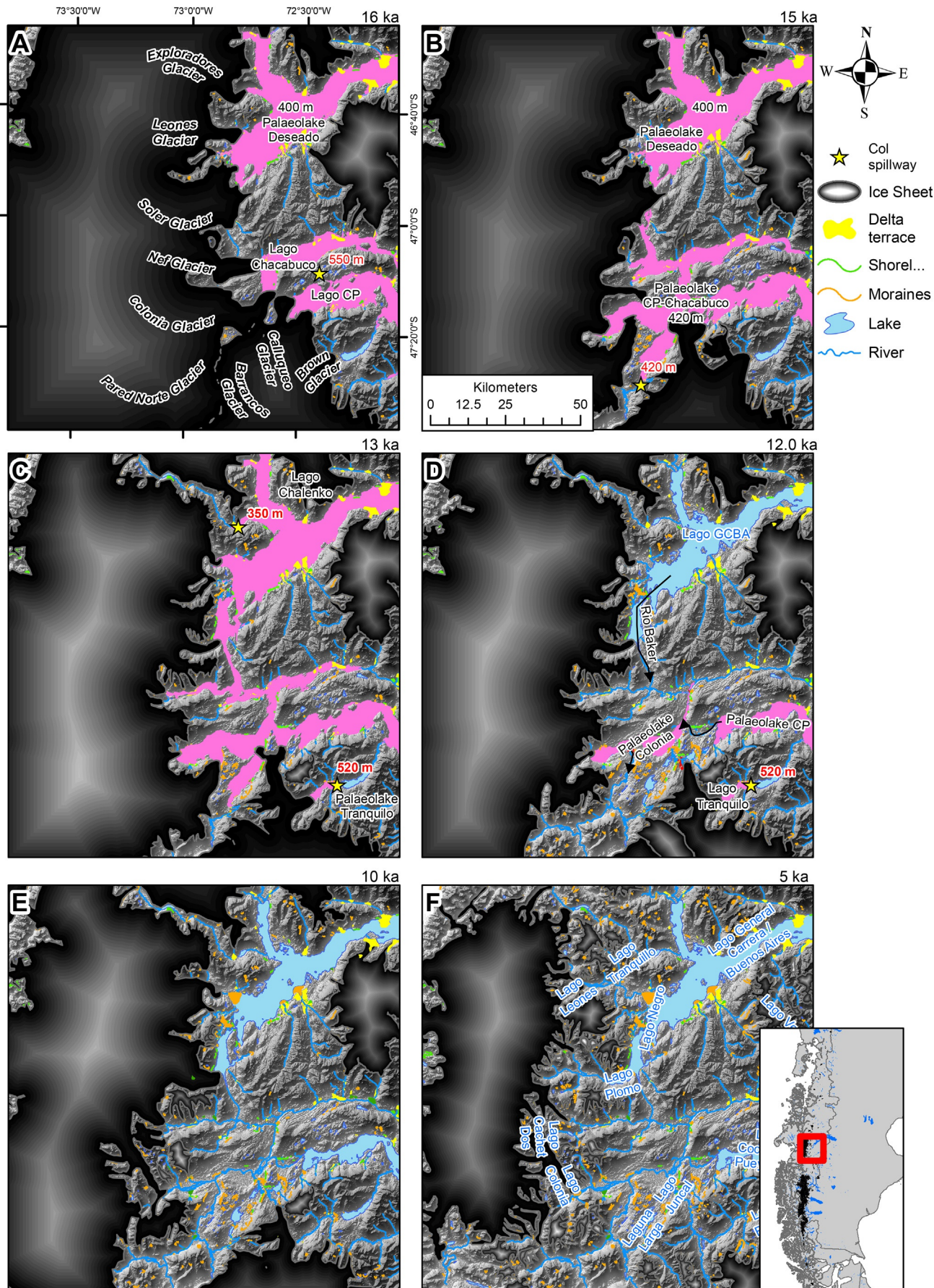


Figure 22



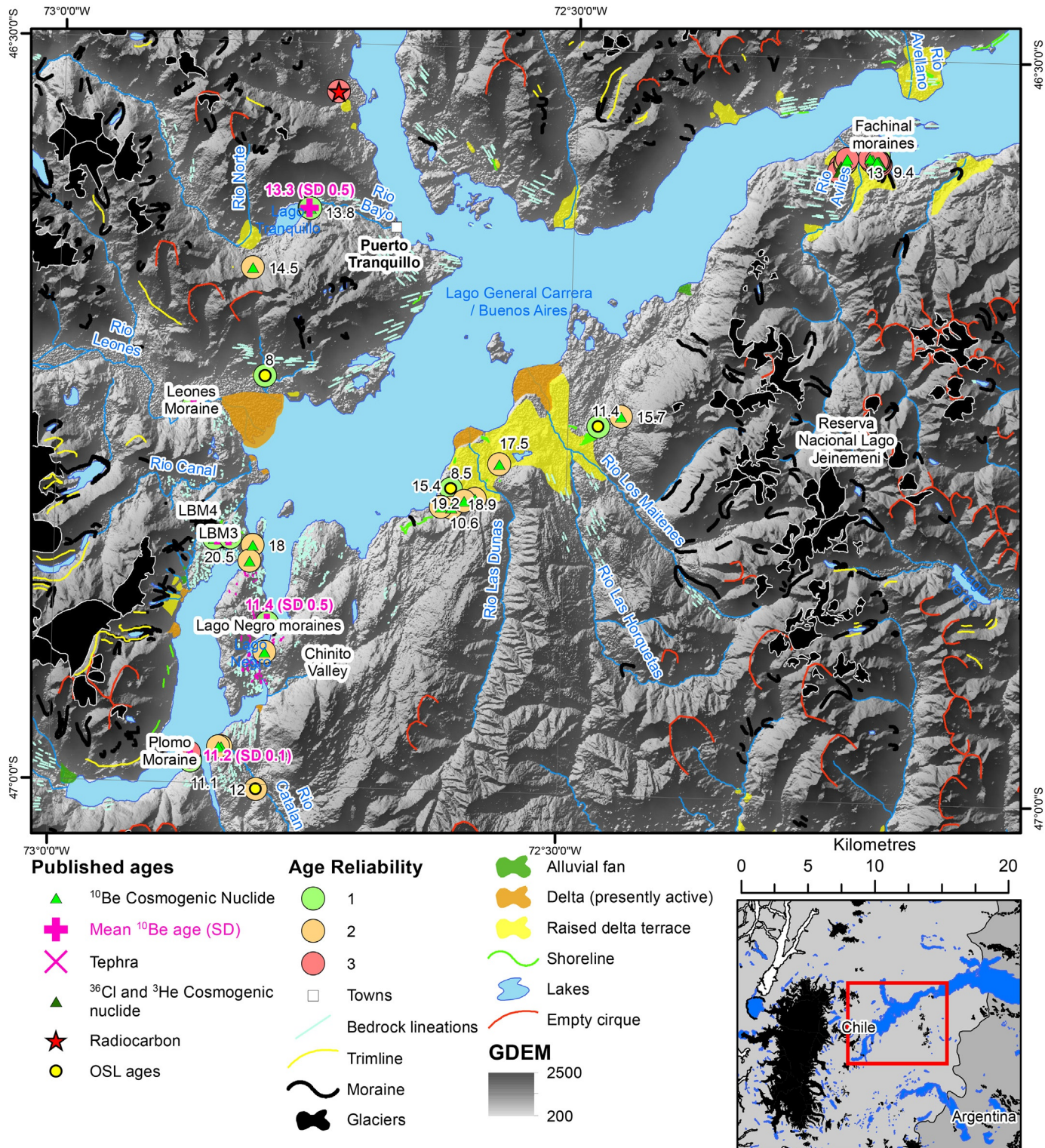


Figure 23



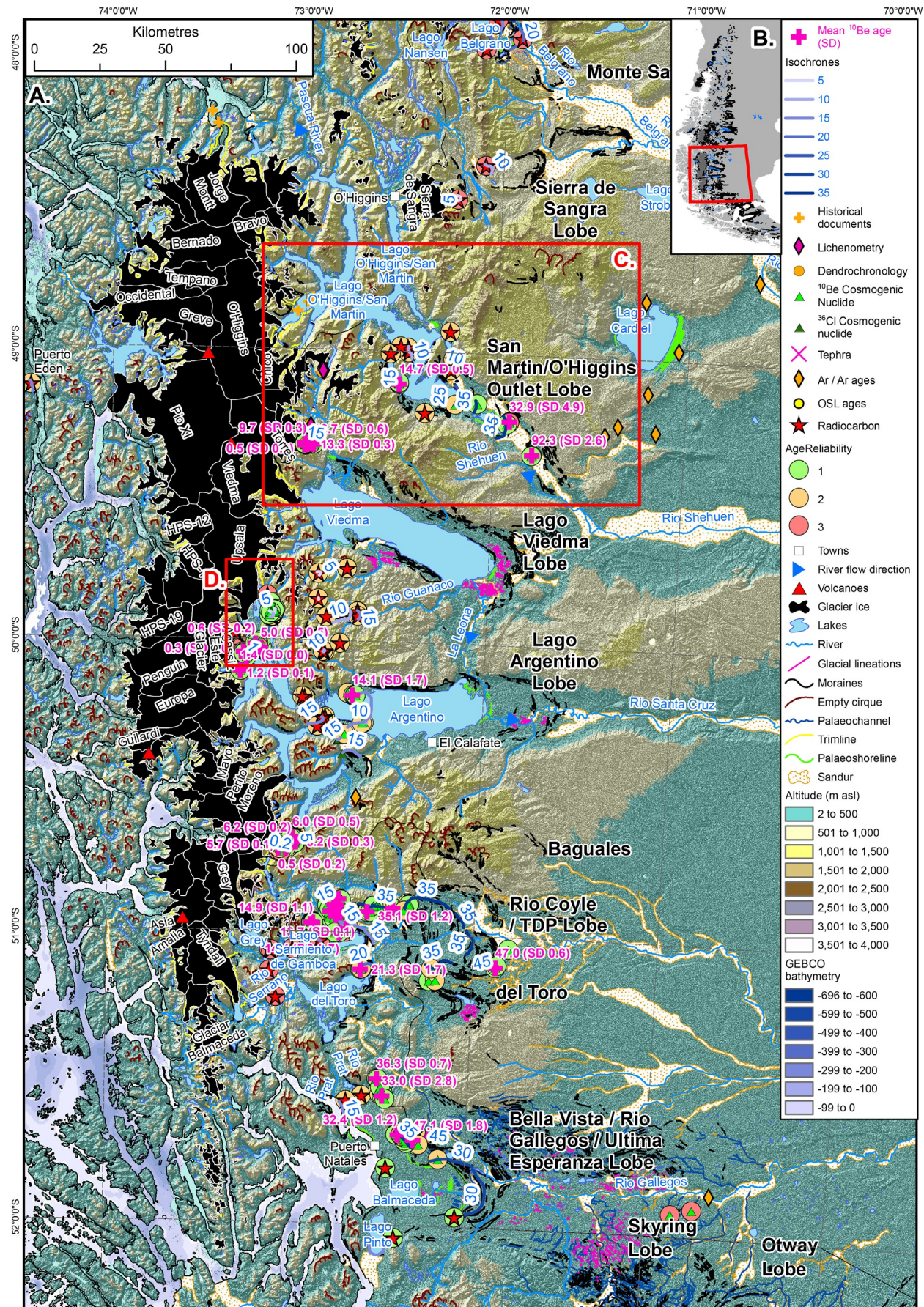


Figure 24



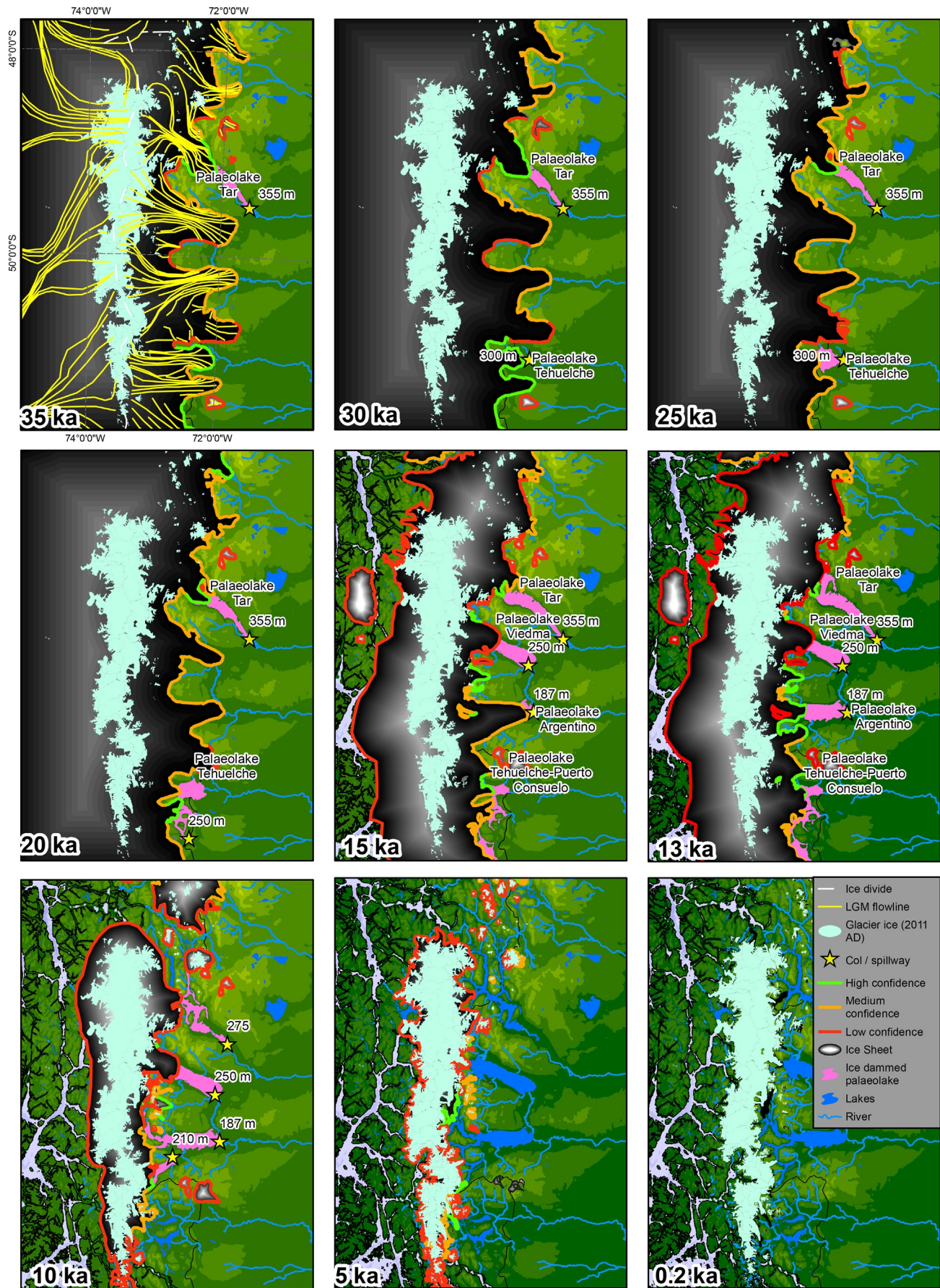


Figure 25



73°0'0"W

72°0'0"W

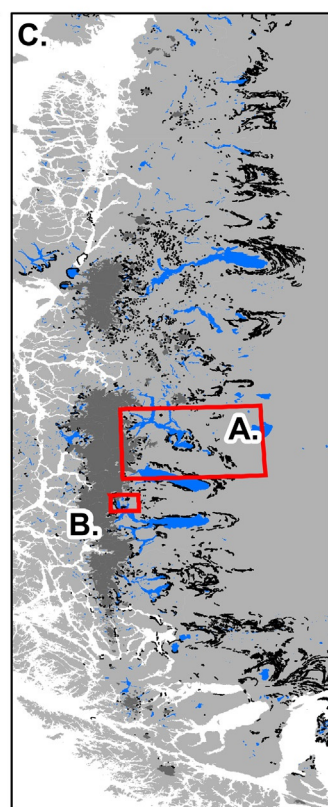
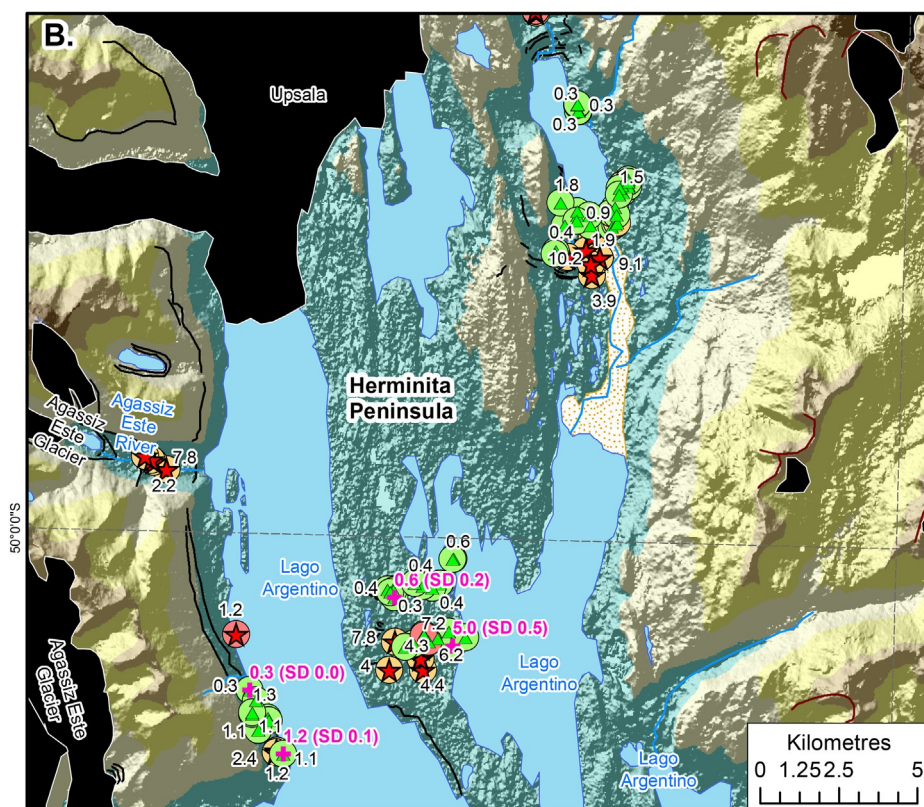
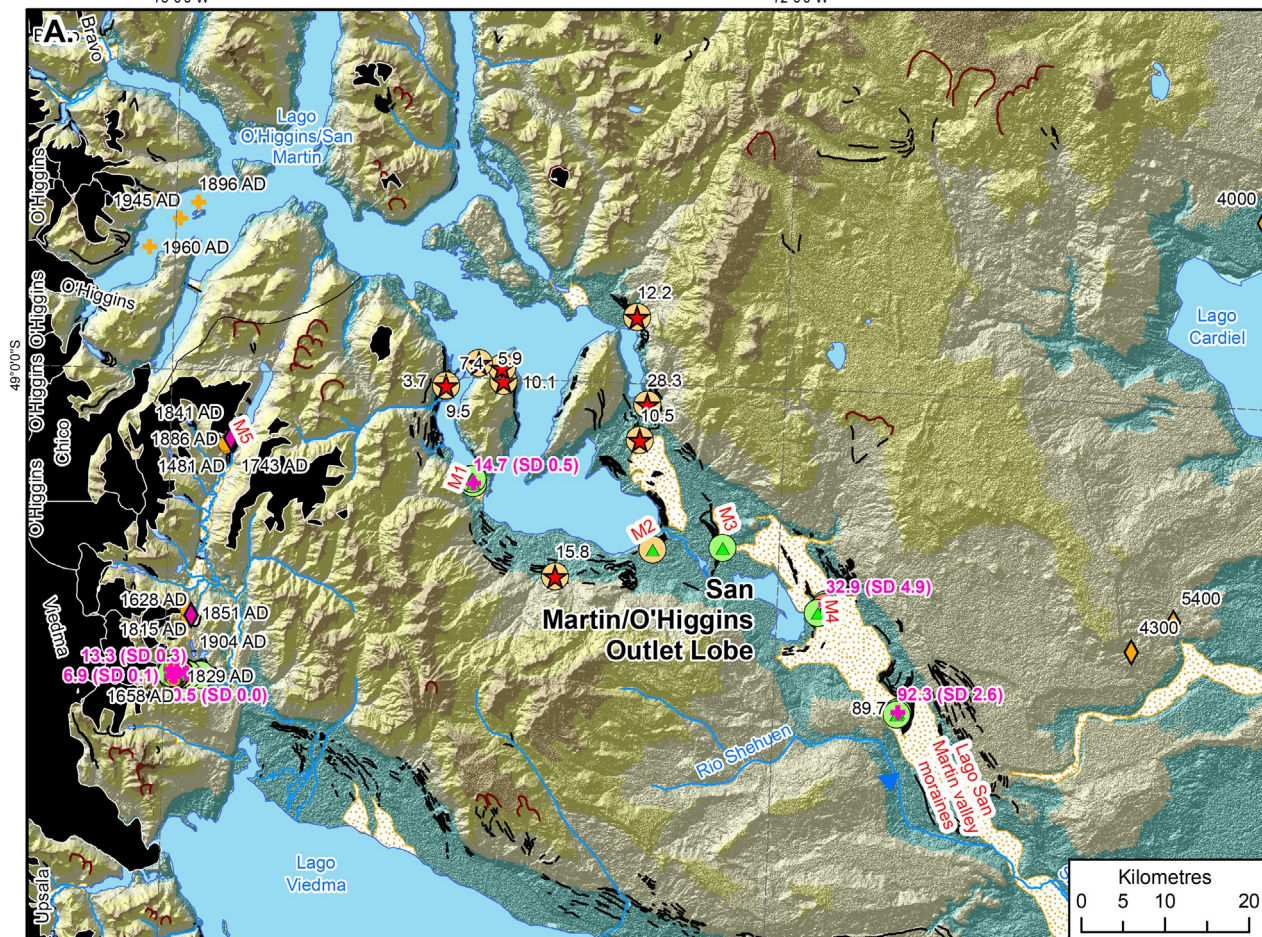


Figure 26







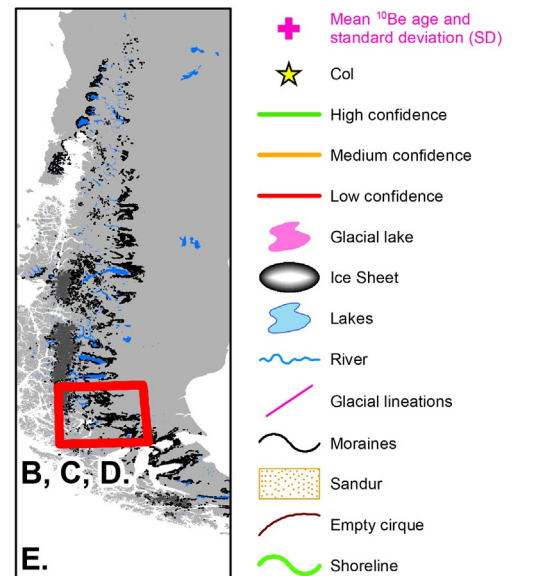
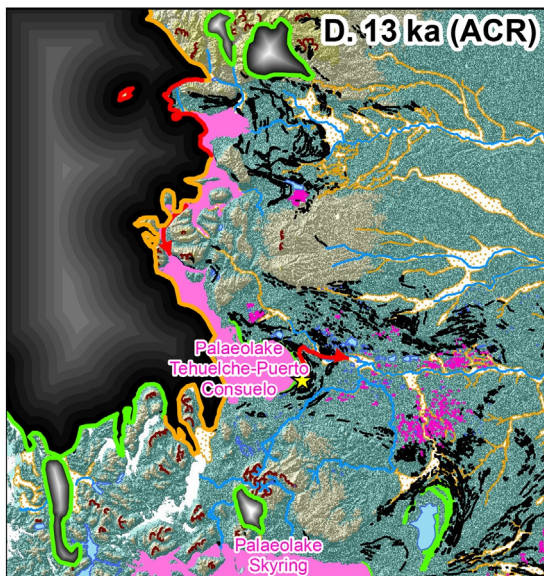
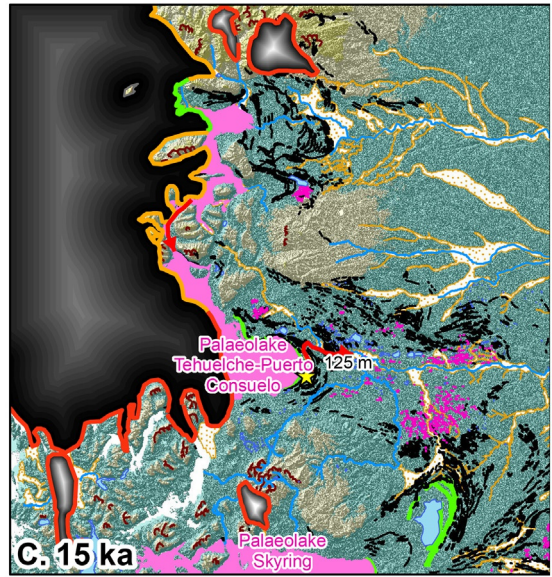
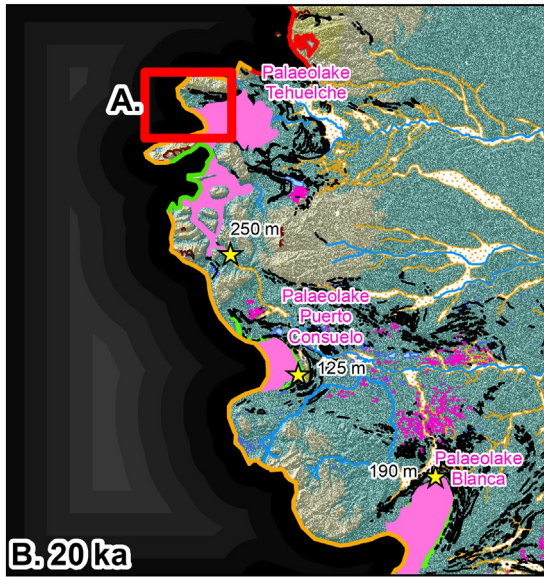
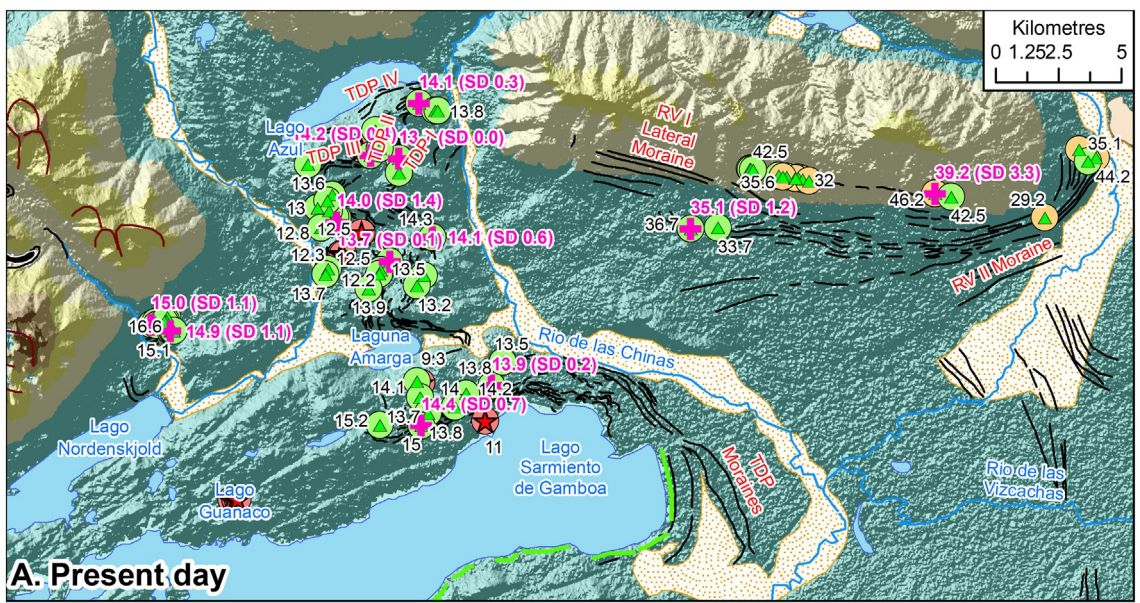


Figure 28







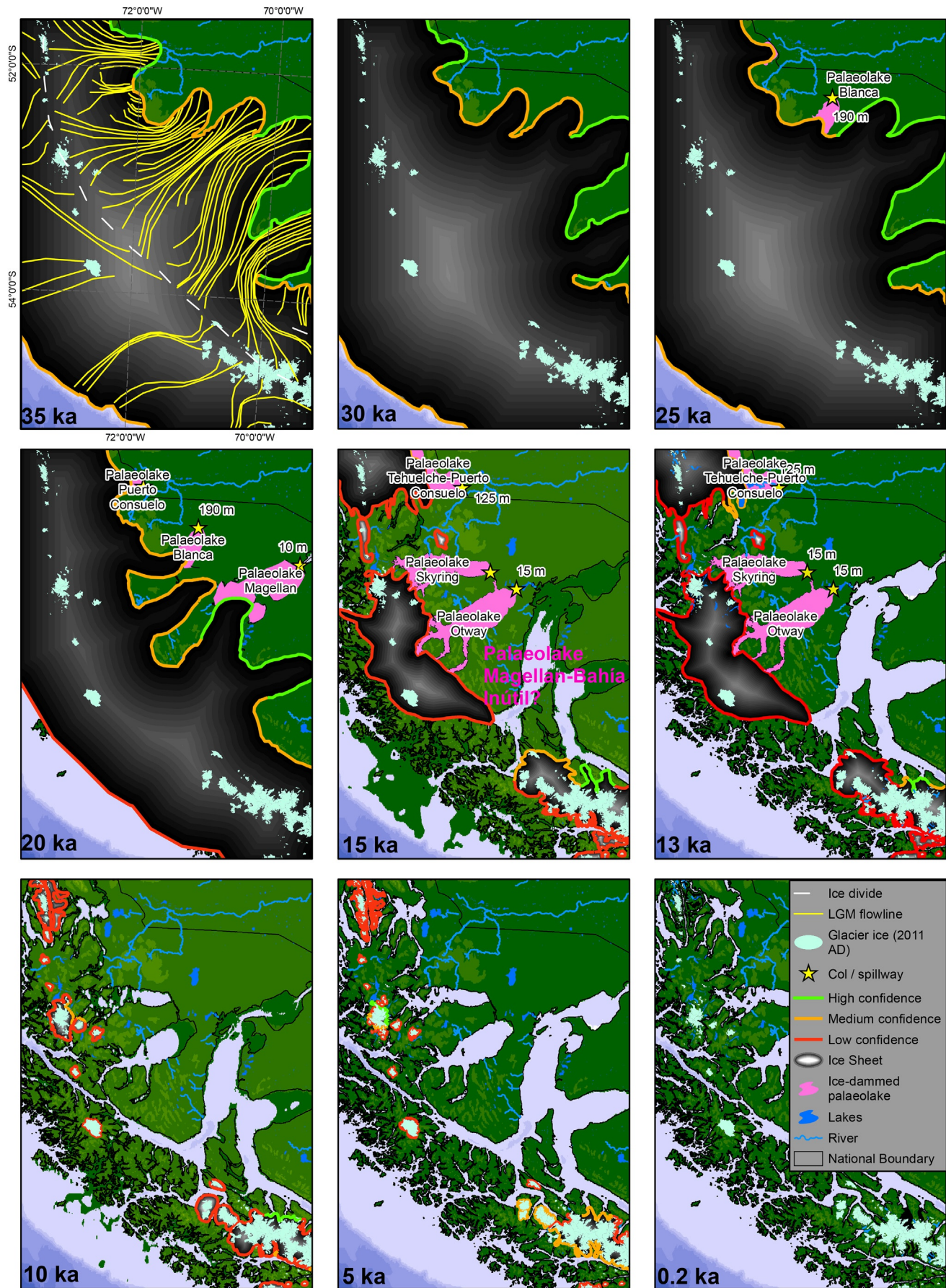


Figure 30



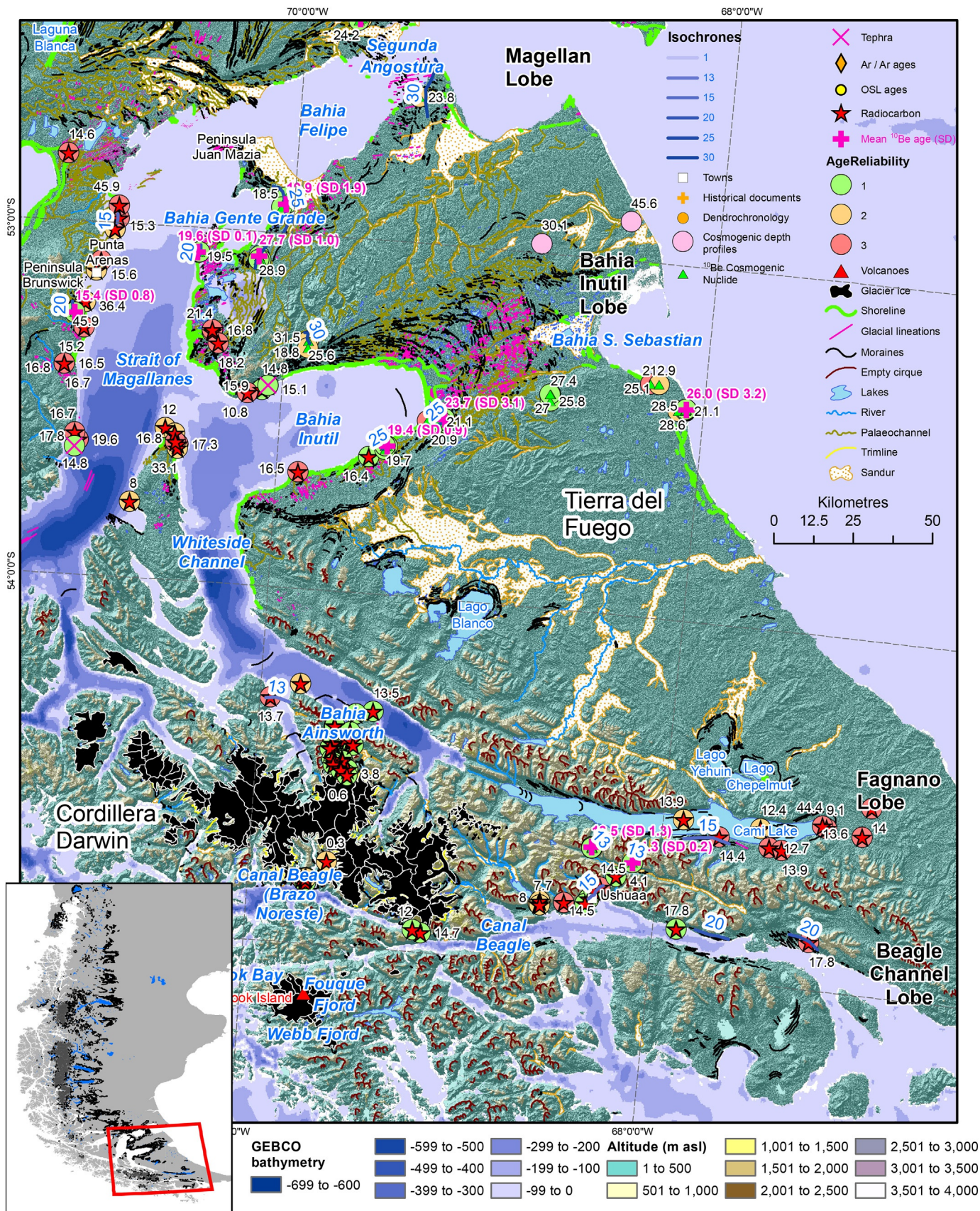


Figure 31



70°0'0"W

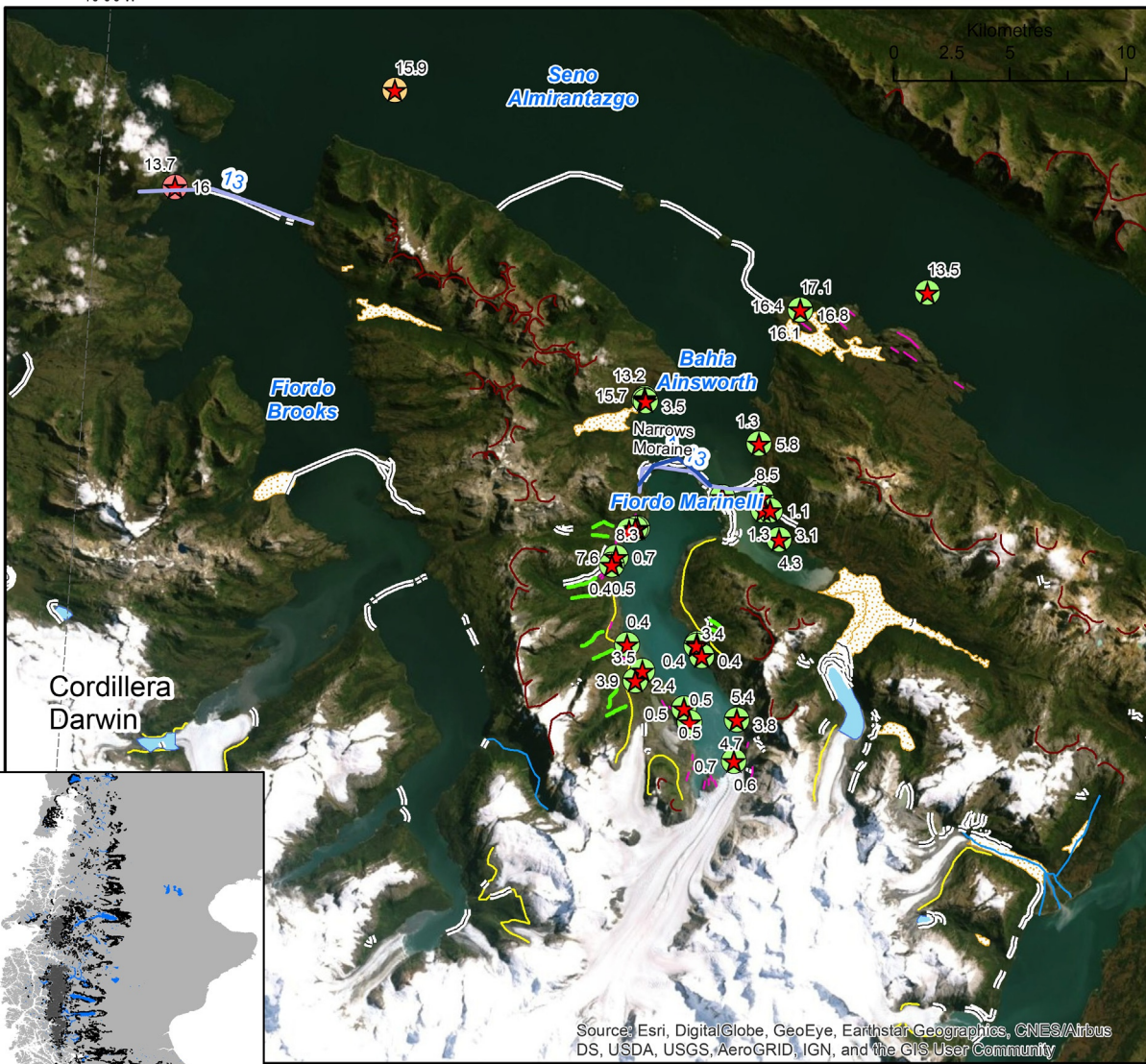


Figure 32



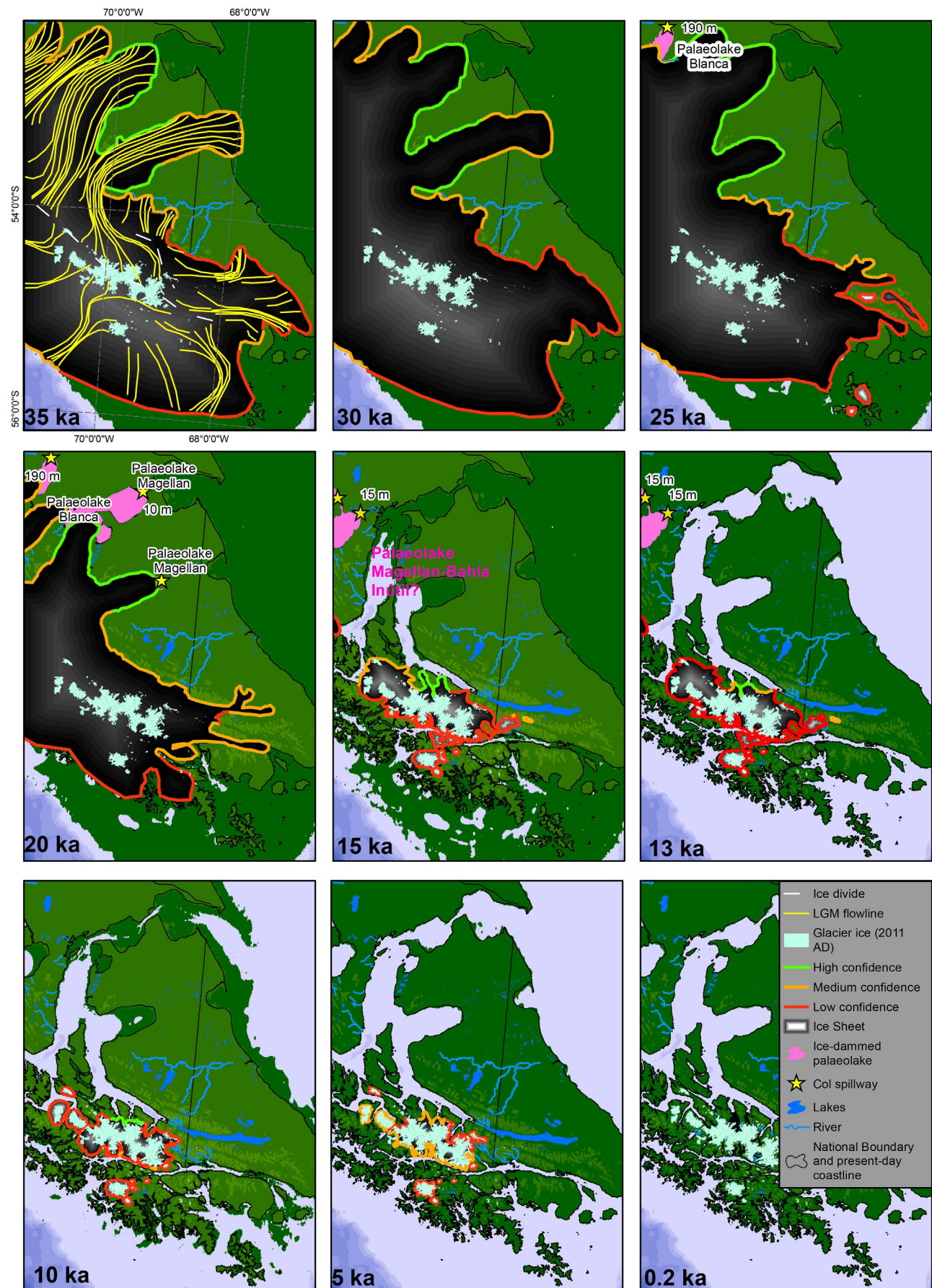


Figure 33



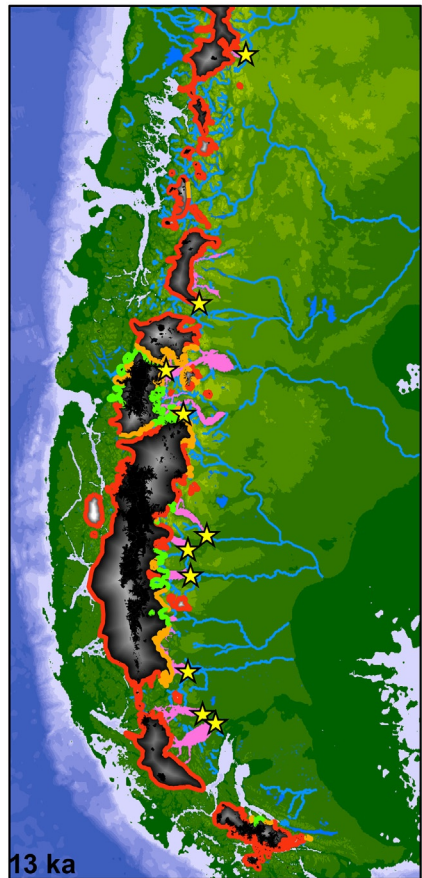
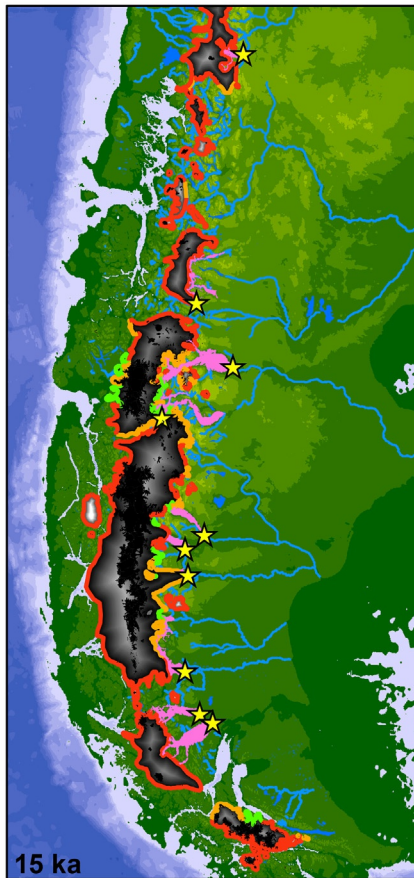
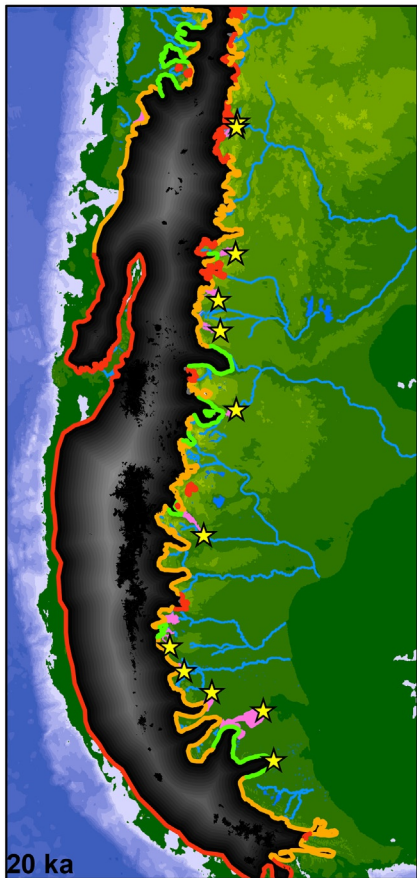
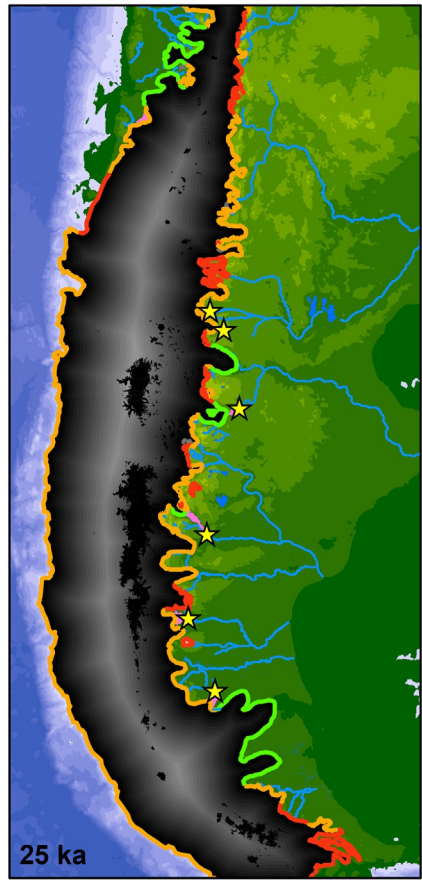
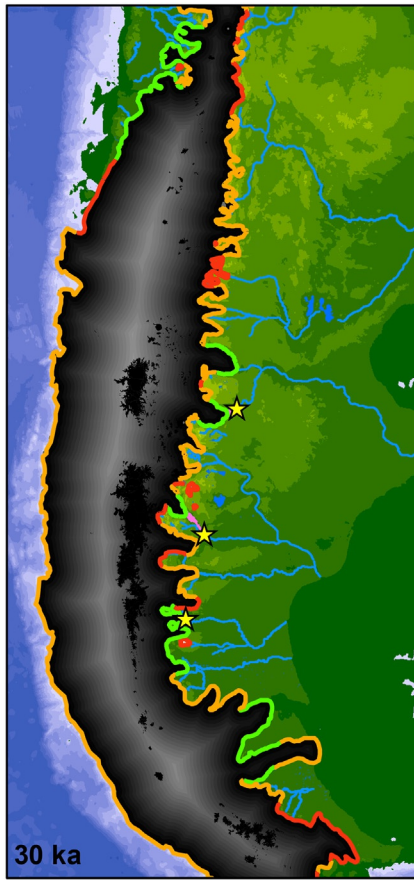
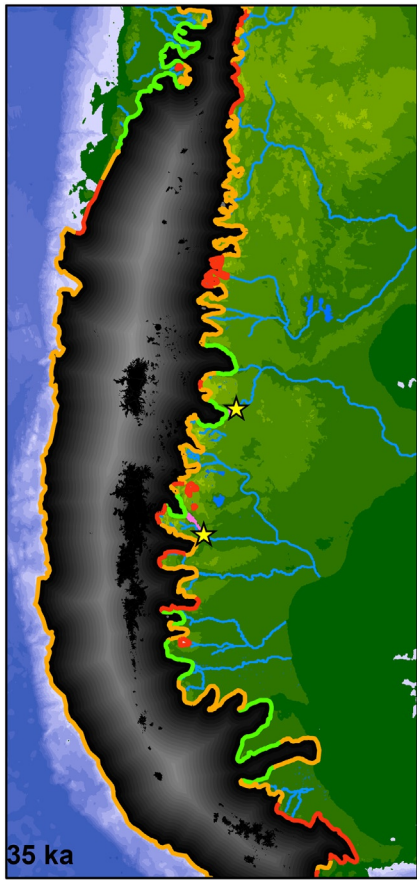
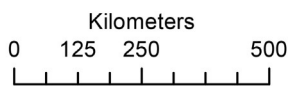
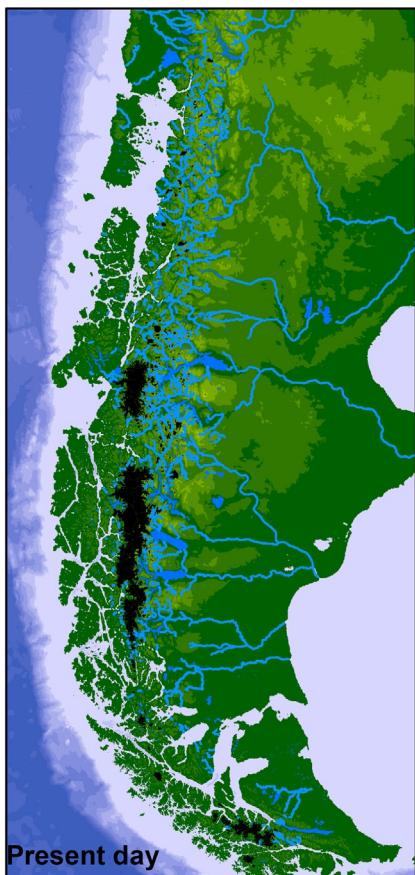
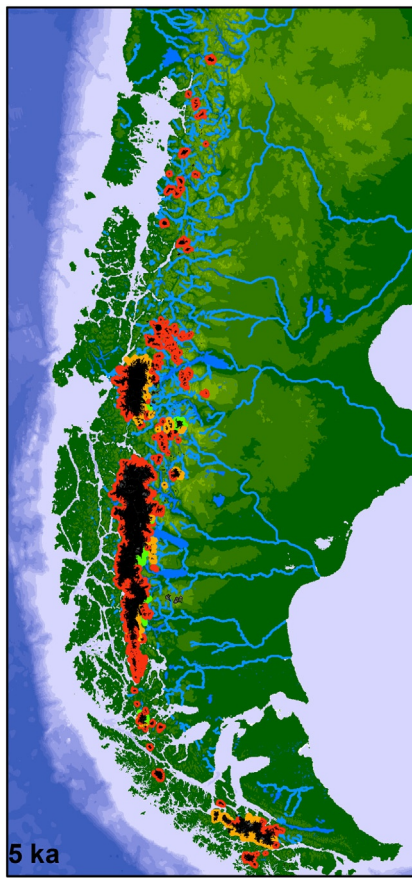
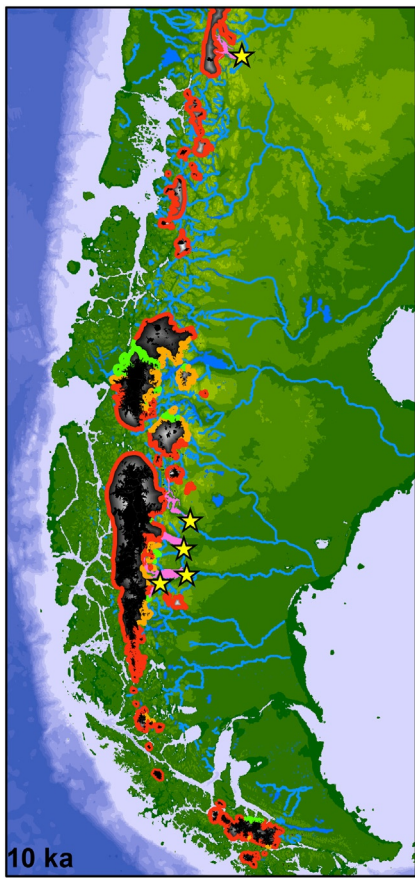


Figure 34A





- Glacier ice
- High confidence
- Medium confidence
- Low confidence
- Ice Sheet
- Lakes
- River
- Glacial lake
- Col spillway

Figure 34B





Figure 35

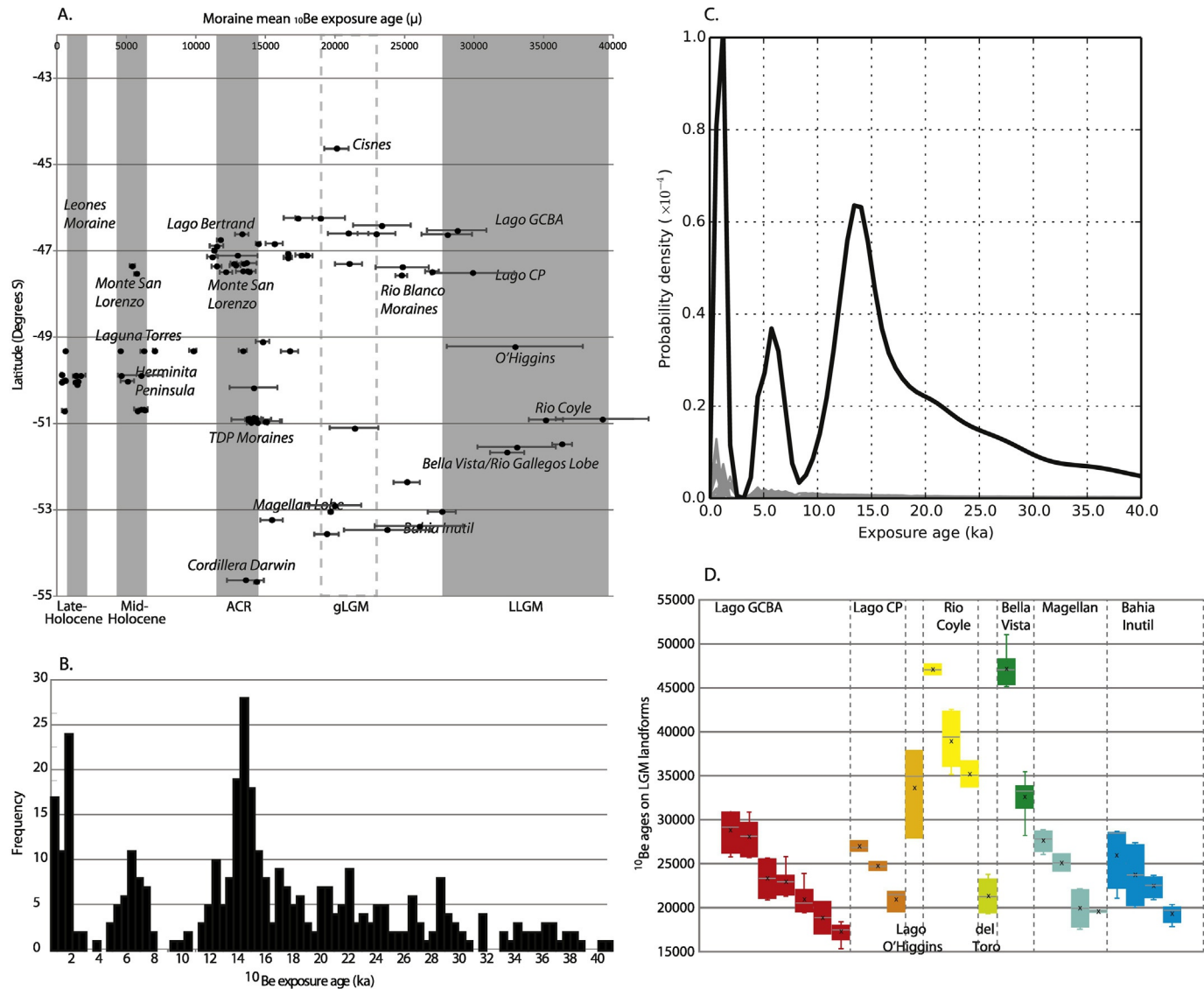


Figure 36

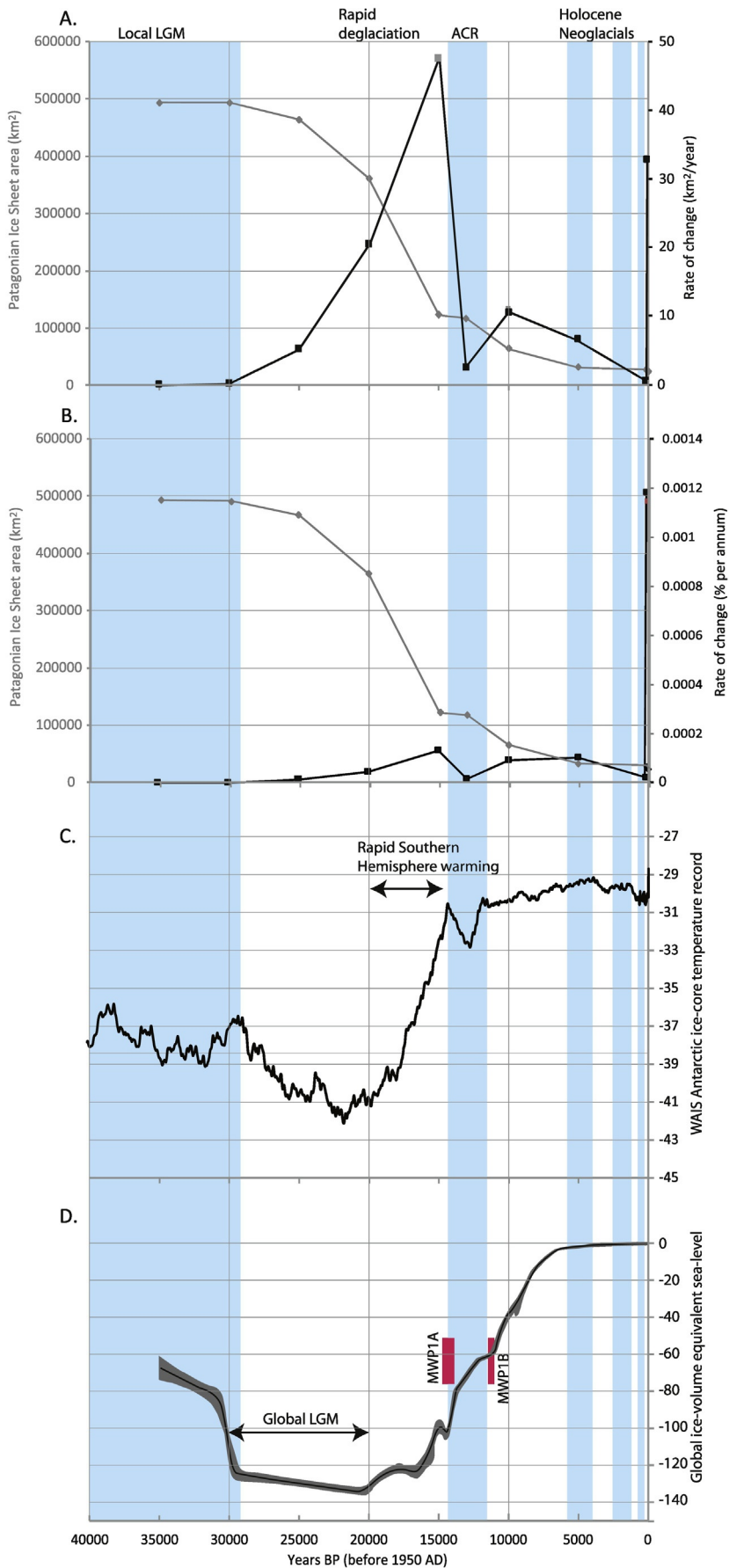


Figure 37

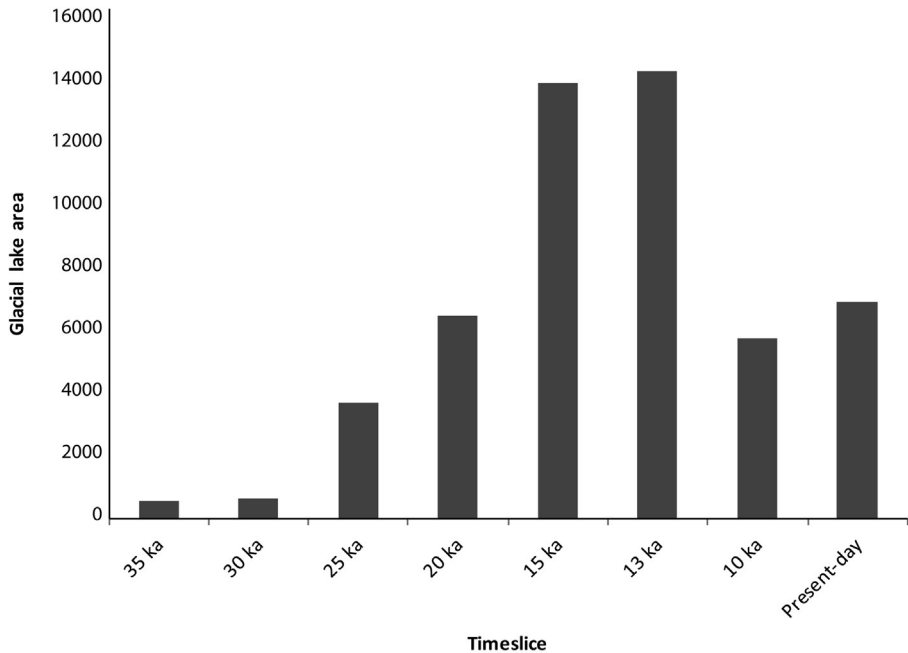


Figure 38